Title
Performance-Based Seismic Demand Assessment of Concentrically Braced Steel Frame Buildings

Author
Chen, Chui-Hsin

Publication Date
2010

Peer reviewed|Thesis/dissertation

Performance-Based Seismic Demand Assessment of Concentrically Braced Steel Frame Buildings

by

Chui-Hsin Chen

A dissertation submitted in partial satisfaction of the requirements for the degree of

Doctor of Philosophy

in

Engineering – Civil and Environmental Engineering

in the

Graduate Division

of the

University of California, Berkeley

Committee in charge:

Professor Stephen A. Mahin, Chair

Professor Bozidar Stojadinovic

Professor Haiyan Huang

Fall 2010

Performance Based Seismic Demand Assessment of
Concentrically Braced Steel Frame Buildings

by

Chui-Hsin Chen

Abstract

Performance-Based Seismic Demand Assessment of
Concentrically Braced Steel Frame Buildings

by

Chui-Hsin Chen

Doctor of Philosophy in Engineering – Civil and Environmental Engineering

University of California, Berkeley

Professor Stephen A. Mahin, Chair

The special concentrically steel braced frame (SCBF) system is one of the most effective structural systems to resist lateral forces. Because of its effectiveness and straightforward design, many SCBFs are incorporated in structures throughout the world. However, the highly nonlinear behavior associated with buckling and non-ductile fracture of braces reduces the ability of the system to dissipate energy resulting in undesirable modes of behavior. While many studies have investigated the cyclic behavior of individual braces or the behavior of subassemblies, the dynamic demands on the structural system under various seismic hazard levels needs additional study for performance-based earthquake engineering.

Archetype buildings of SCBFs and buckling restrained braced frames (BRBFs) were analyzed using the computer program OpenSees (the Open System for Earthquake Engineering Simulation) to improve the understanding of the seismic behavior of braced frame systems, and to assess seismic demands for performance-based design. Numerical models were calibrated using test data determined from testing of conventional buckling braces, buckling restrained braces, and the braced frame specimens. In addition, fiber-based OpenSees models were constructed and compared with results of a sophisticated finite-element model that realistically captured local buckling and local fracture of structural elements. Because the OpenSees models are reasonably accurate and efficient, they were chosen to perform set of parametric computer simulations.

The seismic demands of the system and structural elements were computed and interpreted for 3-, 6-, and 16-story SCBFs and BRBFs under various hazard levels. The analysis results show large seismic demands for the 3-story SCBF, which may result in unexpected damage of structural and non-structural elements. The median expected probability of a brace buckling at one or more levels in a 3-story SCBF is more than 50% for an earthquake having a 50% probability of exceedance in 50 years (the service-level event). The possible need to replace braces following such frequent events due to brace buckling should be considered in performance-based earthquake engineering assessments. In addition, brace fracture in SCBFs is likely for an earthquake having a 2% probability of exceedance in 50 years (the MCE-level event). Analyses show that in general, BRBF models had larger drift demands and residual drifts compared to SCBF systems, because of the BRBF's longer fundamental period. However, the tendency to form a weak story in BRBFs is less than that in SCBFs.

Evaluation of seismic demand parameters were performed for 2-, 3-, 6-, 12-, and 16-story SCBFs

and BRBFs, which demonstrated that short-period braced frame systems, especially SCBFs, had higher probability of collapse than longer-period braced frame systems. Substantially improved response was observed by lowering the response reduction factor of the 2-story SCBF building; this reduced the collapse risk at the hazard level of 2% probability of exceedance in 50 years. For long-period (taller) structures, although the collapse probability was lower compared to the short-period structures, weak story behavior was commonly observed in conventionally designed SCBF. A design parameter related to the ratios of story shear demand and capacity under a pushover analysis is proposed to modify member sizes to reduce weak story behavior efficiently. This is demonstrated for a 16-story SCBF building.

Regarding local deformation and force demands, simple methods to estimate out-of-plane buckling deformation of braces and column axial force demands are proposed. The investigation of system performance and member behavior provides seismic demands to more accurately assess the socio-economic losses of SCBFs and BRBFs for performance-based earthquake engineering.

To Yu-Ting, my parents, brother, and sister

CONTENTS

List of Figures

List of Tables

Acknowledgments

First and foremost, this dissertation never would have been completed without many years of support and guidance from my research advisor, Prof. Stephen A. Mahin. His insightful vision on earthquake engineering and brilliant ideas on the research topic have promoted the accomplishment of this work. I am deeply grateful for his patience and constant encouragement during my study. I sincerely thank Prof. Bozidar Stojadinovic and Prof. Haiyan Huang for serving as the members of my dissertation committee and giving me constructive advice on my dissertation work. I also thank the participation of Prof. James Kelly and Prof. Sanjay Govindjee as members of my qualifying exam committee. Their suggestions on my doctoral work were extremely valuable.

This work was assisted by many professors, graduate students, and engineers. Special thanks are due to Dr. Patxi Uriz, who has provided assistance in developing the numerical models for extensive analyses in computer clusters and interpreting test data on braces and braced frames. Rafael Sabelli, Director of Seismic Design at Walter P Moore, provided advice related to interpretation of code requirements of the SCBF and BRBF structures considered herein. Rafael's efforts contributed to the success of this work. The assistance of Drs. Andreas Schellenberg, Matthew Dryden, Yuli Huang, Tony Yang, Frank McKenna and Silvia Mazzoni in developing the OpenSees models is gratefully acknowledged. I am thankful for Claire Johnson's effort in proofreading the manuscript, and the technical assistance from Charles James, the EERC Library Director. I also appreciate the academic support from my friends at Berkeley. To my friends, Sangjoon Park, Matias Hube, Hong Kim, Jiun-Wei Lai, Tracy Becker, Troy Morgan, and Ken Orgozalek, thank you for sharing your creativity with me.

As ever, my deepest gratitude goes out to Yu-Ting Huang, an endless source of love, warmth, inspiration, and friendship. I am indebted to her for her patience, understanding, self-sacrifice, tolerance, forgiveness, and being always there by my side. Her invaluable support for my life and advice on developing my academic strategies have greatly contributed to the completion of my doctoral program.

Lastly, I would like to acknowledge the financial support provided by the National Science Foundation under Grants CMS-0600625 and CMS-0619161, and by the University of California at Berkeley through Prof. Mahin's Byron and Elvira Nishkian Chair funding. I also thank the Dr. and Mrs. James C.Y. Soong Fellowship provided through UC Berkeley Graduate Division, and financial support through Taiwan Merit Scholarship TMS-094-2-A-025.

Part of the work herein is part of the report prepared for the Building and Fire Research Laboratory of the National Institute of Standards and Technology under contract number SB134107CQ0019, Task Orders 67344 and 68002. The statements and conclusions contained in this study are those of the authors and do not imply recommendations or endorsements by the National Institute of Standards and Technology.

Chapter 1

Introduction

1.1 Motivation

Special steel moment-resisting frames (SMRF) were considered to be one of the best structural systems for use in areas of high seismicity. The simple configuration of structural elements and straightforward design criteria increased the popularity of this structural system among the engineers, architects and owners. However, the 1994 Northridge, 1995 Hyogo-ken Nanbu and other recent earthquakes have shaken the confidence of engineers in these systems due to widespread brittle fractures that occurred in special welded steel beam-to-column connections [FEMA, 2000a]. The Federal Emergency Management Agency (FEMA) initiated a six-year program of investigation and guideline development by the SAC Joint Venture (comprised of the Structural Engineers of Northern California, Applied Technology Council, and California Universities for Research in Earthquake Engineering) [FEMA, 1997a through 1997c; FEMA, 2000b through FEMA, 2000d].

Although these guidelines have restored the confidence of engineers and the public in the use of SMRF, ,more stringent requirements and restrictions are now required for the design using this structural system, and more rigorous checks are stipulated for quality control to achieve the required ductility of beam-to-column connections. Research on SMRF systems has also demonstrated that very large story drift may occur during a severe earthquake leading to serious damage to the structural and non-structural components. Because the design of SMRF is usually controlled by code-designated story drift limits, the member sizes maybe much larger than those designed solely on the basis of force. This has resulted in cost increases and complex construction configurations, with engineers and owners now seeking more efficient and economical systems.

The special concentrically steel braced frame (SCBF) system is one of the candidates that are simple to design, effective in resisting the lateral force and efficient in limiting lateral deformation. Currently, SCBF systems comprise about forty percent of the market for office and hospital buildings in California and the trend is believed to be increasing [Ferch, 2004].

Although the SCBFs are now widely used, damage to concentrically braced frames observed during the past earthquakes, including the 1985 Mexico [Osteraas and Krawinkler, 1989], 1989 Loma Prieta [Kim and Goel, 1992], 1994 Northridge [Tremblay et al., 1995; Krawinkler et al., 1996], and 1995 Hyogo-ken Naubu [AIJ/Kinki Branch Steel Committee, 1995; Hisatoku, 1995; Tremblay et al., 1996] events should be noted. The failure mode generally observed was fracture of the braces at the locations of local buckling or plastic hinges. In some cases, fractures were observed at the weld of the connections to the gusset plate or the weld in the boundary of

the gusset plates. Researches demonstrated that this structural system is prone to concentrating the damage to a single story, which results in significant story drift and floor acceleration [Khatib et al., 1988], and design codes have been updated to reduce such common forms of damage.

Despite such code updates, the seismic performance of concentrically braced frames is not considered as robust as it should be. Several factors possibly degrade the performance of SCBF systems:

- Braces dissipate energy by yielding in tension and by inelastic buckling in compression. The buckling of braces often decreases their ductility and energy-dissipating capacity under cyclic loading [Black et al., 1980; Tang and Goel, 1989; Kim and Goel, 1992]. It is observed that braces fracture after only a few cycles due to the limited ductility capacity.
- The nonlinear behavior of braces as well as braced frames is complex. Therefore, the intensity and distribution of forces, and deformations over the building are difficult to predict numerically. The failure of braces can result in large story drift and frame instability. Some damage occurs because of the unexpected concentration of deformation or force at few stories [Aguero et al., 2006].
- There are a variety of failure modes for SCBF systems. From the observations of previous earthquakes and experiments, damage occurred in braces, gusset plates, beam-column connections, brace-to-framing connections, and beams and columns. The occurrence of failure modes is sensitive to characteristics of earthquakes, structural configurations proportions of structural members and detailing of the connections.

Several experiments have conducted in recent years to assess the seismic responses of concentrically braced frame systems. Despite the available experimental or field data, it is remains difficult to establish confidence in current design methods. Over the past decades, research efforts have strived to develop quantitative probabilistic methods to evaluate the performance of structures [Hamburger et al., 2003; Moehle et al., 2005]. These are quite versatile in terms of addressing engineering-centric goals, such as continued occupancy or collapse prevention, or in terms of societal-centric goals such as maximum probable losses (or down time or injuries) over the life of a structure or given the occurrence of a scenario event (see, for example, Miranda and Aslani, 2003). Thus, a significant opportunity exists to validate and improve design methods for concentrically braced frame structures by developing and validating realistic numerical models and using these models in combination with modern performance-based evaluation framework [Moehle, 2003].

Most of the previous analytical studies investigated the behavior of structural components in a braced frame or the behavior of tested specimens. Such preliminary studies indicate the need for additional system studies. Studies are still limited regarding system performance [Uriz and Mahin, 2008].

1.2 Objectives

The objectives of this study are to:

1. Investigate the sensitivity of global and local engineering demands to parameters used in the design and analysis of concentrically braced frames.

2. Develop further understanding of the seismic behavior of concentrically braced frame systems in terms of the engineering demand parameters.
3. Use performance based evaluation concepts to understand the tradeoffs between the stiffness, strength, and ductility, and the global and local demands associated with various performance goals.

The objectives are being achieved by:

1. Evaluating and improving numerical models to predict the response of concentrically braced frames consistent with the efficiency and accuracy needs of performance-based earthquake engineering (PBEE).
2. Studying the sensitivity of seismic demands to seismic hazard and structural characteristics.
3. Examining various engineering demand parameters to characterize performance.
4. Applying a probabilistic PBEE framework to the assessment of structural performance.
5. Assessing the design parameters of current codes for steel braced frames using the methodology of FEMA P695 (ATC-63).
6. Identifying the global and local seismic demands for performance-based design.
7. Developing schemes to improve system performance.

1.3 Scope

Performance-based earthquake evaluation criteria have been developed by several researchers to assess the seismic hazard, structural responses, expected damage and possible losses for various hazard levels and structural systems. Figure 1.1 illustrates the framework of PBEE as developed by the Pacific Earthquake Engineering Research Center (PEER) of the University of California, Berkeley [Moehle, 2003]. By constructing an appropriate conditional probability function, the relationship between the ground motion intensity and socio-economic variables is established using the total probability theorem.

Based on extensive numerical simulations, the engineering demand parameter (EDP) model characterizes the relationship between the intensity measure and the EDPs. The damage model relates the EDPs to the damage measures; which is usually constructed by summarizing the observations from test data and field work to relate EDPs to damage. The loss model defines the relationship between the damage measure and the decision variables, which are usually expressed in terms of death, dollar losses and downtime; the construction of this model require the efforts from industry to help estimate the possible losses.

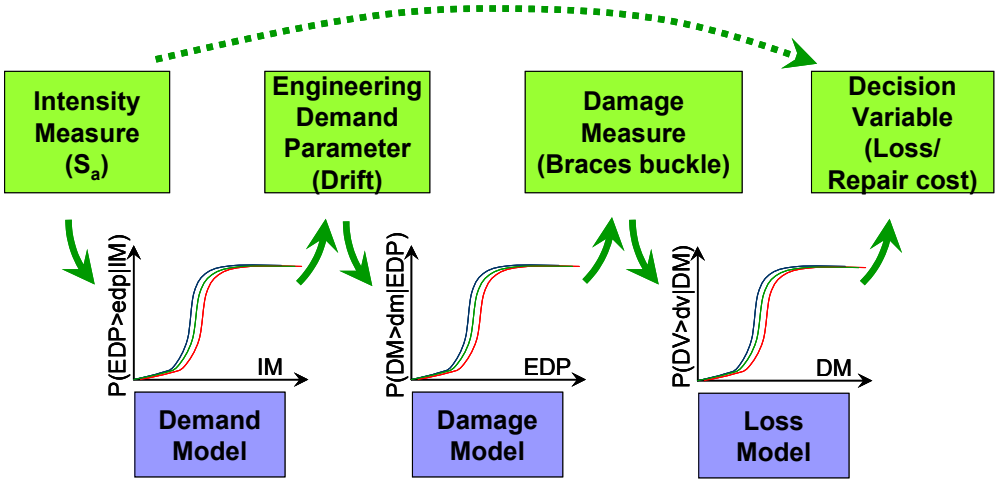

$$\lambda(DV) = \iiint P(DV \mid DM) \cdot dP(DM \mid EDP) \cdot dP(EDP \mid IM) \cdot d\lambda(IM)$$

Figure 1.1 Illustration of PBEE framework

The research presented herein emphasizes the demand model for braced frame systems. Efficient and accurate nonlinear numerical models were constructed, and the numerical models were carefully calibrated with existing test data for braces and two-story braced frames. To determine the accuracy of the extensive nonlinear dynamic analyses performed for simulations for system behaviors, the results for system performance of the numerical models were compared with a more sophisticated but more computational expensive finite-element model, which has been proved to accurately simulate global and local failure of braced frames.

The investigated braced frame systems included SCBF systems that conform to current building codes [ASCE 7-05, 2005] as well as previous versions of the codes, and BRBF systems. Because of the large variety of possible brace configurations, it is not practical to include all configurations. Only structures with a double story X configuration are discussed, which is currently one of the most efficient and commonly used configurations.

To verify the capacity of the braced frame systems to resist collapse under extreme ground motion excitations, the design parameters detailed in the current code for SCBF and BRBF are evaluated. Structures with different number of stories representing various period ranges are analyzed with the selected ground motions. The response reduction factor (R-factor) is the primary design parameter evaluated, but the discussion also includes overstrength factor and the deflection amplification factor, C_d.

To understand how the collapse-resisting capacity of braced frame buildings can be improved, the effects of changing the response reduction factor are evaluated. Also, new design parameters are proposed to better control the deformation concentration observed in high-rise SCBF buildings.

This research also identifies the global and local force and deformation demands of SCBF and BRBF for various hazard levels using the SAC ground motion set [Somerville, 1997] representing various hazard levels. Simple methods to estimate the out-of-plane deformation of buckling braces and column axial force demands are proposed.

This dissertation is organized as follows. Chapter 2 reviews recent studies on the numerical

simulation of braced system behavior and the evaluation of design parameters of braced frame systems. Chapter 3 constructs the numerical models and calibrates them by using test data and results of more detailed finite element models. Chapter 4 examines in detail the performance of a three-story SCBF designed with different criteria and a three-story BRBF. Chapter 5 evaluates the seismic performance factors (R-factor, Ω_0 and C_d factor) found in current design codes using the methodology of FEMA P695. Chapter 6 presents the global force and deformation demands of SCBF and BRBF systems having different number of stories; the effects of changing the design criteria to improve the system performance of SCBF are evaluated. Chapter 7 examines the force and deformation demands of braces, beams, and columns under various hazard levels; this chapter also proposes simple methods to estimate the out-of-plane deformation of buckling braces and column axial force demands. The concluding remarks and recommendations are given in Chapter 8.

Chapter 2

Literature Review

The typical failure modes experienced by SCBF buildings due to earthquake excitation include damage to braces, brace-to-framing connections, columns and base plates [Kato et. al., 1980; Hanson and Martin, 1987; Osteraas and Krawinkler, 1989; Kelly et. al., 2000; Bonneville and Bartoletti, 1996; WJE, 1998; Naeim, 1997, 1998; Architectural Institute of Japan, 1995; Tremblay et. al., 1995]. Much experimental and analytical research has been conducted on the performance of braces [Tremblay, 2002; Lee and Bruneau, 2005; Yang, 2005], gussets [Astaneh-Asl, 1998; Roeder et al., 2005; Chambers and Ernst, 2005] and frames [Khatib and Mahin, 1987; Fukuta et al., 1989; Lee and Lu, 1989; Wallace and Krawinkler, 1989; Bertero et al., 1989; Archambault, 1995; Tremblay et al., 1995; Tremblay and Filiatrault, 1996; Sabelli et al., 2000, 2003; Tremblay et al., 2003; Uriz and Mahin, 2008]. Recently research of SCBF and BRBF buildings has focused on the experimental and numerical performance of braces [Han et al., 2007; Tremblay et al., 2008; Fell et al., 2009], brace-to-framing connections [Packer, 2006; Willibald et al., 2006; Lehman et al., 2008; Shaw et al., 2010; Wigle and Fahnestock, 2010] and systems [Fahnestock et al., 2007a, 2007b; Tsai et al., 2008; Broderick et al., 2008; Annan et al., 2009; Tremblay et al., 2009] in response to updated design codes [ASCE/SEI 7-05 (2005)] or using construction details that are similar to those in the US.

This chapter discusses research that has focused mainly on the numerical simulations of system performance of SCBF and BRBF systems. Studies that evaluate design parameters— ductility, overstrength and response modification factors— are also examined. Because of the considerable amount of literature on this topic, this section provides a brief synopsis of recent work.

2.1 Literature on System Performance of Braced Frame System using Numerical Simulations

Several researchers have used numerical simulations to investigate the behavior of braced frame systems [Sabelli et al., 2000; Ding, 2006; Uriz and Mahin, 2008; Yoo et al., 2008; Khandelwal et al., 2009; Huang, 2010]. Seismic demands of several prototypes of SCBF and BRBF buildings were investigated by Sabelli et al. [2000; 2003] using phenomenological models in SNAP-2DX [Rai et al., 1996]. The model buildings were designed to assess the design and analysis procedures of the then current design, NEHRP Recommended Provisions for Seismic Regulations for New Buildings and Other Structures [FEMA, 1997b, 1997c]). The structural configurations included are shown in Figure 2.1. Table 2.1 lists the analytical results of the model buildings with chevron configuration subjected to a suite of 20 ground motion records with 10% exceedance in 50 years. The 1997 NEHRP provisions allowed the unbalanced tension/compression capacity of braces to be disregarded in the design of beams on the roof level;

therefore, the inelastic response was concentrated at the roof level for almost all ground motions considered. Fracture of braces, which was observed in many of the analyses, occurred mostly at the roof level and early in the record. In this study, the 6-story SCBF was designed based on the performance of the 3-story SCBF, whereby the design of the roof beams of the 6-story SCBF were stronger and stiffer than the requirement in 1997 NEHRP provisions; the damage was less concentrated and smaller peak story drift ratios were observed (see Table 2.1). In the double story X configuration of 6-story SCBF, the 1997 NEHRP provisions did not require a vertical unbalanced load for the design of the beams and no significant beam hinging was observed when subjected to all ground motions.

Analytical results of the model BRBF buildings studied show that the BRBF effectively reduced the damage concentration and the vertical unbalanced load in beams. In addition, the response of BRBFs was more sensitive to proportioning rather than to varying the design R-factors ranging from 6 to 8. Table 2.1 shows that the maximum story drift ratios of 3- and 6-story BRBF were similar. Also, the drift ratio of BRBFs was similar to that of 6-story SCBF, but much less than that of 3-story SCBF, which had relatively weaker roof beams. While the study identified some important parameters associated with structural configurations, proportioning, and modeling, it was suggested that the confidence of the results would be improved by calibrating the analytical model with experimental research and employing more detailed models that account for bending and shear forces in the braces.

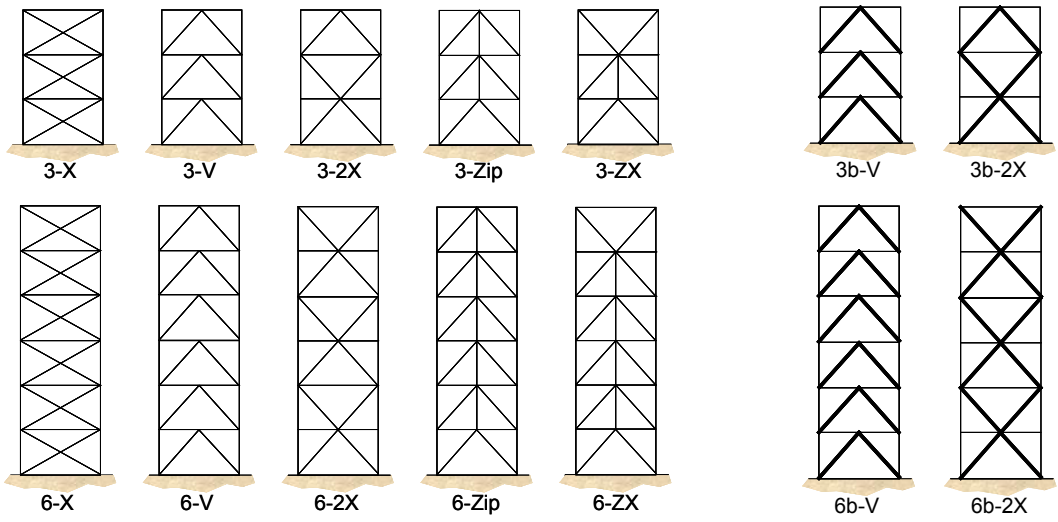

(a) SCBF (b) BRBF

Figure 2.1 Considered structural configurations of 3- and 6-story SCBF and BRBF in Sabelli et al. 2003

Table 2.1 Response summary for 10% in 50 year events (after Sabelli, 2000)

	Frame	Story Drift Ratio (%)		Residual Story Drift Ratio (%)	
		Mean	+1σ	Mean	+1σ
6-Story	BRBF (6b-V, R=8)	1.6	2.2	0.7	1.1
	SCBF (6-V)	1.8	2.6	0.4	0.7
3-Story	BRBF (3b-V, R=8)	1.4	2.1	0.5	1.0
	SCBF (3-V)	3.9	7.0	2.5	5.6

A series of experimental and analytical study on SCBFs and BRBFs was conducted to assess the performance of chevron braced frame structures by Uriz and Mahin [2008] with improved simulation models. Simulations were done using OpenSees [McKenna, 1997] models. Braces were modeled considering large local displacements; fiber sections were used to model plastic hinge behavior including low-cycle fatigue effects. The effects of fatigue did not account for true fracture mechanics; rather, Rainflow cycle counting and Manson-Coffin fatigue criteria was used to fail individual fibers at a plastic hinge. Eventually, all fibers at a section would fail under severe loading conditions. The investigation examined many parameters including: the net section reinforcement at brace connections, the effects of fatigue modeling parameters, the dynamic characteristics of SCBFs and BRBFs, as well as the responses of low-rise and mid-rise braced frame buildings. Table 2.2 summarizes some of the response quantities of three-story and six-story chevron SCBF and BRBF. The brace proportions and details are identical to the buildings found in Sabelli [2000].

The results showed that the drift demands of low-rise SCBFs were slightly greater than that of BRBF at various hazard levels. Nonetheless, the out-of-plane deformation of buckling braces is observed even at the 50% probability of exceedance in 50 years hazard level. The performance of the mid-rise SCBF was even poorer than the low-rise SCBF in some aspects; the residual displacement at the 50% probability of exceedance in 50 years hazard level was greater in the six-story model, while the demand on the braces was also greater at the 10% probability of exceedance in 50 years hazard level. Also, the damage was concentrated in the lower stories in low-rise and mid-rise SCBFs. Compared to the SCBF system, the BRBFs showed a consistent tendency to distribute deformation more uniformly along the height of building at various hazard levels. Moreover, no brace fracture was observed for the BRBFs and no incidence of collapse was found.

In general, the response of SCBFs demonstrated large variation under severe earthquake excitation. Variations also exist for different numerical models. The results of SNAP-2DX and OpenSees simulations show a range of difference in predicting engineering demands for the same model buildings.

Table 2.2 Median (and standard deviation) of drifts for 3- and 6-story SCBF and BRBF at various hazard levels (after Uriz and Mahin, 2008)

ID	Hazard Level (% in 50 years)	Peak Story Drift Ratio at Any Level (%)	Residual Roof Drift (%)
3VF (SCBF)	50	0.4(0.7)	0(0.1)
	10	1.6(0.9)	0(0.2)
	2	5.7(2.4)	0.7(1.0)
3VB (BRBF)	50	0.6(0.6)	0(0.1)
	10	1.3(0.7)	0.1(0.4)
	2	3.8(2.1)	2.1(2.2)
6VF (SCBF)	50	0.4(0.3)	0.02(0.1)
	10	1.1(0.6)	0.06(0.15)
	2	4.4(2.2)	0.7(1.1)
6VB (BRBF)	50	0.4(0.3)	0.08(0.1)
	10	1.4(0.8)	0.3(0.7)
	2	4.4(2.5)	1.37(2.2)

Finite element models overcome the limitations of phenomenological models (such as the SNAP-2DX model) and physical-theory models (such as OpenSees fiber-based model) and are able to simulate local damage in braced frame buildings. Khandelwal et al. [2009] developed macro-models to conduct progressive collapse analysis of 10-story SCBF and EBF buildings, which were the combination of beam-column and discrete spring finite elements. These models were implemented and run on LS-DYNA. A few assumptions and limitations were chosen in developing this model: the gusset plates and beam-column connections in the model were simulated with simplification. The gusset plates were assumed to remain elastic and designed to be so. The beam-column connections were simulated as fully-restrained and the panel zones were assumed to be elastic, even under collapse conditions. Additional factors were not included by Khandelwal et al. [2009] such as the strain rate effect, debris impact during collapse and the uplift of the foundation. Nonetheless, the study successfully simulated the collapse behavior of the selected steel braced frame buildings.

Also utilizing LS-DYNA, Huang and Mahin [2010] developed a new continuum damage mechanics material model to capture the inelastic behavior and deterioration of mechanical properties. The model was implemented for SCBF buildings with the parameters calibrated from test data of braces and braced frames [Yang, 2005; Uriz and Mahin, 2008]. Shell elements were employed in the model building with selected meshes which were determined from a sensitivity study. The beam-column connections, gusset-to-framing connections, and gusset-to-brace connections were modeled in detail and the connected bolts were modeled as springs. Under extensive analysis of a preliminary case study, the seismic demand of a three-story, double-story X braced frame building was examined for PBEE. In recognition of the detailed and accurate information provided by the finite-element model as well as the excess of computational cost for the study of PBEE, Chapter 3 discusses the results from the finite-element and fiber-element based models.

Nonlinear finite-element analyses were conducted to investigate the behavior of multi-story X-braced frames and their gusset plate connections [Yoo et al., 2008]. ANSYS [2005] model with four-node quadrilateral shell elements were used for members, and bilinear kinematic hardening material was adopted to simulate nonlinear behavior of test specimens. The numerical model was calibrated with test data of single story, one-bay diagonal braced frame [Lehman et al., 2008] and then used to investigate the parameters that impact the local and global behavior of two-story double-story X braced frame specimens to then be tested under cyclic loading. The results illustrated that the proposed methodology for designing gusset plates was economic and effective in reducing premature gusset-plate buckling. It was also noted that neglecting the composite effects of concrete slab in numerical models resulted in underestimating the stress and strain demands of the mid-span gusset plates. Also, the potential damage was reduced by adopting the proposed details of gusset plates. Yoo's research also suggested that the double story X SCBF configuration has the potential to decrease deformation concentration in a single story.

A performance evaluation of three-dimensional SCBF structures under earthquake excitations was conducted by Ding [2006]. The study investigated the redundancy of a SCBF system, where 3-, 8-, and 12-story chevron braced frame buildings were designed as model buildings. The responses of structures were simulated in ABAQUS [2003]. Beams and columns were modeled as three-dimensional Euler beams. The modeling scheme of the brace connections is illustrated in Figure 2.2 considering the rigid-end zones and three times the thickness of the gus-

set plates for the flexibility of global brace buckling and gusset bending. For each brace, 20 beam elements were used in the models and brace fracture was simulated with user-defined element. In these simulations, brace fracture caused torsion of the buildings resulting in large displacements. For some ground motion excitations, brace fracture was observed even after the ground motion peak had already occurred. Ding's research also recognized the huge computational costs for numerical simulations for refined analytical models and recommended that numerical models for system performance evaluation should be simplified.

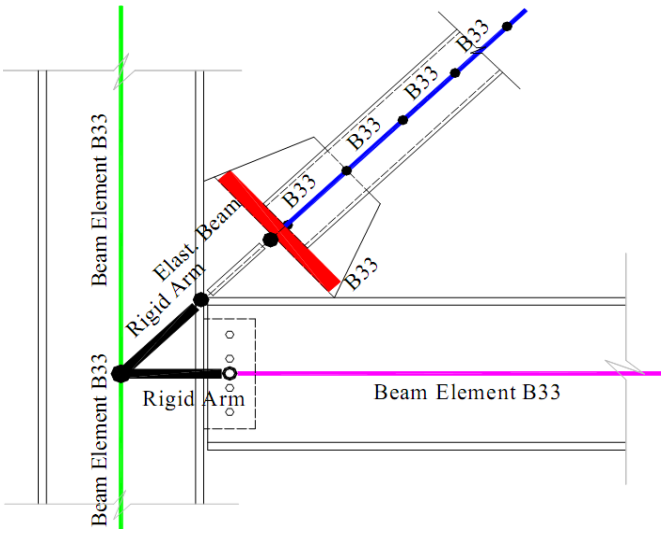

Figure 2.2 The modeling scheme of the brace connections in [Ding 2006]

Consideration of numerical models for PBEE is discussed in other studies [Chenouda and Ayoub, 2009; Ruiz-García and Miranda, 2009]. Chenouda and Ayoub [2009] conducted a probabilistic analysis of the collapse of a degrading multi-degree of freedom system on steel MRF buildings and identified the impact of degradation on displacements of MDOF systems because the degradation strongly affected the higher-mode responses, especially for short-period structures. Chenouda and Ayoub also demonstrated that while an equivalent first-mode SDOF system with degrading property might not collapse, a MDOF counterpart could collapse. These studies highlight the benefits and necessity of including the degradation of properties when study the collapse potential of the MDOF systems. Ruiz-García and Miranda [2009] conducted seismic demand analyses of residual drift on one-bay generic frame buildings of steel MRF and noted several issues when computing residual drift demand hazard curves. Using the lumped plasticity approach might result in larger residual drift when using a fiber-element modeling [Yazgan and Dazio, 2006]. Also, a degrading element model might lead to large uncertainty for residual drift demand when estimated by different software packages. In Ruiz-García and Miranda's research, the results concluded that besides the lateral-load resisting structural system, the fundamental period of structural also had great influence on residual drift demand.

In this study, OpenSees analysis framework [McKenna, 1997] is used as an analytical tool based on its computational efficiency and accuracy. Fatigue properties were adopted from Uriz and Mahin [2008]. The realism of local failure modes were assessed by comparing with test

results and predictions using LS-DYNA [LSTC, 2007] numerical models [Huang, 2010].

2.2 Literatures on the Evaluation of Design Parameters

Some recent studies have evaluated the effect of design parameters of the performance of building structures. A few of them use nonlinear dynamic analyses to investigate SCBF and BRBF buildings over a wide period range and designed according to current seismic codes (ASCE 7-05) for regions of high seismic hazard.

The ductility and overstrength factors of structural systems were investigated by Balendra and Huang [2003]. The model buildings were 3-, 6- and 10-story MRF and CBF buildings conforming to BS 5950 code [BSI 1990], which does not have any seismic provisions. Nonlinear pushover analyses and the N2 method [Fajfar, 2000] were conducted to evaluate the performance of these structures. Balendra and Huang concluded that the steel frames currently being designed according to the BS5950 code were able to resist the base shear caused by the ''design earthquake'' for Singapore. The data in Table 2.3 also show that the overstrength of braced frame buildings is about 70% of that of MRF for various numbers of stories. The ductility capacity of the investigated CBF systems is about 1.5 for various numbers of stories. In general, the smaller overstrength of CBF systems results in smaller effective R factors (the ratio of computed capacity/elastic demand) in CBF systems compared to MRF systems. The trend also shows the R factors were smaller as the number of stories increased. Chapter 6 presents a similar discussion related to SCBF and BRBF systems designed for seismic design category D of current U.S. codes.

Table 2.3 Overstrength, Ductility, Response Modification, Effective R, for Steel Frames under Most Common Vertical Load Combinations [after Balendra and Huang, 2003]

Type of steel frame	Number of stories	Overstrength	Ductility	R
MRF	3	8	1.95	15.6
	6	4.66	1.94	9.04
	10	3.77	1.67	6.30
CBF	3	5.57	1.53	8.52
	6	3.33	1.57	5.23
	10	2.48	1.51	3.74

Similarly, the overstrength, ductility and response modification factors of SCBF and OCBF were evaluated by Kim and Choi [2004]. A variety of model buildings was investigated including 3-, 6-, 9-, 12-, 15-, 18- and 21-story SCBF systems and 3-, 6- and 9-story OCBF systems. The model buildings were designed in accordance with IBC2000 [ICC, 2000] and AISC Seismic Provisions [2002]. Static nonlinear pushover analyses were conducted to evaluate the design parameters for all the model buildings, and an IDA was performed on the 6-story SCBF model structure. Six ground motion records that adequately matched with the design spectrum were selected from SAC project ground motion library to perform the IDA. In general, the IDA results showed smaller overstrength factors, but greater ductility demand. The response modification factors obtained from the IDA and static pushover approaches were similar. The pushover analysis revealed that the overstrength factors were greater in lower-rise SCBF, and for the cases studied, the overstrength factors were greater than the code (Ω_0) value of 2.0. The results

also showed that the lower-rise SCBF tended to have greater effective response modification factors. It was suggested that further research was required to define the effective response modification factors at various performance levels accounting for seismic hazard levels, number of stories, target ductility ratios, etc.

The performance of low-ductility chevron braced frame buildings in moderate seismic regions was assessed by Hines and Grynuik [2006]. The model buildings included the design of 3-, 6-, 9- and 12-story buildings in the Boston Area with R =3. Frame analyses were conducted using fourteen ground motion records that matched closely the IBC2003 [ICC, 2003] MCE-level earthquake spectrum for Site Class B and scaled to simulate Site Class D conditions. The results showed that the 9- and 12-story model buildings were more vulnerable to collapse than the 3- and 6-story counterparts. Higher mode effects were believed to contribute to the collapse potential in the upper stories. Similarly, Hines and Appel [2007] investigated a 9-story chevron braced frame with R=3 but brace connection fracture capacity corresponding to systems with R ranging from 2 to 7, according to ASCE 7-02. In the case study, the braced frame with brace connection fracture capacity of R=3 experienced more collapse instances than other values of R factor. Increasing the strength of the brace connections was not a guarantee of reduction in the potential for collapse, because the drift and damage tended to concentrate in a few stories while other stories still provided substantial strength and stiffness. The drift and damage concentration was one of the primary factors to influencing the collapse performance.

Asgarian and Shokrgozar [2009] conducted research on ductility, overstrength and response modification factors of BRB frame buildings. To investigate these design parameters, Opensees two-dimensional models were subjected to nonlinear static pushover, nonlinear IDA, and linear dynamic analyses. The material characteristics were modeled as being bilinear without degrading properties. The model buildings were designed conforming to the Iranian Earthquake Resistant Design Code [BHRC, 2005] and Iranian National Building Codes for Structural Steel Design. Structural configurations included two braced bays having double story X, chevron, and V bracings for 4-, 6-, 8-, 10-, 12- and 14-story buildings. The results showed that the overstrength factors ranged between 1.5 and 2.0, and the resulting effective response modification factors for ultimate limit state design method were between 4.5 and 16. The effective R-factors decreased as the number of stories increased.

Evaluating the design parameters of both conventional braced frames (CBF) and BRBFs in Iran, Mahmoudi and Zaree [2010] performed static nonlinear analyses on single and double bracing bays, 3-, 5-, 7-, 10- and 12-story model buildings. Different configurations, such as chevron, V and X bracings, were included. The CBFs were designed according to the Iranian Earthquake Resistant Design Code where R = 6 for CBF. For BRBFs, an R of 8 was used. All the beam connections in the CBFs and BRBFs were assumed to be pinned and the braces were designed to take 100% of the lateral loads. The effective R factors of both CBF and BRBF decreased (results corroborated in other research [Asgarian and Shokrgozar, 2009]) with increasing structural height. Also, the effective R factors increased as the number of bracing bays increased. In conclusion, because variations of R factors existed among different structural configurations, the number of bracing bays, and building height, and as the constant R factors in design codes did not reflect these variations, it was suggested that the R factors for both CBF and BRBF buildings in codes be modified.

In recognition of lack of rationale to determine R-factors in current seismic design codes, Lee and Foutch [2006] investigated the issue by designing 3-, 9- and 20-story steel MRF with differ-

ent R-factors (8, 9, 10, 11, and 12). Static nonlinear pushover analyses with displacement controlled loading were conducted to evaluate the strength capacity and post-yielding performance; IDA was also performed to analyze the seismic drift capacity. In addition, nonlinear dynamic analyses were carried out to investigate the seismic demands using 20 SAC ground motion records representing 2% probability of exceedance in 50 years. The results showed that the 20-story steel MRF model buildings tended to concentrate drift in the lower stories. For the 3- and 9-story model buildings designed for an R of 12, the buildings provided 95% confidence of avoiding global collapse and better than 50% confidence for avoiding local connection failure, (determined according to FEMA 350). In conclusion, current seismic design that adopt R-factors and minimum bound on design base shear (C_s factor) provides adequate protection against dynamic instability for high-rise buildings where P-Δ effects have greater impact on dynamic responses of structures.

2.3 Summary

Based on the results from prior research efforts, SCBF and BRBF buildings covering a range of building heights should be designed as per ASCE 7-5 and AISC 2005 and evaluated numerically. Nonlinear static pushover analysis, nonlinear dynamic analysis, and incremental dynamic analysis should be conducted to investigate the system's performance. Results suggest numerical models should incorporate strength degrading and stiffness softening properties as well as element fracture behavior. In addition to PBEE studies for different hazard levels, FEMA P695 [2009] provides a good basis for such evaluations of design parameters (R-factor, overstrength factor, and C_d-factor) related to collapse potential.

Chapter 3

Preliminary Numerical Simulation

PBEE depends on numerical simulation of structural response to future seismic events. As such, analytical models should realistically represent structural behavior and numerical procedures should be efficient enough to permit a large number of events to be simulated. In braced frames, brace characteristics dominate seismic behavior. As the braces yield in tension and/or buckle in compression, the braces provide lateral load resistance and energy dissipation. The complex nonlinear behavior of the braces results in the complex response of the structural system. It is thus essential to model the braces as accurate as possible. This chapter constructs numerical models of braces and braced frames and tests their accuracy by the model with the test data. The numerical models developed here are also compared with high fidelity (but computational expensive) finite-element numerical models. A preliminary PBEE study of a 3-story SCBF is performed to assess capabilities of different analytical models, and to understand better the effects of these models on demand parameters. The results are presented in terms of the EDPs to identify the system performance.

3.1 Simulation tool

OpenSees is employed herein as the primary simulation tool. The brace models used for the numerical simulations were based on the pervious work by Uriz and Mahin [2008] with some simplifications considering the large number of analysis to be performed. The OpenSees framework is depicted in Figure 3.1. An object-oriented software framework used mostly for structural and geotechnical engineering simulations, most of its modules are developed on an open-source basis and implemented in C++. The Tcl command language [Ousterhout, 1994; Welch, 2003] is used to define and execute the analysis. Users construct their models from the module ModelBuilder and the program adds the related objects to the Domain. In Domain, the program holds the state of the model at each time step. In the meantime, users can use a Recorder to record these states to monitor response. The Analysis module analyzes the responses of the model as it moves from the current state to the next state.

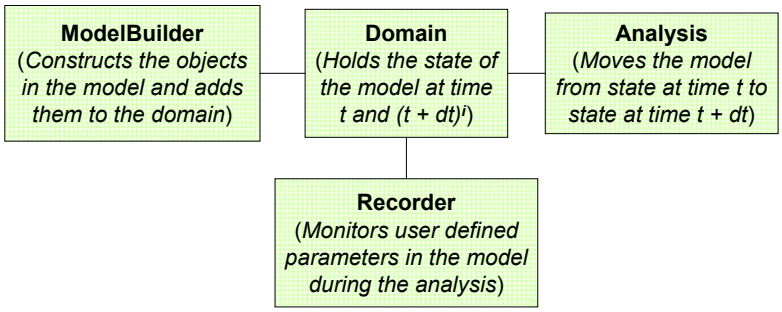

Figure 3.1 Framework of OpenSees

Figure 3.2 illustrates the beam-column element for modeling the structural members. In this study, a model consisted of beam, column and brace members. Each element was modeled by either displacement-based beam-column element or force-based beam-column element [Neuenhofer and Filippou, 1997]. For each element, the number of integration points selected was based on a previous parametric study [Uriz and Mahin, 2008]. Cross sections at each integration points were represented by an assembly of uniaxial fibers. For each fiber, the uniaxial stress-strain relationship was used considering material properties that account for failure due to low-cycle fatigue [Uriz and Mahin, 2008]. The material was modeled by Menegotto-Pinto model with isotropic strain hardening. The co-rotational geometric transformation was adopted here to account for local and global geometric nonlinearities. As such, the effects of lateral buckling of braces were explicitly taken into account.

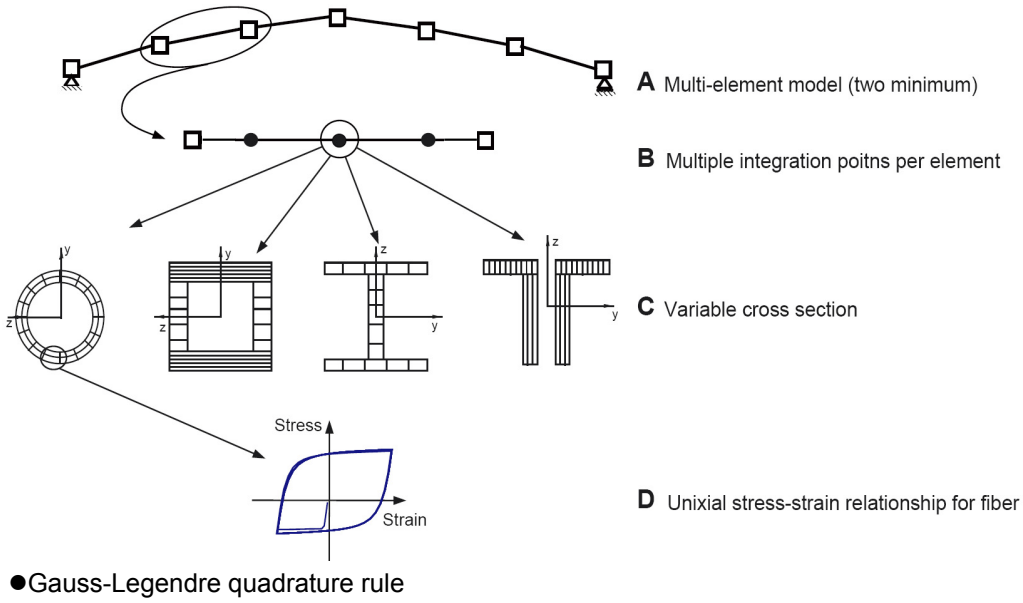

Figure 3.2 Illustration of the beam-column element for modeling the braces (After Uriz and Mahin, 2008)

The numerical model shown in Figure 3.3 demonstrates the geometric parameters of the brace member model. An initial camber is imposed along the middle of the brace to induce buckling. To better capture the behavior of the brace, the brace models have denser element distribution in the middle, where the inelastic behavior is more likely to occur if the brace buckles. Summarized in Table 3.1, the previous study by Uriz and Mahin [2008] investigated the

sensitivity of cyclic response to the initial camber, the number of elements, the number of integration points per element, and number of fibers at each section. An initial camber between 0.05% and 0.1% of the brace length in the mid-span was chosen. The results for 4, 7, 10 and 30 elements were similar. A minimum of 3 integration points in each element was suggested. Ten to 15 layers of fibers across the depth of the cross section were determined to accurately estimate the inelastic strains at the critical sections in braces.

Table 3.1 Suggested modeling parameters of braces in OpenSees [Uriz and Mahin, 2008]

Parameter	Initial camber	Number of elements	Number of integration points	Number of fibers
Suggestion	0.05% to 0.1% of brace length	4, 7, 10, 30	Minimum of 3	10 to 15 layers

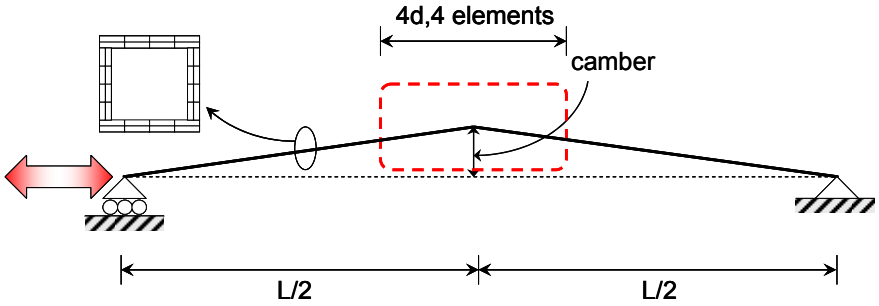

Figure 3.3 Illustration of brace model

3.2 Modeling Fatigue Behavior under Cyclic Loading

Low-cycle fatigue is explicitly simulated using an approach suggested by Uriz and Mahin and implemented in OpenSees models. As noted previously, fracture of braces due to low-cycle fatigue has such profound impact on the global and local behavior of an SCBF system. The mechanics of fatigue is discussed as follows.

Basquin [1910] observed that the stress amplitude and number of cycles to failure are linearly related when plotted on a log-log graph. The relation can be expressed as equation 3.1.

$$\frac{\Delta\sigma}{2} = \sigma_f^{'}(2N_f)^b \tag{3.1}$$

where

$\frac{\Delta\sigma}{2}$ = the constant stress amplitude applied to the material. $\Delta\sigma$ is the stress range.

$\sigma_f^{'}$ = fatigue strength coefficient.

N_f = fatigue life, or number of cycles the material can sustain before the failure occurs. $2N_f$ in the equation means the number of reversals to failure (1 reversal = 1/2 cycle)

b = fatigue strength exponent (Basquin's exponent), which usually varies between -0.05 and -0.12.

In the 1950's, Coffin[1954] and Manson[1953] proposed that the plastic strain amplitude and fatigue life also had a linear log-log relationship. The relation is expressed in equation (3.2):

$$\frac{\Delta\varepsilon_p}{2} = \varepsilon_0 (2N_f)^m \tag{3.2}$$

where

$\frac{\Delta\varepsilon_p}{2}$ = the constant plastic strain amplitude applied to the material. $\Delta\varepsilon_p$ is the plastic strain range.

ε_0 = fatigue ductility coefficient.

N_f = fatigue life, or number of cycles the material can sustain before the failure occurs.

m = fatigue ductility exponent, which usually varies between -0.5 and -0.7.

From the relation of stress amplitude and elastic strain amplitude, and from equation (3.1), the relationship between elastic strain amplitude and fatigue life can be written as equation (3.3).

$$\frac{\Delta\varepsilon_e}{2} = \frac{\Delta\sigma}{2E} = \frac{\sigma_f^{'}(2N_f)^b}{E} \tag{3.3}$$

where the total stain $\Delta\varepsilon$ is the summation of elastic strain and plastic stain. In terms of strain amplitude, the relation is shown in equation (3.4).

$$\frac{\Delta\varepsilon}{2} = \frac{\Delta\varepsilon_e}{2} + \frac{\Delta\varepsilon_p}{2} \tag{3.4}$$

If we substitute equation (3.2) and equation (3.3) into equation (3.4), then the strain-life relation can be written as equation (3.5).

$$\frac{\Delta\varepsilon}{2} = \frac{\sigma_f^{'}}{E}(2N_f)^b + \varepsilon_0 (2N_f)^m \tag{3.5}$$

Figure 3.4 is the graphic expression of equation (3.5). The low-cycle fatigue behavior is the primary failure mode in the braces. In the low-cycle fatigue range, the total strain amplitude is relatively large, and the plastic strain amplitude reflects most of the total strain amplitude. As such, equation (3.5) can be approximated as equation (3.6).

$$\frac{\Delta\varepsilon}{2} \approx \frac{\Delta\varepsilon_p}{2} = \varepsilon_0 (2N_f)^m \tag{3.6}$$

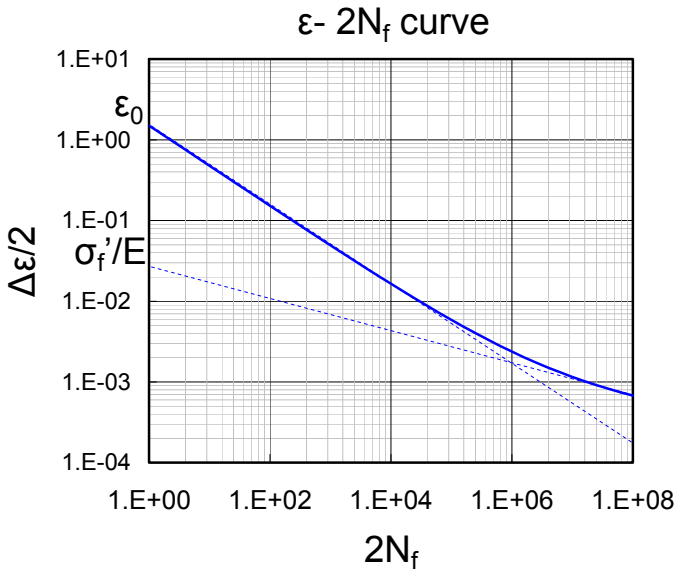

Figure 3.4 The relationship between strain amplitude and fatigue life

3.2.1 Rainflow Cycle Counting

The strain-life of a material is counted in terms of the number of cycles it can sustain under constant strain amplitude. Although this is an efficient way to define the fatigue life of a material in the laboratory, the earthquake response will not emulate a constant strain range in structural members. To identify the fatigue life of a material under varying strain amplitude, the Rainflow cycle counting algorithm is employed, where the number of cycles having a particular strain range is counted through the whole seismic ground excitation. The Rainflow counting algorithm is illustrated in Figure 3.5. Water flows down a pagoda-like structure representing the strain history with a vertical time axis. Specific rules have been developed to quantify the amplitude and number of cycles [ASTM 2003].

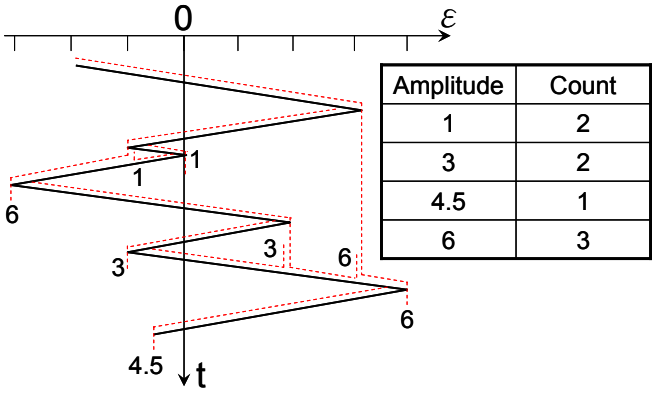

Amplitude	Count
1	2
3	2
4.5	1
6	3

Figure 3.5 Illustration of Rainflow cycle counting

Earlier research by Matsuishi and Endo [1968] using Rainflow cycle counting required a complete loading history. As such, failure of a member could not be simulated during an analysis run. Other studies [Anthes, 1997; Downing and Socie, 1982; Glinka and Kam, 1987; Hong, 1991; Uriz and Mahin, 2008] proposed the "one-pass" algorithm where the cycles are

counted before the entire loading history is acquired.

As cycle counting proceeds, fatigue life of a material is estimated by counting the cycles of various amplitudes during a complex loading history. One of the most popular approaches to identify the damage progress is the linear damage rule proposed by Palmgren [1924] and Miner [1945]. The damage index *DI* in equation (3.7) varies from 0 to 1. Zero means there is no damage and one means the fatigue life is exhausted.

$$DI = \Sigma \frac{n_i}{N_{fi}} \tag{3.7}$$

where n_i is the number of cycles applied at a stress level corresponding to failure in N_{fi} cycles. N_{fi} is calculated from equation (3.6) given the fatigue parameters ε_0 and m. Also, the history of $\Delta\varepsilon$ is calculated from Rainflow cycle counting algorithm and substituted into equation (3.6) to determine N_{fi} [Uriz and Mahin, 2008].

OpenSees incorporated the Rainflow cycle counting algorithm in the fatigue material module. When the damage index of a fiber exceeds unity, the fatigue life of that fiber is flagged as being exhausted and the fiber is removed from the cross section by reducing its strain and stress to zero.

3.2.2 Fatigue Material Parameters

The fatigue parameters, ε_0 and m, for the OpenSees model were obtained by calibrating the model with test data. To illustrate this, HSS6x6x3/8 brace with slenderness ratio KL/r = 51.9 was analyzed. Test results are from Yang and Mahin [2005]. Different combinations of ε_0, ranging from 0.03 to 0.3, and m ranging from -0.5 to -0.70, were analyzed, and the dissipated energy of the analytical result was compared with that of the test results. By observing the correlation of test and analysis results, the optimal combination of fatigue parameters relevant to this study were calculated to be ε_0=0.09 and m=-0.6, which are similar to those values obtained in the previous study [Uriz and Mahin, 2008]. The analytical results of the behavior of a brace were compared with the experimental results in Figure 3.6. The tension and compression strength of the brace hysteresis characteristics and the fracture points were generally captured by the analysis.

It is important to note that the fatigue model only considers unidirectional material properties, and the OpenSees beam-column model does not consider local buckling. As such, the fatigue life prediction requires careful calibration to test results representing the members being modeled.

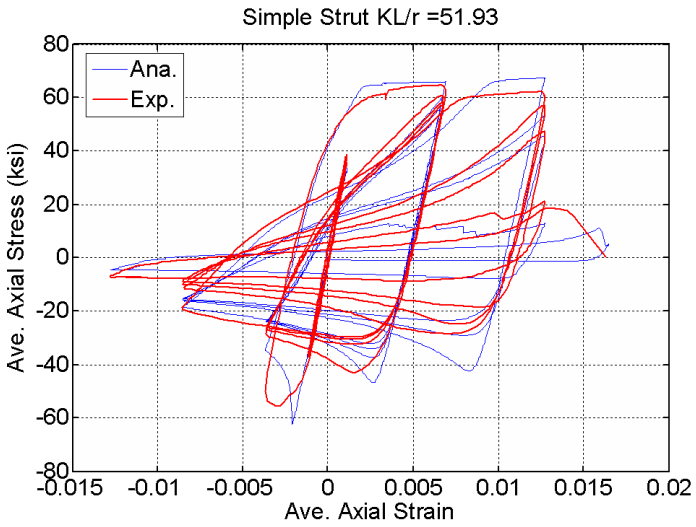

Figure 3.6 Comparison of analytical and experimental responses of HSS6x6x3/8 brace with KL/r =51.93.

3.3 Two-story Tested SCBF

As shown in Figure 3.7, the previous research [Uriz and Mahin, 2008] conducted a test on large-scale, two-story conventional chevron braced frame. The test results were simulated in a three-dimensional model; the analytical results by Uriz and Mahin [2008] captured the responses of the specimen satisfactorily. In order to reduce the computational effort, this model was simplified to a two-dimensional frame model with the modeling parameters discussed earlier and the brace members were modeled with ideal pin ended connections. In the two-dimensional model, the out-of-plane deformation was constrained. As such, only the in-plane failure modes were accounted for and the braces were arranged to buckle in the plane of the frame by aligning the orientation of the pin ends.

An illustration of the two-story model is shown in Figure 3.8. The story height is 20 ft in total with a 20-ft span. Lateral force was applied at only the upper level to achieve a desired cyclic displacement history. Because the lateral force was applied only on the upper level, the story shears of both upper and lower levels were the same. Because the braces comprise the majority of the story shear, the design and size of braces in both stories were identical. The member sizes are also shown in Figure 3.8. The column size is W10x45; the beam size is W24x117; the brace size is HSS 6x6x3/8. No axial load was applied to the column during the test. The beams were designed to take the unbalanced force induced by the buckling of the braces and the drag force transferred by column and braces from the actuator.

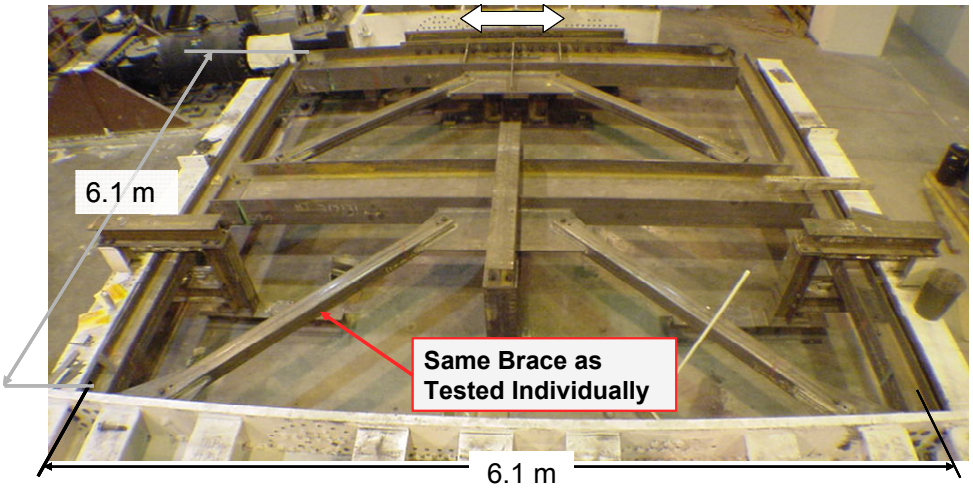

Figure 3.7 Test specimen of two story chevron braced frame [Uriz and Mahin, 2008]

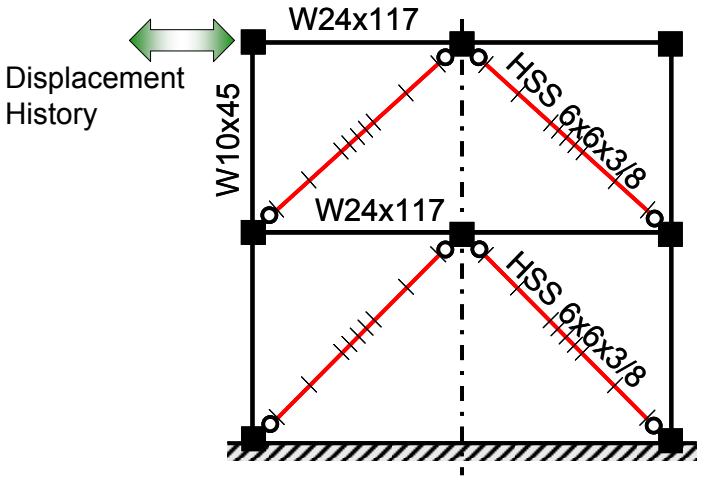

Figure 3.8 Numerical model of two story chevron braced frame

Several studies [Scott et al., 2004; Neuenhofer and Filippou, 1997] have demonstrated the advantages of a force-based beam-column element over a displacement-based beam-column element. As such, the force-based nonlinear beam-column element was chosen. Beams were represented by 2 of force-based beam-columns. Columns were modeled by 1 of force-based beam-columns; they were continuous and assumed fixed at their base. The hysteretic characteristics of the braces were modeled using an approach developed by Uriz and Mahin [2008]. Each brace was subdivided into 10 force-based beam-column elements, with fibers used to model the shape and hysteretic characteristics of the brace at the integration points along each element.

The beam-to-column connections were fully constrained in the numerical model. At connections with gusset plates, the behavior was considered to be very nearly fixed, even if such connections were not detailed as being fully restrained. Although finite element analyses [Huang and Mahin, 2010] and tests [Uriz and Mahin, 2008] suggest that shear-tab-only connections may rupture in the presence of large lateral story drifts or the effects of unbalanced forces applied to a beam when a brace connected to its mid-span ruptures, this mode of failure is diffi-

cult to model without more test data; therefore, all beam-to-column connections in the braced bay are assumed to be fully restrained in the OpenSees fiber-based models.

For the sake of simplicity, and consistent with recommendations by Uriz and Mahin [2008], the beam-column connections and the region between the fold line in the gusset plate and the center of the beam-column connections were idealized as being rigid due to the high stiffness and strength of these regions compared to adjacent members.

For the fatigue sensitive models, the strain history in each fiber in the braces, beams, and columns was tracked, and a Rainflow cycle counting algorithm was used to determine the amplitude of each inelastic cycle. A Manson-Coffin relation, calibrated to multiple tests of HSS6x6x3/8 braces and other sections, was used to characterize low-cycle fatigue damage to each fiber during a particular cycle of response. Miner's rule was used to cumulate cyclic damage throughout the response. If a fiber's fatigue life was exceeded during the analysis, that fiber was removed from the numerical model. This approach has been successfully used to model yielding, buckling, and low-cycle fatigue rupture of braces and braced frames [Uriz and Mahin, 2008].

The actual material strength (shown in Table 3.2) was used to model the frame members. The measured yielding stresses for all the structural components were greater than the nominal values. For the braces, the yielding stress for modeling was 32% higher than the nominal stress.

Table 3.2 Material properties of two-story chevron braced frame test

Member	Average F_y (ksi)	Average F_u (Ksi)	% elongation
Column (W10x45)	55.8 (Gr. 50)	73.7	23.9
Beam (W24x117)	58 (Gr. 50)	74.5	26
Brace (HSS 6x6x3/8)	60.6	65.9	36

The analytical and experimental results are compared in Figure 3.9 and Figure 3.10. Figure 3.9 presents the hysteretic loops of the braces in the lower level. The strength degrading and the fracture of the braces were estimated to a satisfactory degree. Figure 3.10 depicts the roof displacement-base shear relation and shows that the computed initial elastic stiffness of the braced frame is almost identical to the experimental stiffness. Also, the analytical maximum strength of the braced frame approximates the experimental results. The pinching behavior of the braced frame due to the buckling of the braces was well captured. Note that the fracture of the braces leading to a sudden observed drop of strength was also reasonably accurate. At the end of the test, the remaining strength of the braced frame was primarily from the contribution of the moment resisting frame and that strength was well captured.

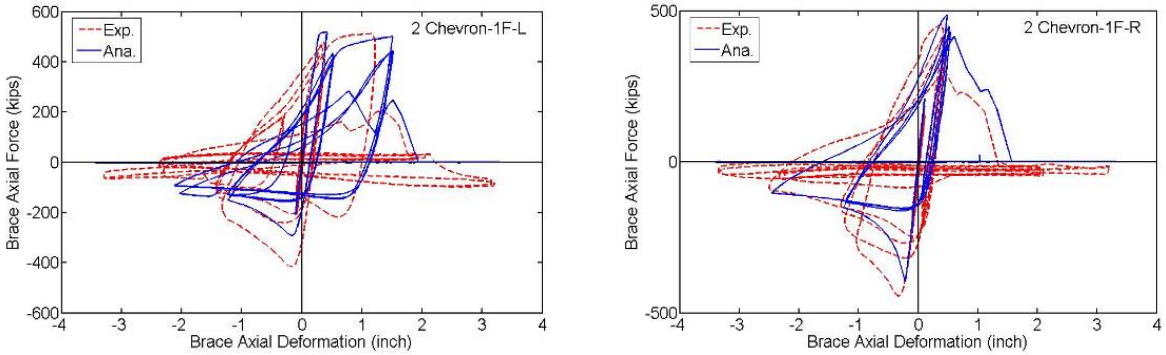

Figure 3.9 Comparison of analytical and experimental responses of braces in the first story

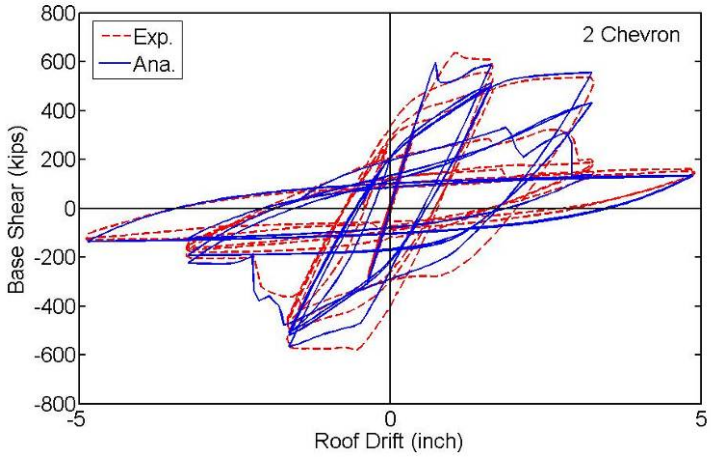

Figure 3.10 Comparison of analytical and experimental response of two-story chevron braced frame

3.4 Preliminary Studies of a Three-story Model Building

The performance of a typical three-story steel braced building was assessed. The previous modeling approach was used and the sensitivity of performance to material and global modeling assumption was examined. No test results were available for this model. As shown in Figure 3.11, the model building has regularly spaced gravity-resisting frames (continuous columns with ideal pin connections to the beams and foundation); the lateral earthquake-load resistance is provided by special concentric braced frames (SCBF) located on the perimeter of the building. Designed to conform to the provisions of ASCE/SEI 7-05 [DASSE, 2007], this building was located in downtown Los Angeles, California, for use as a commercial office building. Table 3.3 lists some of the principal attributes of the structure and the key parameters used in the seismic design.

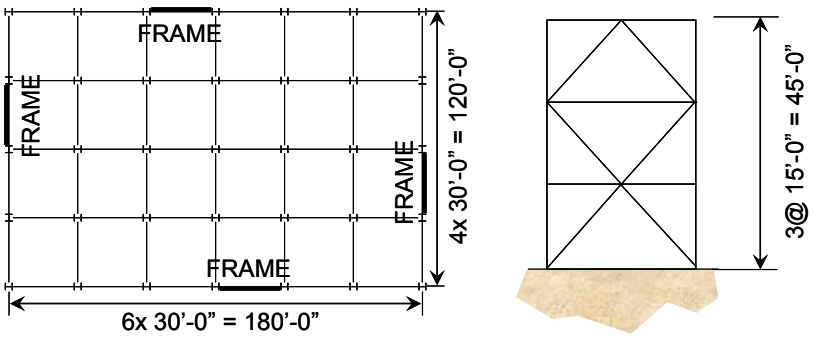

Figure 3.11 Model building floor plan and elevation

Table 3.3 Design parameters of model buildings

Code	ASCE/SEI 7-05
Building Location	Los Angeles, CA
Seismic Design Category	D
Occupancy Category	II (Office)
Importance Factor	1.0
Short Period Spectral Acceleration, S_s	2.2g
1 sec. Period Spectral Acceleration, S_1	0.74g
F_a	1.0
F_v	1.5
R	6
Design Base Shear	0.24W
Code Approximated Period (T_a)	0.35 sec.

Table 3.4 lists the member sizes used in the model. The same size column is used over the whole height of the building. Note that the roof beam is heavy compared to the lower two floor beams, because the configuration of the braces adopted results in small unbalance force in the lower two levels. Where braces intersect along the length of the beam in chevron braced frames, the beam was typically designed for the vertical component of the maximum unbalanced load produced by the tension and compression braces, in addition to axial and other forces associated with the applied earthquake forces. For design, the tension brace was assumed to carry R_yP_y while the compression brace was assumed to carry the post-buckling load of only $0.3\varphi_c P_n$.

Table 3.4 Member sizes

Floor/Story	Braced Frame Columns	Braced Frame Beams	Brace Size
Roof/3	W14x176	W36x210	HSS 10.0x0.375
3rd/2	W14x176	W30x116	HSS 11.25x0.50
2nd/1	W14x176	W27x84	HSS 12.5x0.50

3.4.1 Design Spectra

The design response spectrum (ASCE 7-05) used in the archetype structure's design is shown

in Figure 3.12. A vertical line was included on the plot to represent the archetype structure's computed elastic fundamental period (0.5 sec.) in numerical models.

The structure was analyzed considering sixty ground motion records taken from the SAC ground motion ensembles developed consistent with 1997 NEHRP seismic hazard curves for Los Angeles [Somerville, 1997]. The sixty records represent three different hazard levels: the service-level earthquakes (50% probability of exceedance in 50 years, 50/50), the design-level earthquakes (10% probability of exceedance in 50 years, 10/50) and the MCE-level earthquakes (2% probability of exceedance in 50 years, 2/50). Median pseudo-acceleration and displacement spectra for the 20 ground motion records corresponding to each hazard level are shown in Figure 3.12. Note that for the period of this archetype building, the median spectral values for the twenty records corresponding to the design-level event are less than the corresponding ASCE/SEI 7-05 code spectra. Thus, the records used in this study are smaller on average than those that correspond to the seismic hazard at the site.

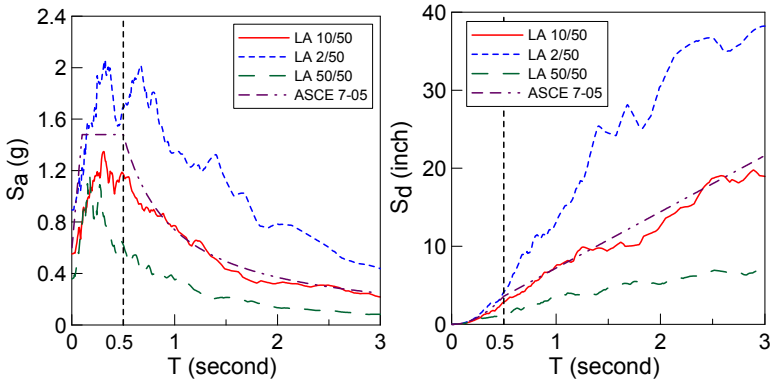

Figure 3.12 Response spectra

Rather than using the median values of results for records corresponding to that hazard level, in this case the spectral displacement corresponding the basic site hazard curve and structural fundamental period were used in conjunction with a regression analysis of the responses for the parameters of interest to interpret the response at a particular hazard level. The median elastic spectral displacements corresponding to the computed fundamental period of the SCBF structure are shown in Table 3.5 for the three hazard levels.

Table 3.5 Median of $S_{d,Elastic}$ (inch)

Fundamental Period	Hazard Level 50% in 50yrs	10% in 50yrs	2% in 50yrs
T =0.50 sec.	1.70	2.74	4.13

3.4.2 Numerical Models at Phase I

Several variations of numerical models were considered. Analyses were conducted in two phases. The parameters varied in Phase I for a single ground motion were:

1. First story height,
2. Mass considered in vertical direction,
3. Effect of rigid end zone in the mid-span of beams,
4. Beam-column connections type,

5. Effect of fatigue material, and
6. Comparison of force-based and displacement-based beam column elements.

These results were compared with one another and to a full finite element model implemented in LS-DYNA and used to refine the OpenSees model. The numerical models were further refined in Phase II by comparing their responses to a single ground motion as well as statistical responses to the ground motion set. The parameters varied were:

1. Axial load modeling in beams,
2. The viscous damping ratios, and
3. Fatigue material parameters.

For both phases, the basic assumptions for the models were the same.

Fiber-based models of the archetype structure were used for the OpenSees analyses and shell-based finite element models were used for the LS-DYNA [LSTC, 2007]. Although two separate software packages were used, the modeling was conducted to be as identical as possible. In both cases, only one braced bay was considered, subjected to vertical gravity dead loads and in-plane horizontal seismic excitations applied at the base. Half of the tributary reactive mass of the building was assigned to a single frame; the torsional response of the structure about a vertical axis was not considered. The gravity-load-only framing was idealized as a leaning column; therefore, it provided no structural strength or stiffness, but it resulted in appropriate geometric nonlinearity effects. For the sake of clarity and simplicity, the vertical component of seismic excitation and the mechanical characteristics of the floor slabs were ignored.

3.4.2.1 OpenSees model

Figure 3.13 shows the illustration of the numerical models including the braced frame and the leaning column. The numerical models are based on the parameters previously discussed with improved details in the brace-to-frame connections. Additional parameters for dynamic analysis are discussed in this section.

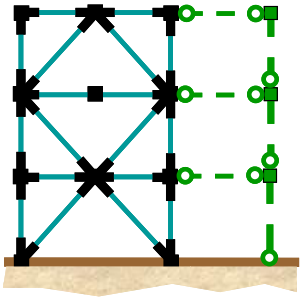

Figure 3.13 Sketch of basic OpenSees model

The vertical floor mass tributary to the braces intersecting a beam or column was included in the models. Earlier studies [Khatib et. al., 1988] showed that this vertical mass has a significant effect on dynamic response during brace buckling.

Because only mass proportional viscous damping could be modeled with the current implicit solver version of LS-DYNA, an OpenSees model with mass-proportional damping was used for some of the analyses for comparison. For mass proportional viscous damping, the damping co-

efficient was selected to produce viscous damping equal to 4% of critical at the computed first mode period (T) of the structure. Raleigh damping, based on the mass and tangent stiffness proportional damping, was used in most of the OpenSees analyses, with the damping coefficients selected to give viscous damping of 4% of critical at the first and third mode periods.

P-Δ effects were represented using either one or two leaning columns. Each leaning column was constrained to have the same lateral displacement as the most adjacent column at the same level in the braced bay. The axial and flexural stiffness of the columns were assumed to be large, but a pin was introduced at the bottom of the column in each story. Thus, bending of the gravity-load only columns did not contribute to the lateral stiffness or strength of the structure. Applied axial loads on the leaning column were taken as half or one quarter of the total dead load of each floor (less the dead load directly tributary to the braced bay) depending on whether one or two leaning columns were included in the model. A co-rotational formulation was used to simulate P-Δ effects for these columns. A single leaning column was commonly used to represent gravity-only framing. Since axial deformability and axial load-moment interaction is considered in the OpenSees model for the beams, the axial forces introduced in the beams in the braced bay by the leaning columns can significantly alter behavior. Thus, cases with one or two leaning columns were considered. For the plan configuration shown in Figure 3.11, two leaning columns would be the most realistic case.

Instead of being modeled as ideal pins, the fold line in the gusset plate of the brace ends was modeled by one force-based beam-column element with fiber section. The dimension of this element was (L x W x t) = ($2t_g$ x b_g x t_g), where t_g is the thickness of the gusset plate and b_g is the width of the gusset at the central location of folding line. This provided adequate modeling constraint to the braces of the braced frames with fully-restrained brace-to-gusset connections.

While the OpenSees fiber-based elements accounted for many aspects of the behavior of braces (and beams and columns), they did not explicitly account for the effects of local buckling and fracture-mechanics-related phenomena. Three-dimensional related behavior modes (such as the torsion and twist of beams, columns, braces and gussets) were not simulated in the OpenSees model. No attempt was made in this study to model potential in-plane or out-of-plane buckling of columns (although comparison of peak column axial forces suggests that column lateral buckling was unlikely). Although of interest to the current study, it is unclear whether the low-cycle fatigue damage parameters used and derived on the basis of the behavior of small- and mid-sized square HSS braces are entirely appropriate for the size and shape of braces used in archetype structure.

3.4.2.2 LS-DYNA model

The finite element models [Huang, 2009] of the archetype structure were formulated in three dimensions using LS-DYNA. The analysis models explicitly simulate local buckling and evolution of damage due to low-cycle fatigue [Huang and Mahin, 2008b]. To be consistent with the OpenSees models, lateral-torsional response of beams and lateral buckling of columns were neglected.

Based on an assessment of computational effectiveness, shell elements were chosen instead of solid or beam elements. Mesh convergence was examined using progressively refined finite element meshes. A final choice of a shell element size corresponding to about the shell thickness achieved an overall model that is believed to be simple with reasonable accuracy. Unlike

the OpenSees model, the gusset plates and connection regions in the LS-DYNA model were fully represented using shell elements. Net reduced sections at the connections of the braces to gusset plates were adequately reinforced per AISC [2005] requirements so that premature rupture at those locations was avoided. A significant difference between the fiber and shell element models was that the beam-to-column connections away from gusset plates were modeled in LS-DYNA as welded shear tab connections, rather than as the moment connections (when modeled in OpenSees).

Crack initiation and propagation were modeled by element erosion (shell element removal) using a cyclic damaged plasticity material model developed by Huang and Mahin [2008b, 2009]. This mechanics-based approach simulates materials that follow a Manson-Coffin model and Miner's rule. Material property specifications similar to the OpenSees model were used. The plasticity and damage properties of steel material were calibrated against braces and validated with a SCBF subassembly experiment conducted in University of California at Berkeley [Yang and Mahin, 2005; Uriz and Mahin, 2008]. A comparison of experiment and numerical results is shown in Figure 3.14; note that buckling and fracture of brace is accurately modeled (Figures 3.14d and 3.8e). In addition, the simulated damage and fracture at the beam-column connections match the experiment (Figure 3.14c and 3.14f). These simulations show that the cyclic damaged plasticity model is reasonable and useful for damage evaluation in steel structures.

a) Test step b) Brace fracture c) Connection fracture

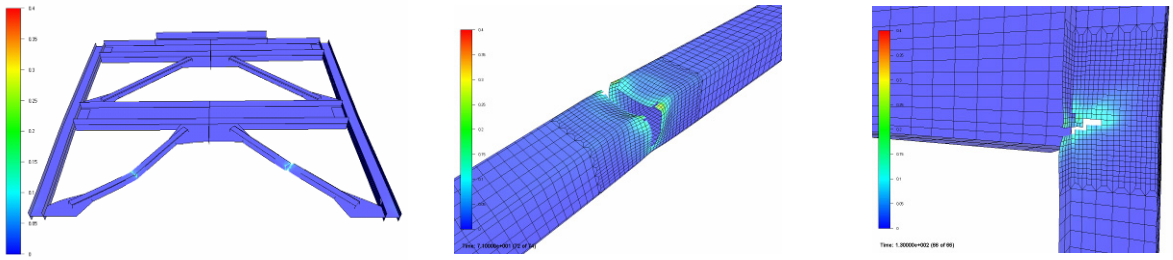

d) Damage of subassembly e) Brace fracture f) Connection fracture

Figure 3.14 Comparison of experiment and LS-DYNA simulation results

The SCBF columns were fixed at the base. Although the top and bottom flanges of all beams were laterally restrained to prevent lateral-torsional motion and out-of-plane buckling, the columns were unrestrained between floors so in- and out-of-plane column buckling could be detected.

The finite element for the three-story SCBF archetype is shown in Figure 3.15. All components except the leaning columns incorporated the damaged plasticity material model and were

modeled as shell elements. No rigid elements were incorporated in the model. Similar to the OpenSees model, the vertical floor mass tributary to the braces and the dual pin-connected leaning column were modeled on each floor level to account for P-Δ effects. The beams in the gravity-only system were disregarded.

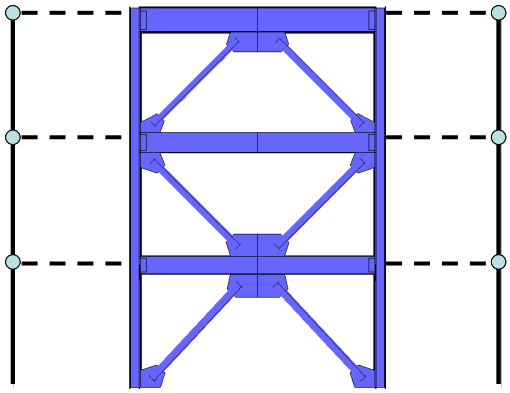

Figure 3.15 Sketch of basic LS-DYNA model

3.4.3 Phase I Analysis

A basic numerical model was developed to monitor the sensitivity of response to variations in model characteristics and ground motions. The displacement time histories of the structural response to SAC ground motion LA32 (simulated time history for a magnitude 7.1 earthquake on the Elysian Park fault) shows pulses in both positive and negative directions; this record was chosen in this section to compare with results from various models. Eleven OpenSees models were compared to determine the sensitivity to geometric configuration, boundary conditions and the analytical element types. The models were all three story, double-story X SCBFs designed following the building code of ASCE/SEI 7-05 (Model B). The detailed parameters of the models are listed in Table 3.6. Model name beginning with 3BF represents the three-story model with Fixed beam-column connections, with gusset plates modeled in the brace ends, and with non-lateral-resisting leaning columns. Model name beginning with 3BP is similar to 3BF except the beam-column connections are Pin ended. Model name with H and R means the story height of the first story is taller than the other stories because the work point in the column base is actually under the ground. However, in real practice, the first-story height is sometimes counted from the ground level. Both the H and R models were analyzed to account for the influence of the story height. The difference between H models and R models are as follows: the R models include the rigid-end-region in the mid-span of the beams while H models do not. Model name with V means the assigned effective vertical mass is more than the tributary mass and equals to the effective mass in the horizontal direction; models name without V means the assigned effective vertical mass equals to the tributary mass. Models with subscript "d" represent that the displacement-based nonlinear beam-column element was employed. Models without subscript "d" mean that the force-based nonlinear beam-column element was used to model the structural members.

The responses are shown in Figure 3.16 to Figure 3.27. The influence of changing parameters is discussed next.

Table 3.6 Model names and their properties in Phase I analysis

Model	Fix-ended beam	Pin-ended beam	taller first story	Same vertical mass as horizontal mass	Tributary vertical mass	Rigid end region in the mid-span of beam	No fatigue	Displace-ment-based element	Force-based element
$3BFHV_d$	X		X	X				X	
$3BFRV_d$	X		X	X		X		X	
$3BFV_d$	X			X				X	
$3BFH_d$	X		X		X			X	
$3BFR_d$	X		X		X	X		X	
$3BF_d$	X				X			X	
3BFHV	X		X	X					X
3BFRV	X		X	X		X			X
3BFR	X		X		X	X			X
$3BPR_d$		X	X		X	X		X	
3BFRN	X		X		X	X	X		X

3.4.3.1 Effect of first-story height

The effect of uniform story height can be seen by comparing models $3BFV_d$ and $3BF_d$ with the other models that have taller first stories. The taller first story tends to concentrate the story drift in only the first story, whereas the lateral deformation of the models with uniform story height tends to concentrate in both the first and second stories. The energy-dissipating mechanism is different for models with taller first story. Models $3BFV_d$ and $3BF_d$ dissipated energy due to the nonlinear behavior of the first- and second-story structural members, while the other models dissipated energy largely via first-story structural members. Models $3BFV_d$ and $3BF_d$ had smaller maximum story drift among all levels compared to all other models.

3.4.3.2 Effect of rigid end zone in the mid-span of beams where braces meet

By comparing model $3BFHV_d$ with $3BFRV_d$, $3BFH_d$ with $3BFR_d$, and 3BFHV with 3BFRV, the effect of rigid end region in the mid-span of beam was demonstrated. For models $3BFHV_d$ and $3BFRV_d$, brace fracture occurred at different times and therefore the permanent story drifts were different. For model $3BFH_d$, the permanent story drift was positive and different compared to the other models. The model with rigid end zone, $3BFR_d$ had negative permanent story drift and the response was smoother compared to model $3BFH_d$. For models 3BFHV and 3BFRV, the shape of the hysteretic loops was similar. Generally, the effect of the rigid-end region at the mid-span of beams where braces intersect was less significant compared to the effect of story height.

3.4.3.3 Effect of vertical mass

The effect of vertical mass on story drifts was investigated by comparing model $3BFHV_d$ with $3BFH_d$ and $3BFRV_d$ with $3BFR_d$. Larger vertical mass did not necessarily result in a larger story drifts under horizontal excitation. In model $3BFHV_d$, the larger vertical mass caused large permanent story drift on the first story, while in model $3BFRV_d$, the story drift on second story was less compared to model $3BFR_d$. Comparing $3BFRV_d$ with $3BFR_d$, the model with larger vertical mass had jagged response, which was due to the dynamic effect of the vertical mass.

3.4.3.4 Effect of analytical element types

The different responses of displacement- and force-based elements can be seen by comparing $3BFHV_d$ with 3BFHV and $3BFRV_d$ with 3BFRV. The results of $3BFRV_d$, 3BFHV and 3BFRV were similar, but in general, the force-based models had smoother responses.

The force-based model was improved by using smaller time steps. The time step changes during the dynamic analysis until convergence occurs. For example, model 3BFR used a time step as small as 10^{-6}.

The story drift of 3BFR was similar to the results obtained using LS-DYNA which employed shell elements to capture detailed responses. The major difference between 3BFR and LS-DYNA results was that the braces fracture in 3BFR resulted in a sudden drop of strength which was similar to what occurred in earlier experimental results. In LS-DYNA, strength still degraded, but because the braces did not completely fracture, there was no sudden drop of strength.

Based on the preceding results, a force-based beam-column element accurately estimates the nonlinear responses of the three-story, double-story X braced frame. In addition, the use of a smaller time step is recommended not only to increase the accuracy but also improve the convergence. As to the vertical mass, the results demonstrate that it is not as significant a factor on the response compared to the other parameters, such as the story height and the element type.

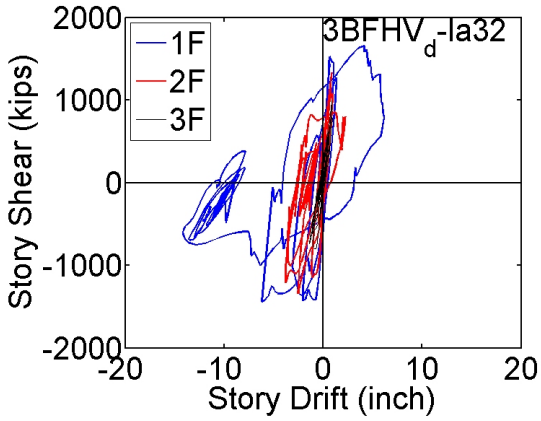

Figure 3.16 Taller first-story height with same vertical mass as horizontal mass (disp.-based element)

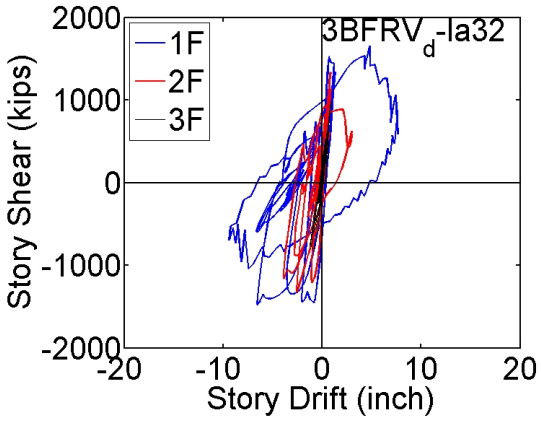

Figure 3.17 Taller first-story height with same vertical mass as horizontal mass and rigid end region in the mid-span of beam (disp.-based element)

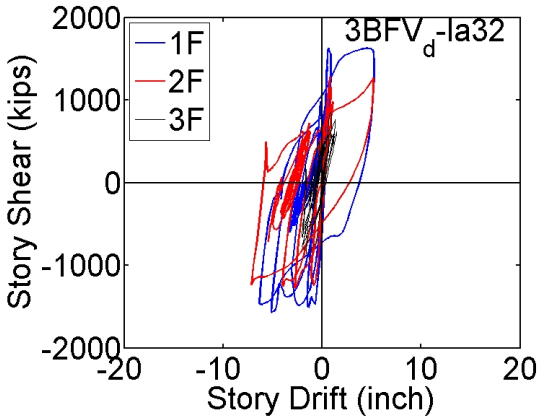

Figure 3.18 Uniform story height with same vertical mass as horizontal mass (disp.-based element)

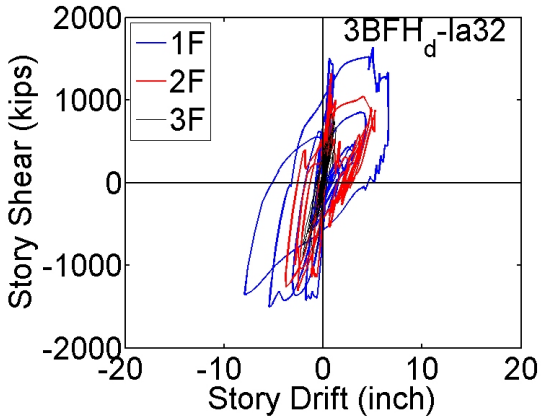

Figure 3.19 Taller first-story height with less vertical mass than horizontal mass (disp.-based element)

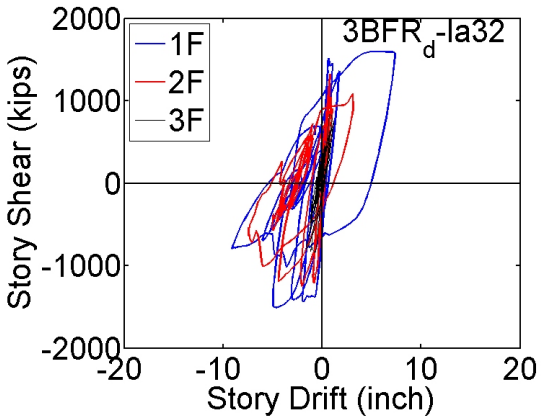

Figure 3.20 Taller first-story height with less vertical mass than horizontal mass and rigid end region in the mid-span of beam (disp.-based element)

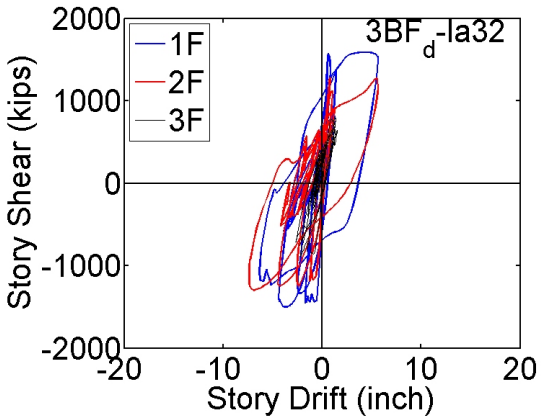

Figure 3.21 Uniform story height with less vertical mass than horizontal mass (disp.-based element)

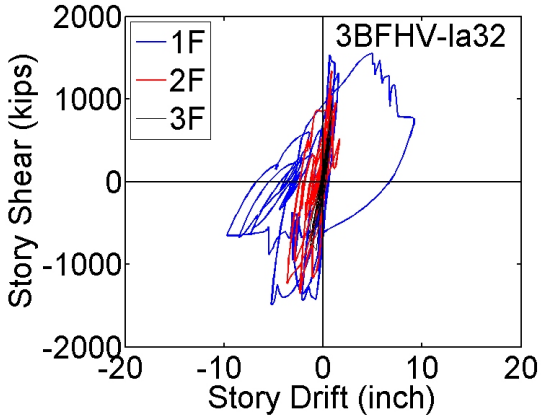

Figure 3.22 Taller first-story height with same vertical mass as horizontal mass (force-based element)

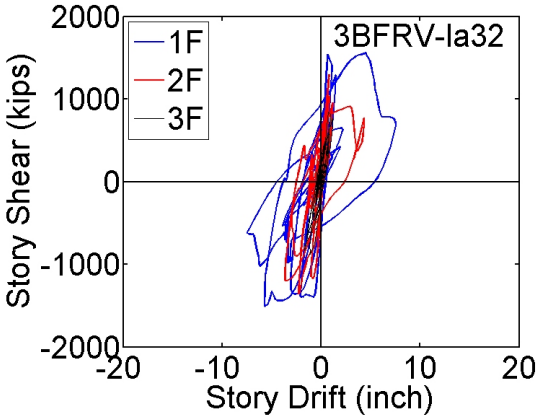

Figure 3.23 Taller first-story height with same vertical mass as horizontal mass and rigid end region in the mid-span of beam (force-based element)

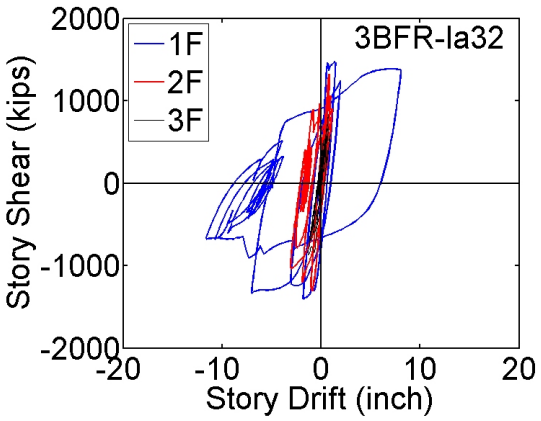

Figure 3.24 Taller first-story height with less vertical mass than horizontal mass and rigid end region in the mid-span of beam (force-based element)

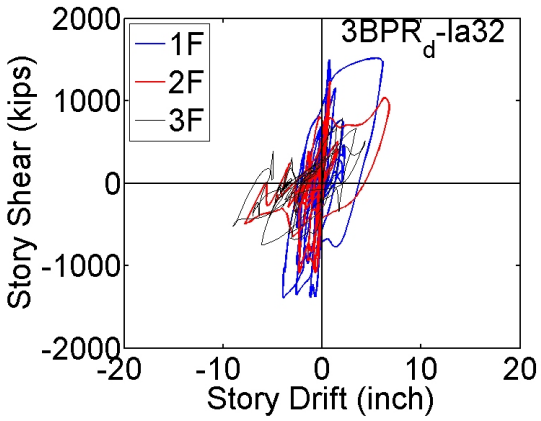

Figure 3.25 Taller first-story height with less vertical mass than horizontal mass, rigid end region in the mid-span of beam and pin-ended beams (disp.-based element)

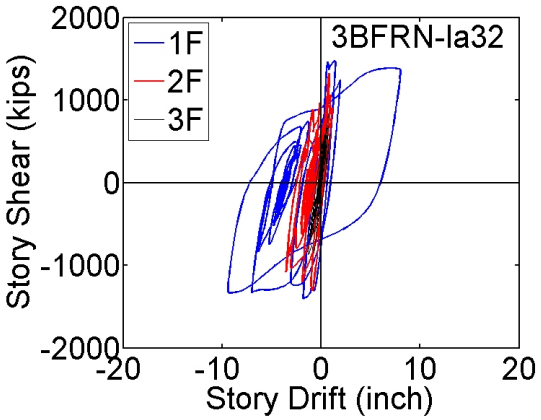

Figure 3.26 Taller first-story height with less vertical mass than horizontal mass, rigid end region in the mid-span of beam and non-fatigue materials (force-based element)

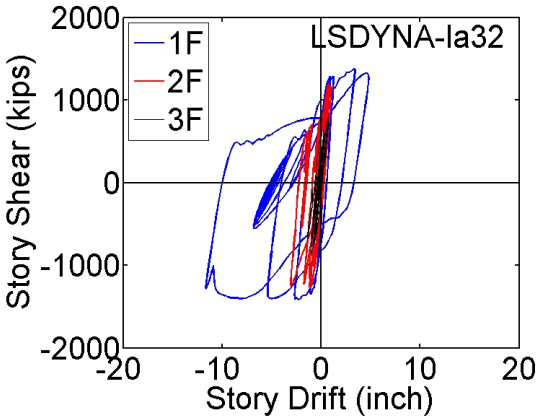

Figure 3.27 LS-DYNA

3.4.4 Phase II Analysis

Results were presented in this section for the five two-dimensional (planar) models. These models allowed for comparison of the effects of (1) mass proportional viscous damping versus combined mass and tangent stiffness proportional viscous damping; (2) the number of leaning columns used to represent geometric nonlinearities; and (3) whether rupture due to low-cycle fatigue is considered or not.

These models were designated 3BF1L, 3BF2L, 3BF2LN, 3BF2LM, and 3BF2LMN, according to the naming convention shown in Table 3.7. For example, model 3BF2LMN was a three-story, double story X SCBF designed to comply with ASCE/SEI 7-05, with fully constrained beam-column connections, with two leaning columns (one on each side of the frame),

and mass-proportional damping; fatigue was disregarded in the modeling of all structural components. The responses to pushover analyses (nonlinear static analyses) and to nonlinear dynamic analyses under a single ground motion and large ensembles of ground motions were investigated. Results obtained with LS-DYNA were used to further study difference between fiber-based and finite element-based models

Table 3.7 OpenSees model names

Abbreviation	Denotation
B	Double story X SCBF designed to comply with ASCE/SEI 7-05
F	Model building with fully constrained beam-column connections
1L or 2L	1 leaning column or 2 leaning columns
M	Mass-proportional damping (Rayleigh damping without this notation)
N	Non-fatigue material (fatigue material without this notation)

3.4.4.1 Pushover Analysis of Phase II Models

Nonlinear pushover analyses were carried out on the models. Lateral forces were distributed over height according to the models elastic first mode shape. The resulting relations between roof lateral displacement and base shear are shown in Figure 3.28. The initial loading stiffnesses of the OpenSees model and LS-DYNA models were similar. At a roof drift index (roof lateral displacement divided by the roof elevation) about 0.3%, one of the braces at the ground story buckled globally in the OpenSees model, resulting in a sudden loss of frame strength and an overall negative tangent lateral stiffness. In the LS-DYNA model, stiffness decreased gradually before reaching the brace's buckling load, and the peak system strength was slightly smaller compared to the OpenSees prediction. This gradual decrease in initial stiffness was associated with several possible factors: e.g., frame action resulting in greater initial stress and sway in the braces, local stress concentrations resulting in earlier local yielding throughout the frame, and initiation of minor local buckling prior to global brace buckling.

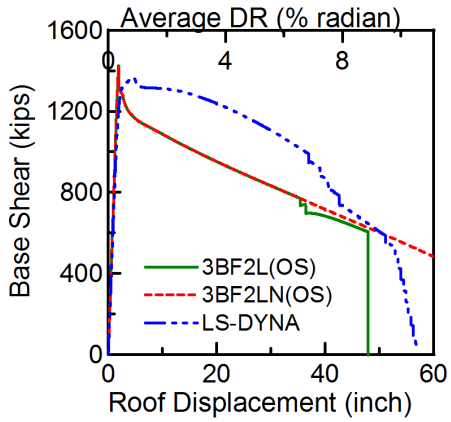

Figure 3.28 Base shear as a function of roof displacement for three models

After the brace-buckling load was reached, the base shear dropped rapidly in the OpenSees model, while reducing much more gradually in LS-DYNA model. The greater post buckling

strength of the LS-DYNA model was attributed to increased post-buckling contributions of the braces through in-plane bending to the overall structural stiffness and strength. For the planar OpenSees model, the braces were pinned to the connections and their contribution to frame response was thus only associated with their axial load-axial deformation characteristics. However, in the finite element model, additional strength contributed to counter the deteriorating axial load capacity of the buckled brace(s) by (1) the moment capacity of the gusset plate to out-of-plane motion of the braces, slowing the deterioration of brace axial load capacity, and especially, (2) by the gusset plates developing brace bending in the plane of the SCBF.

The OpenSees models exhibited steady reduction of base shear capacity with increasing lateral roof displacement. This is associated with the post-buckling characteristics of the braces, but also with the effects of geometric nonlinearities. The damage was concentrated almost entirely in the ground story, with buckling occurring in one of the ground-story braces, followed by tensile yielding of the other brace in the ground story. Limited tension yielding of the second-story brace was predicted. The third story remained essentially elastic in the OpenSees model.

For the OpenSees models including low-cycle fatigue rupture of individual fibers, a small additional reduction of shear capacity was seen at a roof drift index of about 6.5%. This is associated with compression brace at the ground story brace losing all of its capacity. A final loss of capacity was observed at a roof drift index of about 8.5%. This is associated with rupture of the tension brace. As noted in Uriz and Mahin [2008], the Rainflow cycle counting approach counts tension and compression cycles equally, so that failures may occur in tension or compression cycles. Even under compression loading, one side of a plastic hinge in a brace will actually be loaded in tension. The Manson-Coffin relation used in both the OpenSees and LS-DYNA models resulted in much larger drift capacity under monotonic loading than would be expected during cyclic or earthquake loading.

For the LS-DYNA analysis, buckling of the ground story brace occurred quite early, followed by tension yielding of the brace in the same level. There was minor yielding in the second-story tension brace. Although similar to the progression of events in OpenSees, brace fracture was not predicted. However, at about 7-8% roof drift ratio, the tension column began to fracture near the bottom of the shear tab at the end of the lowest beams. At a roof drift ratio of about 9-10%, the connection of the bottom tension brace to gusset plate failed. This is associated with combined tension, in-plane bending and stress concentration at the tip of the gusset plate. These later two modes of failure were not modeled in OpenSees. The base shear goes to zero in LS-DYNA, which was gradually due to the residual capacity of the compression side column and compression brace. In OpenSees, the failure of both braces at the bottom level led to numerical instability.

The results showed that the roof drift index (roof lateral displacement divided by the roof elevation) was about 0.30 % at first buckling of a brace, about 6 % to 8 % at rupture of the first brace, and 8.5% for numerical instability due to excessive damage to the structure. Because the connections in OpenSees model were idealized, their failure was not explicitly simulated in the analysis. It was assumed that the connections remained intact under the seismic demand analyzed.

3.4.4.2 Individual Case Studies of Dynamic Response of the Phase II Models

The six model buildings were subjected to the sixty SAC ground motions described previously. Before looking at a statistical analysis of the sensitivity of key EDPs to ground motion intensity, it is useful to examine in more detail the response of the systems to an individual ground motion. Time histories of critical story drift and vertical mid-span beam displacement, and hysteretic loops for critical braces and for the frame roof displacement-base shear are examined in this section for Record LA32 (a simulated time history for a magnitude 7.1 earthquake on the Elysian Park fault), which is part of the ensemble scaled to be representative of the MCE hazard level. This ground motion caused the largest displacement responses in the model buildings.

Figure 3.29 plots the story drift and brace axial deformation time histories at the first (bottom) story for record LA32. The bottom story suffered the largest story drifts for this (and most other) records, while the upper two stories remained essentially elastic.

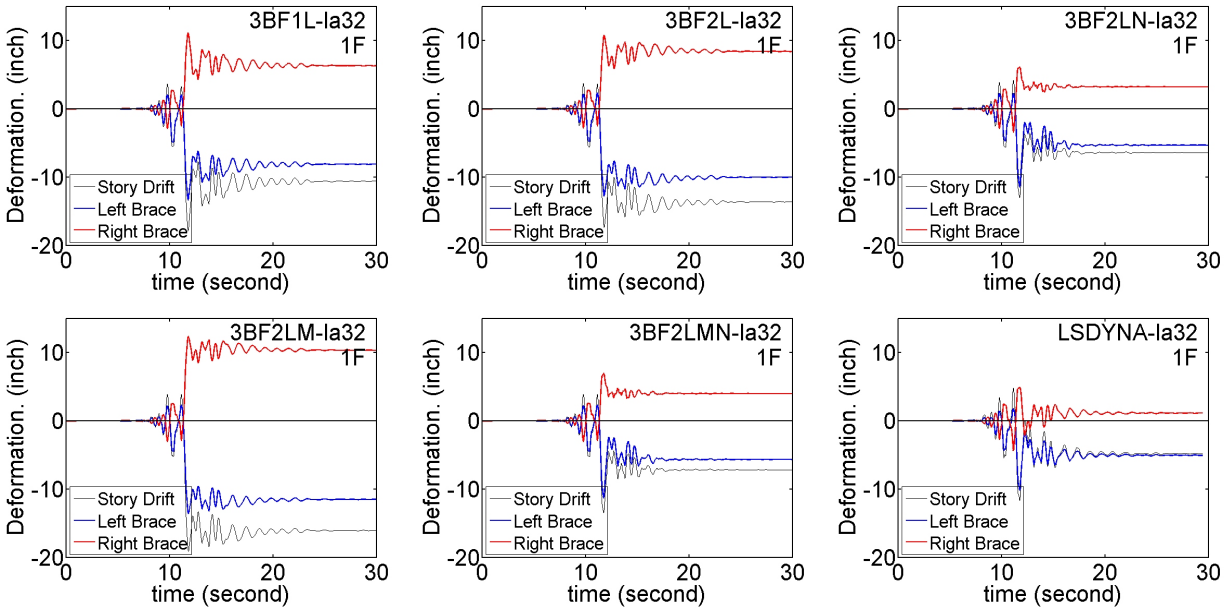

Figure 3.29 Time history of story drift and brace axial deformation in the ground story due to LA32

For OpenSees models 3BF1L, 3BF2L, 3BF2LN, 3BF2LM and 3BF2LMN, response to LA32 is characterized by a single very large story displacement excursion to about 14 to 20 inches in the first story corresponding to story drift ratios of around 8 to 11 percent. Permanent lateral roof displacements at the end of the record ranged from about 6 inches to 16 inches. This level of permanent lateral displacement is difficult to repair. Results show that the displacement time histories for model 3BF1L, 3BF2L and 3BF2LM, all of which included material models accounting for low-cycle fatigue, are similar. For model 3BF2LN and 3BF2LMN, which disregarded fatigue, the time history responses were similar, but had smaller story drifts and residual story drifts compared to the other models. On the contrary, story drifts in the fatigue sensitive models increase significantly once fracture occurred and had larger residual deformations. The strength response of the LS-DYNA model was decreased gradually; this is more similar to the

OpenSees models which did not include fatigue material properties.

Due to the slight sag of the beam at the brace-to-beam intersection, the brace axial deformation time histories show that the tension braces tended to have smaller axial deformation than the compression braces (comparing the absolute values). . Thus, the compression damage in the OpenSees models was greater than in tension (see Figure 3.29).

Figure 3.30 shows the vertical displacement at the mid-span of the beams for different stories. Because the responses in the second and third stories were essentially elastic, the vertical displacement in these stories was relatively small. For OpenSees models 3BF2LN and 3BF2LMN without fatigue sensitive materials and for the LS-DYNA model, the peak mid-span vertical displacements were about 3.5 to 4 inches, and the residual mid-span vertical displacements were about 1.5 to 3 inches. For models 3BF1L, 3BF2L and 3BF2LM, the peak mid-span vertical displacement was between 1.8 inch and 2.3 inches. The residual mid-span vertical displacements of OpenSees models with fatigue materials were similar to those without fatigue materials, while the LS-DYNA model had the largest vertical residual displacement among all the models.

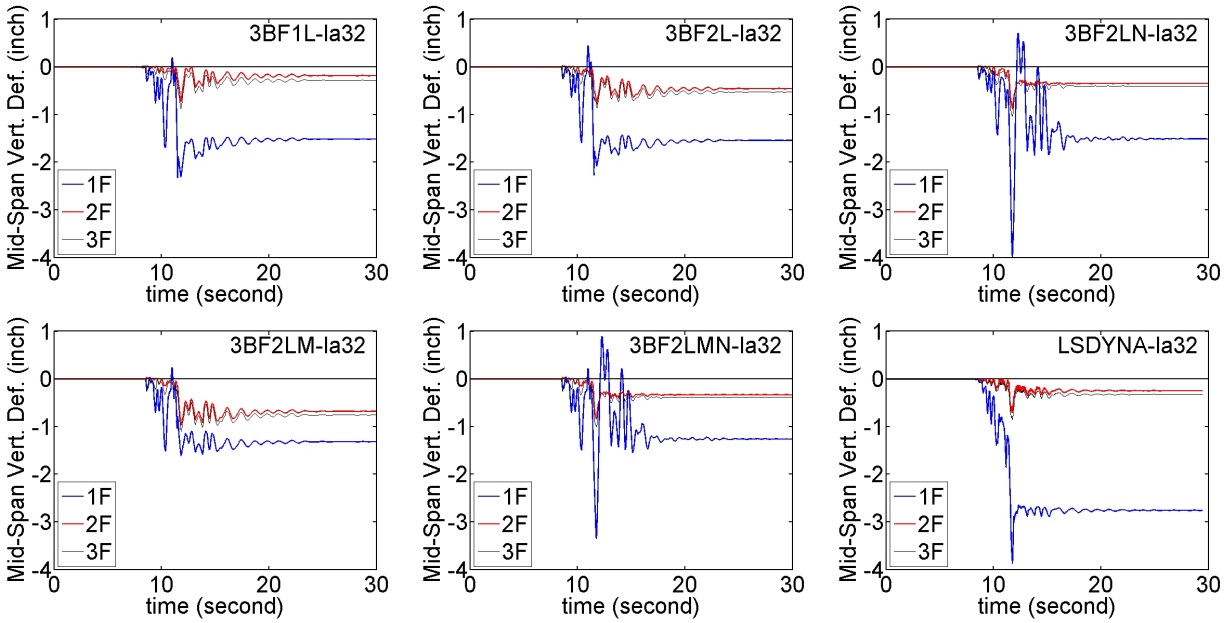

Figure 3.30 Time history of vertical displacement at mid-span of beams on each level

The hysteresis loops of braces in the first story are depicted in Figure 3.31. The buckling and yielding behavior of all the models before initiation of fracture was similar. Models with same damping type responded similarly, i.e. 3BF1L was similar to 3BF2L and 3BF2LN, while 3BF2LM was similar to 3BF2LMN. The OpenSees models with fatigue sensitive material properties had their braces fracture at about the same time (although some variations exist, which are due to the differences in other modeling parameters). Complete fracture of the braces in the first story did not occur for the LS-DYNA model, which might reflect the fact that the LS-DYNA model distributes yielding and damage throughout the structure to a greater degree compared to the OpenSees models.

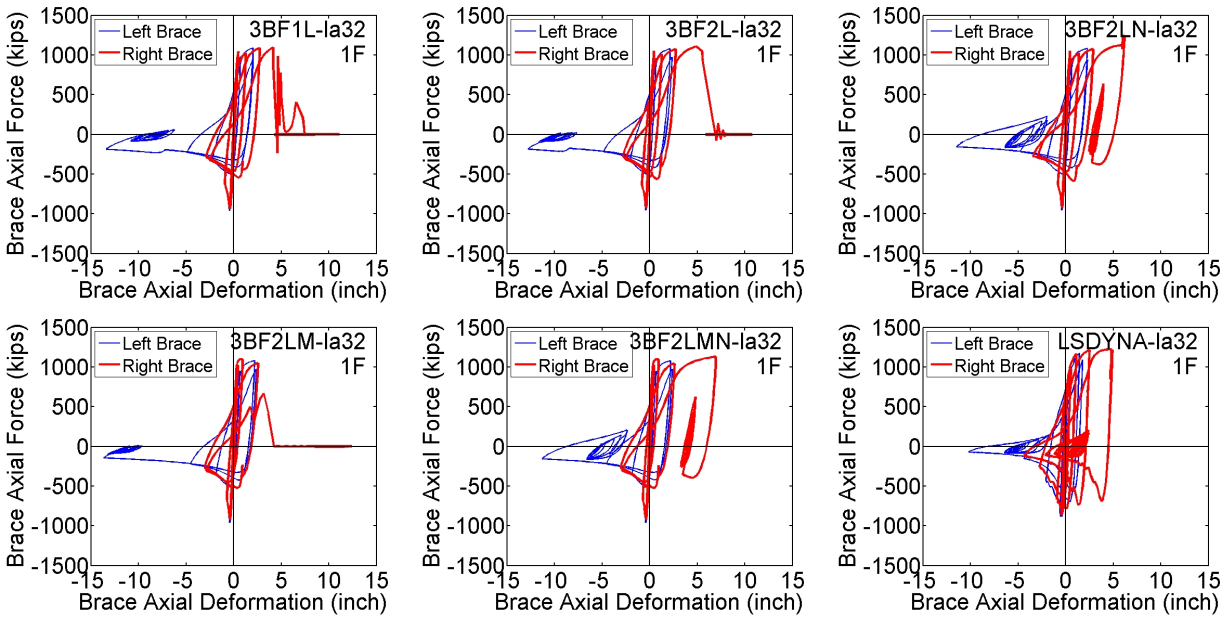

Figure 3.31 The relationship between axial force and axial deformation of braces on the first story due to LA32

The lateral drift–story shear hysteresis loops of each story are depicted in Figure 3.32, providing a direct comparison of the global behavior. Initially, all stories had similar drifts, but once a brace buckled, drifts tended to be concentrated in the bottom story, with only minor inelastic drifts in the second story. The third story remained nearly elastic during the excitation. The behavior of the OpenSees fiber models with material models including low-cycle fatigue was typified by fracture of the tension brace in the bottom level. The resulting vertical displacement at the mid-span of the second floor beam increased the story drift considerably compared to a story drift calculated from the brace elongation alone. The models with fractured braces tended to have greater residual drifts compared to models without fractured braces. The hysteretic responses showed that the strength and stiffness were reduced significantly after brace fracture occurred.

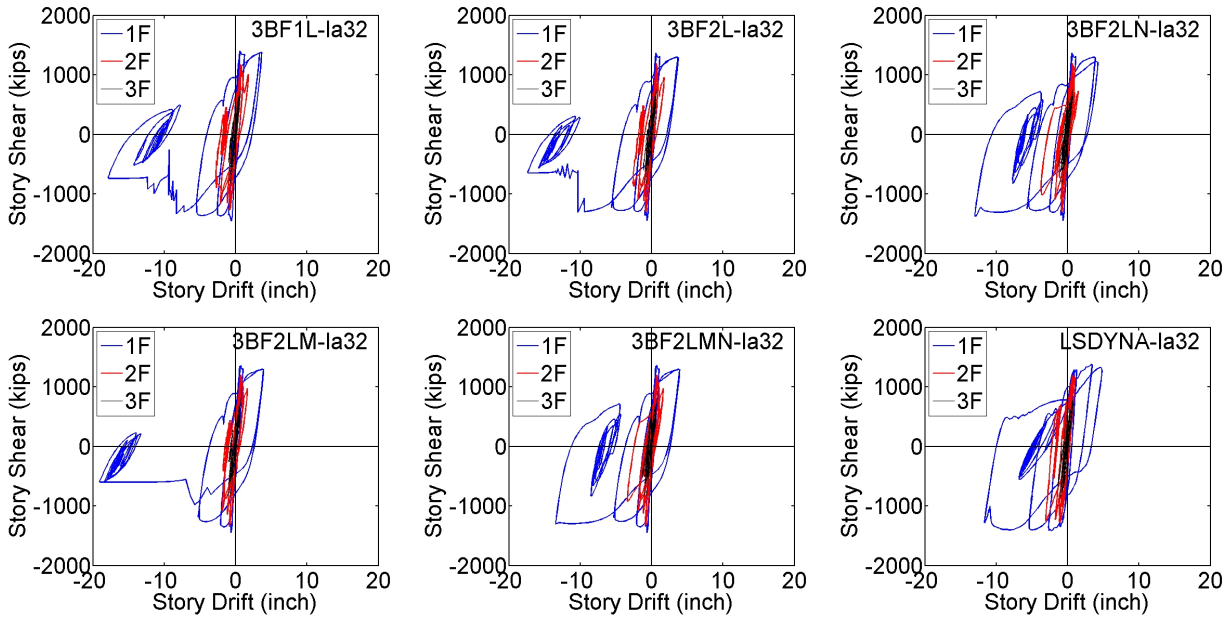

Figure 3.32 The relationship between story shear and story drift due to LA32

Although the braces in the bottom story fractured during record LA32, they did not fracture under some MCE ground motions, even if the fatigue sensitive material model was included. In such cases, the hysteresis loops were more similar to the models without fatigue, and the hysteresis behavior was more similar to the simulation obtained using LS-DYNA.

In general, the effect of beam axial forces on response was investigated by comparing the responses of models with one and two leaning columns (models 3BF1L and 3BF2L); Figure 3.29 demonstrates that the braces fracture at different times and responses time histories show slight differences. The difference of peak story drift on the first story was less than 2%. The effect of low-cycle fatigue was investigated by comparing 3BF2L with 3BF2LN and 3BF2LM with 3BF2LMN. Note that the displacement time histories were different as well as the residual story strength after the braces fractured. The post-fracture stiffness was also different for different models. The damping effect was investigated by comparing 3BF2L with 3BF2LM and 3BF2LN with 3BF2LMN. The story drifts were similar for the mass only and Raleigh (mass and stiffness) damping models. Fracture of the braces had greater impact on the responses of different models than the type of damping adopted in the models.

3.4.4.3 Statistical Evaluation of Story Drift Demands of Phase II Models

Figures 3.27 through 3.31 show the relation of peak story drift ratio to $S_{d,Elastic}$ for each record used in the analysis. $S_{d,Elastic}$ is defined as the elastic spectral displacement for the record used in the analysis at the fundamental period of the model being simulated. In these plots, DR1 is the peak story drift ratio of the first story for each record considered; DR2 is that of the second story; DR3 is that of the third story; DRave is the peak roof displacement divided by the total height of the model building (which is thus the average story drift ratio); and DRmax is the maximum story drift ratio occurring at any of the three stories. The ratio of DRmax/DRave is regarded as the index of the tendency of the system to form a soft story. The higher the ratio, the more concentrated the damage is in a single story.

Linear regression analyses were performed considering all of the results for a particular model in the lognormal form $ln(DR) = b + m \cdot ln(S_{d.Elastic})$. Table 3.8 lists the slope *m* and the intercept *b* of the regression for all the models. σ^2 denotes the variance of the lognormal distribution of DRmax.

Table 3.8 The slope, intercept and standard deviation of the regression relation of DRmax and $S_{d,Elastic}$ for all OpenSees models.

Model	m	b	σ^2
3BF1L	1.58	-5.78	1.08
3BF2L	1.55	-5.67	1.12
3BF2LN	1.53	-5.66	1.19
3BF2LM	1.56	-5.68	1.06
3BF2LMN	1.53	-5.62	1.19

The regression parameters were so similar that the differences of *m* and *b* between each model were within 3%. Consequently, the regression lines plotted in Figures 3.27 to 3.31 are also very similar. Although the trends are similar, several data points show large inelastic demands when $S_{d.Elastic}$ becomes large. For the case study, ground motion LA32, is among the cases that produced demands larger than predicted by the regression relation. To account for this increased response at large $S_{d,Elastic}$ values, a nonlinear regression model may be more suitable for these structures. Improved results obtained using an intensity measure based on inelastic spectral displacement are presented later.

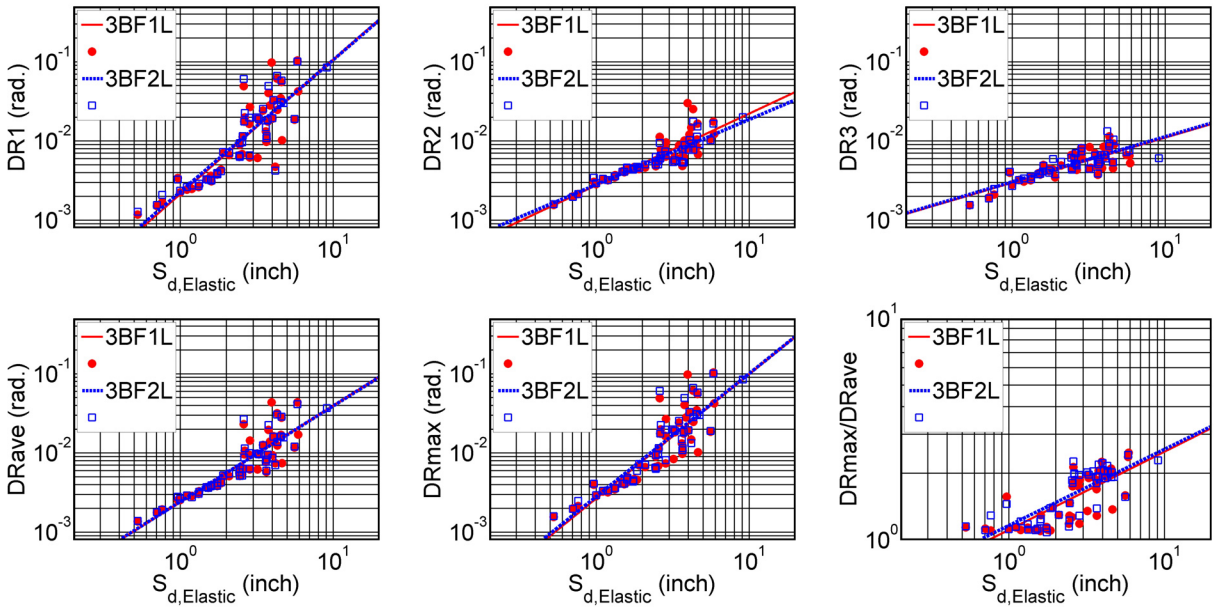

Figure 3.33 Comparison of Story Drift Ratios between one-leaning-column model (3BF1L) and two-leaning-column model (3BF2L)

Figure 3.33 compares regression analysis results for models 3BF1L and 3BF2L. The data of DR1 shows more dispersion than DR2 and DR3, because the first story experienced more

nonlinear deformation. The peak drifts on the first story contributed most of the maximum DR values, but the dispersion was slightly less for the DRmax values. The dispersion on the average DR was even smaller due to the less scattered data on DR2 and DR3. DRmax/DRave plots show that all the ratios were below 3.0 and most of them were below 2.0.

EDPs predicted from these regression lines corresponding to different hazard levels are listed in Table 3.9. These were determined from the regression lines identified in Figures 3.27 to 3.31, and the values of $S_{d.Elastic}$ in Table 3.5 corresponding to the hazard spectra for the site and the computed fundamental period of the structure. For the most severe hazard level (the MCE-level event), the median expected maximum DR values were slightly over 3.0%. For the design-level event, the expected median maximum DR were over 1.5%. Using the story drift index at the onset of brace buckling (about 0.3%) as the yield displacement of the structure, these maximum DRs corresponded to story drift ductility of more than 10 and 5 for the MCE- and design-level events, respectively.

Table 3.9 Median expected EDPs corresponding to different hazard levels based on elastic displacement spectra

Eng. Demand Parameters	Hazard Level	3BF1L	3BF2L	3BF2LN	3BF2LM	3BF2LMN
DRmax (radian)	50/50	0.73%	0.78%	0.78%	0.79%	0.81%
	10/50	1.58%	1.64%	1.62%	1.66%	1.69%
	2/50	3.01%	3.10%	3.04%	3.14%	3.17%
DRave (radian)	50/50	0.52%	0.54%	0.54%	0.53%	0.55%
	10/50	0.96%	0.96%	0.97%	0.96%	0.99%
	2/50	1.57%	1.57%	1.60%	1.59%	1.63%
DRmax/DRave	50/50	1.39	1.46	1.44	1.47	1.48
	10/50	1.66	1.72	1.68	1.73	1.71
	2/50	1.92	1.97	1.90	1.98	1.94
Res. DR (rad.)	50/50	0.04%	0.05%	0.05%	0.05%	0.05%
	10/50	0.24%	0.31%	0.22%	0.28%	0.23%
	2/50	1.06%	1.40%	0.77%	1.29%	0.89%

Note that for all the models, the expected median maximum story drift ratio at the service-level event (50% probability of exceedance in 50 years) exceeded the drift that will cause a brace to buckle (about 0.3%). Thus, following a frequent (service level) earthquake, the analyses show that at least one brace is likely to buckle, and it will be necessary to replace one or more braces and repair nonstructural damage in the adjacent elements.

Figures 3.34 and 3.35 compare responses for the different types of damping, for models with and without fatigue sensitive materials. Figures 3.36 and 3.37 compare the effect of fatigue sensitive materials. Statistically, the results exhibited very little difference. Although the case study of the response to the LA32 record indicated that responses of different models could differ significantly, regression curves based on response to many records were quite similar.

For the application of performance-based design, a relation was developed from the regression analyses that included the probability that a value of DRmax would be exceeded for a given value of $S_{d.Elastic}$. In Figure 3.38, fragility curves are presented for maximum story drifts ratios

of 0.3% and 2.5%. These values were simplified proxies for the initiation of brace buckling and the maximum drift accepted by standard code design methods for a Design Basis Event (ASCE/SEI 7-05).

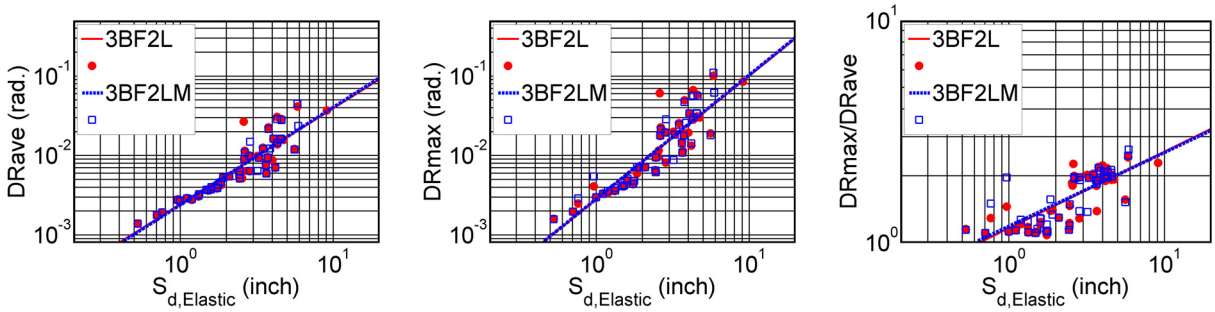

Figure 3.34 Comparison of Story Drift Ratios between Rayleigh damping model (3BF2L) and mass proportional model (3BF2LM)

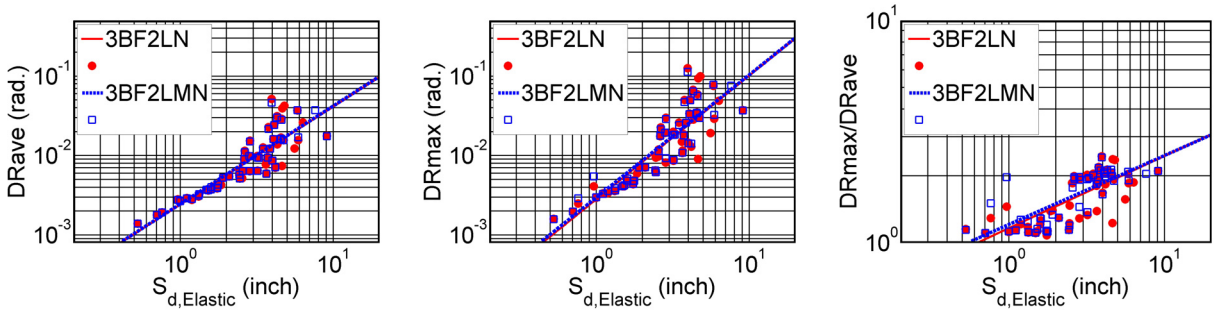

Figure 3.35 Comparison of Story Drift Ratios between Rayleigh damping model (3BF2LN) and mass proportional model (3BF2LMN) without braces fatigue

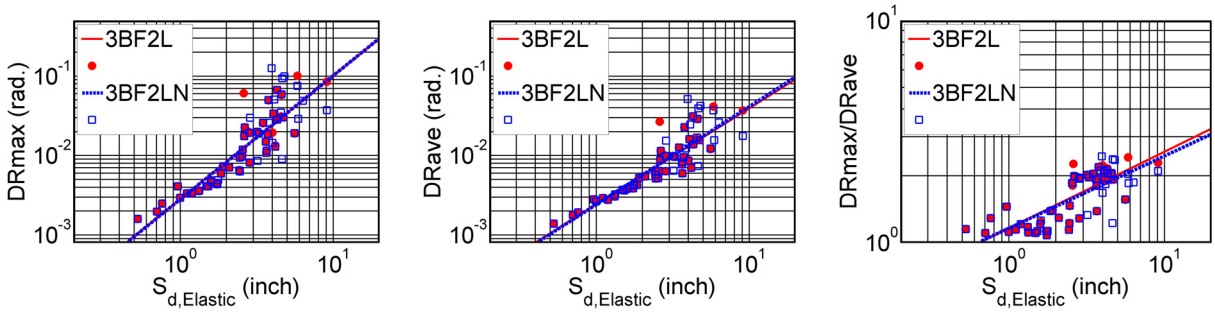

Figure 3.36 Comparison of Story Drift Ratios between fatigue model (3BF2L) and non-fatigue model (3BF2LN) with Rayleigh damping

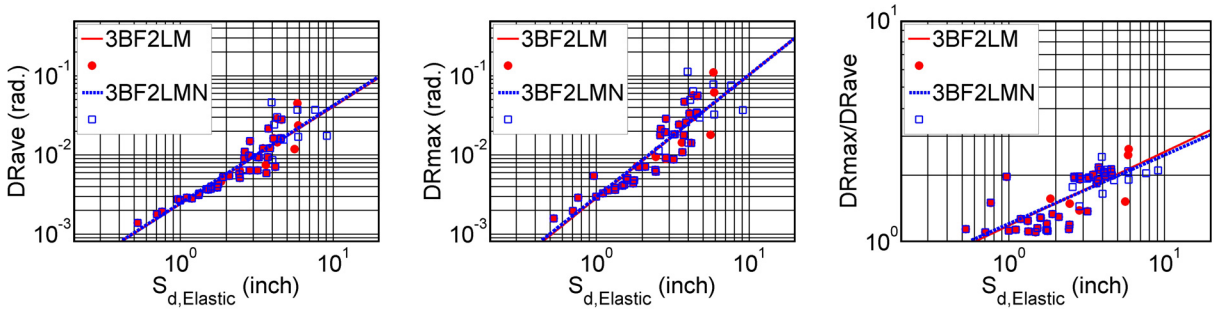

Figure 3.37 Comparison of Story Drift Ratios between fatigue model (3BF2LM) and non-fatigue model (3BF2LMN) with mass proportional damping

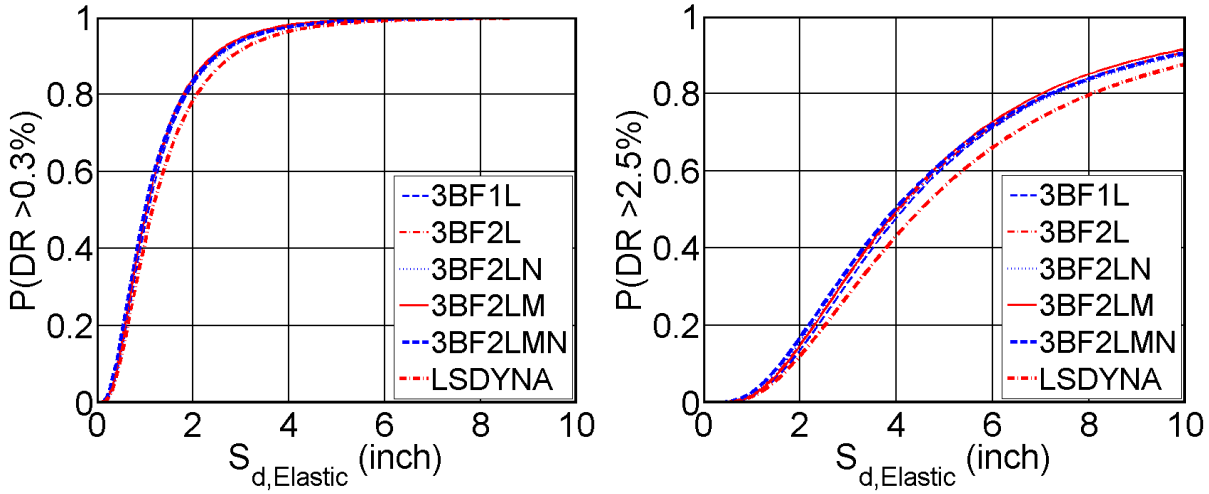

Figure 3.38 Probability of exceeding critical drifts for different models (compare between different models)

Obtained from Figure 3.38, Table 3.10 lists the probability that the maximum story drift ratio will exceed 0.3% and 2.5% for earthquakes with a given probability of exceedance for each OpenSees model. For the MCE-level event, the OpenSees models all have more than a 57% probability of developing maximum story drifts greater than 2.5%. For the design-level event, these probabilities drop to 33%. Considering the service-level event, the models have more than 80% probability of buckling a brace on one or more stories. Obviously, to minimize significant local nonstructural damage during the service-level event, the likely motion of the brace in the buckled configuration must be considered, along with the possibility of replacing braces following such events due to permanent lateral offsets.

Figure 3.39 illustrates the displacement time histories of different models. Among all analyses for the sixty ground motions, record LA32 shows the peak value of maximum DR. LA28 and LA40 show the maximum positive and negative difference between OpenSees model (3BF2L) and the LS-DYNA model.

Table 3.10 Probability of exceeding critical DR values for different models based on elastic displacement spectra

Model		Hazard Level 50%, 50yrs	10%, 50yrs	2%, 50yrs
3BF1L, T =0.50 sec.	P(DR>0.3%)	80.4%	94.6%	98.7%
	P(DR>2.5%)	11.7%	33.0%	57.1%
3BF2L, T =0.49 sec.	P(DR>0.3%)	81.8%	94.6%	98.6%
	P(DR>2.5%)	13.6%	34.5%	58.0%
3BF2LN, T =0.49 sec.	P(DR>0.3%)	81.0%	93.9%	98.3%
	P(DR>2.5%)	14.4%	34.6%	57.1%
3BF2LM, T =0.49 sec.	P(DR>0.3%)	82.4%	95.1%	98.8%
	P(DR>2.5%)	13.1%	34.5%	58.8%
3BF2LMN, T =0.49 sec.	P(DR>0.3%)	81.9%	94.3%	98.5%
	P(DR>2.5%)	15.2%	36.0%	58.6%

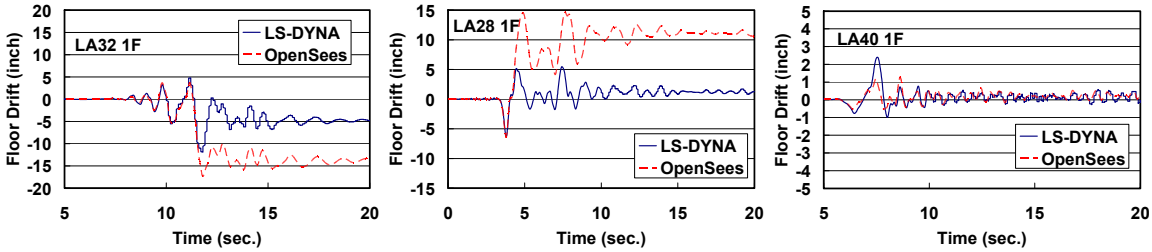

Figure 3.39 Floor displacement time histories of OpenSees model and LS-DYNA model

In most analyses under the same ground motion, the OpenSees models tended to have larger story drift because of the characteristics of the low-cycle fatigue and brace models used as demonstrated in Figure 3.39 for the LA32 and LA28 time histories. The differences between the OpenSees and LS-DYNA models were evident at the peak response, leading to different residual floor drift. Given that, it is also possible that the peak floor drift predicted by LS-DYNA might be larger than that of OpenSees if the peak response is less severe, as shown for the LA40 time history.

3.4.4.4 Statistical Evaluation of Residual Story Drift Demands of Phase II Models

Another response parameter of interest is the residual displacement in a structure, which is used to determine whether it is feasible or cost effective to repair a structure after an earthquake. Figures 3.40 to 3.44 are similar to those presented in Figures 3.33 to 3.37, except the vertical axes are related to the maximum residual story drift remaining at the end of the earthquake. Plots are presented for the roof residual displacement, the peak residual drift index at any floor, and the ratio of the peak residual displacement to the maximum displacement at that story. The points presented on the plots show the data for individual records. Two lines are superimposed for the plot of maximum residual drift index, where one represents the median linear regression analysis result for the residual story drift ratio, whereas the other represents the previously reported maximum story drift ratio.

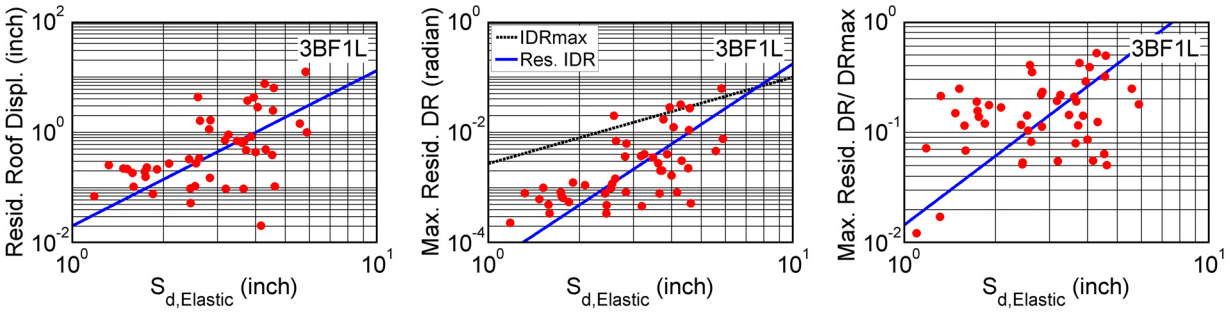

Figure 3.40 Relationship between residual deformation and $S_{d,Elastic}$ of Model 3BF1L

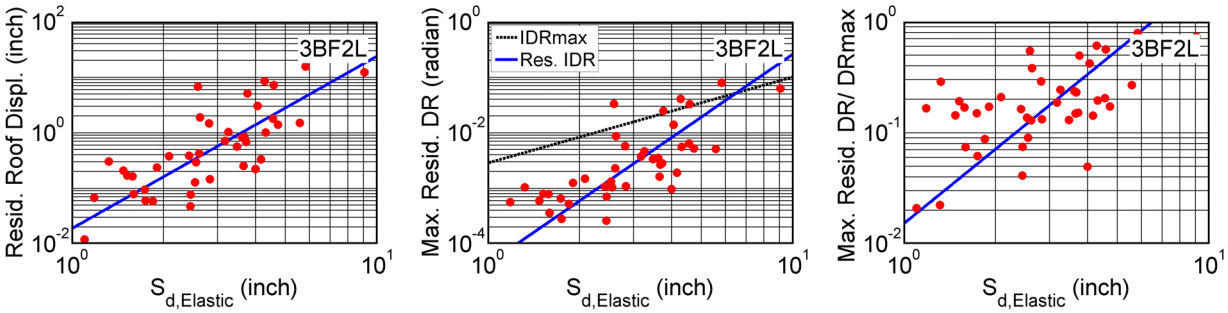

Figure 3.41 Relationship between residual deformation and $S_{d,Elastic}$ of Model 3BF2L

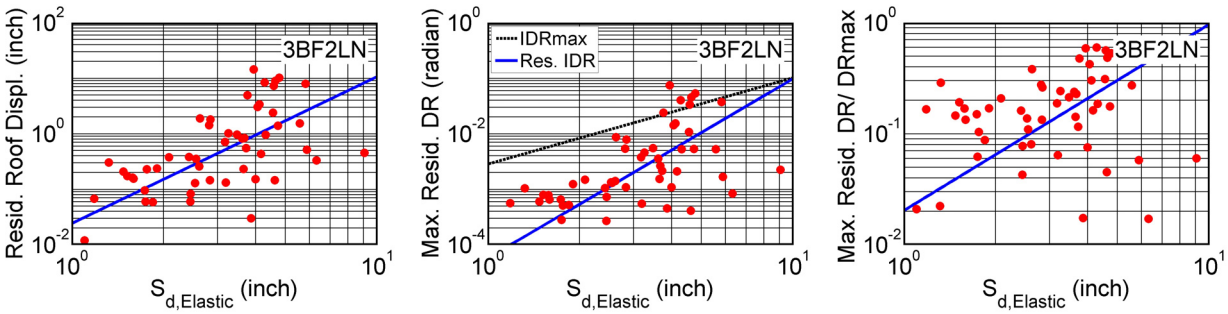

Figure 3.42 Relationship between residual deformation and $S_{d,Elastic}$ of Model 3BF2LN

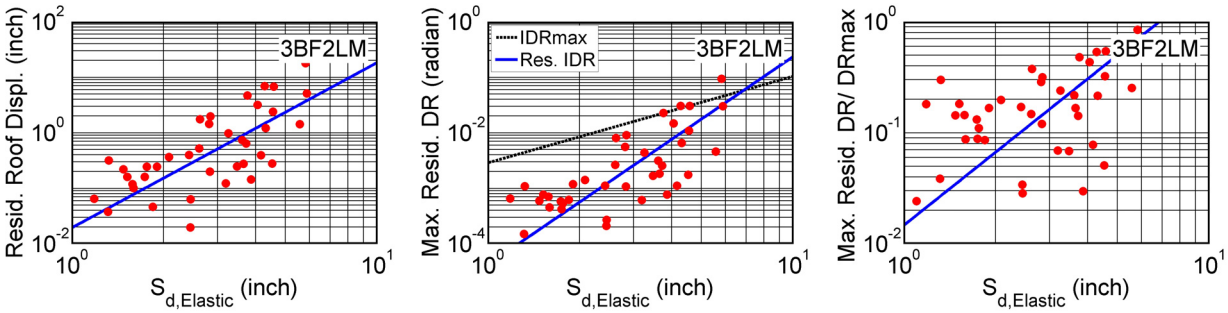

Figure 3.43 Relationship between residual deformation and $S_{d,Elastic}$ of Model 3BF2LM

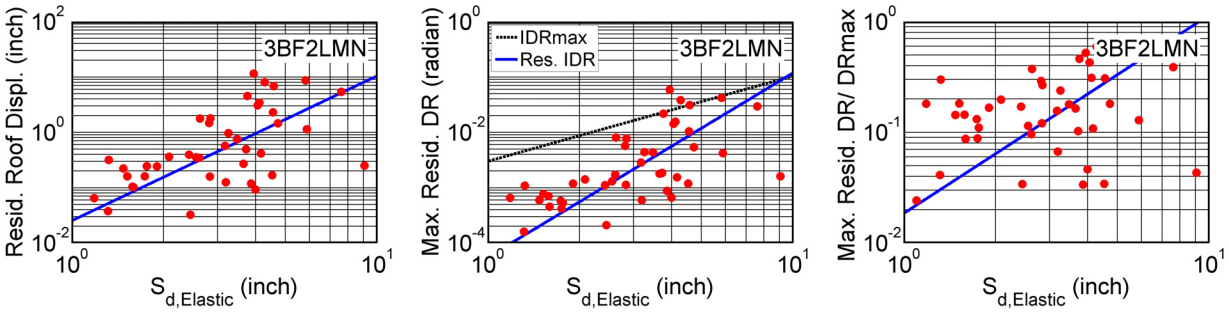

Figure 3.44 Relationship between residual deformation and $S_{d,Elastic}$ of Model 3BF2LMN

In Figures 3.40 to 3.44 it is obvious that there is tremendous scatter in the peak story residual displacements. In some cases, the residual displacement significantly exceeded the median expected maximum displacement at a particular value of $S_{d.Elastic}$, while in other cases the residual displacement is quite small.

In the plots of maximum residual DR/maximum DR, the residual displacement became a more significant fraction of the peak story drift for larger intensity shaking. The models without fatigue included in the material models tended to have smaller residual displacements, although the maximum and average story drifts do not show much difference among all the models.

For the models in which the braces may fracture, considering the spectral displacement corresponding to this structure at the MCE and design levels, the expected median maximum residual story drifts listed in Table 3.9 were about 1.25% and 0.28%, respectively. For the models without fatigue incorporated, the expected median maximum residual story drifts were reduced to about 0.83% and 0.22% corresponding to the MCE- and design-level events.

3.4.4.5 Inelastic spectrum displacement as ground motion intensity measure

To investigate whether the substantial dispersion of the results plotted in Figures 3.33 through 3.44 can be reduced, alternative ground motion intensity measures (IM) was considered [e.g., Ruiz-Garcia and Miranda, 2006]. Results are shown below for the case where an inelastic spectrum displacement is used as the ground motion IM.

The inelastic spectrum displacement was based on the first mode characteristics of the model building and generated from the software application BiSpec [Hachem, 2005]. The strength and stiffness properties of the equivalent single degree of freedom system were based on the static pushover analyses results (Figure 3.28) using the procedure outline by Chopra [2006]. A bilinear model was used to represent the hysteretic behavior of the structure. Inelastic displacements were computed for each of the 60 ground motions used in the study, and the peak displacements $S_{d,Inel}$ are used instead of $S_{d,Elastic}$ to plot the peak EDPs.

As can be seen in Figure 3.45, the scatter of the results for peak DR was significantly reduced compared to previously plotted cases using $S_{d,Elastic}$. Table 3.11 presents the R-square of the fit of the DRmax-$S_{d,Inel}$ relation. The inelastic spectrum displacement substantially improved the dispersion of the DRmax-$S_{d,Inel}$ relation, and the tendency of the DR to exceed the regression curve for high intensity shaking was no longer apparent. It appears that this discrepancy may be thus associated with the "energy preserved" tendency that has been noted for sin-

gle-degree-of-freedom inelastic structures with relatively short periods [Chopra, 2006]. This is captured by the nonlinear analysis for the single-degree-of-freedom systems used to obtain $S_{d,Inel}$. This may not be appropriate for systems for systems having greater contributions of higher modes to response or for systems with longer periods.

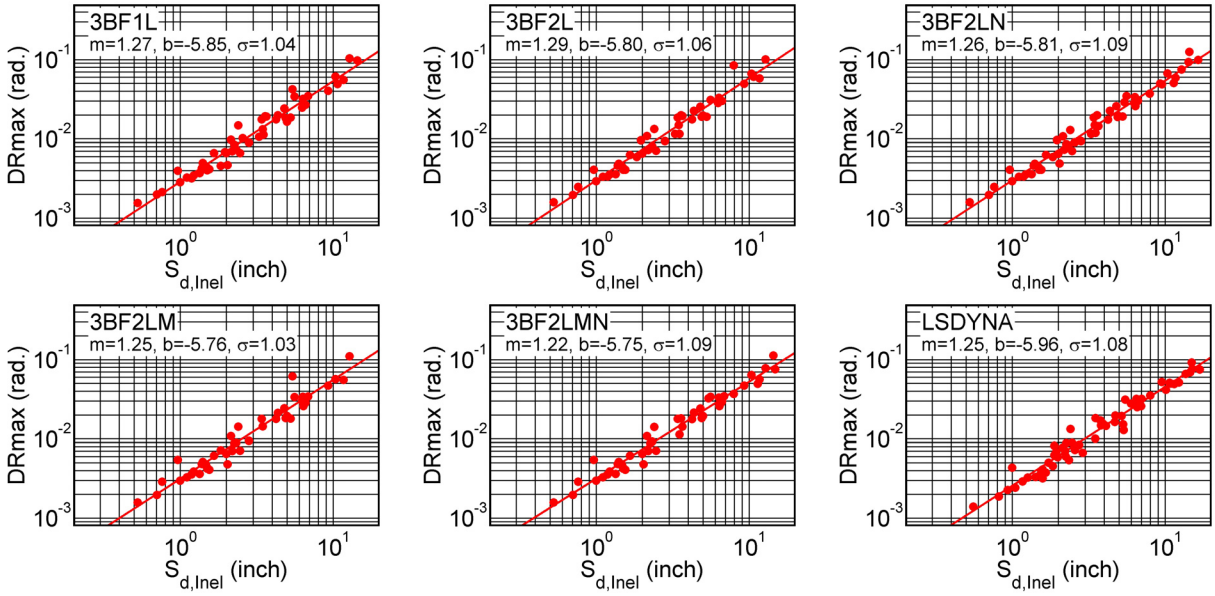

Figure 3.45 Relationship between Maximum Story Drift Ratio and inelastic spectrum displacement for different models

Table 3.11 R-square of the fit of DRmax and S_d relation for different models

Model	3BF1L	3BF2L	3BF2LN	3BF2LM	3BF2LMN	LS-DYNA
R-square of DRmax vs. $S_{d,Elastic}$ relation	0.7531	0.8021	0.7473	0.8246	0.8059	0.7577
R-square of DRmax vs. $S_{d,Inel}$ relation	0.9588	0.9618	0.9728	0.9438	0.9662	0.9642

Table 3.12 shows the expected EDPs based on the inelastic displacement spectra. The values for the service- and design-level events are generally smaller in the EDP- $S_{d,Inel}$ relation than in the EDP- $S_{d,Elastic}$ relation (see Table 3.9); however, for the MCE-level event, the expected EDPs are larger in the EDP- $S_{d,Inel}$ relation than in the EDP- $S_{d,Elastic}$ relation.

Table 3.12 Median expected engineering demand parameters corresponding to different hazard levels based on inelastic displacement spectra

Eng. Demand Parameters	Hazard Level	3BF1L	3BF2L	3BF2LN	3BF2LM	3BF2LMN
DRmax (radian)	50/50	0.66%	0.69%	0.68%	0.70%	0.70%
	10/50	1.42%	1.52%	1.45%	1.50%	1.46%
	2/50	4.72%	5.15%	4.80%	4.91%	4.67%
DRave (radian)	50/50	0.48%	0.49%	0.49%	0.49%	0.49%
	10/50	0.88%	0.90%	0.89%	0.89%	0.88%
	2/50	2.24%	2.33%	2.27%	2.26%	2.22%
DRmax/DRave	50/50	1.36	1.42	1.39	1.44	1.43
	10/50	1.62	1.69	1.64	1.69	1.66
	2/50	2.11	2.21	2.11	2.18	2.10
Res. DR (rad.)	50/50	0.03%	0.04%	0.04%	0.04%	0.04%
	10/50	0.18%	0.24%	0.17%	0.21%	0.17%
	2/50	2.44%	3.97%	1.79%	3.09%	1.87%

A comparison of different models with IMs based on elastic and inelastic displacement spectra is shown in Figure 3.46. The period of the LS-DYNA model is 0.52 seconds while that of OpenSees model is 0.5 seconds; the values of S_d for the OpenSees and LS-DYNA models are virtually the same. The difference in expected DRmax values for OpenSees model and LS-DYNA models is less than 10%.

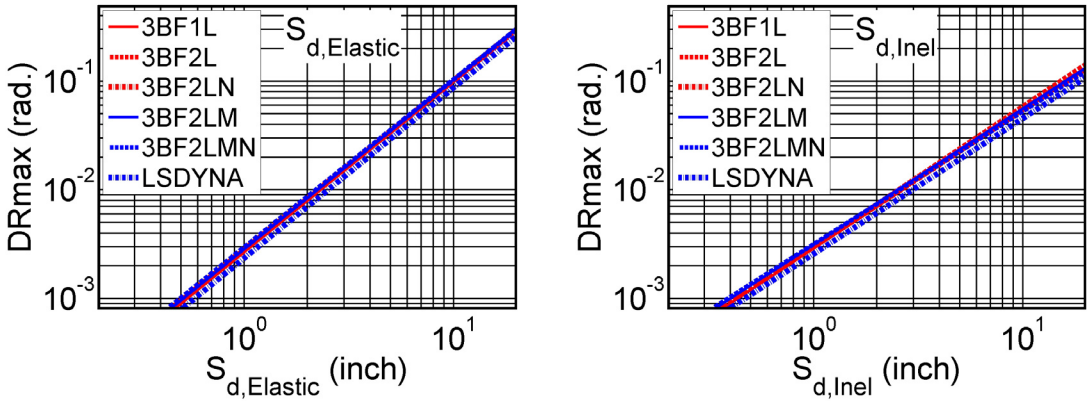

Figure 3.46 Trend lines of DRmax and S_d for different models

3.5 Summary

Analytical studies of a three-story tall SCBF building were conducted using fiber-based models from the computational platform OpenSees and using shell elements from the finite element software program LS-DYNA. Analytical results of each model were interpreted and compared in terms of nonlinear static pushover analyses, a case study under a single earthquake record and a probabilistic analysis of results using sixty ground motions representative of different hazard levels.

In the Phase I analysis, the force-based beam-column element was recommended to better estimate the nonlinear responses of the three-story double-story X braced frame. In addition, a relatively small time step was employed to improve the accuracy of the results and the convergence of the analysis. An adequate working point at the column base should be defined so that the taller first story may be included in the numerical model and reflect the more realistic structural behavior.

In the Phase II analysis, the pushover analysis showed that the braces in the ground story began to buckle globally at a story drift ratio of about 0.3% in both the OpenSees and LS-DYNA models. The LS-DYNA model, being more sensitive in capturing localized stress concentrations and local buckling, showed a more gradual change in strength before and after reaching the peak strength. The OpenSees fiber model exhibited a sudden drop in strength at the ignition of buckling or fracture initiates. The LS-DYNA model suggested an ultimate failure mode that is different than the fiber models in OpenSees. Both identified a soft first story response, but OpenSees suggested a failure by severe buckling of the compression brace and fracture of the tension brace. The shell element model in LS-DYNA suggested that final failure is associated with fracture in the column at the top of the first-story tension-side column, and in-plane deformation related fracture of the brace to gusset plate connection at the bottom of the tension brace.

The case study of structural behavior under ground motion record LA32 showed that adding low-cycle fatigue to the OpenSees fiber models resulted in larger story drifts (for records where a brace fractures) and led to larger residual story drifts. The vertical displacement at mid-span of beams predicted results in the tension braces having smaller axial deformations than the compression braces. In OpenSees models with fatigue sensitive materials, when the braces fractured, the overall strength and stiffness of the structure were reduced after the fracture. The drift demands increased significantly whenever fracture occurred. Comparing the effects of beam axial forces, fatigue materials and damping types, material properties that fail in low-cycle fatigue affected the response more than the other phenomena do.

The OpenSees analyses suggest that since the number of cases where fracture occur is small on a statistical basis, fatigue sensitive materials do not change the overall response significantly. . However, when examining the response to a single ground motion, fracture of a brace has an important impact on structural response. OpenSees results show that the expected median maximum story drift ratio at the service-level event (about 0.75%) exceeded the drift needed to cause buckling of a brace (about 0.3%). OpenSees models predicted that for this hazard level, there is more than 80% probability of buckling a brace at one or more stories in. For a 2% in 50 year-hazard level, the OpenSees models had more than a 57% probability of developing maximum story drifts greater than 2.5%. For the design-level event, the probability dropped to 33%.

Results for this short-period SCBF system demonstrate that using inelastic spectral displacements instead of those based on elastic analysis substantially reduced dispersion of the results especially for large intensity events. The predicted story drifts for maximum considered hazard levels increased, however, when inelastic spectral displacements were used as IM. Additional research is needed on this topic.

OpenSees fiber models suggest that residual displacement becomes a more significant fraction of the peak story drift for larger intensity shaking. However, according to observations from the analyses, the relationship between residual displacements and ground motion durations did not show clear trend. The effect of fatigue sensitive materials was more important for the

residual displacement than for the peak displacement. For the OpenSees models that employed fatigue sensitive materials, the expected median maximum residual story drifts were about 1.25% and 0.28% for the MCE- and design-level events, respectively.

Comparison of inelastic behavior predicted by fiber models with OpenSees and shell elements with LS-DYNA for individual ground motion records shows that the difference between beam-element and shell element models can be significant for some ground motion excitations. For the ground motions used in this study, shell-element models in LS-DYNA predicted smaller maximum story drift and residual story drift, but larger maximum vertical displacement at mid-span of the beam and stiffness reduction. Moreover, the ultimate failure modes may differ significantly for the two models. On the other hand, from a statistical perspective (when inelastic spectrum displacement is used as the IM), the difference between OpenSees beam-element model and LS-DYNA shell-element model results was less than the dispersion for different ground motions by the same model. For the case considered herein, if inelastic spectrum displacements are used to predict the structural responses, corresponding inelastic properties can be obtained from analysis using beam- or shell-element model, resulting in equally accurate median response prediction.

In general, the parameters in Phase II models did not result in any significant differences statistically. For the final models, either the one-leaning column or two-leaning column option will be used, and the fatigue material will be included. Because the scatter in statistical data was reduced by using the inelastic spectrum displacement, the probability relation will be generated based on inelastic spectrum displacement.

Chapter 4

Performance Evaluation of Braced Frame Buildings

A detailed performance evaluation is conducted for three-story braced frame buildings. The SCBF buildings were designed according to both older and current codes are to investigate the impact of code change on structural response. A BRBF building was also analyzed to evaluate the advantage and disadvantage of different braced frame systems. To improve the system performance of the SCBF, the response reduction factor for design using code approaches is reduced to limit the demands in the building; the effectiveness of this strategy is investigated. This chapter compares statistically the drift demands of four structures based on the numerical models developed and evaluated in Chapter 3.

4.1 Design Criteria

The seismic responses of three-story tall steel buildings are investigated. Figure 4.1 shows the model buildings with lateral earthquake-load resistance provided by special concentric braced frames (SCBF) or buckling restrained braced frames (BRBF) located on the perimeter of the building. These buildings were designed by others [Sabelli, 2000, DASSE, 2007]. Model A was designed in conformance with the provisions of the 1997 NEHRP seismic design provisions, and Model B and Model C were designed to comply with the provisions of ASCE/SEI 7-05. Model B is the same model building as discussed in Chapter 3. The importance factor and redundancy factor were assumed to be unity for all designs. Table 4.1 lists some of the principal attributes of the structures and the key parameters used in the seismic design.

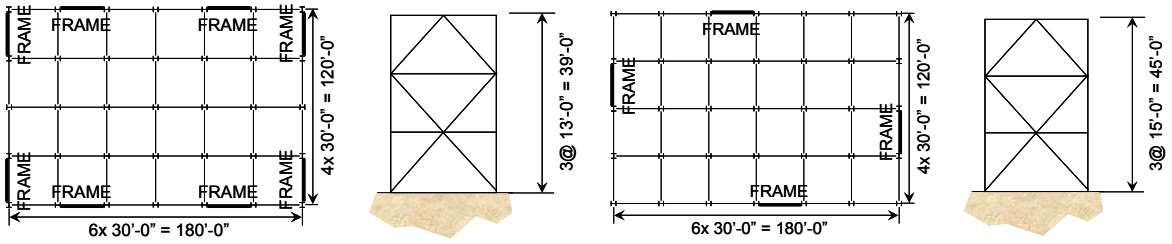

(a) Model A (b)Model B and C

Figure 4.1 Model building floor plan and elevation

Table 4.1 Design parameters of model buildings

Model	A	B (SCBF), C (BRBF)
Code	1997 NEHRP	ASCE/SEI 7-05
Building Location	Los Angeles, CA	Los Angeles, CA
Seismic Design Category	D	D
Occupancy Category	II (Office)	II (Office)
Importance Factor	1.0	1.0
Short Period Spectral Acceleration, S_s	2.09g	2.2g
1 sec. Period Spectral Acceleration, S_1	0.77g	0.74g
F_a	1.0	1.0
F_v	1.5	1.5
R	6	6 (SCBF), 8 (BRBF)
Design Base Shear	0.23W	0.24W (SCBF), 0.13W (BRBF)

4.2 Model Buildings

Table 4.2 lists the member sizes used in the models. Model A represents the typical SCBF bent designed based on 1997 NEHRP provisions, while Models B and C represent SCBF and BRBF systems designed based on ASCE/SEI 7-05. The configuration of lateral load-resisting frames were also different, with Model A having twice as many lateral load resisting bents. The story height for Model A is 13 feet, whereas that for Models B and C is 15 feet. Model B is the same building as modeled in Section 3.4.

The roof beam of Model A is particularly light compared to the lower two floor beams because the 1997 AISC Seismic Provisions [AISC, 1997] contains an exception to the normal strong beam design requirement at the roof of chevron SCBF systems. The beams are typically designed to account for the unbalanced load produced by the tension and compression braces (described in section 3.4). According to 1997 AISC seismic provisions, this provision was not required for the roof, so the roof beam was significantly smaller than at the other levels. In contrast, the roof beam of Model B is considerably heavier than the second and third floor girders. This is because the unbalanced loads induced from the buckling of braces on the top story were considered in accordance with the 2005 AISC Seismic Provisions [AISC, 2005]. The tension force used to compute the unbalanced load on the beam was based on R_yP_y instead of P_y, and the unbalance loads in the lower two stories were small,. In Model C, the member sizes are typically smaller because of the greater R value, the reduced brace unbalanced forces, and the longer fundamental period and therefore smaller design acceleration.

Table 4.2 Member sizes

Floor	Model	Braced Frame Columns	Braced Frame Beams	Brace Size
Roof	A	W12x96	W18x46	HSS 6x6x3/8
	B	W14x176	W36x210	HSS 10.0x0.375
	C	W14x132	W24x76	4 in^2
3rd	A	W12x96	W27x84	HSS 8x8x1/2
	B	W14x176	W30x116	HSS 11.25x0.50
	C	W14x132	W24x76	6 in^2
2nd	A	W12x96	W30x90	HSS 8x8x1/2
	B	W14x176	W27x84	HSS 12.5x0.50
	C	W14x132	W24x76	7.5 in^2

4.3 OpenSees Numerical Models

Four model buildings, designated 3AF, 3BF, $3BF_3$, 3CF, were analyzed and discussed. The notation used for the model names is listed in Table 4.3. All the beams were considered to be rigidly connected to the columns in all models including the beams with braces connected in the middle span and in the ends. Model $3BF_3$ was similar to Model 3BF, except twice as many braced bents were used, thus, a effective force reduction factor R of 3 (rather than 6) was used for Model $3BF_3$; therefore, the member sizes of Model $3BF_3$ were the same as those of Model 3BF, but the effective seismic mass of Model $3BF_3$ was half that of Model 3BF. Model 3CF was also similar to Model 3BF except for the use of buckling restrained braces. The OpenSees modeling parameters of Model 3CF were essentially the same as those for the SCBF models, except for the modeling of the braces. Adopting the fatigue model, Model 3CF was modeled to conform to the code requirement on the ductility capacity for testing of braces. (The BRBs were required to achieve a cumulative inelastic axial deformation of at least 200 times the yield deformation). Fracture occurs when the fatigue life in BRBs was exhausted. Compared to the SCBF model, the modeling of braces in BRBFs was more straightforward because there was no need to apply the initial camber to the BRBs. Only one force-based nonlinear beam-column element was used for each BRB. The modeling properties were calibrated from test data (BRBs had the cyclic deformation capacity that conforming to the code minimal requirement). Rigid end zones were used to increase the stiffness computed using only the steel core to get more accurate stiffness of BRBs accounting for the stiffness contribution from tapered and connection areas of an actual BRB.

Table 4.3 Model names

Abbreviation	Denotation
A	Double story X SCBF designed to comply with 1997 NEHRP
B	Double story X SCBF designed to comply with ASCE/SEI 7-05
C	Double story X BRBF designed to comply with ASCE/SEI 7-05
F	Model building with fully constrained beam-column connections
Subscript 3	Model building designed with R=3 instead of R=6 for SCBF

4.4 Design Spectra

The seismic spectra considered in the design of the three model buildings are shown in Figure 4.2. The spectra are quite similar, although in the constant amplified acceleration range, the ASCE/SEI 7-05 spectrum is slightly larger than that in the 1997 NEHRP provisions.

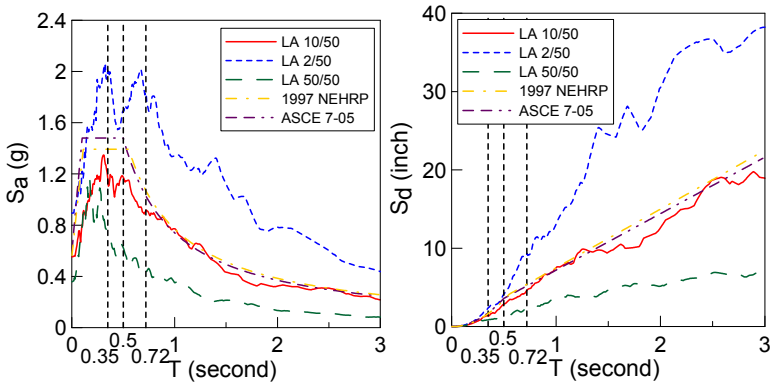

Figure 4.2 Response spectra

The SAC ground motion suite which is used to conduct nonlinear dynamic analysis is the same as the suite described and used in Chapter 3. The median of the pseudo-spectral acceleration and spectral displacement corresponding to a particular hazard level are shown in Figure 4.2. The median elastic spectral displacements corresponding to the fundamental period of the various models for the three hazard levels considered are summarized in Table 4.4.

Table 4.4 Median of $S_{d,Elastic}$ (inch)

Model	Hazard Level		
	50% in 50yrs	10% in 50yrs	2% in 50yrs
3AF, T_1=0.36 sec.	1.12	1.63	2.44
3BF, T_1=0.49 sec	1.70	2.74	4.13
$3BF_3$, T_1=0.35 sec.	1.07	1.56	2.30
3CF, T_1=0.72 sec.	2.86	4.67	9.31

4.5 Statistical Evaluation of Story Drift Demands

4.5.1 Story Drift Ratio

Figure 4.3 compares the responses of structures (Model 3AF and Model 3BF) that were designed under different design code. The regression lines of the story drift ratios in the first story were similar for the Models 3AF and 3BF. For the second story, the regression curve of Model 3BF was slightly steeper than that of Model 3AF. In the plot of DRave, the slopes of both models were similar but the regression curve of 3BF fell below that of 3AF. Similar observations were noted in the plot of DRmax, but the regression curves were more parallel. The data in DRmax/DRave plot was less scattered for Model 3BF, with the ratios mostly less than 3.0.

While the trend line offers a general comparison regardless of the intensity of the ground mo-

tions, the comparison of the EDPs with respect to different hazard levels should take into account the difference of the fundamental periods. As shown in Table 4.5, corresponding to different hazard levels, Model 3BF has larger maximum DR than Model 3AF for all three hazard levels. Particularly, at the MCE-level event, the maximum DR of 3BF was almost twice as much as that of 3AF. This difference is primarily due to the longer period of 3BF and also the resulting larger $S_{d,Inel}$. Nonetheless, at the MCE-level event the soft-story index (DRmax/DRave) of 3BF was only slightly greater than that of 3AF. At the service-level event, the soft-story index of 3BF was even smaller than that of 3AF. The weaker roof beam in 3AF may contribute to this difference.

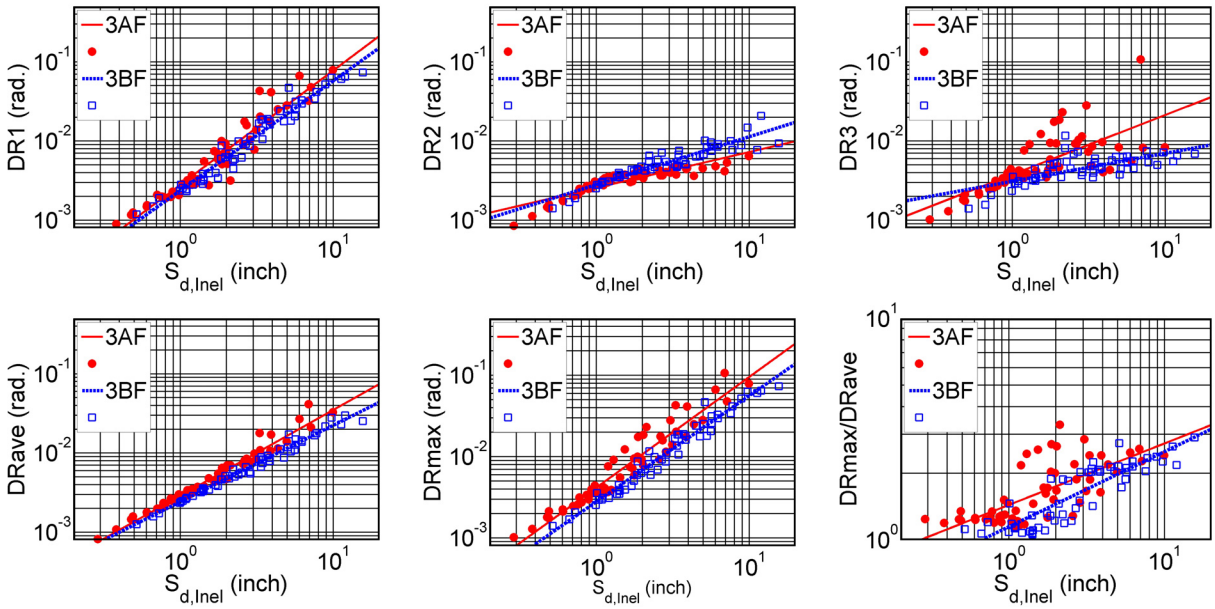

Figure 4.3 Story drift ratio for Models 3AF(1997 NEHRP) and 3BF(ASCE/SEI 7-05)

Table 4.5 Median expected EDPs corresponding to different hazard levels based on inelastic displacement spectra

Eng. Demand Parameters	Hazard Level	3AF	3BF	$3BF_3$	3CF
$S_{d,Inel}$ (inch)	50/50	1.08	1.90	1.12	2.63
	10/50	1.67	3.24	1.63	6.00
	2/50	3.60	8.36	2.82	16.20
DRmax (radian)	50/50	0.46%	0.69%	0.31%	0.84%
	10/50	0.84%	1.52%	0.51%	1.95%
	2/50	2.38%	5.15%	1.04%	5.37%
DRave (radian)	50/50	0.32%	0.49%	0.26%	0.61%
	10/50	0.50%	0.90%	0.38%	1.37%
	2/50	1.16%	2.33%	0.65%	3.68%
DRmax/DRave	50/50	1.47	1.42	1.20	1.39
	10/50	1.66	1.69	1.34	1.42
	2/50	2.05	2.21	1.59	1.46

Figure 4.4 compares results for Model 3BF and Model $3BF_3$ for different hazard levels corresponding to the inelastic displacement spectra. Model $3BF_3$ was twice as stiff and strong as Model 3BF. Thus, the fundamental period and spectrum displacement for Model $3BF_3$ are significantly less than those for Model 3BF (see Table 4.4). The regression curves at all levels (except for the top story) —the average DR and maximum DR— are almost identical for Model 3BF and Model $3BF_3$. In the DRmax/DRave plot, the regression curves of the two models are similar, but because the spectrum displacement of Model $3BF_3$ is smaller, the tendency to form a soft story is actually reduced. The median story drift ratios listed in Table 4.5 show that reducing the R value decreases the drift demand of SCBF. In the service-level event, the maximum story drift ratio is about 0.3%, and the braces may not buckle at this hazard level. For the other hazard levels, the drift demand is lower and therefore the deformation demand of braces is smaller.

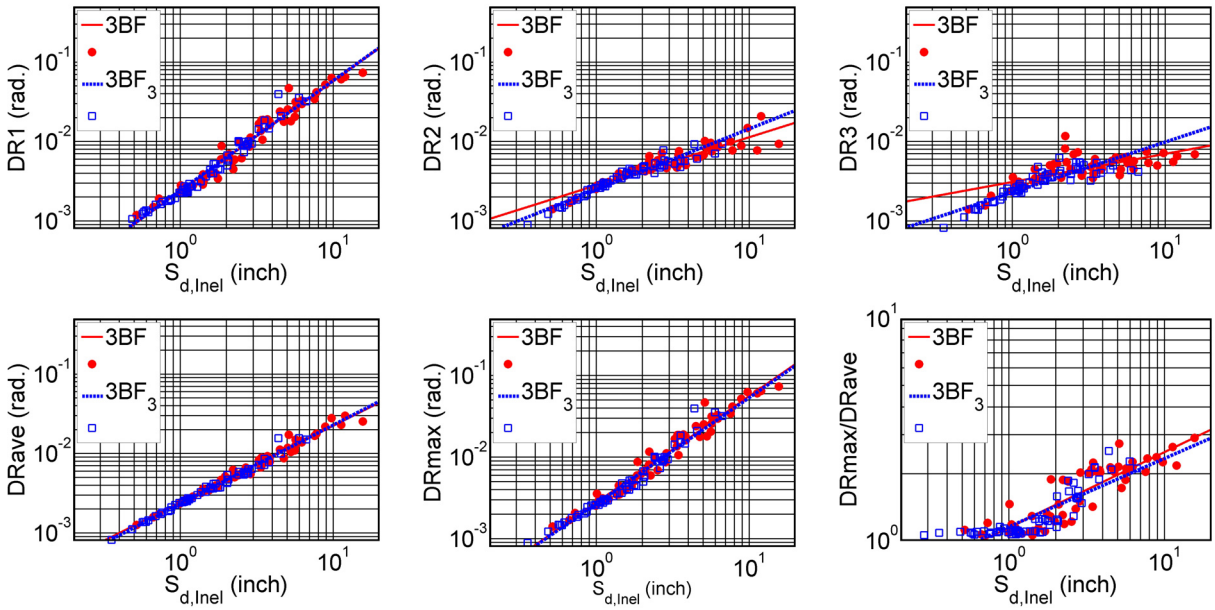

Figure 4.4 Story drift ratio for 3BF (R=6) and $3BF_3$ (R=3)

A comparison of the regression curve of DRave for Models 3BF and 3CF shows that both models are rather similar (Figure 4.5). The DRs in each story, however, show differences between Models 3BF and 3CF, demonstrating that the BRBF tends to have a more uniform DR throughout the whole building, as the braces do not buckle and deteriorate. As shown in Figure 4.5, the tendency to form a soft story\ies is much less than with SCBF. Considering the difference of spectrum displacement, the maximum DR of Model 3CF is greater than that of Model 3BF at different hazard levels (see Table 4.5). The shift in fundamental period greatly increases the spectrum displacement resulting in high drift demands for different hazard levels.

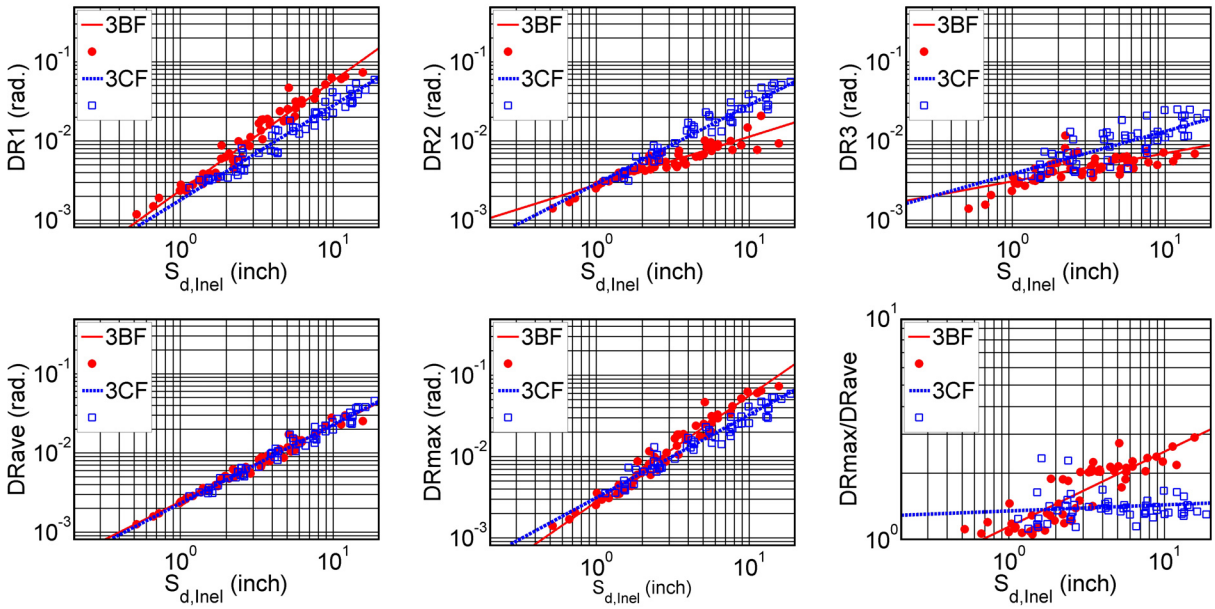

Figure 4.5 Story drift ratio for 3BF (SCBF) and 3CF (BRBF)

Using the data in Figures 4.4 through 4.6, it is possible to develop a relation describing the probability that a maximum story drift ratio is exceeded for a given inelastic spectrum displacement. The probability that the maximum story drift ratio will exceed 0.3% and 2.5% radians is shown in Figure 4.6, which is representative of initiation of buckling and the maximum drift accepted by standard code design methods for a Design Basis Event. The probability curves show different results for Models 3AF and 3BF. However, it is not clear whether this difference is due to the differences in code provisions or simply the sizes and shapes of the members selected. Thus, the response of a SCBF designed according to a particular code may be very sensitive to designer selection of member sizes, slenderness ratios and degree of compactness. A comparison of Models 3BF and $3BF_3$, demonstrates that the probability curves are similar. However, if the structure is designed with R equals 3, the stiffness usually increases resulting in a shorter fundamental period smaller displacement demand and lower probability of exceeding the critical drifts levels. Similar observations are noted when 3BF(SCBF) and 3CF(BRBF) are compared. Because the code prescribes an R of 8 for BRBF, the fundamental period of a BRBF is usually longer.

Considering the service-level event, Models 3AF, 3BF and $3BF_3$ have 65.6, 76.6 and 51.6% probabilities of buckling a brace at one or more levels, respectively (see Table 4.6). This illustrates the need to consider likely local nonstructural damage during service-level events, and the possible need to replace braces following such events due to permanent lateral offsets. Considering the MCE-level event, Models 3AF, 3BF, $3BF_3$ and 3CF have 48.1, 70.8, 16.4 and 81.8% probabilities of exceeding 2.5% drift, respectively. Severe damage is expected for the models with high probabilities of exceeding the critical drifts.

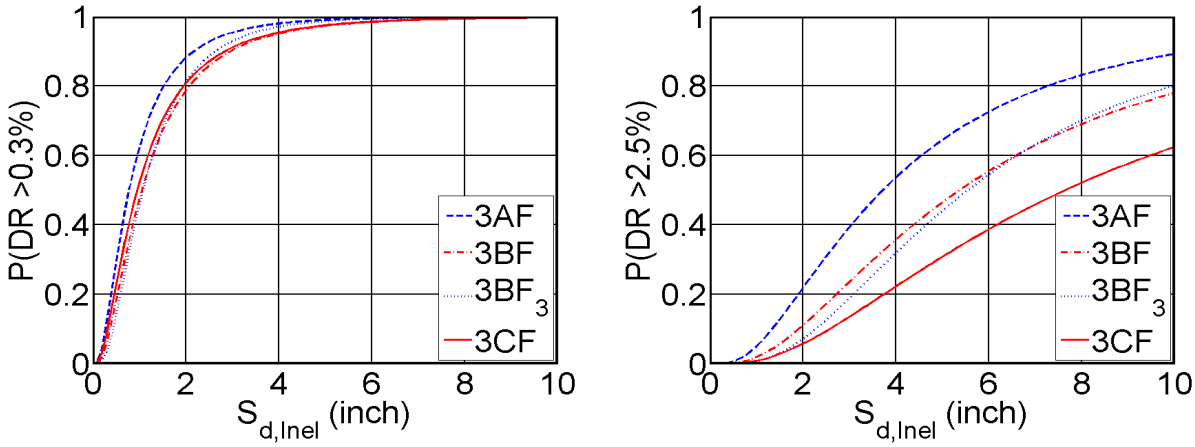

Figure 4.6 Probability of exceeding critical drift level for different models

Table 4.6 Probability of exceeding critical DR values for different models based on inelastic displacement spectra

Model		Hazard Level		
		50%, 50yrs	10%, 50yrs	2%, 50yrs
3AF,	P(DR>0.3%)	65.6%	82.8%	97.2%
T =0.36 sec.	P(DR>2.5%)	6.0%	15.6%	48.1%
3BF,	P(DR>0.3%)	76.6%	91.8%	99.5%
T =0.49 sec.	P(DR>2.5%)	9.7%	26.4%	70.8%
$3BF_3$,	P(DR>0.3%)	51.6%	72.1%	91.5%
T =0.35 sec.	P(DR>2.5%)	1.0%	3.9%	16.4%
3CF,	P(DR>0.3%)	88.3%	98.5%	100.0%
T =0.72 sec.	P(DR>2.5%)	10.4%	38.7%	81.1%

4.5.2 Residual Story Drift Ratio

Another response parameter of interest is the residual displacement in a structure, which is used to determine whether it is feasible to repair a structure following an earthquake. The residual story drift ratios of each model corresponding to different hazard levels are listed in Table 4.7. Figures 4.8 to 4.10 present the relation of the maximum residual story drift remaining at the end of the earthquake and spectrum displacement. The dots presented show the data points related to residual drift ratios. Two lines are superimposed, where one represents the median linear regression analysis result for the residual story drift ratio, whereas the other represents the previously reported maximum story drift ratio. The trend for residual displacements is such that the residual drifts become a larger fraction of the maximum drifts as the intensity of shaking increases.

Table 4.7 Median expected residual story drift ratio corresponding to different hazard levels based on inelastic displacement spectra

Eng. Demand Parameters	Hazard Level	3AF	3BF	$3BF_3$	3CF
Res. DR (rad.)	50/50	0.02%	0.04%	0.01%	0.10%
	10/50	0.07%	0.24%	0.03%	0.39%
	2/50	0.56%	3.97%	0.15%	1.95%

Figure 4.7 shows the residual drift for Model 3AF. The median expected maximum residual displacement became a more significant fraction of the peak story drift as the intensity of shaking increased. Although there are no data points that show the residual displacement exceeding the median peak story drift ratio, in some data points the residual displacement was rather close to the median peak story drift ratio. Considering the spectral displacement corresponding to Model 3AF at the service- and design-level events, the expected median maximum residual story drifts were 0.02% and 0.07%, respectively. For the MCE-level event, the expected median maximum residual story drift ratio was 0.56% radian.

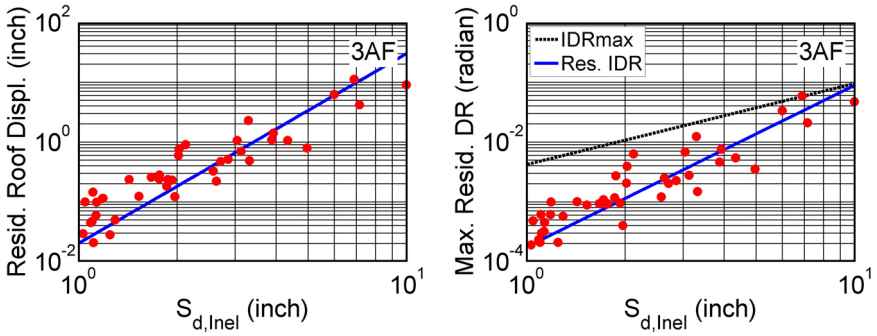

Figure 4.7 Relationship between residual deformation and $S_{d,Inel}$ of Model 3AF

Considering Model 3BF, there are no data points that show the residual displacement exceeding the median peak story drift ratio. Compared to Model 3AF, the residual displacement comprised a smaller portion of the peak story drift although the residual displacement of Model 3BF was larger for the three hazard levels. For the design- and MCE-level events, the expected median maximum residual story drift ratios were 0.24% and 3.97% radians, respectively. For the service-level event, the expected median maximum residual story drift ratio was 0.04%.

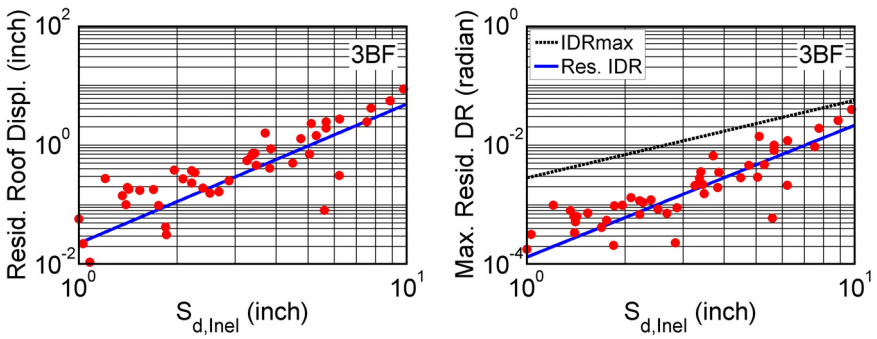

Figure 4.8 The relationship between residual deformation and $S_{d,Inel}$ for Model 3BF

For Model $3BF_3$ the maximum residual story drifts were considerably smaller than for Model 3BF. At the MCE-level event, the median expected maximum drift was on the order of 0.15% radian. This was in part, due to smaller lateral displacements, but also because the stronger and stiffer braces remained intact even under this large level of excitation.

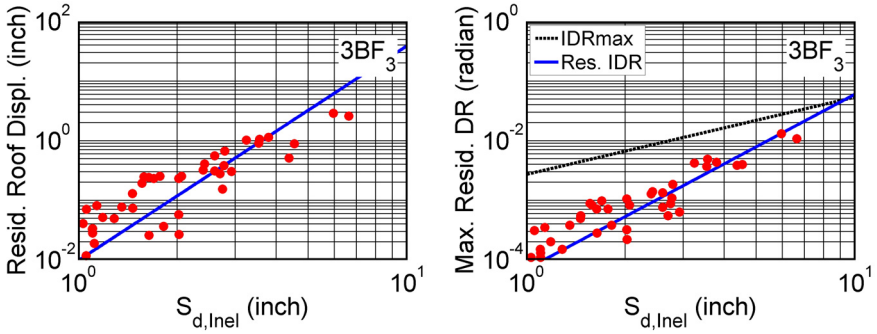

Figure 4.9 Relationship between residual deformation and $S_{d,Inel}$ of Model $3BF_3$

Figure 4.10 shows the residual drift for Model 3CF. Note that the residual drifts became a larger fraction of the maximum drifts as the intensity of shaking increased for the other models, but this trend was less pronounced in Model 3CF, because the regression lines were more parallel. In addition, Model 3CF tended to have larger residual displacement than the other models partly because of the longer fundamental period and partly because of the properties of the buckling restrained braced frames. The braces yielded rather than buckled under severe events because more energy was required to reverse the displacement as the yielding strength was normally greater than buckling strength. Consequently, Model 3CF exhibited larger residual displacement; its larger period and inelastic deformation were believed to be the cause of this increase. For the service-, design-, and MCE-level events, the expected median maximum residual story drift ratios were 0.10%, 0.39% and 1.45% radian, respectively.

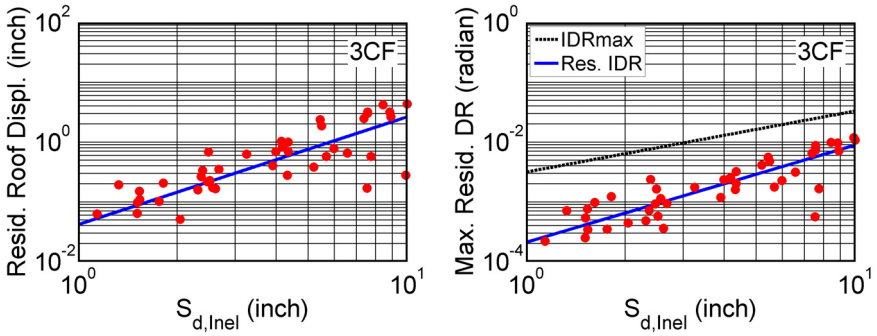

Figure 4.10 Relationship between residual deformation and $S_{d,Inel}$ of Model 3CF

4.6 Summary

According to the analyses, the performance of SCBF designed in compliance with ASCE/SEI 7-05 and 1997 NEHRP are quite similar.

Generally, the expected median maximum story drift ratios of SCBF with R of 6 were in excess of the values likely to cause buckling of the braces considered at the service-level event. Thus, after a frequent (service-level) earthquake, it would be necessary to replace one or more braces, and repair nonstructural damage to adjacent elements. The expected median maximum story drift ratios were also likely to exceed 2.5% radian at the MCE-level event, whereby the integrity of the beam to column connections can be assessed with confidence.

In contrast, Model $3BF_3$ resulted in median expected maximum DRs less than those needed to initiate buckling at the service-level event, and less than those likely to fracture the beam to column connections at the MCE-level event.

To provides a more useful indication of the response characteristics of the various models, the fragility curves were integrated with respect to the seismic hazard to obtain the probability for a given hazard level whereby, the maximum DR will exceed some key threshold. For the MCE-level event, Models 3AF and 3BF had 48.1% and 70.8% probabilities, respectively, of developing maximum story drifts greater than 2.5%. In Model $3BF_3$, the probability reduces to 16.4%. For the design-level event, these probabilities dropped to 15.6%, 26.4% and 3.9% for Models 3AF, 3BF and $3BF_3$, respectively. Interestingly, considering the service-level event, Models 3AF, 3BF, and $3BF_3$ had 65.6%, 76.6% and 51.6% probabilities, respectively, of having a brace buckle in one or more stories. Consideration of the likely motion of the brace in the buckled configuration is required to minimize significant local nonstructural damage during the service-level event. It is also necessary to consider replacing braces following service-level events due to the buckling of braces.

Residual lateral drifts were considered for all models as the intensity of ground shaking increased. In Model $3BF_3$, the residual drifts were in the reasonable range for post-earthquake repair for different hazard levels. The residual story drift ratio was 0.15% radian for the MCE-level event. Among all the analyses, the BRBF model had the largest residual drift partly because of the longer fundamental period and partly because of the characteristics of the buckling restrained braced frames.

Finally, the tendency to form a soft story was reduced for different seismic hazard levels if the R value is reduced from 6 to 3. Although the cost of constructing SCBF with an R of 3 would be higher and significant elastic response would be expected, the demands would be more consistent with the capacity of the connections and buckling braces considered herein. In the case of BRBF, although higher maximum drift demands and residual drift demands were expected, the tendency to form a soft story was less than for SCBF.

Chapter 5

Evaluation of Seismic Performance Factors Using FEMA P695 (ATC-63) Methodology

5.1 Introduction to FEMA P695 (ATC-63) Methodology

The FEMA P695 (ATC-63) project entitled "Quantification of Building System Performance and Response Parameters" developed a methodology to quantify building system performance and response parameters that can be used in seismic design. One of the key parameters investigated is the response modification coefficient (R factor). Other related design parameters including the system overstrength factor (Ω_0) and deflection amplification factor (C_d) were also addressed.

5.1.1 Seismic Performance Factors

Seismic performance factors are the key parameters for designing buildings. Figure 5.1 visually depicts these factors:

R: Response modification factor
Ω: Effective overstrength factor
C_d: Deflection amplification factor
V_{Ela}: Base shear of elastic system under design earthquake ground motions
V_{max}: Maximum base shear of the yielded system
V: Design base shear from building codes
Δ_{Ela}: Roof drift of elastic system under design earthquake ground motions
Δ_u: Roof drift corresponding to 80% of the maximum base shear after building yields
Δ_y: Idealized yielding roof drift
Δ_{des}: Roof drift corresponding to the design base shear
Δ: Roof drift of yielded system under design earthquake ground motions.

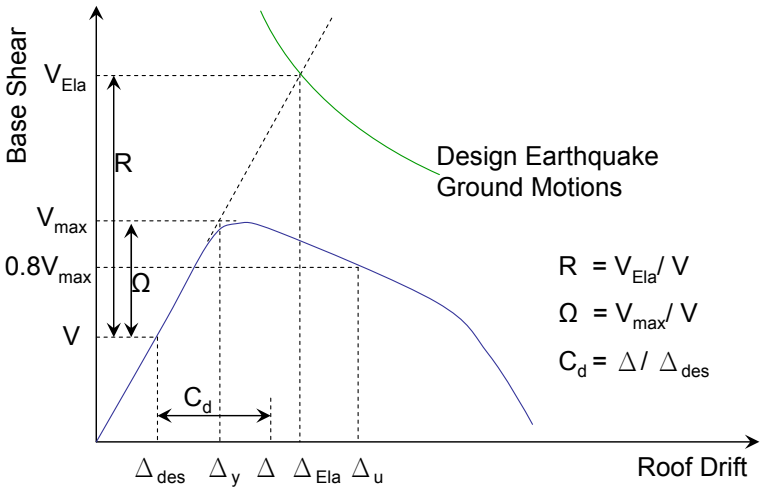

Figure 5.1 Illustration of the seismic performance factors as defined in the Commentary to the FEMA 450

FEMA P695 (ATC-63) quantified the system performance and response parameters considering the collapse-level response of buildings. The seismic performance factors (R, Ω ,C_d) are illustrated in Figure 5.2 in terms of single-degree-of-freedom spectral parameters (S_A, S_D) instead of base shear and roof drift. The conversion to spectral coordinates assumes that 100% of the effective seismic weight of the structure, W, participates in fundamental mode at the fundamental period, consistent with equation (5.1).

$$V = C_s W \tag{5.1}$$

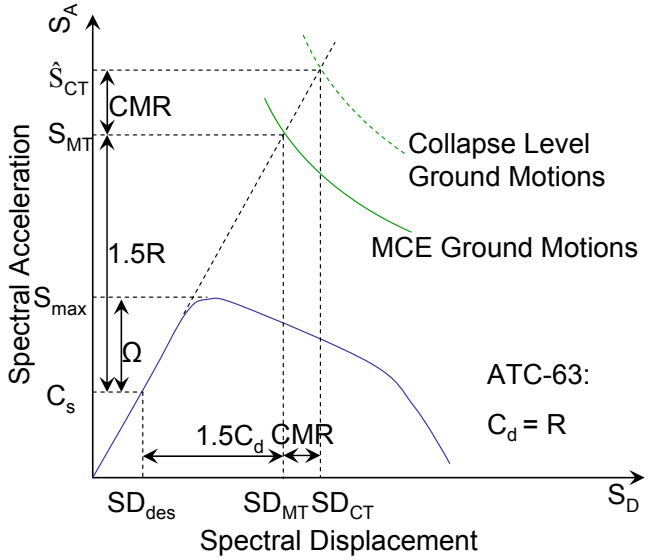

Figure 5.2 Illustration of the seismic performance factors as defined by FEMA P695

Figure 5.2 defines the seismic performance factors used in FEMA P695. The following terms are used:

$\hat{S}_{CT}$: Median spectral acceleration of collapse level earthquakes at the fundamental period of the building

S_{MT}: Spectral acceleration of Maximum Considered Earthquake (MCE) at the fundamental period of the building

S_{max}: Maximum lateral force of the yielded system normalized by the effective seismic weight of the building, W

C_s: Seismic response coefficient as determined in Section 12.8.1.1 of ASCE/SEI 7-05

SD_{CT}: Median spectral displacement of collapse level earthquakes at the fundamental period of the building corresponding to spectral response acceleration, $\hat{S}_{CT}$.

SD_{MT}: MCE spectral displacement at the fundamental period of the building corresponding to spectral acceleration, S_{MT}.

SD_{des}: Spectral displacement at the fundamental period of the building corresponding to seismic response coefficient, C_s.

CMR: Collapse Margin Ratio

The relationship in equation (5.2) is illustrated in Figure 5.2. The 1.5 factor accounts for the definition of design earthquake ground motions in ASCE/SEI 7-05 as being two-thirds of MCE ground motions.

$$1.5R = S_{MT}/C_s \tag{5.2}$$

The overstrength parameter Ω in Figure 5.2, which is calculated from a pushover analysis, is different from the overstrength factor Ω_0 of ASCE/SEI 7-05, which is used for design of non-ductile elements. Naturally, different designs of a building have different Ω values, and most appropriate Ω for a specific design can be considered to be Ω_0. The notation follows the definition of FEMA P695.

FEMA P695 (ATC-63) assumes the displacement of the yielded system at the MCE-level event is equal to $1.5C_d$ times SD_{des} and is equal to the MCE elastic system displacement, SD_{MT}. This relationship leads to:

$$C_d = R \tag{5.3}$$

Note that equation (5.3), instead of the prescribed values in ASCE/SEI 7-05, is used later in this chapter in the design of archetype buildings to evaluate system collapse resistance.

5.1.2 Collapse Margin Ratio

FEMA P695 (ATC-63) defined the collapse level ground motions as the intensity that would result in median collapse of the archetype building of interest. Nonlinear dynamic analyses were conducted by scaling up the intensity of 22-pair ground motion records until the median collapse intensity ($\hat{S}_{CT}$) was reached, where one-half of the ground motions caused collapse of the archetypes. The collapse margin ratio (*CMR*) was defined as the ratio of $\hat{S}_{CT}$ to the Maximum Considered Earthquake ground motion demand (S_{MT}, determined directly from the response

spectrum) at the fundamental period, T. As shown in Figure 5.2, the collapse level intensity is greater than the MCE-level intensity. The CMR defined in equation (5.4) is an index of the probability that a building will collapse at the MCE-level ground motion.

$$CMR = SD_{CT}/SD_{MT} = \hat{S}_{CT}/S_{MT} \tag{5.4}$$

5.2 Overview of FEMA P695 (ATC-63) Methodology

The methodology of FEMA P695 (ATC-63) is illustrated in Figure 5.3. It requires the use of a ground motion set, analysis methods, test data, design requirements, and a peer review.

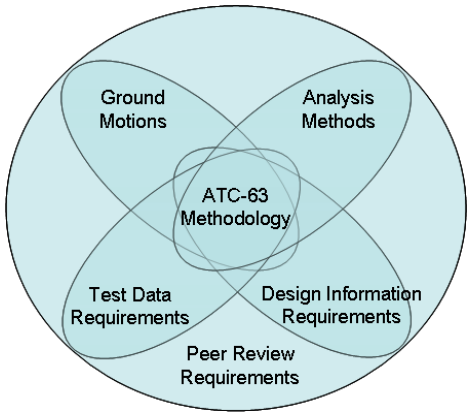

Figure 5.3 Illustration of FEMA P695 (ATC-63) methodology

Generally, FEMA P695 (ATC-63) is used to evaluate the design requirement of existing structural systems and also the newly developed systems. This chapter uses FEMA P695 (ATC-63) to evaluate special concentrically braced frames (SCBF) and buckling restrained braced frames (BRBF) designed according to the design provisions in ASCE/SEI 7-05. The application of FEMA P695 (ATC-63) approach focused on developing archetype buildings and nonlinear analysis models, and then performing and interpreting nonlinear analyses to assess collapse resistance. The next sections follow the FEMA P695 process step-by-step to evaluate current design requirements for SCBF and BRBF systems. Systems studied ranged from two to 16 stories in height. The archetypes were not re-designed to improve their collapse resisting force where needed.

Figure 5.4 gives more details of this evaluation process. The evaluation methodology consisted of requiring the system information, developing archetype buildings, constructing numerical models, performing nonlinear analysis, and evaluating the collapse resistance of a structural system.

The archetype buildings were designed covering a selected range of structural geometry and design parameters including structural configurations, seismic design categories, fundamental periods, etc. These archetypes were assembled into "performance groups" reflecting major changes in structural behaviors within the archetype design space.

The numerical models were developed with the calibration of available test data. The CMR was determined from the nonlinear dynamic analyses. Because the methodology in FEMA

P695 was a generalized procedure using a constant set of ground motions for different site, hazard level, and structural period of interest, to account for the frequency content (spectral shape) of the set of ground motions [Baker, 2005; Baker and Cornell, 2006], the CMR was modified by simplified spectral shape factors (SSF). The adjusted collapse margin ratio (ACMR) was computed by multiplying CMR by SSF (ACMR = SSF×CMR). The SSF depended on fundamental period, period-based ductility, and seismic design category of the building and was tabulated in Table 7-1 of FEMA P695.

Performance of each archetype and each performance group was evaluated by comparing the ACMR to the acceptable ACMR. The acceptable ACMR was determined based on the uncertainty factors of structural system; the quality of design requirements, test data, numerical modeling, and a prescribed set of ground motions contributed to the total system collapse uncertainty, which was denoted as $\beta_{TOT} = \sqrt{\beta_{RTR}^2 + \beta_{DR}^2 + \beta_{TD}^2 + \beta_{MDL}^2}$, where β_{RTR} was the record-to-record uncertainty, β_{DR} was the design requirement-related uncertainty, β_{TD} was the test data-related uncertainty, and β_{MDL} was the modeling-related uncertainty. Quality ratings for design requirements, test data, and numerical modeling were quantified by the following scale: (A) Superior, β = 0.10; (B) Good, β = 0.20; (C) Fair, β = 0.35; and (D) Poor, β = 0.50. The details to determine these uncertainty factors were described in FEMA P695.

The total system collapse uncertainty was used to determine the acceptance criteria, which is conditional probability of collapse (under MCE ground motions) of 10% in average for a performance group, and 20% for individual archetype. The acceptable $ACMR_{10\%}$ and $ACMR_{20\%}$ were tabulated in Table 7-3 of FEMA P695 based on the total system uncertainty and the acceptable probability of collapse. If an individual archetype or a performance group failed the evaluation (ACMR < Acceptable ACMR), the archetypes needed to be redesigned with modified seismic performance factors. The iterative process continued until adequate seismic performance factors were identified to provide a structural system with adequate collapse resistance.

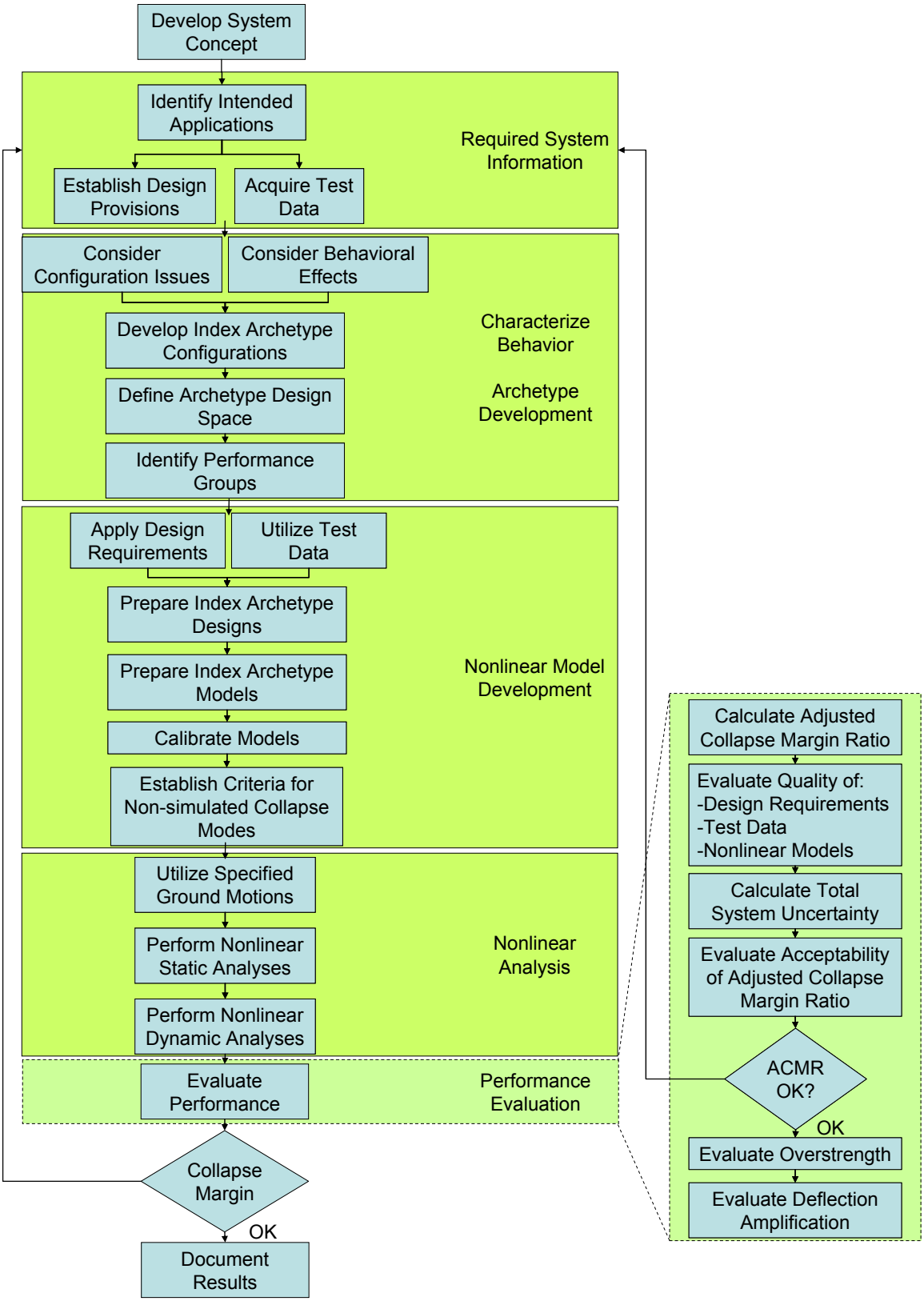

Figure 5.4 Process of evaluating seismic performance factors of buildings using FEMA P695 (ATC-63) methodology

The evaluation was conducted for both SCBF and BRBF systems; however, the evaluation in this section was not a complete study of the braced frames as there are a variety of structural configurations and design options. Here, only few of the representative braced frames were investigated. In the analyses, the global buckling behavior and possible rupture of the braces were explicitly considered in the computational models. Based on available test data, other critical non-simulated collapse modes were indirectly accounted for in beams, columns and other components based on available test data.

5.3 Structural System Information

5.3.1 Design Requirements

The archetype design — described in Appendix A — carefully followed the ASCE/SEI 7-05 design requirements. The beam-column connections and brace-to-framing connections of the archetypes were not designed in detail. It was assumed that they had adequate stiffness and strength, and detailed such that they would not fail before the braces fractured. The ASCE/SEI 7-05 requirements mainly focused on braces, beams and columns; therefore, many assumptions were used to design the beam-column connections, gusset-to-framing connections and brace-to-gusset connections, with the understanding that these assumptions might have an effect on the overall behavior of the system. Therefore, these design requirements should not be categorized as "A-Superior" according to the FEMA P695 methodology; however, a designation of "B-Good" reflects the degree of confidence in the design requirements for the SCBF and BRBF archetypes.

5.3.2 Test Data

Testing of braces, braced frame components, and braced frames has a long history [Black et al., 1980, 2004; Zayas et al., 1980; Tremblay, 2002, 2008; Powell et al., 2008; Yoo et al., 2008; Yang and Mahin, 2005; Uriz and Mahin, 2008]. The material properties derived from these tests may vary depending on the date and location of the tests. To calibrate the numerical models used herein, data from recent tests conducted on braces and braced frames [Yang and Mahin, 2005; Uriz and Mahin, 2008] at Pacific Earthquake Engineering Research Center were adopted. The test data included the cyclic responses of tube braces, pipe braces, buckling restrained braces, conventional buckling chevron braced frames, and chevron BRB frames. Although considerable test data are available, important limitations need to be considered:

1. Variations in member sizes
   The brace size of the SCBF test specimens and conventional braces were similar, around six inches across the section. The archetypes may incorporate heavier or lighter sections, which might affect local and global cyclic responses. In addition, the beam and column sizes likely differ from those encountered in the archetypes.
2. Variations in loading conditions
   Due to the limitations of the test setup for laboratory tests, the SCBF and BRBF were not subjected to gravity load during the tests. Also, the cyclic load was applied only on the roof level. The idealized load pattern reduced the complexity in order to examine the

component responses, hence the uniform force distribution may or may not representative of seismic loading.

3. Absence of slabs
   The concrete slabs were not included in the test specimens; therefore, changes in stiffness and strength because of the intended or accidental composite behavior were not reflected in the test results used to calibrate the models.
4. Variations in drift range
   The frame specimens tested were subjected to large story drifts able to significantly damage the critical elements. For the safety and protection of the experimental facilities, the tests did not continue until the specimens collapsed; therefore, the structural response between the stages of significant damage and total collapse remains largely unknown.

In sum, although test data are available for SCBF and BRBF elements and frames, due to limitations and variations of experimental procedures and intentions, the test data cannot provide the exact requirements of model parameters and behavior. Accordingly, for the purpose of assessing the total uncertainty, the test data is categorized as "B-Good" in FEMA P695 (ATC-63).

5.4 Identification of Archetype Configurations

The configuration of double story X was adopted for the archetypes because of its cost benefit and compared to chevron or inverted V braced frames, the loading path in double story X braced frames is more straightforward. The unbalanced load in beams due to the buckling or fracture of braces in chevron and inverted V braced frames can be avoided if the double story configuration is used, allowing for a reduction the size of the beam. In addition, the double story X configuration does not have the braces intersect within a story as the single-story X configuration does, and the potential failure in the brace-to-brace connections can be avoided. This configuration reflects current design trends in real practice.

There were ten archetypes designed for SCBFs (summarized in Table 5.1) and ten designed for BRBFs (summarized in Table 5.2). The ten archetypes represented the combination of two seismic demand intensities and five building heights, namely 2, 3, 6, 12, and 16 stories. Figure 4.1(b) shows the typical layout of the archetypes. The braced bays (for both SCBFs and BRBFs) were located at the perimeter of the structures. For the 2, 3 and 6-story archetypes, one bay of braced frame was used in each side of the perimeter. For the 12 and 16-story archetypes, two nonadjacent bays of braced frame were used in each side of the perimeter. The story height for all archetypes was 15 ft, except for the 2-story series, which had a story height of 10 ft. The floor plan was 180 ft by 120 ft. Beam spans were 30 ft typically, except for the 2-story archetypes where the span was 20 ft.

Table 5.1 and Table 5.2 show the performance groups of SCBFs and BRBFs archetypes, respectively. The archetypes intended to cover braced frames in both the short- and long-period range, and were evaluated for high- and low-seismic demands. The performance groups are summarized as follows:

- Maximum seismic design criteria (SDC D_{max}), short period
- Maximum seismic design criteria (SDC D_{max}), long period
- Minimum seismic design criteria (SDC D_{min}), short period
- Minimum seismic design criteria (SDC D_{min}), long period

The high- and low-seismic demands were represented by the minimum and maximum de-

mands possible in Seismic Design Category (SDC) D. The archetypes were designed for a Site Class D soil conditions and design lateral loads of S_s = 1.5g and S_1 = 0.6g for SDC D_{max}, and S_s = 0.55g and S_1 = 0.13g for SDC D_{min}.

Table 5.1 Performance groups for evaluation of special steel concentrically braced frame archetypes

Group No.	Grouping Criteria				Number of Archetypes
	Basic Config.	Design Load Level		Period Domain	
		Gravity	Seismic		
PG-1SCB	Double Story X-Braces	Typical	SDC D_{max}	Short	2[1]
PG-2SCB				Long	3[2]
PG-3SCB			SDC D_{min}	Short	2[1]
PG-4SCB				Long	3[2]

1. Short-period performance groups, PG-1 and PG-3, include 2-story and 3-story archetypes.
2. Long-period performance groups, PG-2 and PG-4, include 6-story, 12-story and 16-story archetypes.

Table 5.2 Performance groups for evaluation of buckling-restrained brace frame archetypes

Group No.	Grouping Criteria				Number of Archetypes
	Basic Config.	Design Load Level		Period Domain	
		Gravity	Seismic		
PG-1BRB	Double Story X-Braces	Typical	SDC D_{max}	Short	2[1]
PG-2BRB				Long	3[2]
PG-3BRB			SDC D_{min}	Short	2[1]
PG-4BRB				Long	3[2]

1. Short-period performance groups, PG-1 and PG-3, include 2-story and 3-story archetypes.
2. Long-period performance groups, PG-2 and PG-4, include 6-story, 12-story and 16-story archetypes.

Table 5.3 Special steel concentrically braced frame archetype design properties

Archetype Design ID Number	No. of Stories	Key Archetype Design Parameters						
		Analysis Procedure	Seismic Design Criteria					$S_{MT}(T)$ [g]
			SDC	*R*	*T* [sec]	T_1 [sec]	*V/W* [g]	
Performance Group No. PG-1SCB								
2SCBFDmax	2	ELF	D_{max}	6	0.26	0.40	0.167	1.50
3SCBFDmax	3	ELF	D_{max}	6	0.49	0.58	0.167	1.50
Performance Group No. PG-2SCB								
6SCBFDmax	6	ELF	D_{max}	6	0.82	1.02	0.122	1.10
12SCBFDmax	12	ELF	D_{max}	6	1.38	1.91	0.073	0.65
16SCBFDmax	16	RSA	D_{max}	6	1.71	3.16	0.059	0.53
Performance Group No. PG-3SCB								
2SCBFDmin	2	ELF	D_{min}	6	0.28	0.55	0.083	0.75
3SCBFDmin	3	ELF	D_{min}	6	0.52	0.80	0.064	0.58
Performance Group No. PG-4SCB								
6SCBFDmin	6	ELF	D_{min}	6	0.88	1.51	0.038	0.34
12SCBFDmin	12	ELF	D_{min}	6	1.47	2.64	0.023	0.20
16SCBFDmin	16	RSA	D_{min}	6	1.83	4.67	0.022	0.16

Table 5.4 Buckling-restrained brace frame archetype design properties

Archetype Design ID Number	No. of Stories	Key Archetype Design Parameters						
		Analysis Procedure	Seismic Design Criteria					$S_{MT}(T)$ [g]
			SDC	*R*	*T* [sec]	T_1 [sec]	*V/W* [g]	
Performance Group No. PG-1BRB								
2BRBFDmax	2	ELF	D_{max}	8	0.40	0.50	0.125	1.50
3BRBFDmax	3	ELF	D_{max}	8	0.73	0.80	0.103	1.23
Performance Group No. PG-2BRB								
6BRBFDmax	6	ELF	D_{max}	8	1.23	1.35	0.061	0.73
12BRBFDmax	12	RSA	D_{max}	8	2.06	2.82	0.044	0.44
16BRBFDmax	16	RSA	D_{max}	8	2.56	3.73	0.044	0.35
Performance Group No. PG-3BRB								
2BRBFDmin	2	ELF	D_{min}	8	0.43	0.68	0.059	0.70
3BRBFDmin	3	ELF	D_{min}	8	0.78	1.25	0.032	0.38
Performance Group No. PG-4BRB								
6BRBFDmin	6	ELF	D_{min}	8	1.31	2.34	0.022	0.23
12BRBFDmin	12	RSA	D_{min}	8	2.21	3.49	0.022	0.14
16BRBFDmin	16	RSA	D_{min}	8	2.74	4.83	0.022	0.11

Table 5.3 and Table 5.4 summarize the properties of the SCBF and BRBF archetype designs needed to evaluate SDC D, including code-calculated structural period, fundamental period of numerical model, and the design base shear.

The building height limit for steel braced frames was 240 ft in this evaluation, which was ex-

tended from the limit of 160 ft prescribed in ASCE/SEI 7-05. Diaphragms were assumed to be constructed with concrete filled metal deck with a length to width ratio of less than 3. The structures were assumed to have no horizontal irregularities allowing them to be idealized as being rigid in plane. The archetypes were regular in plan and the braced frames were located at the perimeter of the buildings. The redundancy factor (ρ) was equal to 1.0 for the archetypes as determined by analysis. The analytical procedures used in the design of the archetypes are listed in Table 5.3 and Table 5.4 (ELF represents Equivalent Lateral Force analysis and RSA represents Modal Response Spectrum Analysis). The selection of analytical procedures followed ASCE/SEI 7-05. The design of the archetypes was not governed by P-delta effects according to design analyses.

Braces in the SCBF and BRBF models were assumed to have pin connections to the framing. Rigid in plane offsets were assumed at the beam-column connections and brace-to-framing connections. The effective length of the braces corresponded to 70 percent of the work-point-to-work-point length. The effective stiffness of the BRBs was modified to 1.4 times the stiffness computed using only the steel core to account for the stiffness contribution from tapered and connection areas of BRBs.

Fully restrained connections were adopted in designing the beams, which were assumed to be laterally supported at quarter points along the span. In addition to the typical load combinations, axial forces due to the yielding and fracture of braces were applied to the beams where the braces intersect at the ends. The axial forces conservatively accounted for the over-strength and strain hardening of the brace under tension and neglected the compression strength of the other. According to the current code, those beams where the braces intersect at the mid-span were not explicitly required to be designed to take the unbalanced axial loads from differences in tension and compression of the braces. As such, the beam sizes on the even numbered stories were usually greater than those at the odd numbered stories.

Columns of the braced frames are fixed at the base. They were orientated to resist lateral force by strong-axis bending. Overstrength factors for the seismic load were taken from ASCE/SEI 7-05.

The gravity systems were idealized as leaning columns, and P-delta effects were considered by applying gravity load on the leaning columns. The gravity systems were assumed to be axially rigid and as stipulated in FEMA P695 to have no lateral resisting capacity. Their failure was not considered in analyses of the archetypes.

Two-dimensional frames were designed disregarding possible lateral-torsional behavior of structural members. It was assumed that the frame members are adequately supported laterally. Also, global torsion effects due to mass and stiffness eccentricities were not accounted for in the design.

5.5 Archetype Analysis Models

The numerical models were developed based on the parameters discussed in Chapters 3 and 4. OpenSees fiber models were used considering the fatigue material property, Rayleigh damping, and one leaning column.

5.5.1 Collapse Modes Simulation

The evaluation in FEMA P695 uses non-simulated collapse limit states to consider the significant failure modes that are not possible or not practical to be directly simulated. Non-simulated collapse limit states were established in cooperation with the Methodology peer review panel. In the analytical models of the archetypes, the collapse modes due to the damage of the braces were well calibrated with test data. Although the brace failure was one of the most critical indices to identify if the archetypes collapse, there were other collapse modes that were not explicitly simulated but the force and deformation were tracked (i.e. non-simulated collapse modes) for limit state checks; these collapse modes needed to be incorporated in this evaluation through post-processing or adequate capacity design. These failure modes considered in the numerical models are summarized in Table 5.5; all the failure modes listed were incorporated in the evaluation for limit state checks except for the neglected failure modes.

Table 5.5 Critical deterioration modes of steel braced frame buildings

Critical Deterioration Modes	Explicitly Modeled	Non-Simulated	Neglected in Model	Empirical Criteria
Braces				
Local buckling		◎		
Global buckling	◎			
Net-section failure			◎	
Low-cycle fatigue fracture	◎			
Beam				
Lateral torsional buckling			◎	
Column				
Torsion			◎	
Fracture				◎ (10% Drift)
Tension failure (at splice/ base plate)		◎		
Global buckling		◎		
Connections			◎	
3D torsion of system			◎	

Many non-simulated collapse modes and neglected failure modes can be avoided by detailed design and quality control during construction. The global buckling of columns was not explicitly modeled, but the force and deformation demand of columns were tracked to check if the columns failed.

Earlier tests [Newell and Uang, 2006] on wide flange columns under cyclic interactions of axial and lateral loading demonstrated that the columns begin to loss their capacity after 7% to 9% story drift ratio. The member sizes of the column test specimens in that study were similar to those of the archetypes. The critical story drift capacity of columns was modified to be incorporated in component limit state checks for collapse modes. Because the boundary condi-

tions of the test specimens were more constrained than those of the archetypes studied herein, the story drift capacity for the non-simulated collapse of columns was modified to 10% radians and was used in the evaluation as the collapse criteria. If the numerical model of these archetypes doid not show collapsing responses at large ground motion intensity, it was assumed to collapse if the drift exceeded 10% due to the high probability of column failure.

5.5.2 Uncertainty Due to Model Quality

For the purpose of assessing uncertainty, this modeling is rated as "B-Good." The brace behavior is believed to control the failure modes of the SCBFs and BRBFs. The brace models were calibrated with test data to capture the failure responses satisfactorily. Moreover, the braced frame models incorporated with the brace models matched the test data of two-story braced frames. Although some non-simulated collapse modes were not explicitly included in the analysis models, they were taken into consideration based on the test data. Although, the fiber-based element had the limited capacity to simulate the local buckling behavior, the modeling capacity of capturing the local buckling behavior can be improved. Also, the 3-D effects were not explicitly modeled. Essentially, this modeling approach was well calibrated to large amounts of data and able to simulate structural response up to collapse, but there was still room for improvement. As such, the model quality in this study is rated as "B-Good" in FEMA P695 (ATC-63) as approved by the peer review panel.

5.6 Nonlinear Structural Analyses

Nonlinear static and dynamic analyses were performed with OpenSees models to identify the system behavior for the evaluation. To compute the system overstrength factor (Ω_0) and to help verify the structural model, monotonic static pushover analysis was used. This pushover was based on the lateral load pattern prescribed in ASCE/SEI 7-05. Figure 5.5 shows examples of the pushover curve for the three-story archetypes.

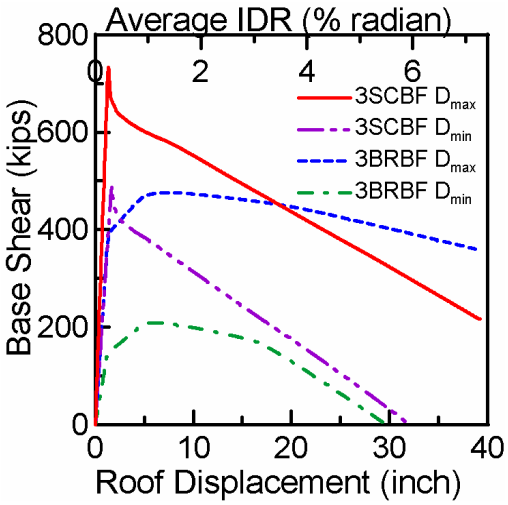

Figure 5.5 Pushover curve for three story archetypes

For 3SCBFDmax, the buckling of braces occurred at about 0.002 roof drift ratio, which was

also the drift ratio of the maximum strength; the corresponding base shear was V_{max} = 730 kips. The strength then dropped quickly, because the braces rapidly lose compression capacity. The P-delta effect contributed to the observed negative stiffness. The overstrength factor can be computed as $\Omega = V_{max} / V$, and the period-based ductility can be computed as $\mu_T = \Delta_u/\Delta_y$, where V_{max}, Δ_u, and Δ_y are defined in Figure 5.1. V_{max} is the maximum base shear strength at any point on the pushover curve; V is the design base shear in equation (5.1); Δ_u is the roof displacement at the point of 20% strength loss ($0.8V_{max}$); and Δ_y is effective yield displacement. For 3SCBFDmax, Ω = 730 (kips)/519 (kips) = 1.41, and μ_T = 0.012 (radian)/0.002 (radian) = 6.01. The overstrength factor and ductility capacity of all SCBF archetypes are listed in Table 5.6.

For 3BRBFDmin, the braced frame yielded at about 0.003 roof drift ratio. The maximum strength of 210k occurred at around 0.01 roof drift ratio with the negative stiffness coming from the P-delta effect. The overstrength factor and ductility capacity of BRBF archetypes are listed in Table 5.7.

To compute the collapse capacity for each archetype design, incremental dynamic analysis (IDA) approach was implemented using the far-field ground motion set and ground motion scaling method. Figure 5.6 illustrates how IDA was used to compute the collapse capacity of archetype 3SCBFDmax. The spectral acceleration at collapse (S_{CT}) was computed for each of the 44 ground motions of the Far-Field Set, and then the median collapse level ($\hat{S}_{CT}$) was computed, which was 2.4 g for 3SCBFDmax. The collapse margin ratio (*CMR*) was 1.60 (see Table 5.6) for archetype 3SCBFDmax.

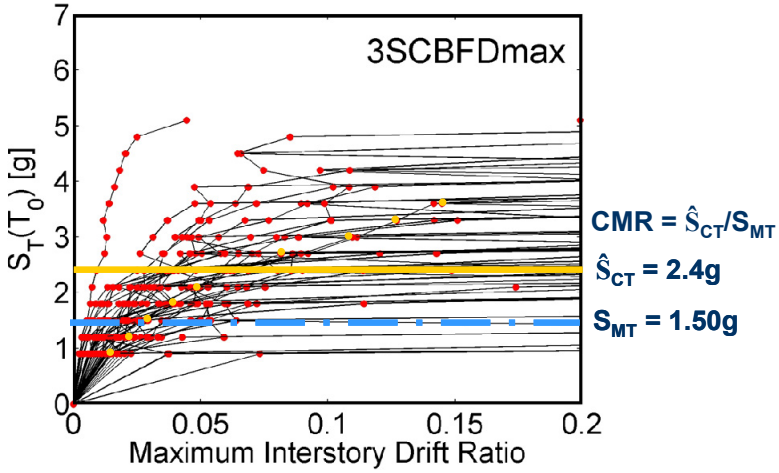

Figure 5.6 IDA of archetype 3SCBFDmax

Static pushover analyses were completed and the IDA method was applied to each of the ten archetype designs for SCBFs and ten for BRBFs. Table 5.6 and Table 5.7 summarize the results of these analyses. These IDA results showed that the two-story SCBFs and BRBFs had lower CMR than the other archetypes. Generally, the 12-story SCBF and 3-story BRBF have higher CMR. The trend also showed that although the SCBFs designed for lower seismic demand had higher CMR, this trend was not obvious for BRBFs.

5.7 Performance Evaluation

Table 5.8 and Table 5.9 show the final results and acceptance criteria for each of SCBFs and BRBFs, respectively. The summary includes the CMR computed from the IDA, the spectral shape factor (SSF), and the adjusted collapse margin ratio (ACMR); Section 5.2 summarized the definition of these parameters.

The results in Table 5.8 show that, generally, the SCBF archetypes with short periods had lower ACMR values and may have unacceptable collapse resistance. The 16-story archetypes were designed using the RSA procedure and had acceptable ACMR values. The two-story SCBF designed for the highly seismic scenario (SDC D_{max}) did not satisfy the FEMA P695 criteria. Although archetypes with long period were more likely to pass the acceptance criteria, 6-story and 3-story SCBF archetypes had similar ACMR. The results also show that the archetypes designed for the highly seismic scenario (SDC D_{max}) tended to have lower ACMR than those designed for the low seismic scenario (SDC D_{min}).

The results for BRBFs in Table 5.9 show more variation, but the BRBF archetypes with short periods generally had lower ACMR values and had the highest collapse probability. The two-story BRBFs had especially low ACMR compared to the other BRBF archetypes. For the long-period performance group, the 12-story archetypes had lower ACMR. The results of two-story and 6-story BRBF archetypes show that the archetypes designed for the highly seismic scenario (SDC D_{max}) did not necessarily have lower ACMR. The ACMR for the three-story BRBFs designed for D_{max} and D_{min} demands were similar.

Comparing the results for SCBF and BRBF archetypes, the SCBFs had smaller ACMR values compared to BRBFs. The two-story SCBF designed for SDC D_{max} did not pass the FEMA P695 criteria, and an adjustment in the design requirements may be necessary. Because of the low ACMR values of the two-story SCBF designed for SDC D_{max}, the mean ACMR of short-period performance group of SCBF designed for SDC D_{max} was too low to pass the acceptance criteria. All other SCBF and BRBF archetypes and performance groups satisfied the collapse resistance criteria.

Table 5.6 Summary of collapse results for special steel concentrically braced frame archetype designs

Archetype Design ID Number	Design Configuration			Pushover and IDA Results			
	No. of Stories	Gravity Loads	Seismic SDC	Static Ω	S_{MT} [T] (g)	S_{CT} [T] (g)	*CMR*
Performance Group No. PG-1SCB							
2SCBFDmax	2	Typical	D_{max}	1.44	1.50	1.5	1.00
3SCBFDmax	3	Typical	D_{max}	1.41	1.50	2.4	1.60
Performance Group No. PG-2SCB							
6SCBFDmax	6	Typical	D_{max}	1.34	1.10	1.8	1.64
12SCBFDmax	12	Typical	D_{max}	1.60	0.65	2.1	3.23
16SCBFDmax	16	Typical	D_{max}	2.11	0.53	1.4	2.64
Performance Group No. PG-3SCB							
2SCBFDmin	2	Typical	D_{min}	1.38	0.75	1.3	1.73
3SCBFDmin	3	Typical	D_{min}	2.41	0.58	2.1	3.62
Performance Group No. PG-4SCB							
6SCBFDmin	6	Typical	D_{min}	1.86	0.34	1.2	3.53
12SCBFDmin	12	Typical	D_{min}	2.20	0.20	1.2	6.00
16SCBFDmin	16	Typical	D_{min}	1.56	0.16	0.7	3.53

Table 5.7 Summary of collapse results for buckling-restrained braced frame archetype designs

Archetype Design ID Number	Design Configuration			Pushover and IDA Results			
	No. of Stories	Gravity Loads	Seismic SDC	Static Ω	S_{MT} [T] (g)	S_{CT} [T] (g)	*CMR*
Performance Group No. PG-1BRB							
2BRBFDmax	2	Typical	D_{max}	1.31	1.50	2.6	1.73
3BRBFDmax	3	Typical	D_{max}	1.48	1.23	5.7	4.63
Performance Group No. PG-2BRB							
6BRBFDmax	6	Typical	D_{max}	1.47	0.73	2.4	3.29
12BRBFDmax	12	Typical	D_{max}	1.17	0.44	1.0	2.27
16BRBFDmax	16	Typical	D_{max}	1.00	0.35	1.1	3.14
Performance Group No. PG-3BRB							
2BRBFDmin	2	Typical	D_{min}	1.44	0.70	1.2	1.71
3BRBFDmin	3	Typical	D_{min}	2.11	0.38	2.1	5.53
Performance Group No. PG-4BRB							
6BRBFDmin	6	Typical	D_{min}	1.28	0.23	0.7	3.04
12BRBFDmin	12	Typical	D_{min}	1.44	0.14	0.4	2.86
16BRBFDmin	16	Typical	D_{min}	1.15	0.11	0.5	4.55

Table 5.8 Summary of collapse performance evaluations of special steel concentrically braced frame archetypes

Arch. Design ID No.	Design Configuration		Computed Overstrength and Collapse Margin Parameters					Acceptance Check	
	No. of Stories	SDC	Static Ω	*CMR*	μ_T	*SSF*	*ACMR*	Accept. *ACMR*	Pass/ Fail
Performance Group No. PG-1SCB									
2SCBFDmax	2	D_{max}	1.44	1.00	4.3	1.22	1.22	1.56	Fail
3SCBFDmax	3	D_{max}	1.41	1.60	6.1	1.28	2.05	1.56	Pass
Mean of Performance Group:			**1.42**	**1.30**	**5.2**	**1.25**	**1.63**	**1.96**	**Fail**
Performance Group No. PG-2SCB									
6SCBFDmax	6	D_{max}	1.34	1.64	6.6	1.36	2.23	1.56	Pass
12SCBFDmax	12	D_{max}	1.60	3.23	3.2	1.32	4.26	1.56	Pass
16SCBFDmax	16	D_{max}	2.11	2.64	1..8	1.21	3.20	1.56	Pass
Mean of Performance Group:			**1.69**	**2.50**	**3.8**	**1.30**	**3.23**	**1.96**	**Pass**
Performance Group No. PG-3SCB									
2SCBFDmin	2	D_{min}	1.38	1.73	5.8	1.12	1.94	1.56	Pass
3SCBFDmin	3	D_{min}	2.41	3.62	3.0	1.08	3.91	1.56	Pass
Mean of Performance Group:			**1.90**	**2.68**	**4.4**	**1.10**	**2.93**	**1.96**	**Pass**
Performance Group No. PG-4SCB									
6SCBFDmin	6	D_{min}	1.86	3.53	3.9	1.15	4.06	1.56	Pass
12SCBFDmin	12	D_{min}	2.20	6.00	3.4	1.23	7.38	1.56	Pass
16SCBFDmin	16	D_{min}	1.56	3.53	1.2	1.06	4.64	1.56	Pass
Mean of Performance Group:			**1.87**	**4.63**	**2.8**	**1.15**	**5.36**	**1.96**	**Pass**

Table 5.9Summary of collapse performance evaluations of buckling-restrained braced frame archetypes

Arch. Design ID No.	Design Configuration		Computed Overstrength and Collapse Margin Parameters					Acceptance Check	
	No. of Stories	SDC	Static Ω	*CMR*	μ_T	*SSF*	*ACMR*	Accept. *ACMR*	Pass/ Fail
Performance Group No. PG-1BRB									
2BRBFDmax	2	D_{max}	1.31	1.73	11.9	1.33	2.31	1.56	Pass
3BRBFDmax	3	D_{max}	1.48	4.63	22.7	1.39	6.44	1.56	Pass
Mean of Performance Group:			**1.40**	**3.18**	**17.3**	**1.36**	**4.37**	**1.96**	**Pass**
Performance Group No. PG-2BRB									
6BRBFDmax	6	D_{max}	1.47	3.29	15.5	1.53	5.03	1.56	Pass
12BRBFDmax	12	D_{max}	1.17	2.27	4.0	1.4	3.18	1.56	Pass
16BRBFDmax	16	D_{max}	1.00	3.14	3.1	1.32	4.15	1.56	Pass
Mean of Performance Group:			**1.21**	**2.90**	**7.5**	**1.42**	**4.12**	**1.96**	**Pass**
Performance Group No. PG-3BRB									
2BRBFDmin	2	D_{min}	1.44	1.71	6.6	1.13	1.94	1.56	Pass
3BRBFDmin	3	D_{min}	2.11	5.53	10.5	1.2	6.63	1.56	Pass
Mean of Performance Group:			**1.77**	**3.62**	**8.5**	**1.17**	**4.28**	**1.96**	**Pass**
Performance Group No. PG-4BRB									
6BRBFDmin	6	D_{min}	1.28	3.04	6.4	1.28	3.90	1.56	Pass
12BRBFDmin	12	D_{min}	1.44	2.86	3.1	1.21	3.46	1.56	Pass
16BRBFDmin	16	D_{min}	1.15	4.55	2.0	1.15	5.23	1.56	Pass
Mean of Performance Group:			**1.29**	**3.48**	**3.8**	**1.21**	**4.19**	**1.96**	**Pass**

5.8 Evaluation of Ω

The overstrength factors for each archetype are given in Table 5.6 for SCBF and Table 5.7 for BRBFs, with no specific identifiable trends. In general, the overstrength factors varied between 1.3 and 2.4 for SCBFs, and not necessarily correlated to SDC. For BRBF archetypes, the overstrength factors varied between 1.0 and 2.1.

Some of the overstrength factors were observed to be low. It appeared this was because the damage was concentrated in a certain story of the archetypes from first-mode pushover analysis. The overstrength factors could even be lower than 1.0. Figure 5.7 illustrates the relationship between story shear demand and capacity; although the story shear capacity of each story was greater than the design story shear, the design story shear demand and capacity were similar in the 9th story. Under the first-mode pushover loads, the 9th story was the first story to reach the capacity. As such, the damage was concentrated in the 9th story under the first-mode pushover loads, resulting in the peak base shear associated with the story shear capacity of the 9th story. The resulting peak base shear was less than design base shear and therefore, the overstrength factor was less than 1.0. The capacity of the story where the damage was concentrated under the first-mode pushover analysis dominated the maximum strength of the building. When the deformation under the first-mode pushover loads was more uniform along the height of the building or was concentrated in the lower stories, the overstrength factor was more likely to be large.

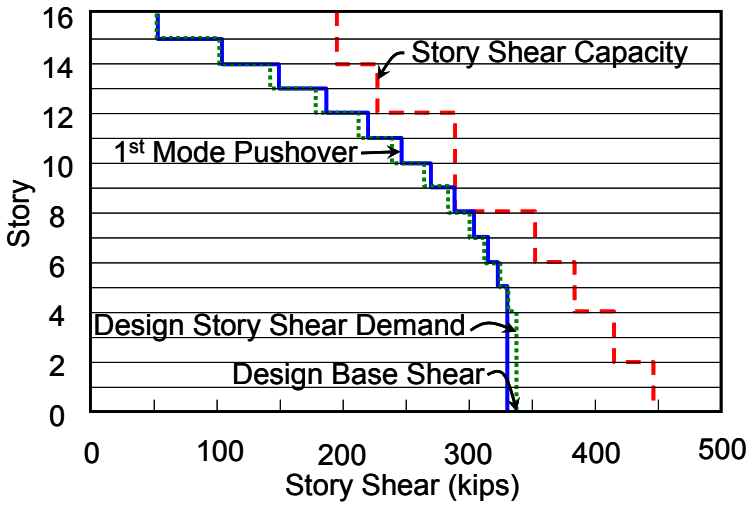

Figure 5.7 Illustration of story shear demand and capacity

5.9 Summary

The BRBF archetypes passed the evaluation but the two-story SCBF designed for SDC D_{max} failed the FEMA P695 criteria. As such, the seismic performance factors of ASCE/SEI 7-05 seem appropriate for BRBFs based on the methodology and the archetypes, but may need adjusting for short-period SCBFs.

5.9.1 Observations on the Methodology

The spectral shape factors (SSF) are dependent on the ductility established by nonlinear static analysis. For the untypical pushover curve of SCBFs with negative post-yield tangent stiffness, FEMA P695 may underestimate the ductility demand of the system and may err on determining the ACMR. The evaluation is likely on the conservative side.

The quality ratings are based on subjective judgment; therefore it is important to study the reviews and comments from engineers and researchers in order to have confidence in the quality ratings.

Although all the archetypes were designed based on the design requirements of current codes, variations do exist between designers as the same design codes can be satisfied with different selections of structural layout, member size and detailing. The subjectivity of the design process warrants that design alternatives be thoroughly studied. The evaluation provided here gave a preliminary assessment of the implementation of the Methodology to SCBFs and BEBFs.

Most of the SCBF and BRBF archetypes passed the evaluation although some performed better than others. The seismic performance factors of ASCE/SEI 7-05 seem appropriate for BRBFs, but may need adjusting for SCBFs based on the Methodology and the archetypes. Those archetypes that barely passed the evaluation may fail if the uncertainty increases. One reason why certain archetypes fail or come close to failing is the R factors may be too large for low-rise archetypes. Because drift may control the design, in the taller archetypes, member sizes are typically increased to obtain more stiffness; with the increase in stiffness comes an increase in strength. Low-rise archetypes typically satisfy drift requirements and members sizes need not be increased beyond those required for strength. They thus have less reserve capacity to resist collapse.

5.9.2 Observations on System Performance

In terms of analysis procedure, the Equivalent Lateral Force Analysis (ELF) and Modal Response Spectrum Analysis (RSA) had a great effect on the member size for higher-rise braced frames than lower-rise braced frames. Take archetype 6SCBFDmax for example, the difference of force demand in the members determined by ELF and RSA is within 10%. For the higher archetype 16SCBFDmax, the difference increase to 50%. For structures, where the force governs the design criteria, the maximum difference of design lateral force between ELF and RSA is 15% according to the current code; for structures, where the drift governs the design criteria, the design lateral force calculated from the RSA can be much smaller compared to the ELF. For high-rise SCBF and BRBF archetypes, because of the selected design configurations (number of bays of braced frames, SDC, gravity, etc.), the ELF resulted in uncommonly large member sizes; as such, to be representative of the evaluation on the structural systems, the RSA was used for the design of the archetypes.

The pushover curve demonstrated that the buckling of braces for some SCBFs caused a sudden drop of strength globally. This kind of response resulted in a small period-based ductility using the PEMA P695 methodology and caused an overestimation in the overstrength factor. In the numerical model adopted here, the buckling strength and drift were affected by the initial imperfection applied in the middle of braces. A constant initial imperfection was adopted for

modeling purpose, implying that the braces were fabricated with the same degree of quality. In real practice, however, the initial imperfection of each brace varies; the pushover responses may or may not be the same as the one shown in numerical models. Although the responses of the frame under larger deformations or after cyclic responses were less sensitive to initial imperfections, the simulated peak strength and buckling (yielding) drift from the pushover analysis should be interpreted with caution.

Instead of distributing deformation uniformly, braced frames tended to concentrate damage in certain stories from first-mode pushover analysis. When the damage was concentrated in higher stories, the overall strength of the braced frames was dominated by the damaged level, which may underestimate the base shear capacity. The overstrength factor, therefore, may be as low as 1.0 or even smaller.

Some of the analyses demonstrated that the archetype frames showed no evidence of collapse response even after the braces ruptured, with loss in their capacity in tension and compression. The moment resisting frames in the model might contribute more than was expected to resist collapse. The models of the braced frames included fiber elements, which were able to capture strength degradation effects associated with brace buckling. The responses associated with deterioration of the beams due to plastic hinging were not explicitly simulated, however. As such, these evaluation results were more representative if the connections were detailed and able to reach the required ductility and strength demand.,

5.9.3 Recommendations for Further Experimental or Analytical Investigation

The evaluation was intended to examine the appropriateness of the seismic performance factors for typical SCBFs and BRBFs designed for SDC D_{max}. Because of the large amount of design choices, such as different floor plan, different vertical configuration and different number of braced bays, only limited but typical braced frames were analyzed. More efforts were required to reduce the uncertainty of seismic performance factors.

Some of the designs of SCBFs used large brace sizes that were not quantified in the previous tests. Because the local and global behavior of large braces is believed to be different than that of the regular braces, more testing is needed to improve the confidence on the quality of test data.

In the archetypes, only the double story X configuration was adopted. Other braced frames with different vertical configurations or the chevron braced frames designed with larger beams to resist the unbalanced load from braces and with different load path may exhibit other failure modes not obvious in double story X braced frames. Further investigation on the different brace configurations should cover a wider range of samples, thereby improving the confidence of the evaluation.

For the taller buildings, it may be not efficient to use only the braced frames to resist the lateral load. Designs incorporating outriggers or multi-bays of braced frames are common. Analyses on such buildings will provide meaningful comparison to the typical archetypes.

A three-dimensional model can be constructed to account for the three-dimensional related failure modes. The torsional effect of the building is important for the braced frames, especially when the structure is subject to near-field ground motions in two orthogonal directions, which may show obvious asymmetric excursions.

Chapter 6

Evaluation of Global Seismic Demands and Design Parameters of Braced Frame Buildings

6.1 Introduction

According to the FEMA P659 evaluation results presented in Chapter 5, low-rise braced frame archetypes have higher probabilities of collapse at the MCE-level event (2/50) than taller ones. The simulation results for the three-story tall, code-conforming braced frame buildings show that the probability of fracturing at least in one brace at the MCE-level event is over 70 percent in SCBF buildings and over 80 percent in BRBF buildings. Fracture of braces significantly reduced the lateral strength and stiffness of the buildings and increased the probability of the collapse of these buildings [also see Uriz and Mahin, 2008]. Although taller braced frame buildings more easily satisfied FEMA P695 collapse prevention safety criteria, the damage tended to be concentrated in just a few stories.

To further investigate how the braced structural systems perform under earthquakes, several of the archetypes were selected for more detailed study. The 3-, 6- and 16-story tall archetypes, 3SCBFDmax, 6SCBFDmax, 16SCBFDmax, 3BRBFDmax, 6BRBFDmax, and 16BRBFDmax were chosen to represent SCBF and BRBF systems with both short and long periods. Examined in this Chapter are the drift and force demand. In addition, collapse and damage characteristics of the 2-story SCBF system are also studied. The numerical models were established according to the parametric studies and results presented in Chapter 3 and 4.

As in Chapters 3 and 4, the SAC ground motions [Somerville, 1997] corresponding to the service (50/50), design (10/50) and MCE (2/50) hazard levels for downtown Los Angeles were used to assess likely demands at different hazard levels. Figure 6.1 shows the medians of SAC ground motions. Note that the median of the 10/50 records is similar to the design spectral acceleration of FEMA P695 at SDC Dmax.

In this chapter, global demands related to story drift, shear and floor acceleration were examined. EDPs related to local or member behavior are presented in Chapter 7.

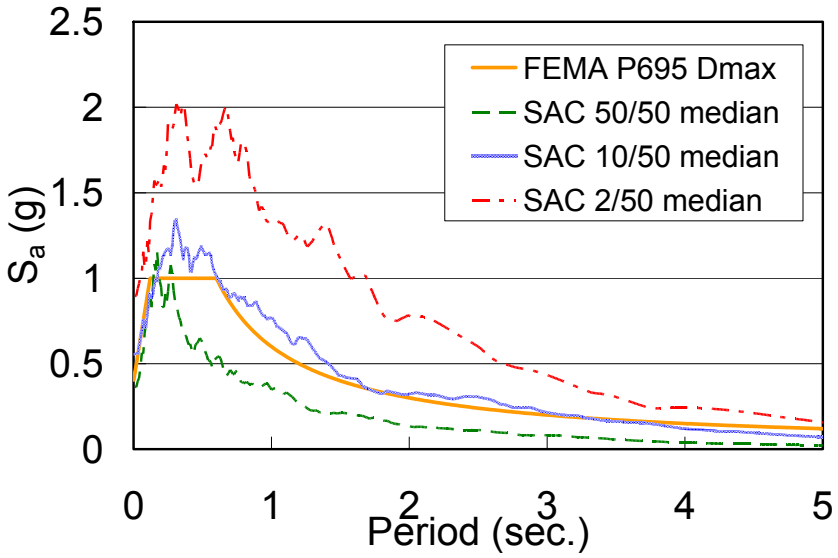

Figure 6.1 Design spectral acceleration of FEMA P695 at SDC Dmax and the median spectral acceleration of SAC ground motions

6.2 Global Drift Demand

Drift demands are discussed here in terms of the maximum story drift that occurs during the response to the seismic excitation and the residual (permanent) story drift ratio that presents at the end of the record. These EDPs can be related to local structural damage (see Chapter 7), to damage to displacement sensitive non-structural components and to difficulty in restoring a structure to operational status.

6.2.1 Story Drift Demands

Figure 6.2 presents the median and 84th percentile of the maximum story drift of the three SCBF archetypes at three hazard levels, which is the value related to the maximum value of the peak story drift at any story. These values are also summarized in Table 6.1. It is assumed that the distibution of the DRmax is lognormal. The number of cases where the buildings collapsed for these records is also shown in this figure; there are 20 records at each hazard level. The results shown are generated from the non-collapse results. If the DRmax of the collapse results were also included, the median and 84th percentile of DRmax would significantly increase, especially for the archetypes with more collapse cases.

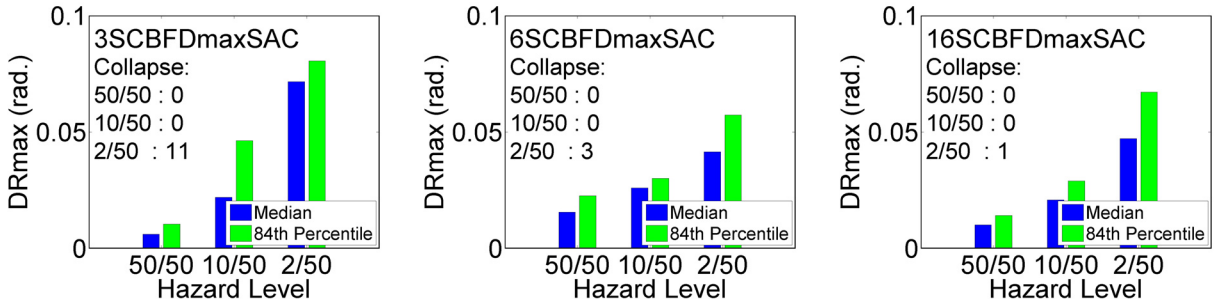

Figure 6.2 Maximum story drift ratios of SCBF archetypes under SAC ground motions corresponding to three hazard levels

Table 6.1 Summary of maximum story drift ratios of SCBF and BRBF archetypes under SAC ground motions corresponding to three hazard levels

Model	50/50		10/50		2/50	
	Median	84th Percentile	Median	84th Percentile	Median	84th Percentile
3SCBFDmaxSAC	0.61%	1.05%	2.19%	4.63%	7.16%	8.06%
6SCBFDmaxSAC	1.56%	2.26%	2.59%	3.01%	4.14%	5.73%
16SCBFDmaxSAC	1.01%	1.41%	2.08%	2.89%	4.71%	6.71%
3BRBFDmaxSAC	0.68%	1.23%	1.95%	3.86%	4.82%	7.96%
6BRBFDmaxSAC	0.89%	1.07%	1.93%	2.70%	3.65%	8.11%
16BRBFDmaxSAC	1.05%	1.38%	1.78%	2.48%	3.27%	5.28%

At the service-level events, the median DRmax of 3SCBFDmaxSAC is the smallest among the SCBF archetypes compared. At the design-level event, the median DRmax values of the three SCBF archetypes are similar; with values are between 2% and 2.6%. The 84th percentile value for 3SCBFDmaxSAC is greater than the other two cases. This large 84th percentile value comes from some near-collapse cases at the design-level event. At the MCE-level event, 3SCBFDmaxSAC shows a total of 11 cases of collapse, which is more collapse cases than the other two archetypes. The median DRmax for the nine excitations where 3SCBFDmaxSAC does not collapse is 7.16%. For 6SCBFDmaxSAC and 16SCBFDmaxSAC, it is 4.14% and 4.71% respecitvely. In general, for 3SCBFDmaxSAC, the DRmax responses changed more from one hazard level to another than the other two cases. In other words, even if DRmax of 3SCBFDmaxSAC at the service-level event is smaller than other archetypes, DRmax of 3SCBFDmaxSAC at the MCE-level event is larger and contributes to a higher risk of collapse than the other archetypes.

Figure 6.3 shows the median and 84th percentile value of the maximum story drift of the BRBF archetypes for three hazard levels. The median DRmax values for a given hazard level of different BRBF archetypes are more similar than found for the SCBFs. The 84th percentile value for 3BRBFDmaxSAC is greater than the other models at the service- and the MCE-level events. A similar trend for SCBFs is evident where the median DRmax of 3BRBFDmaxSAC is smaller than the other BRBF archetypes at the service-level event but greater at the MCE-level event.

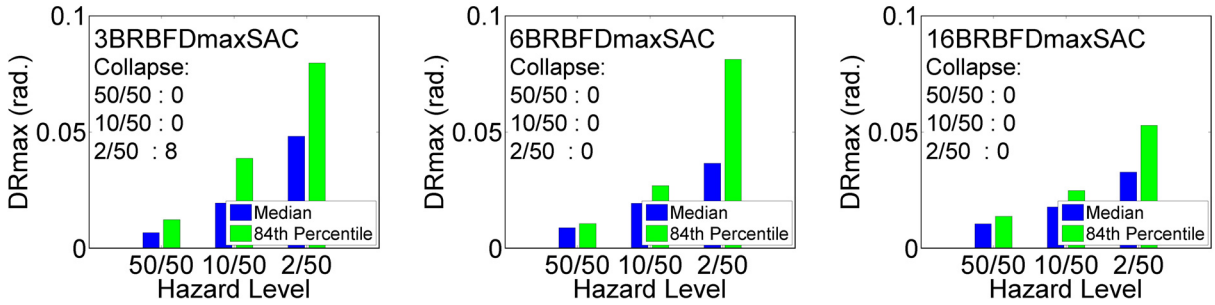

Figure 6.3 Maximum story drift ratios of BRBF archetypes under SAC ground motions corresponding to three hazard levels

In general, for 6-story and 16-story archetypes, the median DRmax is slightly greater for the SCBFs than for the BRBFs at all three hazard levels. The median DRmax for the 3SCBFDmaxSAC for non-collapse cases of the MCE-level event is 7.16% while that of 3BRBFDmaxSAC is 4.82%. The difference between 84th percentile and median is an estimate of standard deviation under normal assumption giving an indication of dispersion. For all the archetypes, this dispersion at the MCE-level event was greater than that at the other hazard levels.

Figure 6.4 plots the distribution of the median and 84th percentile of DRmax over the height of the SCBF archetypes. At the service-level event, the DRmaxs were below 0.1% for all SCBF archetypes. The top story of 6SCBFDmaxSAC had the largest median service level DRmax (1.56%) among the compared models. At the design-level event, 3SCBFDmaxSAC tended to concentrate deformation at the bottom level, while the other archetypes had a more uniform drift profile. For 16SCBFDmaxSAC, the median drifts increased gradually with elevation, but the 84th percentile it the 13th story was large. The drifts at the bottom two stories were small because the available brace sections at these stories were much larger than required and provided extra strength and stiffness. At the MCE-level event, the DRmax profiles were larger than the profile values at the design-level event, but maximum drifts and especially the 84th percentile values tended to be concentrated in a few stories.

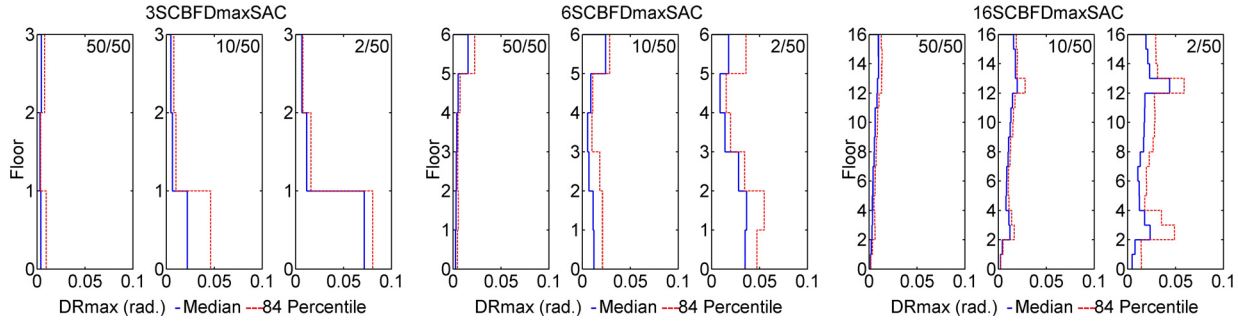

Figure 6.4 Profiles of the maximum story drift ratios of SCBF archetypes under SAC ground motions corresponding to three hazard levels

The distributions of the median and 84th percentile values of DRmax over the height of the BRBF archetypes are shown in Figure 6.5. The median drifts at the MCE-level event show that the drifts of BRBF archetypes changed more gradually than the SCBF archetypes (see Figure 6.6)

where there is no sudden increase of DRmax at a few stories. At the service-level event, the median DRmax of any story of 3BRBFDmaxSAC was greater than that of 3SCBFDmaxSAC while the median DRmax of any story of 16BRBFDmaxSAC was similar to that of 16SCBFDmaxSAC. In 16BRBFDmaxSAC, although the maximum of median DRmax may occur at middle floors, the change was gradual from the adjacent floors, which was different from the sudden deformation change in a few stories in 16SCBFDmaxSAC. The uniform distribution of deformation contributed to a more efficient pattern for energy dissipating for BRBFs.

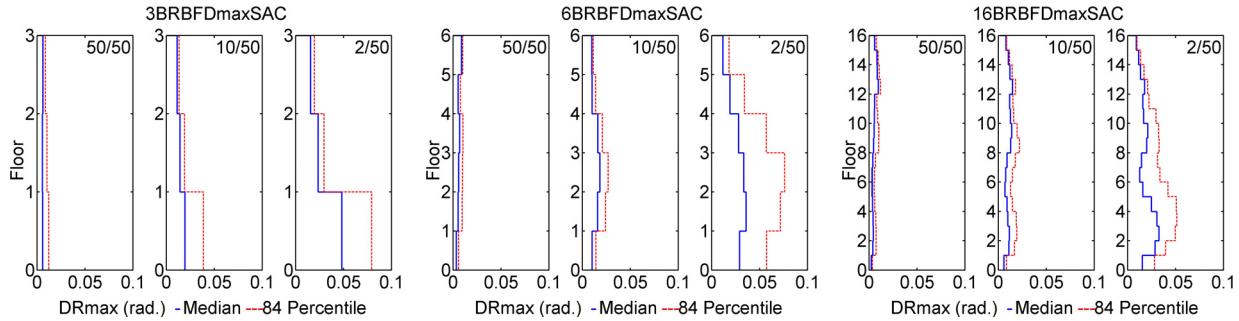

Figure 6.5 Profiles of the maximum story drift ratios of BRBF archetypes under SAC ground motions corresponding to three hazard levels

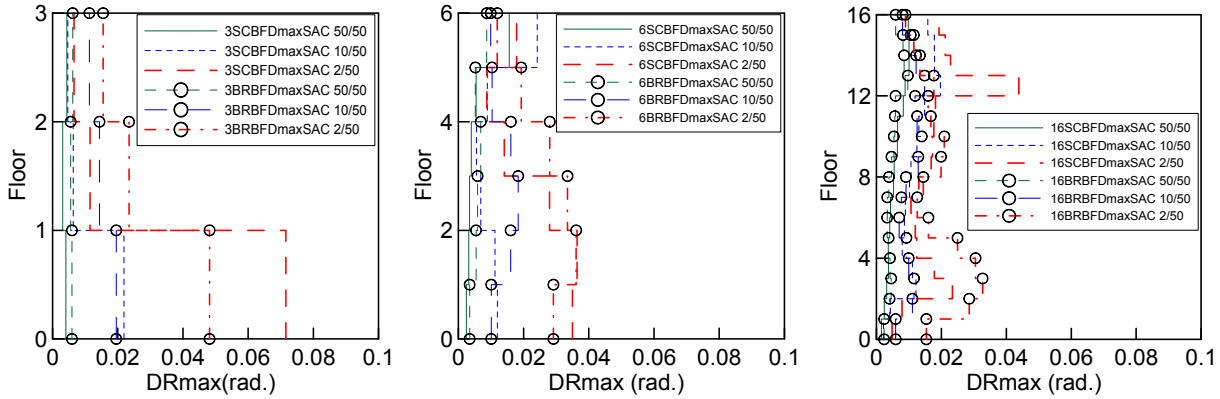

Figure 6.6 Comparison of profile of the maximum story drift ratios of different archetypes under SAC ground motions corresponding to three hazard levels

6.2.2 Residual Story Drift Demands

The median residual DRs of SCBF archetypes are less than 0.1% at the service-level event for all three archetypes (see Figure 6.7). At the design-level event, although the median residual DR of 3SCBFDmaxSAC is 0.52% at the first story, the 84th percentile was more than 2.84%. The median residual DRs of 6SCBFDmaxSAC and 16SCBFDmaxSAC at the design-level event were less than 0.3% and, thus, may be repairable after earthquakes. At the MCE-level event, the residual DRs were especially large at the levels where the median DRmax values were concentrated for all three archetypes. The residual DRs of SCBF archetypes with fewer stories tended to be greater than those SCBF archetypes with more stories. Although the median residual DRs of 16SCBFDmaxSAC were the smallest among the three archetypes, i.e. 0.06%, 0.24% and 1.44% for the service-, design-, and MCE-level events, respectively, the 84th percen-

tile value at the MCE-level event was large at the stories where the median DRmax was concentrated and exceeded 3.9 making repairs problematic.

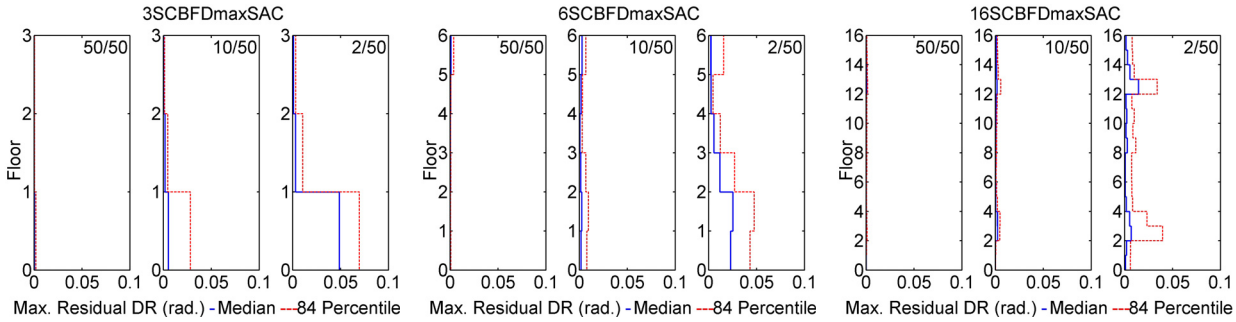

Figure 6.7 Profiles of the maximum residual story drift ratios of SCBF archetypes under SAC ground motions corresponding to three hazard levels

The residual DRs of BRBF archetypes were less than 0.12% at the service-level event for the three archetypes (see Figure 6.8). At the design-level event, the median residual DRs in BRBFs were 0.61%, 0.53% and 0.29% for 3-, 6- and 16-story BRBF archetypes, respectively. At the MCE-level event, the residual DRs were especially large at the stories where the median DRmax values were concentrated. The maxima of the median residual DR of the three BRBF archetypes at the MCE-level event were 2.88%, 1.82% and 2.47% for 3-, 6- and 16-story BRBF archetypes, respectively. Note that it is not a given that the taller BRBF archetypes have smaller median residual DRs (as observed in SCBF archetypes).

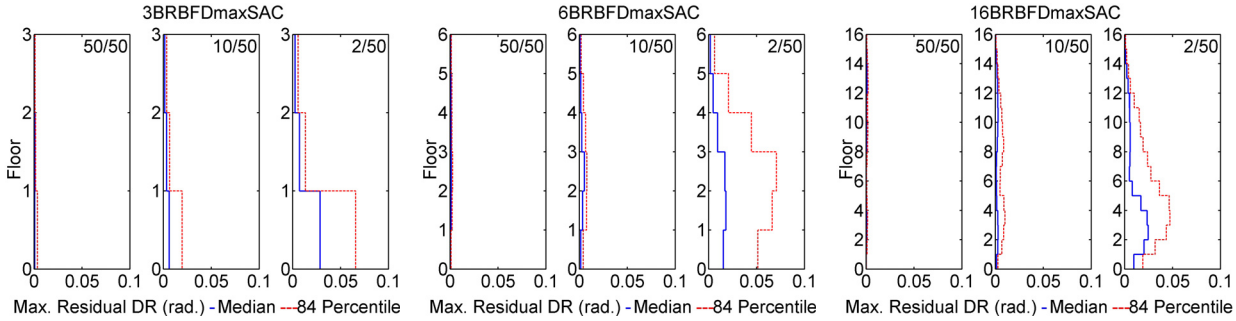

Figure 6.8 Profiles of the maximum residual story drift ratios of BRBF archetypes under SAC ground motions corresponding to three hazard levels

A comparison of the residual DRs at the service- and the design-level events finds that they are similar for the SCBFs and BRBFs at most of the stories (see Figure 6.9). At the MCE-level event, the median residual DR at the first story of 3BRBFDmaxSAC was smaller than that of 3SCBFDmaxSAC, but the median residual DRs at the other stories of 3BRBFDmaxSAC were greater than those of 3CBFDmaxSAC. The difference of the 84th percentile and the median residual DR of 6BRBFDmaxSAC at the MCE-level event was about 5.23%, which is greater than the difference for 6SCBFDmaxSAC (2.24%). At the MCE-level event, the maximum median residual DR of 16BRBFDmaxSAC was about 2.5% and distributed in a few stories while that of 16SCBFDmaxSAC was 1.44% and only occurred in one story. The difference between the median and the 84th percentile of residual DR in 16BRBFDmaxSAC was generally greater than that

in 16SCBFDmaxSAC. In other words, there were more cases of large residual DR in 16BRBFDmaxSAC than 16SCBFDmaxSAC.

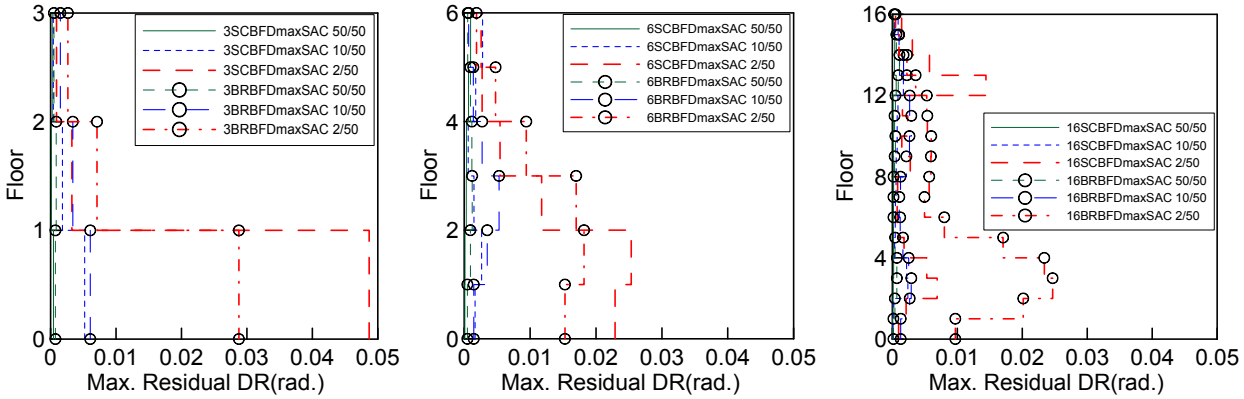

Figure 6.9 Comparison of profile of the maximum residual story drift ratios of different archetypes under SAC ground motions corresponding to three hazard levels

6.3 Global Force Demand

The global force demand examined was the story shear. The story shear identifies the maximum force demand at each story under various hazard levels. The story shear profile illustrates the story shear strength pattern under dynamic loadings.

The R-factor is the force reduction between a elastic system and nonlinear system. It is bounded by the ductility capacity of the structure. Given the limited ductility of the braced frame system, this force-related parameter was investigated. After examining the distribution of median and the 84th percentile values of story shear, these were interpreted in terms of the effective R_{Sa} value of the archetypes and base shear overstrength.

6.3.1 Story Shear

Figure 6.10 shows the story shear distribution of SCBF archetypes over the height of the buildings at the service-, design-, and MCE-level events. For 3SCBFDmaxSAC, the shape and values of the profile of maximum story shear at all three hazard levels were similar. The median of maximum base shears were 744 kips, 749 kips and 753 kips at the service-, design-, and MCE-level events, respectively for 3SCBFDmaxSAC. While similar trends were observed in 6SCBFDmaxSAC, the distribution of story shear in upper story of 16SCBFDmaxSAC was not necessarily smaller than the lower floor for two adjacent stories. The higher mode effects seemed to be reflected in the profile. At the design- and the MCE-level events, the median story shears at ground levels were 1544 kips and 1652 kips, respectively, while the story shears from third story to 12th story were about 1000 kips. The ground levels were subjected to especially higher demand of story shears.

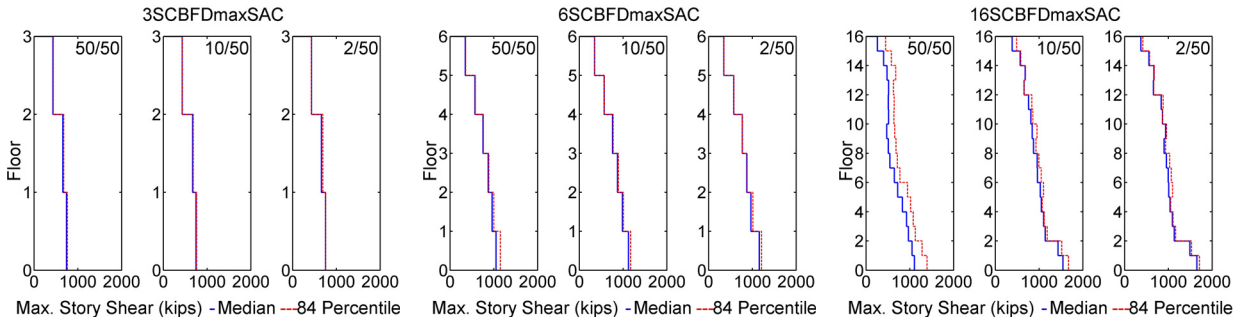

Figure 6.10 Profiles of the maximum story shear of SCBF archetypes under SAC ground motions corresponding to three hazard levels

Figure 6.11 plots the story shear distribution for BRBF archetypes over the height of the buildings at the service-, design-, and MCE-level events. The story shears for 3BRBFDmaxSAC and 6BRBFDmaxSAC tended to increase consistently in each story as the hazard level increased. The median of maximum base shears were 453 kips, 522 kips, and 566 kips at the service-, design-, and MCE-level events, respectively, for 3BRBFDmaxSAC. The median of maximum base shears were 618 kips, 788 kips, and 1019 kips at the service-, design-, and MCE-level events, respectively, for 6BRBFDmaxSAC. For 16BRBFDmaxSAC, increasing the hazard intensity increased shear demand on the lower levels while the shear demands in the 4th story and above did not change as much as the lower levels did. The median of maximum base shears were 481 kips, 597 kips, and 825 kips at the service-, design-, and MCE-level events, respectively, for 16BRBFDmaxSAC. The story shears in the higher stories did not undergo significant change as the hazard intensity increased. In the lower stories, the difference between the median and the 84th percentile value of story shears were also greater than the difference in the higher stories.

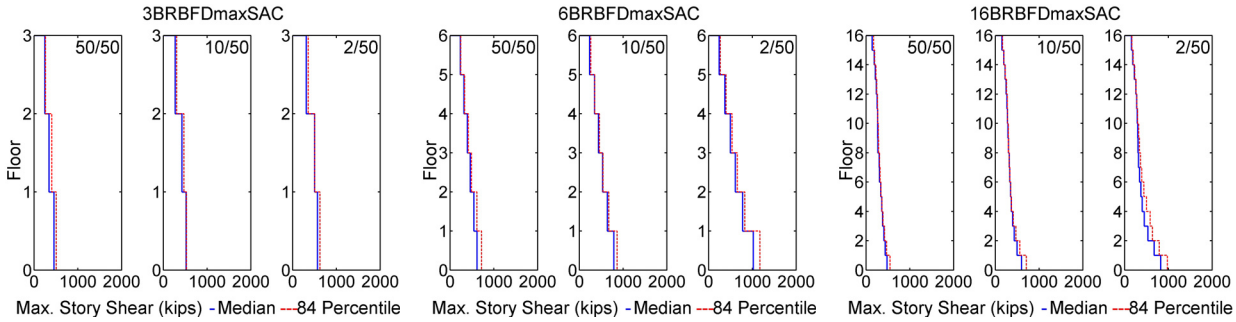

Figure 6.11 Profiles of the maximum story shear of BRBF archetypes under SAC ground motions corresponding to three hazard levels

The median story shears were similar to the 84th percentile values at the design-level event for each archetype. For many cases, the story shears approached the yielding capacity of each story for 3- and 6-story archetypes. Several of the story shears were greater than the story yielding capacity due to the deformation hardening of the yielding components or the additional lateral force resistance from the mechanism of beams and columns. In 16SCBFDmaxSAC, the difference between median and 84th percentile was greater at the service-level event. The archetype still remained essentially elastic; the variation of story shear for elastic structural response was larger than that for nonlinear structural response because as long as the buildings ex-

perienced nonlinear structural response, the maximum story shear demands were near capacity. At design- and the MCE-level events, however, most stories experienced nonlinear behavior; therefore, the story shear demands were similar to the capacity of each story. If a story experienced extensive nonlinear behavior, the profile of story shear demand was similar to that of the capacity. Because most of the archetypes experienced nonlinear response at each story — especially at the design- and the MCE-level events— and the story shear capacity of BRBF archetypes were smaller than the SCBF counterparts, the story shears demands in BRBF were generally smaller than those in SCBFs (see Figure 6.12). The base shear of 3SCBFDmaxSAC was almost 1.5 times that of 3BRBFDmaxSAC, while the base shear of 16SCBFDmaxSAC was almost 2 times that of 16BRBFDmaxSAC. The primary factors that affected the larger base shear demand and capacity of SCBF archetypes include:

1. The shorter fundamental period of SCBF archetypes

   The shorter fundamental period of 3SCBFDmaxSAC relative to 3BRBFDmaxSAC corresponded to larger design spectral acceleration and, therefore, resulted in larger design lateral force. Although the design spectral acceleration in the long-period range varied less, the design spectral acceleration corresponding to the fundamental period of 16SCBFDmaxSAC was about 1.2 times that of 16BRBFDmaxSAC.

2. The greater design R-factor of BRBF archetypes

   The design R-factor for SCBFs and BRBFs is 6 and 8, respectively. The difference resulted in a 1.33 times larger design force for SCBFs given the same design spectral acceleration in both systems.

3. Selection of member sections

   Because it is more convenient to customize the brace sizes of BRBFs, the capacity of the BRBF is usually close to the design force. In contrast, the selection the braces sizes for SCBFs is constrained to available sections. The available sizes can be more than 10% stronger than required. Moreover, because member sizes are based on the design compression force in a brace, and most braces have tensile capacity greater than their compressive capacity, the ultimate capacity of a system where the tension brace yields and the compression brace buckles is greater than the capacity calculated based on first buckling of braces.

The characteristics of materials also affect the ultimate capacity of the structure. Nonetheless, it is assumed that the difference in material properties in the analyses presented have negligible effects on the ultimate capacity. The initial tangent and Bauschinger effect parameters are set to be the same for all the material in the analyses.

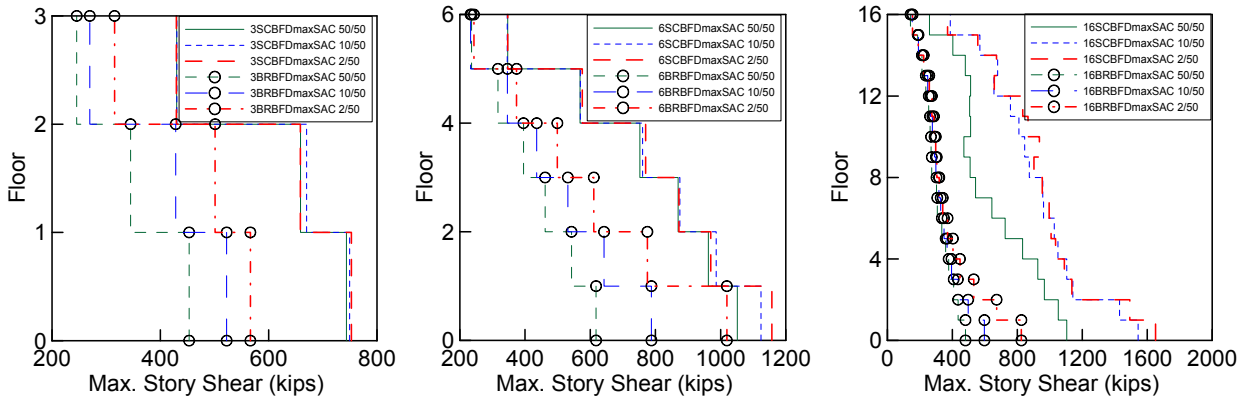

Figure 6.12 Comparison of profile of the maximum story shear of different archetypes under SAC ground motions corresponding to three hazard levels

6.3.2 Effective R-factor

This section investigates the appropriateness of the code response modification factors (R-factor) for the archetypes. Code R-factors consider the ductility and overstrength of a structure and are generally expressed in the following form [Uang, 1991]:

$$R = R_{\mu}\Omega \tag{6.1}$$

where R_μ is the ductility reduction factor and Ω is structural overstrength factor.

For a single-degree-of-freedom (SDOF) system, the relationship between ductility (μ) and R_μ was well established [Newmark and Hall, 1982; Riddell et al., 1989]. The relationship is period dependent and expressed in equations (6.2), (6.3), and (6.4). Linear interpolation was used for different period range.

$$R_{\mu}^{NH} = 1.0 \quad (\mathrm{T} < 0.03\mathrm{s}) \tag{6.2}$$

$$R_{\mu}^{NH} = \sqrt{2\mu - 1} \quad (0.125 < \mathrm{T} < \text{about } 0.4\text{s depending on } \mu) \tag{6.3}$$

$$R_{\mu}^{NH} = \mu \quad (\mathrm{T} > \text{about } 0.6\text{s depending on damping ratio}) \tag{6.4}$$

Overstrength usually accounts for the beneficial effects from other factors such as the material overstrength and the strain rate effect during earthquake excitation. This section will identify response modification factors of the archetypes and examine the Code R-factors.

The overstrength, ductility, and response modification factors of the archetypes obtained from the analyses in Chapter 5 are summarized in Table 6.2, which includes archetype 2SCBFDmaxSAC. Note that the definitions of Ω and Ω_0 in this Chapter are commonly used in other literature [Uang, 1991], but are different from those in Chapter 5. The overstrength factor Ω was obtained from the computed Ω_0, with nominal material properties times the material overstrength 1.05 and strain-rate factor 1.1 [Uang, 1991; Ellingwood et al., 1980]. R_μ^{NH} was calculated from Newmark-Hall R_μ^{NH}-μ relationships given computed structural ductility in Chapter 5

and fundamental period. Conceptually, if the ratio of $R_{code}/(\Omega*R_{\mu}^{NH})$ is greater than 1.0, it means that the overstrength and ductility capacity of the archetype designed with R_{code} are insufficient. The 2-story SCBF and 16-story SCBF and BRBF archetypes have $R_{code}/(\Omega*R_{\mu}^{NH})$ ratios greater than 1.0. However, for 16-story archetypes, the estimation of overstrength factors was affected by more uncertain factors, and Ω and $\Omega*R_{\mu}^{NH}$ may be underestimated in some cases. This issue is presented in the following.

Table 6.2 Overstrength (Ω_0, Ω), ductility (μ) and response modification factors (R_{μ}^{NH}, R_{code}) of the archetypes

Archetypes	Ω_0	Ω	μ	R_{μ}^{NH}	R_{code}	$\Omega*R_{\mu}^{NH}$	$R_{code}/(\Omega*R_{\mu}^{NH})$
2SCBFDmaxSAC	1.44	1.67	4.29	2.75	6	4.59	1.31
3SCBFDmaxSAC	1.41	1.62	6.09	3.78	6	6.14	0.98
6SCBFDmaxSAC	1.34	1.55	6.57	6.57	6	10.19	0.59
16SCBFDmaxSAC	2.11	2.44	1.77	1.77	6	4.31	1.39
3BRBFDmaxSAC	1.48	1.71	22.67	16.26	8	27.85	0.29
6BRBFDmaxSAC	1.47	1.70	15.45	15.45	8	26.25	0.30
16BRBFDmaxSAC	1.00	1.16	3.13	3.13	8	3.61	2.22

The trend that the 16-story archetypes have a smaller ductility capacity than the 3- and 6-story archetypes is obvious in Table 6.2 due to drift concentration and more severe P-delta effect occurred in high-rise archetypes. The values of Ω_0 and μ obtained from pushover analysis should be interpreted with caution for the high-rise archetypes because the force and deformation responses of the first-mode nonlinear static pushover analyses are not representative of the responses obtained from nonlinear dynamic analyses.

From nonlinear dynamic analyses, the base shear and ductility capacity obtained are different than the values from the pushover analyses. Table 6.3 shows the median base shear demands of the archetypes at the design-level event ($V_{10/50}$) and the maximum base shear from first-mode pushover analyses (V_{max}). Because the archetypes experience nonlinear behavior at the design-level event, the corresponding base shear demands were similar to the capacity; the static pushover analyses resulted in smaller base shear compared to dynamic analyses. This difference was more obvious for 16-story archetypes. For 16SCBFDmaxSAC, the mechanism caused by first-mode pushover occurred in the third story, while during SAC ground motion excitations the mechanism mostly occurred in the first story; V_{max} (1035 kips)was associated with the story shear capacity of the third story and smaller than $V_{10/50}$ (1544 kips); as such, Ω_0 and Ω calculated from first-mode pushover is smaller than overstrength calculated from the base shear in dynamic analyses (Ω').

Table 6.3 Median base shear demands at the design-level event of the archetypes and maximum base shear from pushover analyses

Archetypes	First-mode Pushover Maximum Base Shear (V_{max}) (kips)	Median Base Shear Demand at the Design-Level Event ($V_{10/50}$) (kips)	$V_{10/50}/V_{max}$
3SCBFDmaxSAC	730	749	1.03
6SCBFDmaxSAC	1020	1124	1.10
16SCBFDmaxSAC	1035	1544	1.49
3BRBFDmaxSAC	475	522	1.10
6BRBFDmaxSAC	558	788	1.41
16BRBFDmaxSAC	365	597	1.64

The comparison of the SDOF constant ductility spectra at the design-level event and the Newmark-Hall relation is shown in Figure 6.13. The SDOF constant ductility spectra were constructed from the 20 SAC ground motion records representing the events of 10% probability of exceedance in 50 years. The post-yielding stiffness ratio was assumed to be 5% for a bilinear SDOF system and damping ratio of 4% was used for the system. Note that Newmark-Hall approach provides lower R_μ^{NH} than the effective $R_\mu^{10/50}$ factors calculated from SAC ground motions. For example, for target ductility of 6.0, R_μ^{NH} factors calculated using Newmark-Hall approach was 82%, in average, of the effective $R_\mu^{10/50}$ factors for period from 0 to 5 sec.

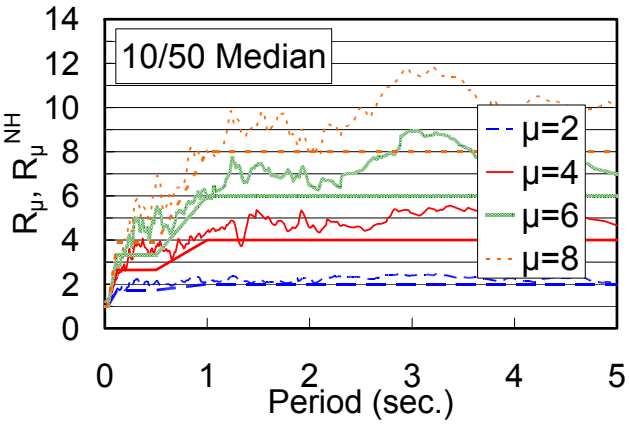

Figure 6.13 Constant ductility spectra of SAC ground motions

For 16-story archetypes, because the dynamic responses exhibited higher overstrength (Ω') than the overstrength factor Ω estimated from first-mode static pushover analysis, the $\Omega' * R_\mu^{10/50}$ factor representing dynamic response was greater than $\Omega * R_\mu^{NH}$ obtained from first-mode static pushover analysis. As such, although the $\Omega * R_\mu^{NH}$ was less than R_{code} for 16-story archetypes, only one collapse was observed when they were subjected to the SAC ground motion excitations at the MCE-level event.

In contrary, for 2SCBFDmaxSAC, because Ω factor was less affected by the difference between the static and dynamic analyses, the large $R_{code}/(\Omega * R_\mu^{NH})$ ratios for 2SCBFDmaxSAC simply resulted from insufficient strength and ductility capacity of the archetypes. To reduce

the probability of damage and collapse of 2SCBFDmaxSAC, it is necessary to either improving the ductility and strength capacity of the archetype or reducing the ductility and strength demands on the archetype.

6.4 Effective R-factors for Design of 2-story SCBF to Resist Collapse

To take advantage of the structural overstrength and ductility, the current code specifies an R-factor. In the case of short-period 2SCBFDmaxSAC, this archetype designed conforming to the current codes does not have sufficient overstrength and ductility to resist collapse at the MCE-level event. Two-story SCBFs were designed with various R-factors and the collapse resistance is discussed in the following.

In current code for SCBFs, a design R-factor of 6 is too large for low-rise SCBF archetypes to resist collapse at the MCE-level event where the probability of collapse is more than 20% (see Chapter 5). Table 6.4 summarizes the number of collapses and DR responses of two-story SCBF archetypes with design R-factors of 6, 4.5, 3.3, and 3. The archetype with the design R-factor of 6 resulted in one collapse at the design-level event, but the archetype exhibited collapse behavior for almost all the ground motion records at the MCE-level event. In the case where design R-factor of 4.5 was incorporated, the collapse cases were reduced to eight at the MCE-level event, but the collapse risk was still high. When the design R-factor were reduced to 3.3 and 3, no collapse cases were observed at the design-level event and the number of collapse cases at the MCE-level event was only three and one for the archetype of R=3.3 and R=3, respectively.

Table 6.4 also shows the median of maximum DR for these 2-story archetypes. Note that the median DRmax of design R-factor of 6 at the MCE-level event is not shown because only two non-collapse cases remained and the statistical results are not representative. The results demonstrated that considering design R-factors of 3.3 or 3.0 for 2-story SCBF archetypes successfully reduces the drift demand at various hazard levels as well as the probability of collapse at the MCE-level event.

Table 6.4 Summary of responses of 2-story SCBF archetypes with different R-factor for design

R (Design)	T_1(Sec.)	Number of Collapses (out of 20 records)		Median DRmax (Non-Collapse)	
		10/50	2/50	10/50	2/50
6	0.4	1	18	0.028	--
4.5	0.35	0	8	0.016	0.033
3.3	0.30	0	3	0.007	0.017
3	0.28	0	1	0.006	0.019

6.5 Demand-to-Capacity Ratio

The damage concentration is common in the analyses of braced frame archetypes. It causes severe nonlinear behavior in a few stories in high-rise archetypes, while other stories still remain

elastic. This section highlights the relationship between the damage concentration and the demand-to-capacity ratio (DCR) of the building.

6.5.1 Capacity

The story shear capacity at the yielding point of the SCBF archetypes is based on the brace capacity only. The typical pushover response of SCBF from OpenSees analyses shows that the response is elastic until the first global buckling of the brace(s). For the double story X braced frame archetypes before the buckling occurs, the tension and compression braces have forces of about the same magnitude but opposite sign. The story shear contributed by columns and other structural elements is generally small (less than 10% of total story shear) at the range of elastic responses. Therefore, it is assumed the major story shear contribution is due to the brace capacity. This is illustrated in equation (6.5).

$$\begin{aligned} V_{br,SCBF} &= \left|P_{compression}\right| \cdot \cos(\theta + \theta') + \left|P_{tension}\right| \cdot \cos(\theta - \theta') \\ &\cong P_{cr} \cdot \cos(\theta) + P_{cr} \cdot \cos(\theta) \\ &= 2P_{cr} \cdot \cos(\theta) \end{aligned} \tag{6.5}$$

where P_{cr} is the compression capacity of the buckling braces at one level

θ is the incline angle of the brace with respect to the horizon

θ' is the story drift angle at the yielding point, which is small compared to θ and may be neglected

The story shear capacity at the yielding point of the BRBF archetypes is estimated similarly and expressed in equation (6.6).

$$\begin{aligned} V_{br,BRBF} &= \left|P_{compression}\right| \cdot \cos(\theta + \theta') + \left|P_{tension}\right| \cdot \cos(\theta - \theta') \\ &\cong P_{y} \cdot \cos(\theta) + P_{y} \cdot \cos(\theta) \\ &= 2P_{y} \cdot \cos(\theta) \end{aligned} \tag{6.6}$$

where P_y is the tension capacity of the BRB at one level

6.5.2 Demand-to-Capacity Ratio Profile

The story shear demand at the yielding point is based on the first-mode pushover analysis. The demand in Figure 6.14 is normalized to the shear capacity of the story where the DCR is the maximum considering all stories of an archetype. As such, the maximum DCR is 1.0 (see Figure 6.14).

Figure 6.14 provides indices to predict precisely where the first yielding will occur under the first-mode pushover analysis. The base shear demand at the yielding strength of structure is not always near the story shear capacity of the base level. Instead, it is estimated given the story shear capacity and the location of the level where the largest DCR occurs along the height. The 3-story and 6-story archetypes demonstrated relatively more uniform profile of DCR along the height of the buildings; all the DCR values are greater than 0.8. For the 16-story archetypes, the DCR of 1.0 occurred in the middle stories, other stories had a DCR smaller than 1.0. Under the first-mode pushover analysis, it is expected that, the levels with higher DCRs will yield earlier and experience more nonlinear behavior, with the likelihood of damage being concentrated

in those stories.

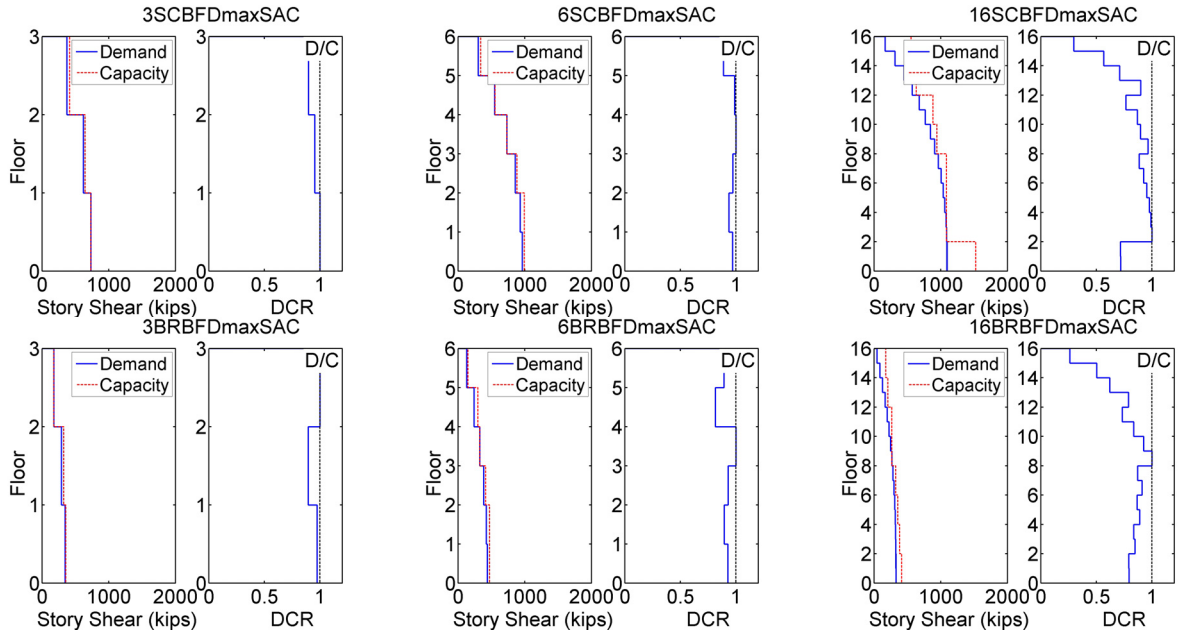

Figure 6.14 Story shear capacity and demand of first-mode pushover analysis and the demand-to-capacity ratio of braced frame archetypes

Figure 6.15 plots the DCR of the braced frame archetypes under dynamic excitations; μ and σ shown in the figure are the mean and variance among all the stories in the archetype. The distribution of the DCR of dynamic responses is different compared to the results from static pushover results. The DCR of dynamic responses was more uniform and close to 1.0 because most of the stories experienced nonlinear responses and the story shear demands approached the "yielding" capacity in each story. Therefore, it was difficult to identify which story yielded first and which story experienced more inelastic behavior from the DCR of dynamic responses. Although using the first-mode load pattern in static pushover analyses to represent the dynamic responses of structures had uncertain accuracy, the DCR of static pushover analyses exhibited a distribution that was possibly associated with the drift concentration. As such, the DCR of pushover analyses was used here as an indicator to investigate the initiation of yielding and the consequent deformation concentration.

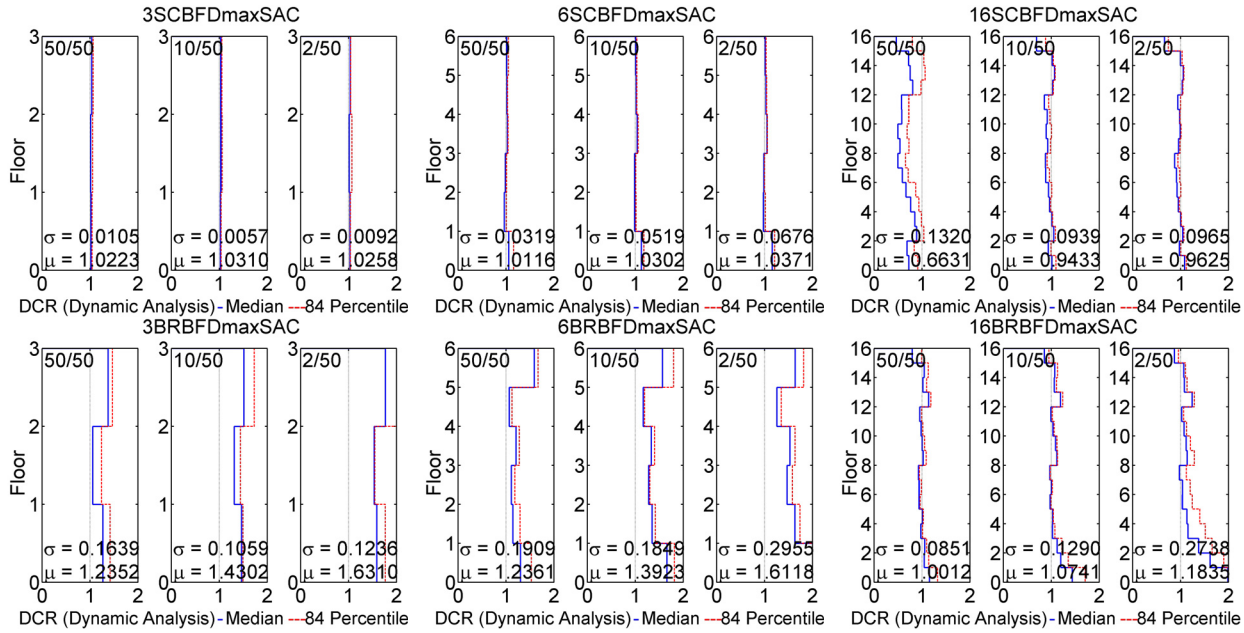

Figure 6.15 Demand-to-capacity ratios of braced frame archetypes with respect to various hazard levels

For pushover analysis, the contribution from P-Δ effect, which presented as the force of leaning column, was greater after the buckling occurred (see Figure 6.16). After the peak loading when the brace buckled, the column force increased rapidly while the contribution from the P-Δ effect also increased. Although both of these two components increased, they are of the opposite sign, which cancels out a possible increase in story shear. Generally, the total story shear reduced more when P-Δ effect was more obvious at larger drift, whereas the column force did not increase much and approached the plastic capacity of the columns. As such, the pushover curve demonstrated a negative slope after a peak force around the occurrence of brace buckling.

At the MCE-level event in the dynamic analyses, DRmax values were about 5%, whereas the contribution from P-Δ effect was about 10% of the peak story shear from static pushover analysis; the mechanisms under dynamic excitations were observed in several stories, mostly in the lower stories. While the capacity of a story was estimated considering only the brace capacity, the seismic loading resulted in the nonlinear responses and plastic hinges at the columns and beams contributing to a large component of the story shear. Therefore, Figure 6.15 shows that the median of story shear demands was close to the yielding capacity of each level (i.e. the DCR was about 1.0); in some stories, especially lower ones, the DCR varied between 1.0 and 2.0.

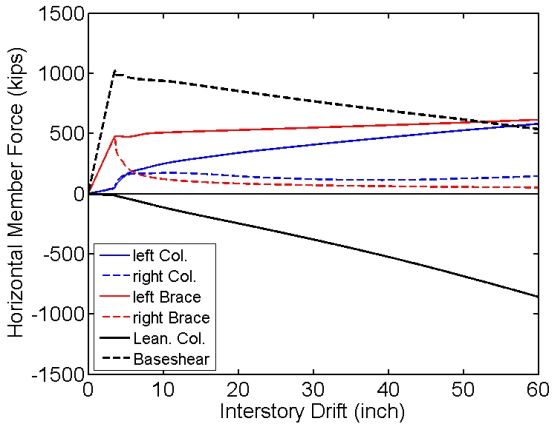

Figure 6.16 Typical pushover curve and force contribution from various structural elements

6.6 Considering Demand-to-Capacity Ratio Profile for Designing a 16-Story SCBF Archetype

For high-rise archetypes, the damage was concentrated in several stories. One of the reasons is the difference of stiffness and/or strength at adjacent floors is too large such that a soft story/weak story mechanism occurs. The proportion of the structural components in the archetypes is not appropriate, and, therefore, although the structural deformation along the height is within the design limits at the service- and the design-level events, the damage concentration becomes more obvious at the MCE-level event which corresponds to the higher nonlinear demand.

The DCR of 16SCBFDmaxSAC from the first-mode static pushover analysis illustrated that the ratio was greater for some stories compared to the others. The results from dynamic analysis also showed a possible trend that the drifts were greater in the stories where these static DCRs were greater. However, the relationship between DCR and drift was not obvious. To simply estimate the relationship between the dynamic responses of a story and the DCR from first-mode pushover analysis, it is assumed that the energy dissipation ratio of two stories is comparable to the pushover DCR ratio for the two stories. For the stories where the pushover DCR is larger, they are assumed to dissipate more energy during the dynamic excitations because the yielding of these stories may occur earlier than the other stories. Note that although DCR of pushover was used here, more appropriate parameter need to be identified as an indication of the energy dissipation in each story subjected to dynamic excitations.

From the simplified bilinear story shear and DR relationship shown in Figure 6.17, the energy dissipated by story *i* and that dissipated by story *j* have a relationship in the form:

$$\frac{E_i}{E_j} = \frac{V_i \cdot DR_i - (1/2) \cdot V_i \cdot DR_y}{V_j \cdot DR_j - (1/2) \cdot V_j \cdot DR_y} \tag{6.7}$$

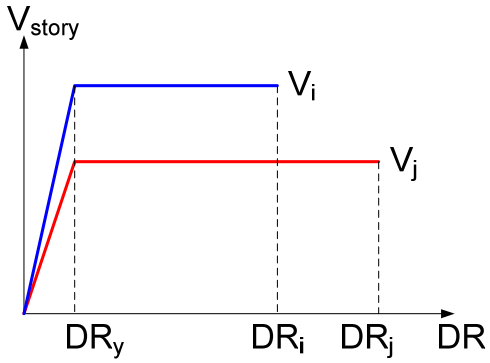

Figure 6.17 Simplified story shear and DR relationship

with primary assumption being

$$\frac{E_i}{E_j} = \frac{D_i / C_i}{D_j / C_j} (= \alpha) \tag{6.8}$$

By substituting equation (6.8) into equation (6.7), and by definition $V_i = C_i$ and $V_j = C_j$, we obtain:

$$\frac{C_i \cdot DR_i - (1/2) \cdot C_i \cdot DR_y}{C_j \cdot DR_j - (1/2) \cdot C_j \cdot DR_y} = \alpha \tag{6.9}$$

For $\frac{C_i}{C_j} = \beta$,

$$\frac{\left(DR_i - (1/2) \cdot DR_y\right)}{\left(DR_j - (1/2) \cdot DR_y\right)} = \frac{\alpha}{\beta} \tag{6.10}$$

Because DR_y is generally small if nonlinear behavior occurs, equation (6.10) can be approximated as:

$$\frac{DR_i}{DR_j} \approx \frac{\alpha}{\beta} = \frac{D_i / C_i^2}{D_j / C_j^2} \tag{6.11}$$

The relation in equation (6.11) implies:

(1) For those stories with similar force demand determined by static pushover analysis, if the story shear capacity of the story is greater, the DR during dynamic excitation is likely to be smaller. This situation usually occurs in adjacent bottom stories.

(2) For those stories with similar story shear capacity, if the DCR of static pushover analysis is greater, the DR during dynamic excitation is likely to be greater. This comparison usually applies to adjacent stories along the height.

(3) For those stories with similar DCR of static pushover analysis, if the capacity of the story is greater, the DR during dynamic excitation is likely to be smaller. The relation usually applies to the stories with DCR close to 1.0.

Figure 6.18 shows the relationship between D_i/C_i^2 (scaled with yielding capacity of the archetypes) and DR of 16SCBFDmaxSAC for three hazard levels. The regression is based on

zero intercept. The largest $D_i \cdot V_y / C_i^2$ —corresponding to the largest median DRmax at the MCE-level event— was the response of the 13th story where the drift was concentrated. The data are summarized in Table 6.5. Note that although $D_i \cdot V_y / C_i^2$ on the third story was not especially large, dynamic analysis contends that the drift concentration was severe in this story indicating that the changes of stiffness and strength in the adjacent stories may be too large. Given the proportional relationship between $D_i \cdot V_y / C_i^2$ and DR, not only $D_i \cdot V_y / C_i^2$ but also the change ratio of $D_i \cdot V_y / C_i^2$ at adjacent levels should be limited such that the DR in adjacent stories was not significantly altered. The constraint on the change of $D_i \cdot V_y / C_i^2$ in adjacent stories also confined the change of the stiffness at adjacent levels. Table 6.5 also lists the change ratio of $D_i \cdot V_y / C_i^2$ at two adjacent levels. The relatively large change ratios in the third and 13th story resulted in relatively large DR in these stories.

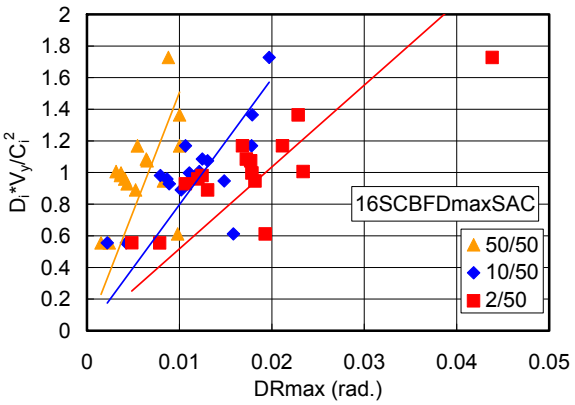

Figure 6.18 Relationship between $D_i \cdot V_y / C_i^2$ and median DRmax of 16SCBFDmaxSAC at different hazard levels

Table 6.5 $D_i \cdot V_y / C_i^2$, change ratio of $D_i \cdot V_y / C_i^2$ and median DRmax of 16SCBFDmaxSAC

Floor/Story	$D_i \cdot V_y / C_i^2$	Change Ratio of $D_i \cdot V_y / C_i^2$	Median DRmax		
			50/50	10/50	2/50
Roof /16	0.63	0.52	0.98%	1.58%	1.93%
16 /15	1.21	0.81	1.00%	1.78%	2.12%
15 /14	1.48	0.79	1.00%	1.79%	2.28%
14 /13	1.88	2.00	0.88%	1.97%	4.38%
13 /12	0.94	0.88	0.83%	1.48%	1.82%
12 /11	1.06	0.95	0.65%	1.31%	1.77%
11 /10	1.12	0.93	0.64%	1.25%	1.72%
10 /9	1.20	1.36	0.55%	1.07%	1.68%
9 /8	0.88	0.96	0.53%	1.02%	1.31%
8 /7	0.92	0.97	0.43%	0.89%	1.07%
7 /6	0.95	0.98	0.41%	0.87%	1.20%
6 /5	0.97	0.98	0.36%	0.80%	1.24%
5 /4	0.99	0.99	0.37%	1.11%	1.79%
4 /3	1.00	2.15	0.32%	1.22%	2.34%
3 /2	0.46	1.00	0.24%	0.43%	0.79%
2 /1	0.47	-	0.15%	0.22%	0.49%

To reduce the drift concentration and the large DRmax of some stories at the MCE-level event, the archetype is redesigned as 16SCBFDmaxSACR. The target chosen was 0.025 radians, which was about the drift ratio to cause brace fracture, corresponding to $D_i \cdot V_y / C_i^2$ =1.3 from the regression at the MCE-level event in Figure 6.18. The difference of $D_i \cdot V_y / C_i^2$ in two adjacent levels was selected to be within 30% to reduce stiffness irregularity. The member size and steel weight of the new design is shown in Table 6.6. Only the brace sizes were changed; the size in beams and columns remained the same as the previous design. The percentage change of the total weight of the steel in the braced frames was less than 5%. It was even less for the total weight of the whole building. Table 6.7 summarizes $D_i \cdot V_y / C_i^2$, the change ratio of $D_i \cdot V_y / C_i^2$, and median DRmax at various hazard levels of 16SCBFDmaxSACR; the relationship between $D_i \cdot V_y / C_i^2$ and DR is depicted in Figure 6.19. The median DRmax was effectively reduced and the DRmax profile under dynamic excitation was obviously more uniform along the height than the original design (see Figure 6.20).

Table 6.6 Member size and steel weight of 16SCBFDmaxSAC and 16SCBFDmaxSACR

Floor/Story		Brace of 16SCBFDmaxSAC	Brace of 16SCBFDmaxSACR	Column	Beam
Roof	/16	HSS9-5/8x0.375	HSS10.75x0.375	W12x45	W18x65
16	/15	HSS9-5/8x0.375	HSS10.75x0.375	W12x45	W18x35
15	/14	HSS8-5/8x0.5	HSS10.75x0.5	W14x82	W18x71
14	/13	HSS8-5/8x0.5	HSS10.75x0.5	W14x82	W18x35
13	/12	HSS11-1/4x0.5	HSS10x0.625	W14x120	W18x86
12	/11	HSS11-1/4x0.5	HSS10x0.625	W14x120	W18x35
11	/10	HSS10x0.625	HSS12.75x0.5	W14x176	W18x86
10	/9	HSS10x0.625	HSS12.75x0.5	W14x176	W18x35
9	/8	HSS11-1/4x0.625	HSS16x0.438	W14x233	W18x97
8	/7	HSS11-1/4x0.625	HSS16x0.438	W14x233	W18x35
7	/6	HSS11-1/4x0.625	HSS16x0.5	W14x283	W18x97
6	/5	HSS11-1/4x0.625	HSS16x0.5	W14x283	W18x35
5	/4	HSS11-1/4x0.625	HSS14x0.625	W14x342	W21x93
4	/3	HSS11-1/4x0.625	HSS14x0.625	W14x342	W18x35
3	/2	W12x96	W12x96	W14x370	W24x146
2	/1	W12x96	W12x96	W14x370	W18x35
Total Steel Weight (kips)		35130	29830	49530	30630

Table 6.7 $D_i \cdot V_y / C_i^2$, change ratio of $D_i \cdot V_y / C_i^2$ and median DRmax of 16SCBFDmaxSACR

Floor/Story		$D_i \cdot V_y / C_i^2$	Change Ratio of $D_i \cdot V_y / C_i^2$	Median DRmax 50/50	10/50	2/50
Roof	/16	0.59	0.52	1.00%	1.85%	2.33%
16	/15	1.13	1.21	1.01%	1.88%	2.40%
15	/14	0.93	0.79	0.99%	1.86%	2.34%
14	/13	1.18	1.04	0.89%	1.70%	2.38%
13	/12	1.13	0.88	0.87%	1.62%	2.22%
12	/11	1.29	1.15	0.67%	1.43%	1.98%
11	/10	1.12	0.93	0.63%	1.42%	1.84%
10	/9	1.20	1.26	0.55%	1.14%	1.64%
9	/8	0.95	0.96	0.54%	1.10%	1.42%
8	/7	1.00	1.25	0.45%	1.00%	1.13%
7	/6	0.80	0.98	0.41%	0.93%	1.10%
6	/5	0.81	1.10	0.38%	0.84%	1.28%
5	/4	0.74	0.99	0.37%	0.79%	1.18%
4	/3	0.75	1.31	0.31%	0.67%	1.04%
3	/2	0.57	1.00	0.28%	0.61%	1.38%
2	/1	0.57	-	0.16%	0.52%	2.14%

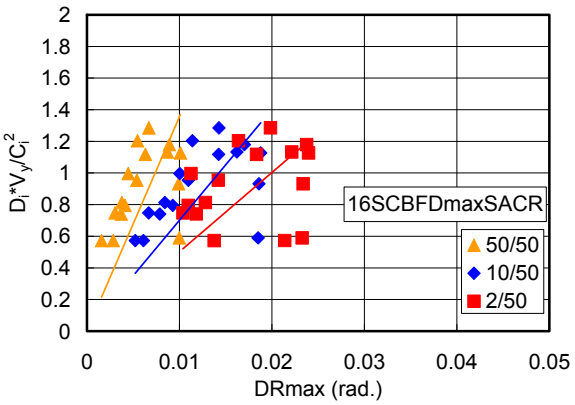

Figure 6.19 Relationship between $D_i \cdot V_y / C_i^2$ and median DRmax of 16SCBFDmaxSACR at different hazard levels

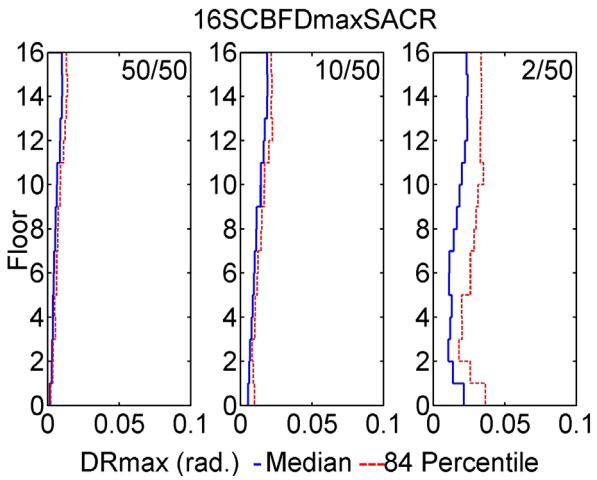

Figure 6.20 Profiles of the maximum story drift ratios of 16SCBFDmaxSACR under SAC ground motions corresponding to three hazard levels

6.7 Floor Acceleration Demand

Life safety hazards can develop as a result of falling objects. The potential for nonstructural elements and contents falling is related to floor level accelerations. In addition to posing a life safety hazard, acceleration sensitive objects can be dislodged or damaged, requiring considerable effort and funds to repair following an earthquake. As such, the maximum peak floor level accelerations are examined.

Figure 6.21 shows the median and 84th percentile of peak floor acceleration (PFA) of all the archetypes corresponding to various hazard levels. Figure 6.22 shows the comparison of median PFA of all the archetypes. Both Figures only accounted for the non-collapse cases. The difference between the 84th percentile and the median shown in Figure 6.21 illustrates that these differences of BRBF archetypes are between 0.13 g and 0.66 g and those of SCBF archetypes are between 0.12 g and 0.88 g. The 6-story archetypes had greater difference than 3- and 16-story archetypes, which meant the PFAs had greater variation in the 6-story archetypes. Figure 6.21 also presents that for all SCBF archetypes, the largest PFAs occur on the bottom and roof floors (or the 5th story of 6SCBFDmaxSAC), but for all BRBF archetypes, the largest PFAs occur on the bottom floors.

Figure 6.22 shows that median PFAs of low-rise archetypes are generally greater than those of high-rise counterparts. Note that PFAs at the MCE-level event were generally greater than those at the other hazard levels; this was especially true on the lower floors of 3-, 6- and 16-story archetypes. For 16-story BRBF archetype, median PFAs on the higher floors were similar at all three hazard levels, and for 16-story SCBF archetype, median PFAs on the higher floors were similar at the design- and MCE-level events and greater than median PFAs at the service-level event. Comparison of the responses of SCBF and BRBF archetypes indicated that median PFAs of 16SCBFDmaxSAC were greater than those of 16BRBFDmaxSAC along the height of the archetypes at three hazard levels due to the longer fundamental period and higher flexibility of BRBF archetypes. For 6-story archetypes, median PFAs of SCBF were greater than those of BRBF on the top two floors at three hazard levels; for 3-story archetypes, median PFAs of SCBF were greater than those of BRBF along the height of the archetypes at three hazard levels, except

on the roof at the MCE-level event. Generally, non-structural damage associated with floor acceleration was more severe for SCBF archetypes than for BRBF archetypes at three hazard levels, and more severe for short-period archetypes than for long-period archetypes.

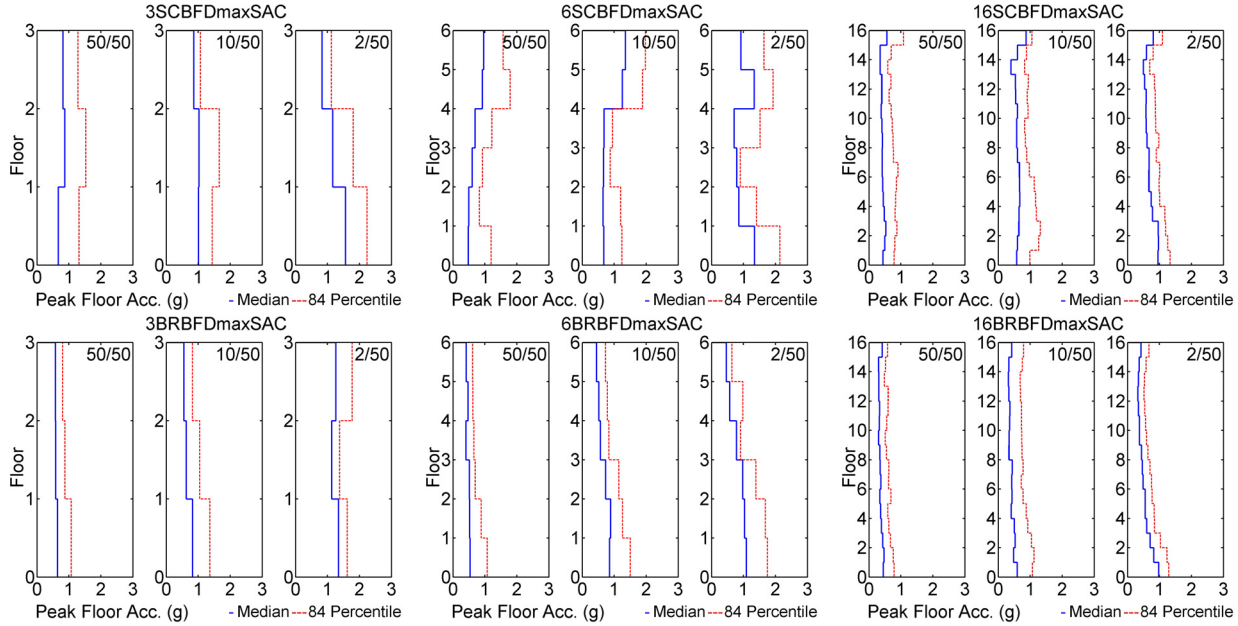

Figure 6.21 Peak floor accelerations of braced frame archetypes with respect to various hazard levels

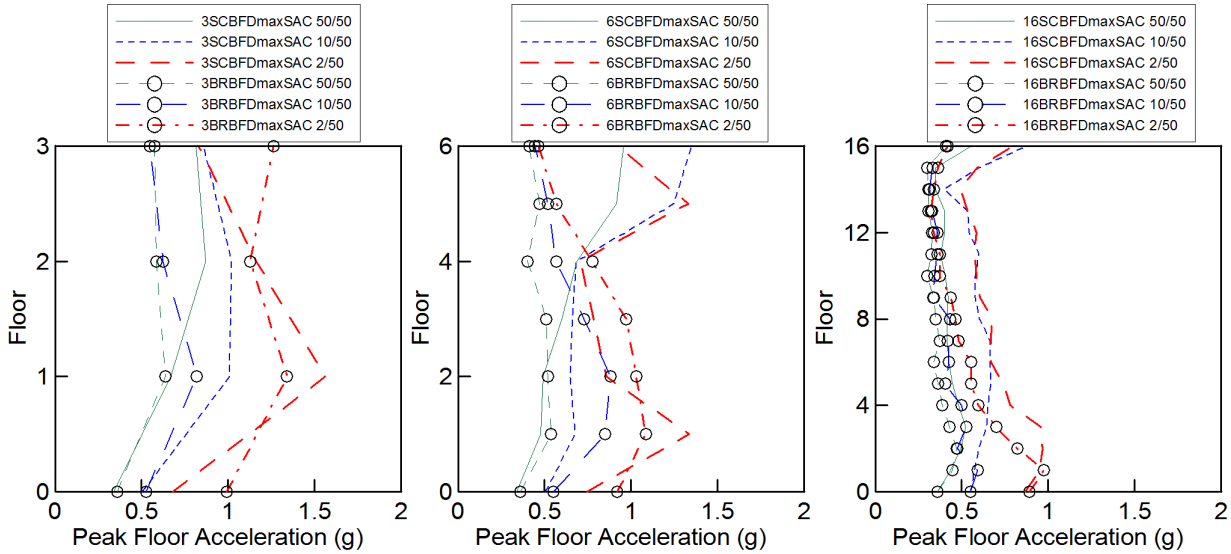

Figure 6.22 Comparison of peak floor accelerations of different archetypes under SAC ground motions corresponding to three hazard levels

6.8 Summary

Sixty SAC ground motions representing three hazard levels were applied to evaluate the per-

formance on 3-, 6- and 16-story SCBF and BRBF archetypes. Low-rise SCBF archetypes showed higher probability of collapse at the MCE-level event according to the evaluation in Chapter 5, while the high-rise SCBF archetypes showed deformation concentrated in a few stories. The design R-factor of the two-story SCBF archetype was investigated for its high probability of collapse. To reduce the deformation concentration, the 16-story SCBF archetype was redesigned based on the proposed parameters. The results are summarized below.

Drift Ratio:

The deformation of 3SCBFDmaxSAC archetype tended to concentrate drift in the bottom story. For 16SCBFDmaxSAC, a few of the middle stories had larger median DRmax and 84th percentile. Deformation and damage concentration in those stories led to weak stories under dynamic excitations, especially at the MCE-level event.

The BRBF archetypes generally had more uniform profile of DRmax than SCBF archetypes. In 16BRBFDmaxSAC, although the maximum of median DRmax occurred in middle stories, the change was gradual between the adjacent floors, a different response scenario compared to the sudden drift change experienced in the 16SCBFDmaxSAC. The uniform distribution of drift contributed to a more efficient pattern for energy dissipation in BRBFs.

Residual Drift Ratio:

The median residual DRs of SCBF and BRBF archetypes at the service- and the design-level events were small (usually in the order of 0.5% radians). At the MCE-level event, median residual DRs of all archetypes increase to 1.0% to 3.0%, leading to unrepairable damage of the buildings. The maximum median residual DR of 16BRBFDmaxSAC was about 2.5% and distributed across a few stories. For 16SCBFDmaxSAC, the maximum median residual DR was 1.44% occurred in only one story.

Story shear:

In general, the median story shears were similar to the 84th percentile of story shears for each archetype. The story shears approached the yielding capacity of each story if the archetype had experienced nonlinear behavior. Because the strength capacity of SCBF archetypes were generally greater than those of BRBF archetypes, the story shear demands in BRBF archetypes are smaller than those found in the case of SCBFs.

Effective R-factor:

The ratio of $R_{code}/(\Omega^*R_\mu)$ was investigated, where the 2-story SCBF and 16-story archetypes had $R_{code}/(\Omega^*R_\mu)$ ratios greater than 1.0. This suggests that the overstrength and ductility capacity of the archetype designed with R_{code} are insufficient. The estimation of overstrength and R_μ needs to be modified to reflect the dynamic responses of archetypes and the characteristic of selected ground motions, respectively. After the modification, the code design parameters are appropriate for the 16-story archetypes. For 2-story SCBF, the overstrength and ductility capacity are still insufficient.

For archetype 2SCBFDmaxSAC, a smaller design R-factor (ex. R = 3.3 or R = 3.0) is more consistent with the ductility capacity of the structural system and more appropriate for the design.

The code mandated R-factors appear to be unconservative for short-period archetypes. The R of 3.3 and 3.0 successfully reduced the drift demand at various hazard levels as well as the probability of collapse at the MCE-level event. It is suggested that for collapse prevention at the MCE-level event, a period-dependent design R-factor is more appropriate for the short-period SCBF archetypes designed for SDC Dmax.

Demand-to-Capacity Ratio:

The demand-to-capacity ratio (DCR) provided indices to predict at which story the first yielding will occur under the first-mode pushover analysis. Although using the first-mode load pattern in static pushover analyses to represent the dynamic responses of structures had uncertain accuracy, the DCR of static pushover analyses exhibited a distribution that was possibly associated with the drift concentration. As such, the DCR of pushover analyses was used here as an indicator to investigate the initiation of yielding and the consequent deformation concentration.

Under the assumption that the energy dissipation profile over the height of the building during dynamic excitations is proportional to DCR distribution of the first-mode pushover analysis along the height, DR of each story is approximately proportional to D_i/C_i^2 (or $D_i \cdot V_y/C_i^2$). The analysis of the 16-story SCBF archetypes demonstrated that by limiting the $D_i \cdot V_y/C_i^2$ ratios, the target DR at different hazard levels can be achieved. The stiffness difference in adjacent stories should also be limited to reduce drift concentration. A difference of 30% for the $D_i \cdot V_y/C_i^2$ ratio in adjacent stories was adopted in the archetype and successfully reduced the stiffness irregularity of the 16-story SCBF archetype.

Peak Floor Acceleration (PFA):

The largest median PFAs occurred on the bottom or roof floors (or the 5th story of 6SCBFDmaxSAC) for SCBF archetypes; for all BRBF archetypes, the largest median PFAs occur on the bottom floors. Analyses showed that the low-rise archetypes had greater median PFAs than the high-rise counterparts, and also showed that PFAs had greater variation in the 6-story archetypes than the other archetypes. In general, median PFAs at the MCE-level event were greater than those at the other hazard levels especially for the lower floor of all SCBF and BRBF archetypes. Note that median PFAs of 16SCBFDmaxSAC were greater than those of 16BRBFDmaxSAC along the height of the archetypes at three hazard levels due to the longer fundamental period and higher flexibility of BRBF archetypes. For 3-story and 6-story archetypes, however, the median PFAs of the BRBF archetypes were not always smaller than those of the SCBF counterparts along the height of archetypes. In general, non-structural damage associated with floor acceleration was expected to be more severe for SCBF archetypes than for BRBF archetypes at three hazard levels, and more severe for short-period archetypes than for long-period archetypes.

Chapter 7

Seismic Demand Evaluation of Structural Members in Steel Braced Frame Buildings

7.1 Introduction

Discussed in this chapter are the EDPs for structural members including the braces, beams and columns corresponding to different hazard levels. These EDPs include out-of-plane deformation of braces in SCBFs, ductility demands of the braces, damage indices of braces, axial force and moment demands in beams and columns, and vertical deformation in the middle span of the beam where braces intersect. A simple and accurate approach is proposed to estimate the out-of-plane deformation of braces. A simplified method to estimate the column compressive axial forces is also proposed.

7.2 Behavior and Demands for Braces

This section discusses the demands of out-of-plane deformation and ductility of the braces and damage of braces. The damage of braces is expressed in terms of damage index to represent the fatigue life of the braces under various hazard levels.

7.2.1 Out-of-Plane Deformation

In previous earthquakes, the out-of-plane deformation of braces was commonly seen in SCBF buildings when the gusset plates were oriented to allow braces to move out of the plane. The major concern of out-of-plane deformation of braces is the damage it may cause to the adjacent walls and non-structural components. To prevent such damage, a few design details can easily be employed whereby the braces deform in-plane; such designs are beyond the scope of this research. Although the numerical models presented herein are two-dimensional assuming in-plane buckling of the braces, the investigation of the out-of-plane deformation of braces is possible by measuring the brace deformation transverse to its longitudinal axis. Figure 7.1 shows the out-of-plane deformation of braces for the SCBF archetypes for three hazard levels. The median out-of-plane deformation at the MCE-level event is 28.7, 22, and 19 inches for 3SCBFDmaxSAC, 6SCBFDmaxSAC, and 16SCBFDmaxSAC, respectively.

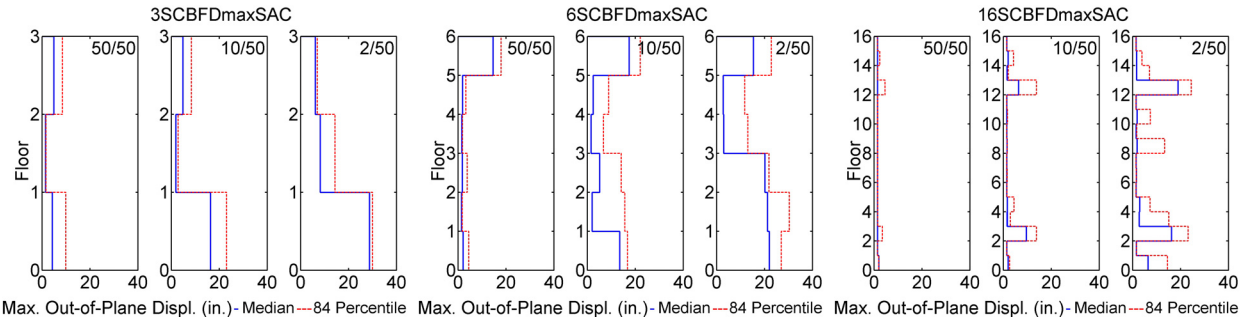

Figure 7.1 Profiles of brace out-of-plane deformation of SCBF archetypes under SAC ground motions corresponding to three hazard levels

The distributions of the out-of-plane deformation along the height of the buildings are similar to the profile of the maximum DR; their relationships were approximately proportional. Figure 7.2 illustrates the relationship between out-of-plane deformation and the story drift. The story drift caused shortening of the compression braces, which led to out-of-plane deformation of the braces. It was assumed that the axial and flexural deformations of the braces were negligible and the deform shape was composed of straight lines.

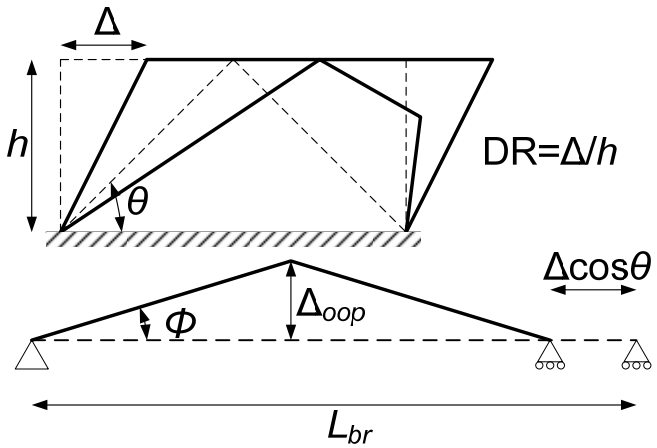

Figure 7.2 Simplified relationship between story drift and brace out-of-plane deformation

The out-of-plane displacement can be expressed as:

$$\begin{aligned}\Delta_{oop} &= \frac{L_{br}}{2}\cdot\sin\phi \\ &= \frac{L_{br}}{2}\cdot\sin\left(\cos^{-1}\left(\frac{L_{br}-h\cdot\cos\theta\cdot DR}{L_{br}}\right)\right) \\ &= \frac{1}{2}\sqrt{2\cdot L_{br}\cdot h\cdot\cos\theta\cdot DR - h^2\cdot\cos^2\theta\cdot DR^2}\end{aligned} \tag{7.1}$$

where $\phi = \cos^{-1}\left(\frac{L_{br}-\Delta\cdot\cos\theta}{L_{br}}\right)$. The brace length is presented by:

$$L_{br} = \eta \cdot \frac{h}{\sin\theta} \tag{7.2}$$

where η is the ratio of hinge-to-hinge length to work point-to-work point length of braces.

In this analysis, the effective brace length was assumed to be 70% of the work point-to-work point length and therefore η = 0.7. Substituting equation (7.2) into equation (7.1), the out-of-plane displacement can be rewritten and approximated as:

$$\begin{aligned} \Delta_{oop} &= \frac{L_{br}}{2}\sqrt{DR \cdot \frac{\sin 2\theta}{\eta}\left(1 - \frac{\sin 2\theta}{4 \cdot \eta} \cdot DR\right)} \\ &\approx \frac{L_{br}}{2}\sqrt{\frac{\sin 2\theta}{\eta} \cdot DR} \end{aligned} \tag{7.3}$$

The out-of-plane deformation is approximately proportional to square root of DR. Note that when the DR is less than the DR that initiates buckling of the brace, the out-of-plane deformation has not yet occurred and Δ_{oop} should be zero. As such, we modify equation (7.3) as follows:

$$\Delta_{oop} = 0 \qquad \text{if } DR \leq DR_{buckle} \tag{7.4}$$

$$\Delta_{oop} \approx \frac{L_{br}}{2}\sqrt{\frac{\sin 2\theta}{\eta} \cdot (DR - DR_{buckle})} \qquad \text{if } DR > DR_{buckle} \tag{7.5}$$

where DR_{buckle} is the DR value that initiates buckling of the brace and about 0.25% radian in the analyses.

Tremblay et al. [2003] has derived a simplified relationship between the brace axial deformation and out-of-plane deformation. The relation is re-written in equation (7.6).

$$\Delta_{oop,Tremblay} = 0.7\sqrt{\Delta \cdot \cos\theta \cdot L_{br}} \tag{7.6}$$

This relation provides a conservative estimate for a low DR demand while giving accurate estimation for large deformations [Tremblay et al., 2003]. Figure 7.3 compares these simplified estimations and the analytical responses of 3SCBFDmaxSAC. Equation (7.5) provides accurate estimations of Δ_{oop} for various DR demands especially when the DR demands are small. In other words, equation (7.5) gives more precise information to evaluate damage and loss of SCBF system at various hazard levels for PBEE.

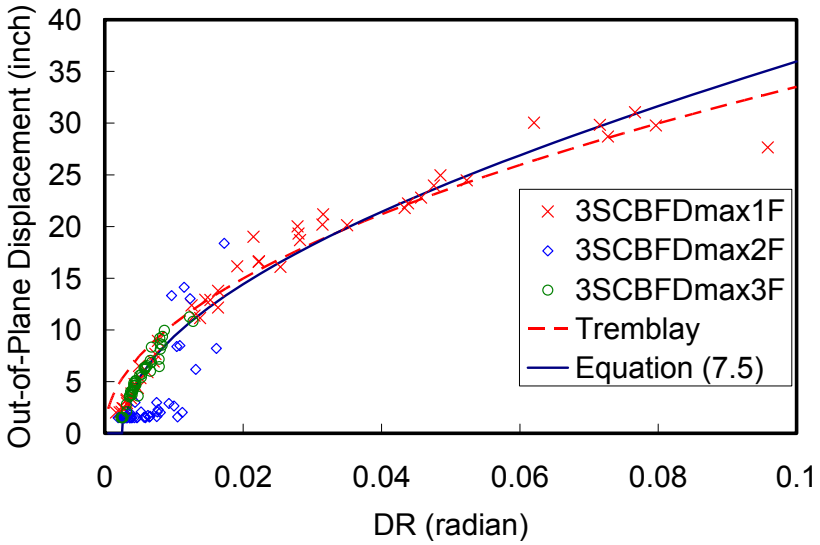

Figure 7.3 Brace Out-of-plane deformation of 3SCBFDmax under SAC ground motions versus predicted relationships

7.2.2 Ductility Demand

Local and global buckling of conventional braces results in damage concentration and limits ductility capacity of the braces. To design the braced frame system within the limitation of the ductility capacity of the braces, the ductility demand of braces is investigated. Figure 7.4 shows a typical hysteresis loop of a conventional buckling brace. In this section, the positive and negative ductility is defined and normalized by the yielding deformation of the brace.

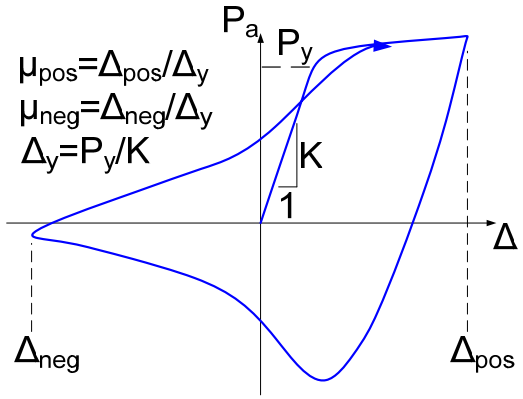

Figure 7.4 Illustration of positive and negative ductility of a conventional buckling brace

Figure 7.5 shows the ductility demand of SCBF archetypes at various hazard levels. The data only included the non-collapse results. The distribution of the ductility demand was assumed to be lognormal. For the given SAC ground motions, most of the response of the SCBFs showed a larger ductility demand in the negative direction. At the MCE-level event, the maximum of negative median normalized brace ductility demand, (as exhibited by 3SCBFDmaxSAC), was 34.4. At the design-level event, this occurred in 6SCBFDmaxSAC and is 14.9. The nor-

malized median brace ductility demands of 6SCBFDmaxSAC were greater than those of 3SCBFDmaxSAC at the service- and design-level events, but smaller at the MCE-level event. Archetype 16SCBFDmaxSAC had the smallest brace ductility demands among the SCBF archetypes for the three hazard levels; the normalized median brace ductility demand was 10.2 at the design-level event.

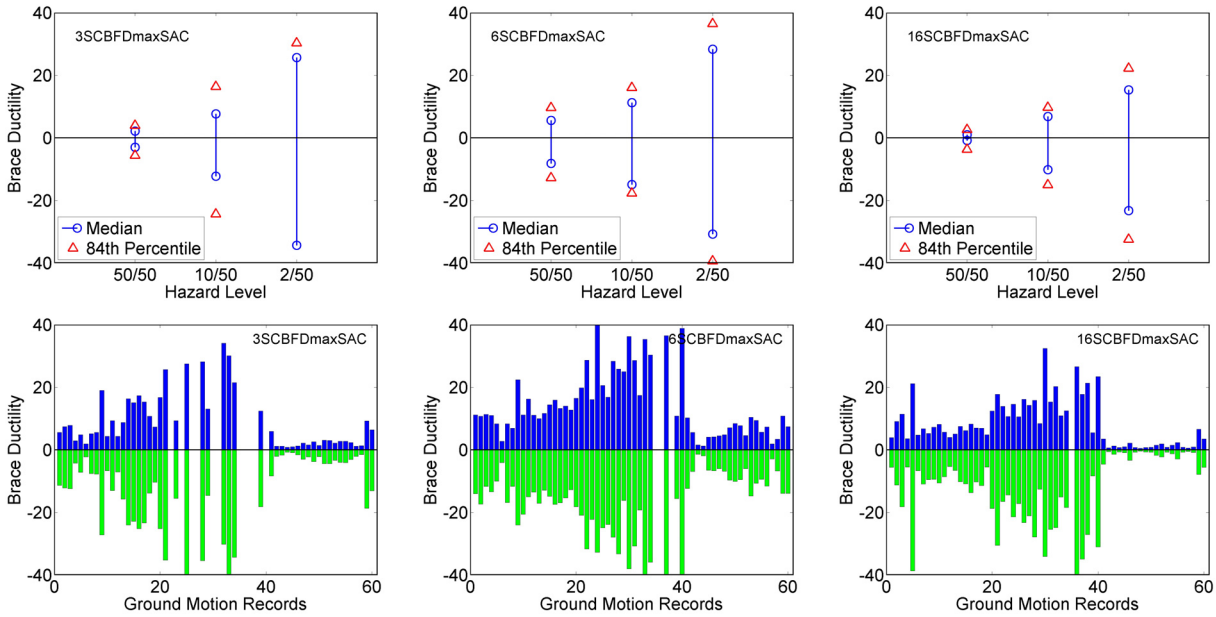

Figure 7.5 Ductility demands of braces in SCBF archetypes under SAC ground motions corresponding to three hazard levels

Figure 7.6 shows the ductility demands for the BRBF archetypes at various hazard levels. The ductility demands of the braces show symmetric responses in both the positive and negative directions. The median ductility demands of 3BRBFDmaxSAC and 6BRBFDmaxSAC were similar at the service- and design-level events, while 3BRBFDmaxSAC was greater than 6BRBFDmaxSAC at the MCE-level event. The median brace ductility demands at the design-level event were 9.0 and 9.3 for 3BRBFDmaxSAC and 6BRBFDmaxSAC, respectively. Archetype 16BRBFDmaxSAC had the smallest brace ductility demand among the BRBF archetypes at all hazard levels. There was only slightly difference noted at the service-level event compared to the other BRBF archetypes; the median brace ductility demands at the service-level event were 3.18, 3.96 and 3.39 for 3-, 6- and 16-story BRBF archetypes, respectively

A comparison between the SCBF with the BRBF archetypes shows that the brace ductility demands of BRBFs were generally smaller at various hazard levels, with larger difference occurring between median and 84th percentile at the design- and MCE-level events. The smaller brace ductility demands and better ductility performance of BRB may lead to a more reliable seismic resisting structural system of BRBFs compared to SCBFs.

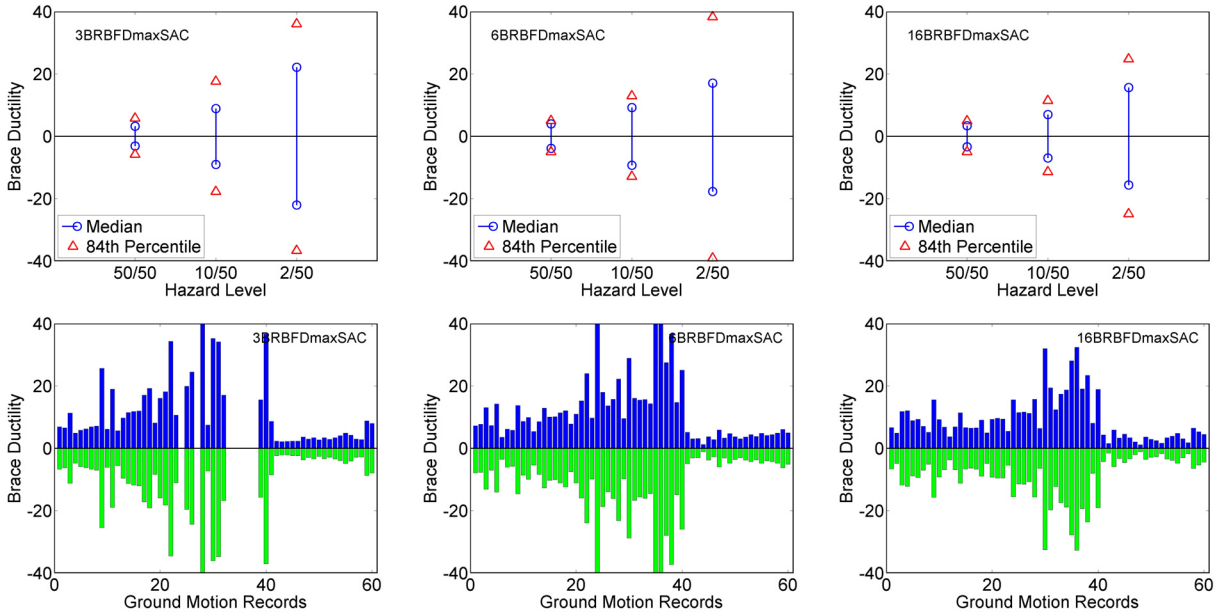

Figure 7.6 Ductility demands of braces in BRBF archetypes under SAC ground motions corresponding to three hazard levels

7.2.3 Damage of Braces

The damage of each brace in the archetypes was monitored. The damage of each fiber at each modeled section was accumulated using Rainflow cycle counting algorithm and Miner's rule as discussed in Chapter 3. The normalized damage index (*DI*) [Uriz and Mahin, 2008] at the modeled brace section is:

$$DI = \frac{\sum_{i=1}^{N} A_i \cdot DI_i}{\sum_{i=1}^{N} A_i} \tag{7.7}$$

where A_i is the representative area of fiber i and DI_i is the damage index of fiber i.

The maximum DI of the two braces in the same story is plotted in Figure 7.7. A DI of 1.0 represents the exhaustion of the fatigue life in a brace or, in other words, the complete rupture of the brace.

For 3SCBFDmaxSAC, the median brace damage indices were less than 0.04 at the service-level event in every story. At the design-level event, the median DI was 0.18 in the first story and less than 0.02 in the other stories. Note that the variation of the DI was large in the first story. The maximum DI in the first story at the design-level event was 0.87 meaning there was no complete rupture of the braces occurred at the design-level event, but rupture is likely to have initiated. At the MCE-level event, the drift was concentrated more in the first story; therefore, the median DI in first story was 1.0 while the median DI values for the other stories were less than 0.05; the maximum DI values for the second and third story at the MCE-level event were smaller than those measured at the design-level event.

For 6SCBFDmaxSAC, the DI at the roof level was larger than the other stories at the service-

and design-level events. Although the braces did not complete rupture at the service-level event, the median and maximum DI values for the 6th story was 0.22 and 0.89, respectively. The braces in the other stories experienced minor damage at the service-level event. At the design-level event, the complete rupture of brace(s) in the 6th story was observed during some earthquake excitations; therefore, the maximum DI for the 6th story is 1.0. The median DI values in all stories at the design-level event were similar to those at the service-level event, but the maximum DI values increased for all stories. At the MCE-level event, the median and maximum DI values for the 6th story were 0.16 and 1.0, respectively, which is similar to those at the design-level event (0.21 and 1.0, respectively). The damage was concentrated more in the lower stories, especially in the first story where the median and maximum DI values were 0.77 and 1.0, respectively. The higher DI at the roof level showed that the deformation due to higher mode effect was greater for the 6-story SCBF archetype compared to the 3-story SCBF archetype.

For 16SCBFDmaxSAC, the median DI values in all stories at the service- and the design-level events were less than 0.02. The maximum DI values occurred in the third and 13th story, where the story drift was concentrated. At the MCE-level event, at the 3rd and 4th story, some complete ruptures occurred; this was also the location where the DR was greater due to drift concentration. The maximum DI for the 13th story was 0.83; this level of damage may cause severe damage to such braces in the event of an aftershock.

Compared to the SCBF archetypes, the BRBF archetypes showed more uniformly distributed DI in the braces along the height of the building. Also, the maximum DI among all the BRB archetypes was less than 0.3, which occurs at the MCE-level event in the first story of 3BRBFDmaxSAC. All DI values were less than 0.3 for 3BRBFDmaxSAC, 0.17 for 6BRBFDmaxSAC and 0.1 for 16BRBFDmaxSAC at the MCE-level event.

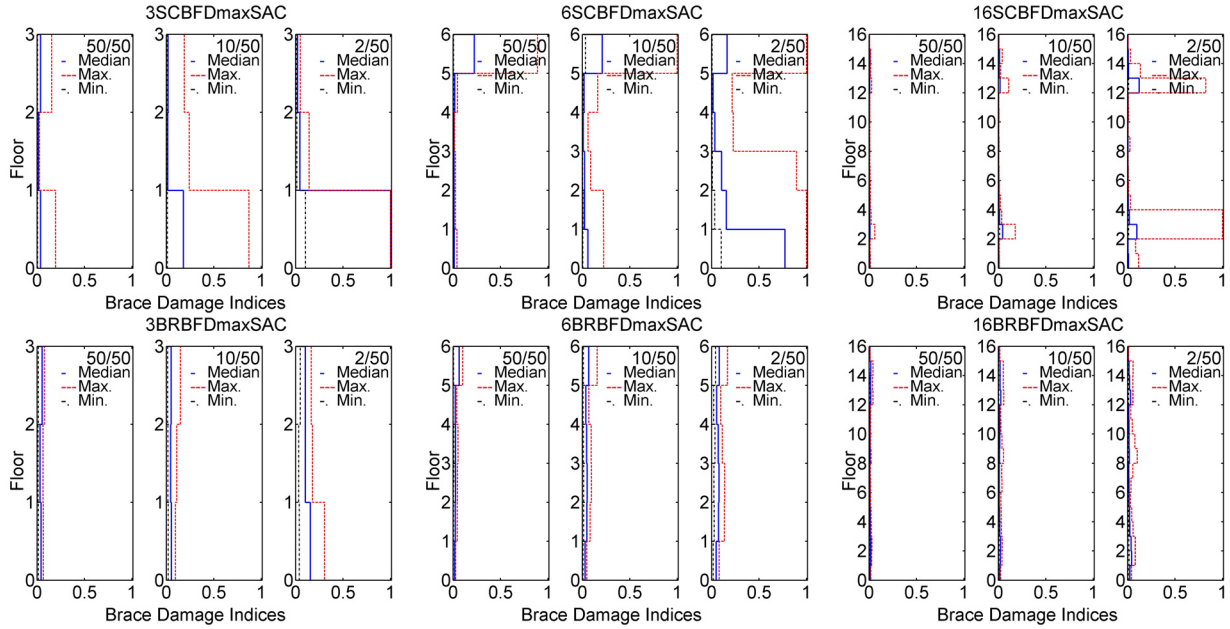

Figure 7.7 Profiles of brace damage indices of SCBF and BRBF archetypes under SAC ground motions corresponding to three hazard levels

Figure 7.8 compares the damage indices for braces at the same story for various archetypes and hazard levels. Note that some values are different from the values of the envelope depicted in Figure 7.7; this is because the sample sizes were different for the two figures. The median DI values for the two braces in the same story were almost identical for most of the archetypes. The maximum DI profile of the BRBF archetypes was symmetric, but that of SCBF archetypes showed some asymmetric distribution. For those stories where one brace ruptured completely (DI = 1.0), the other brace usually also ruptured except for some instances in 16SCBFDmaxSAC. The right braces in the 3rd and 4th story of 16SCBFDmaxSAC ruptured completely according to the maximum DI values; however, the maximum DI in the left brace was only 0.27 for the 3rd story and 0.05 for the 4th story. The drift concentration for few ground motions resulted in an asymmetric profile of the brace damage in the SCBF archetypes. For the BRBF archetypes, the brace damage distribution occurred along the height showed a uniform and symmetric response at various hazard levels.

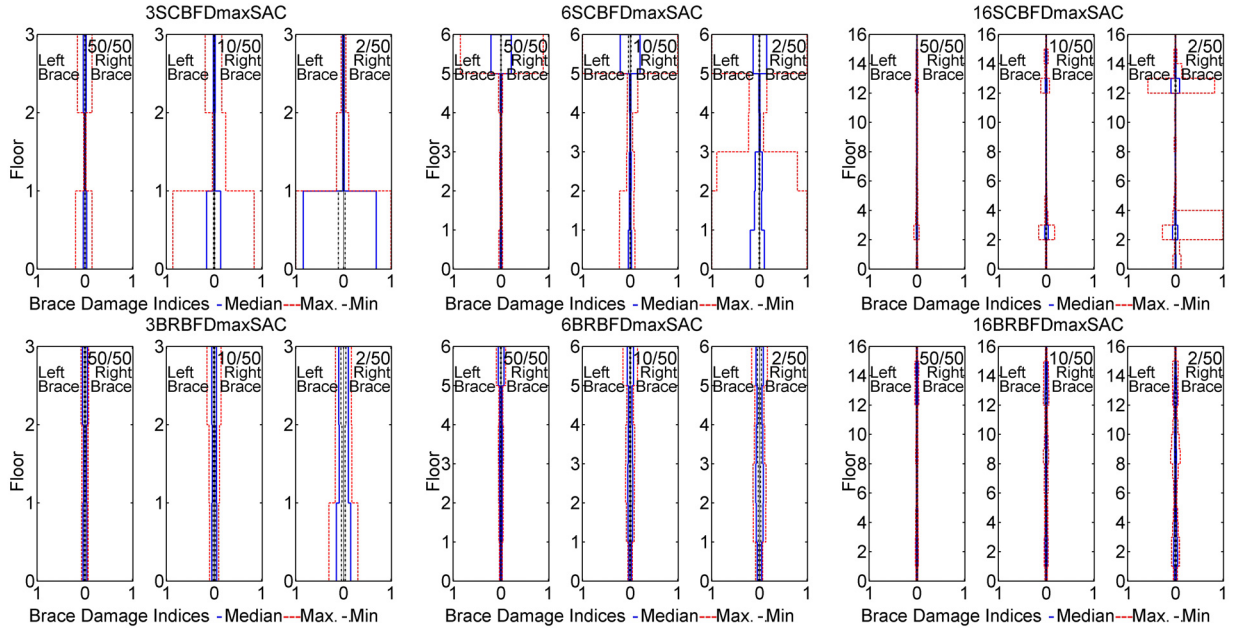

Figure 7.8 Comparison of brace damage indices of two braces at the same level in SCBF and BRBF archetypes under SAC ground motions corresponding to three hazard levels

Figure 7.9 shows the relationship between brace damage indices and DRmax for all archetypes; the responses from all stories were plotted together. Note that the relationship was approximately linear in the figure. The data demonstrate that only few DI data points were between 0.3 and 0.6 with most readings below 0.3 or close to 1.0. In other words, in most cases, the braces had either reached a 30% level of fatigue or were near rupture. For 6SCBFDmaxSAC, the DI values were usually less than 0.3 when DR was less than 2.0%. When the DR was greater than 2.0% for 6SCBFDmaxSAC, many of the DI values became 1.0.

Among the SCBF archetypes, 6SCBFDmaxSAC showed the steepest slope in the relationship between brace damage indices and DRmax. For the data where the brace damage indices were large but with small DRmax, resulted in a steeper relationship. These data points usually occurred at the 6th story.

Figure 7.10 shows the story drift histories and brace axial deformation histories of various SCBF archetypes under the excitation of LA09. In general, the damage of braces is usually occurred as follows: (1) damage with only few large excursions and several small ones such as the response of the first story in 3SCBFDmaxSAC, the first story in 6SCBFDmaxSAC, and the third story in 16SCBFDmaxSAC; and (2) damage with several median-range excursions (such as the responses of the 6th story in 6SCBFDmaxSAC). The brace axial deformation histories at 6th story of 6SCBFDmaxSAC showed a lot of excursions with about ± 2 inch deformation range. These cycles resulted in severe damage to the braces (DI closes 1.0) without an extreme DRmax. Higher mode effect may contribute to such responses, as experienced in the 6th story for 6SCBFDmaxSAC. The responses of the 3rd story in 3SCBFDmaxSAC and the 13th story in 16SCBFDmaxSAC showed higher-frequency and lower-frequency excitations, respectively, but the story drift was smaller than that found for the 6th story in 6SCBFDmaxSAC. As such, the brace damage indices were not as large as the damage index of the 6th story in 6SCBFDmaxSAC. For identifying brace damage, although DR is often used as a quick estimation, brace damage index is more precise as a measurement.

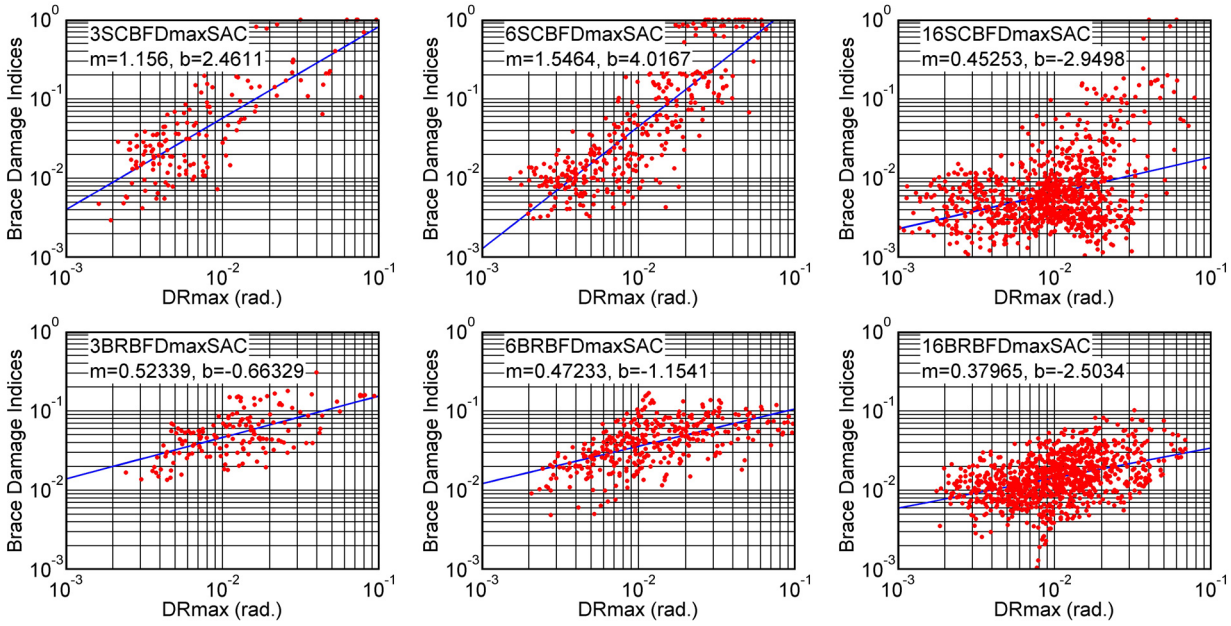

Figure 7.9 The relationship between the maximum brace damage indices of a story and DRmax for all archetypes

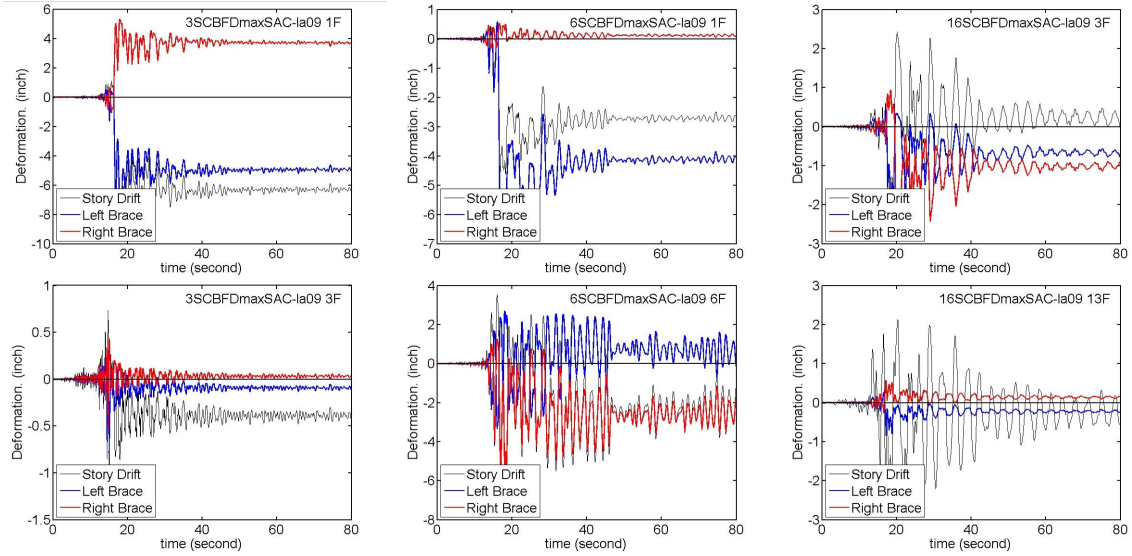

Figure 7.10 Story drift history and braces deformation history of SCBF archetypes subjected to ground motion LA09

7.3 Behavior and Demands for Beams

For beams, the flexural moment demands are generally expected to be more critical than the axial force demand. The beam design for the archetype buildings considered the potential axial force demand from braces such as unbalanced load in chevron braced frames. The structural designs of the archetypes are described in Appendix A. This section examined the axial force demands, flexural moment demands, and the deformation demands in the middle span of the beams where the braces connect in the double story-X configuration.

7.3.1 Beam Axial Force Demand

The axial force demands in the beams of braced frames in the elastic range are expected to be small. The force demands come from the lateral forces (collectors) and the forces transferred from the braces. In the double-story X configuration, the forces transferred from the braces are usually transferred to the braces in the adjacent stories or the columns rather than the beams. As such, the design of these beams is usually not governed by the possible force demand or capacity of the braces and only accounts for the load combinations of dead load, live load, seismic load, etc. However, when the braces yield, buckle and degrade the force of the braces in adjacent stories will need to be transferred by the beams.

Figure 7.11 shows the maximum axial force of the beams at different levels under different ground motion excitations for different archetypes. The beams of the odd stories have the braces intersected in the middle span and those of the even stories have braces connected in the beam-column connections. For the beams in odd stories, if the strength capacity of the braces on adjacent floors are similar, then the unbalanced load applied to the beams in design will be cancelled out. The force demands to consider when designing such beams are small. Because of the conservatism during the design of the archetypes, for the beams in even stories, large axial forces were developed to enable the complete yielding of the tension braces and 30% capacity of

the compressive brace in two adjacent stories. For most of the responses of the archetypes, the beam axial forces did not exceed the capacity of the beams in odd stories where the demand for design was relatively small. The responses also showed that the axial force demands of beams were greater in the lower stories. Generally, the axial force demands in SCBF archetypes were slightly greater than the BRBF archetypes. For the stories where the drift was concentrated, the demands were also greater for both SCBF and BRBF archetypes. There were a few instances in 16SCBFDmaxSAC where the damage was concentrated in certain stories. Many of the maximum beam axial force demands in 16SCBFDmaxSAC approached the capacity of the second floor beam (first story, 1F), which was designed for relatively small demand. Some of the data from the 3rd floor beam (second story, 2F) showed a greater demand than the capacity of the second floor beam. In summary, for the design of beams in even stories, the estimation of beam axial forces demand was very conservative by considering the full capacity of braces on adjacent floors. For the design of beams in odd stories, the estimation of beam axial forces demand was appropriate by considering the full capacity of braces in adjacent stories unless severe drift concentration occurred.

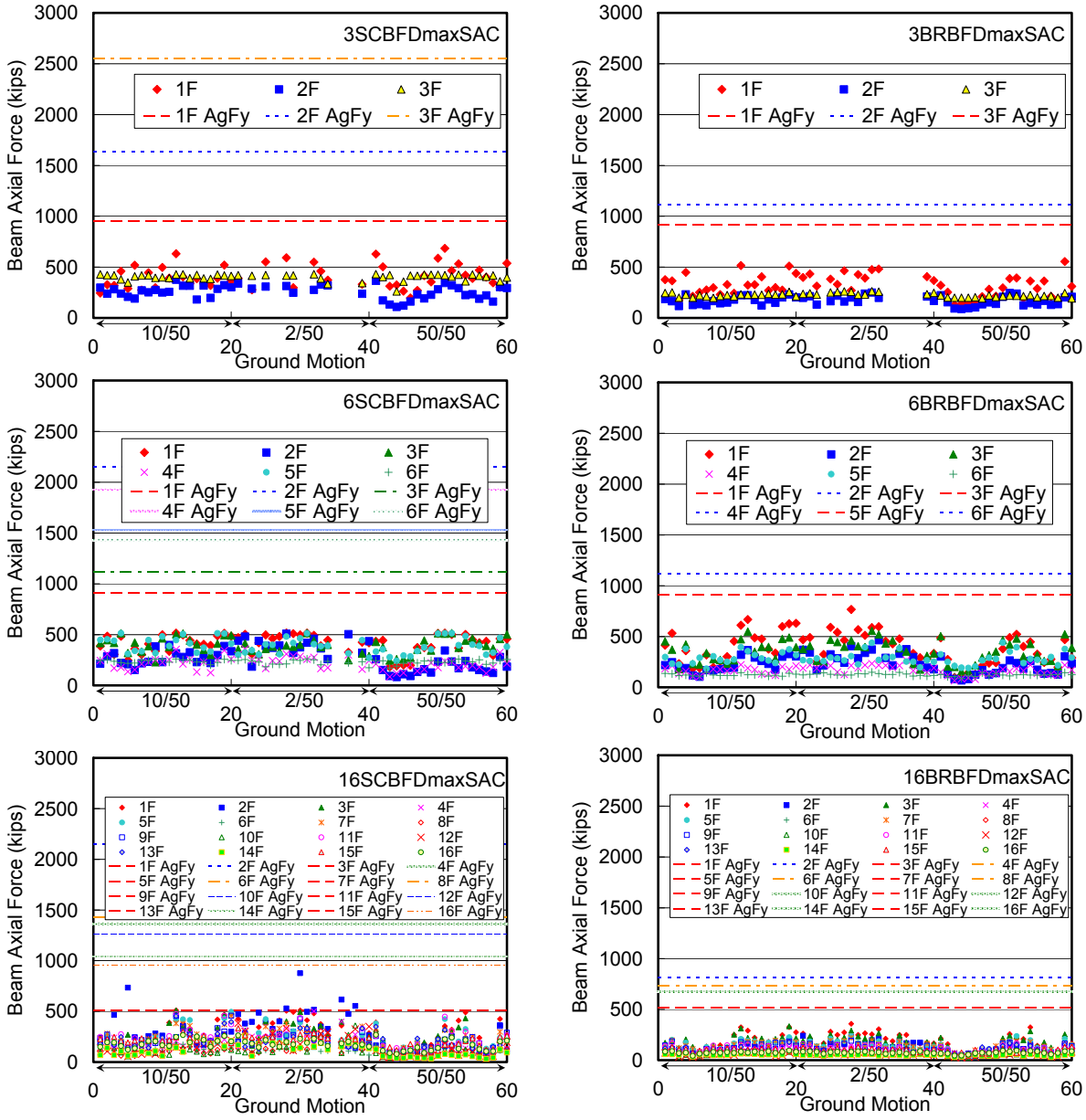

Figure 7.11 Maximum beam axial forces of SCBF and BRBF archetypes under SAC ground motions

Figure 7.12 shows the median and maximum of the beam axial force demands for SCBF and BRBF archetypes at different hazard levels. The median axial force demands were about 40% of the capacity (A_gF_y) in the odd stories and about 10% to 15% in even stories for all archetypes. The beam design for all archetypes estimated the axial force demands by accounting for brace yielding and buckling at extreme conditions, which resulted in greater axial force demands of beams in even stories than those in the odd stories. However, the profile of beam axial force demand under ground motion excitations showed a different trend. The estimations of beam axial force demand for design was much greater than the dynamic responses of the archetypes.

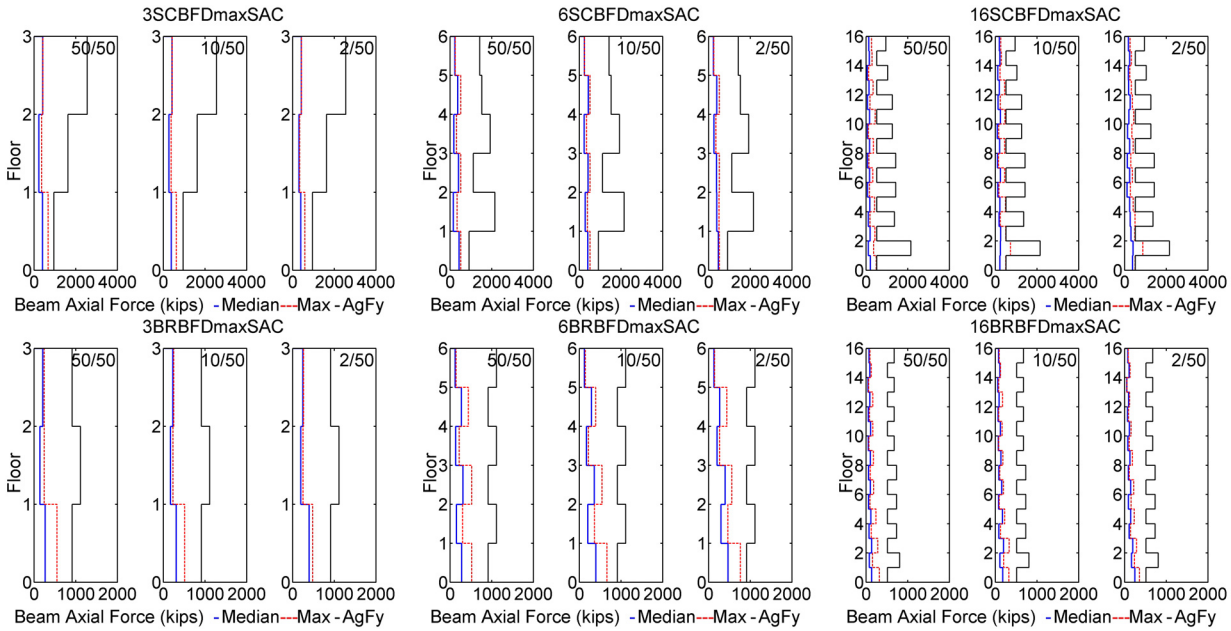

Figure 7.12 Profiles of beam axial forces of SCBF and BRBF archetypes under SAC ground motions corresponding to three hazard levels

7.3.2 Beam Flexural Moment Demand

The profile of moment demands in beams of all the archetypes is shown in Figure 7.13. For 3SCBFDmaxSAC, the median and maximum of moment demands in the first story were approximately equal to the moment capacity of the first story at the design- and MCE-level events, while those on the second and third stories were about 30% of the moment capacity. At various hazard levels for 6SCBFDmaxSAC, none of the beams reached their moment capacity because 6SCBFDmaxSAC had a relatively uniform drift distribution and the force demands were also distributed more uniformly along the height. For 16SCBFDmaxSAC, the drift was concentrated in the 3rd and 13th story at the design- and MCE-level events resulting in highly nonlinear behavior on those floors; the beam moment demands for the 3rd and 13th story of 16SCBFDmaxSAC reached the beam capacity.

The properties of beam moment demands profile for the BRBF archetypes were different from those of the SCBF archetypes. For 3BRBFDmaxSAC and 6BRBFDmaxSAC, the profiles of beam moment demands were rather uniform at three hazard levels; at the design- and MCE-level events, the medians, maxima and the beam capacity were similar in the lower stories. For 16BRBFDmaxSAC at the design-level event, while all the medians of beam moment demands were below the moment capacity, the maxima of beam moment demands almost coincided with the moment capacity; at the MCE-level event, the medians, maxima, and beam moment capacity were almost identical except for the top few floors. Because of strain hardening, some of the maxima were even greater than the capacity of the beam moments.

The difference between the maximum beam moment demand and capacity demonstrates that beam moment demand reached the capacity in many stories for the BRBF archetypes at the design- and MCE-level events. Given that, it would be expected that the BRBF archetypes experienced more nonlinear flexural behavior of beams, dissipating more energy through beam plastic rotations than their SCBF counterparts. The magnitude of beam moment demands were

also greater in the BRBF archetypes.

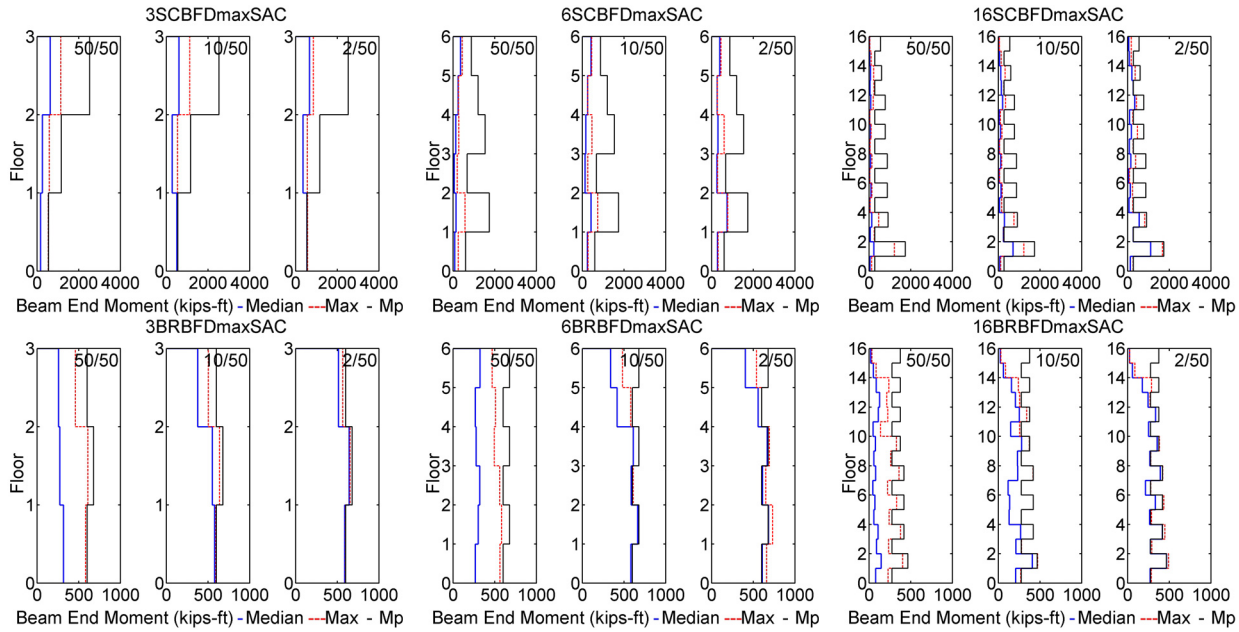

Figure 7.13 Profiles of beam end moments of SCBF and BRBF archetypes under SAC ground motions corresponding to three hazard levels

7.3.3 P-M Relationship of Beams

While the medians and maxima of beam axial force and moment demands provided these peak responses independently, it was more common that the axial forces and moments interact with each other and the peak responses of beam axial force and moment demands did not occur at the same time. Figure 7.14 shows examples of the P-M demands of beams in the first story for all archetypes under the excitation of LA09. In the first story of 3SCBFDmaxSAC, although the beam axial force was below 20% of the beam axial force capacity most of the time, at some instant, it was more than 30% of the capacity. The left beam at left end, which is the beam-column connection and right beam in the middle span, reached the moment capacity (M_p) in this example. In the first story of 6SCBFDmaxSAC, the responses of beam axial force demand was similar to that observed in 3SCBFDmaxSAC with one difference. The moment demands at all beam ends were only about 50% of the beam moment capacity; the left beam at left end and right beam in the middle span had similar moment demands. In the first story of 16SCBFDmaxSAC, the beam axial force demand was about half that of 3SCBFDmaxSAC and 6SCBFDmaxSAC, and the beam moment demand was much smaller than the 3- and 6-story counterparts; the beam moment demand was about 20% of the capacity. Clearly for 16SCBFDmaxSAC that the beam moment demands were higher at beam-column connections (i.e. at the left end of left beam and right end of right beam) than the moment demand in the middle span of these beams.

The P-M responses of BRBF archetypes show more consistency among different archetypes; the beam axial force demands were all about 20% of the capacity and beam moment demands all reached the capacity in the three archetypes. For all BRBF archetypes, the inelastic behavior and moment demands were concentrated at beam-column connections (left end of left beam and

right end of right beam) rather than at the middle span of the beams.

The archetypes were designed with double-story X configuration which reduced the unbalanced load in beams. In SCBF archetypes, although the unbalanced load had been reduced, its effects still cannot be ignored in beam design. Under the unbalanced load, the moment demands in the middle span of the beams are about the same magnitude of the moment demand in the ends of the beams as shown in the first story of 3SCBFDmaxSAC and 6SCBFDmaxSAC. For 16SCBFDmaxSAC, because the deformation and force demands were smaller than the 3- and 6-story counterparts, the unbalanced loads were usually small and the moment demands in the ends of the beams were greater than the moment demands in the middle span of beams; only the floors that had a higher deformation demand had similar magnitude of beam moment demands in the middle and ends of the beams. In the BRBF archetypes, the unbalanced loads had little effects on the beam moment demands in the middle span of beams. All the beam moment demands in the middle span of the beams in BRBFs were far less than those in the ends of the beams.

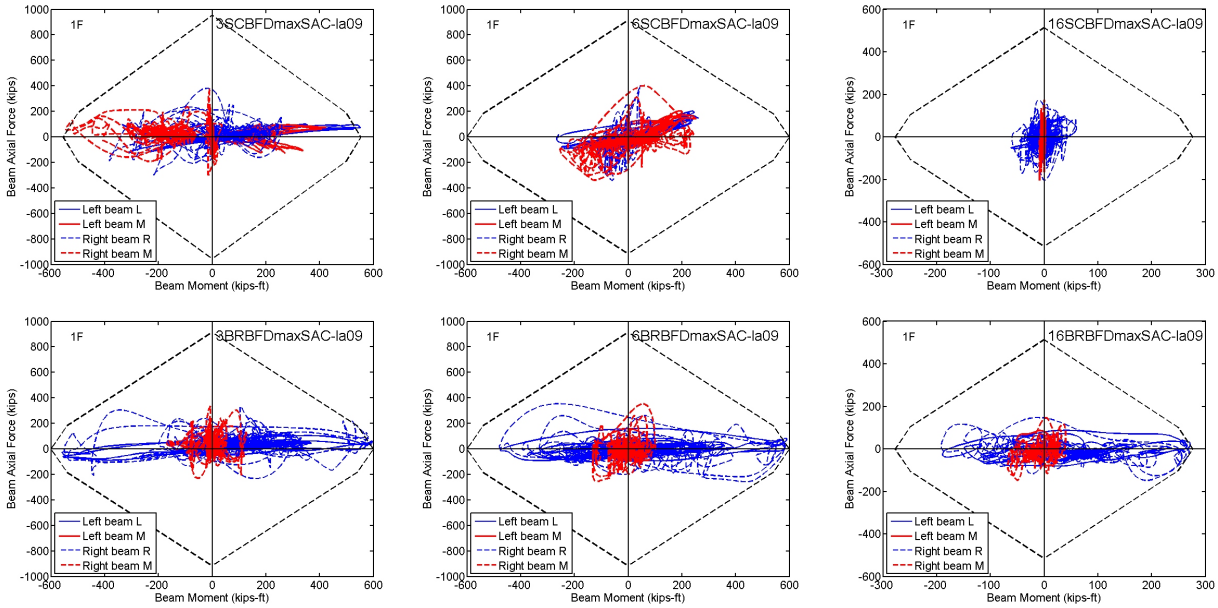

Figure 7.14 P-M interactions of the beams in the first story of SCBF and BRBF archetypes under the excitation of SAC ground motion LA09

Figure 7.15 shows the P-M relation of the beams on the second story. The beam axial force demands were about 10% of the capacity and the beam moment demands dominated the behavior of the second story in all SCBF and BRBF archetypes. The response loops in the SCBF archetypes were relatively small because the capacity of these beams was much greater than the demands. In fact, the maximum beam moment demand of 6SCBFDmaxSAC was similar to that of 6BRBFDmaxSAC (about 700 kips-ft), the maximum beam moment demand of 3SCBFDmaxSAC was smaller than that of 3BRBFDmaxSAC, and maximum beam moment demand of 16SCBFDmaxSAC was greater than that of 16BRBFDmaxSAC. For the even stories, the beam moment demands in SCBF and BRBF archetypes were similar.

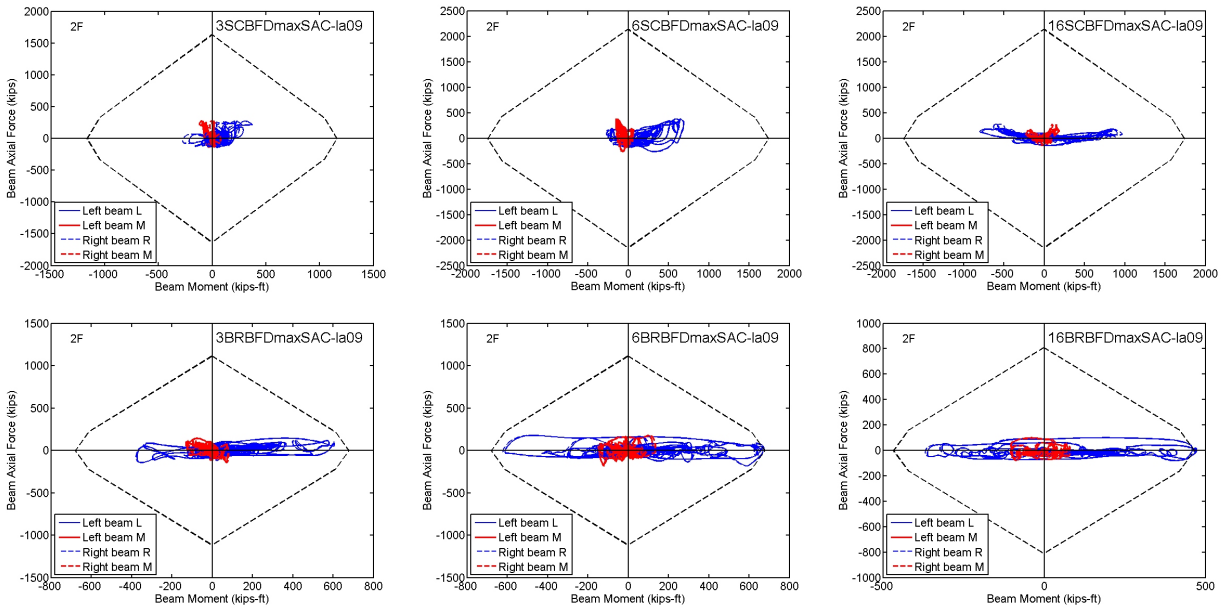

Figure 7.15 P-M interactions of the beams in the second story of SCBF and BRBF archetypes under the excitation of SAC ground motion LA09

7.3.4 Vertical Displacement in the Middle Span

In chevron braced frames, beams are designed to resist the unbalanced loads due to yielding and buckling of the braces. In double-story X configuration, these unbalanced loads are expected to be small. However, some of the analytical results show that the vertical deformation in the middle span of beams where the braces intersect should not be neglected. These beams are designed considering the brace capacity difference, which is small, on adjacent floors. However, when one of the braces intersected in a beam yields, buckles or loses its strength capacity, the unbalanced loads in the beam will be increased leading to a large mid-span vertical displacement.

Figure 7.16 shows the median vertical deformation in the middle span of the beams in the odd stories for all SCBF and BRBF archetypes at different hazard levels. At the service-level event, the median vertical deformations were small; with the maximum deformation of about 0.2 inches occurring in the first and third story of 3SCBFDmaxSAC.

At the design-level event, the median vertical deformations were more than 1.0 inch and 1.5 inches in the first story of 3SCBFDmaxSAC and 6SCBFDmaxSAC, respectively. The vertical deformation of 1.0 inch in the middle span of the beam corresponded to about 0.5% drift ratio in the beam-column connections. In such cases, the deformation demands of the beam-column connections will increase by 0.5% radians, accordingly. Note that the beam vertical deformations in 16SCBFDmaxSAC are relatively large in the stories where the DR is concentrated; the beam vertical deformations were 0.78 inches and 0.22 inches in the 3rd and 13th story, respectively at the design-level event. Although the amount of vertical deformation in the middle span of beams for 16SCBFDmaxSAC at the design-level event may not increase the structural damage to a large extent, it may cause non-structural damage that can not be ignored.

At the MCE-level event, the median vertical deformation was as high as 3.93 inches on the

first floor of 6SCBFDmaxSAC, which corresponded to about 2% drift ratio in the beam-column connections; this increased the deformation demands of the beam-column connections by a large amount, thereby increasing the risk of damaging the beam-column connections. Other large median vertical deformations in the middle span of beams at the MCE-level event occurred in the third story of 6SCBFDmaxSAC (2.15 inches), in the third story of 16SCBFDmaxSAC (1.82 inches), in the first story of 3SCBFDmaxSAC (1.45 inches), and in the 13th story of 16SCBFDmaxSAC (1.1 inches).

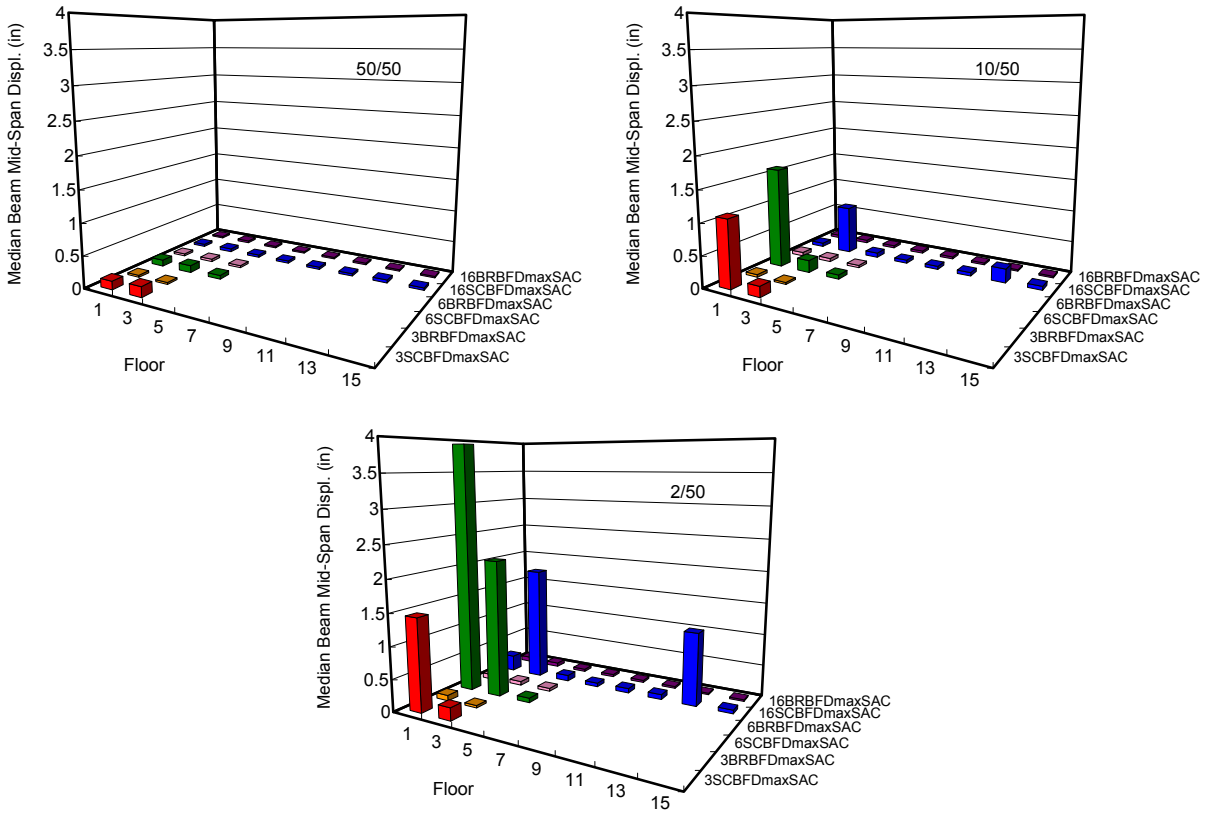

Figure 7.16 Median vertical deformations in the middle span of beams in odd stories in SCBF and BRBF archetypes under SAC ground motions corresponding to three hazard levels

In general, the large median vertical deformations in beams occurred on the floors where the brace DI values of braces had greater differences between adjacent stories (see Figure 7.7). When one of the braces intersected in the beam yielded, buckled or degraded, the unbalanced load was likely to cause large mid-span deformation in the beam.

7.4 Behavior and Demands for Columns

Columns are one of the most critical structural components to protect the buildings from collapse. In this section, column axial force demands (compression and tension), column moment demands and P-M relationships are examined.

7.4.1 Column Axial Force Demand

Axial force is one of the primary components of columns to resist lateral forces. Axial force demand usually governs the design of the columns. In this section, the column axial force demands are extracted from the responses to the combinations of gravity loads and lateral seismic loads, and only include the responses to lateral seismic loads.

Figure 7.17 shows the median column axial force demands under various hazard levels. Positive values represent tensile axial force demands and negative ones represent compressive axial force demands. For all the 3-story and 6-story archetypes demonstrate that the medians and maxima of column axial force demands were similar at the same story and the values were almost identical for various hazard levels. Clearly, the column axial force demands of 3-story and 6-story archetypes were bounded as the medians and maxima coincided with each other. In 16SCBFDmaxSAC, while the maxima of column axial forces were similar to the capacity at all hazard levels, the medians increase as the hazard level increases from the service-level event to the design- and MCE-level events. The maximum axial force demands in 16SCBFDmaxSAC reach the capacity of the columns at the design- and MCE-level events almost on all the floors. In 16BRBFDmaxSAC, the maximum column axial force demands barely change with the hazard levels and are about 40% of the column axial force capacity. Here, the median column axial force demands are smaller than the maximum column axial force demands at the service-level event, but similar to the maximum column axial force demands at the design- and MCE-level events.

The profile of the column axial force demands shows that these demands change every two story. The double-story X configuration contributes to this profile. More specifically, the column axial force demands are related to the force demands and capacity of braces.

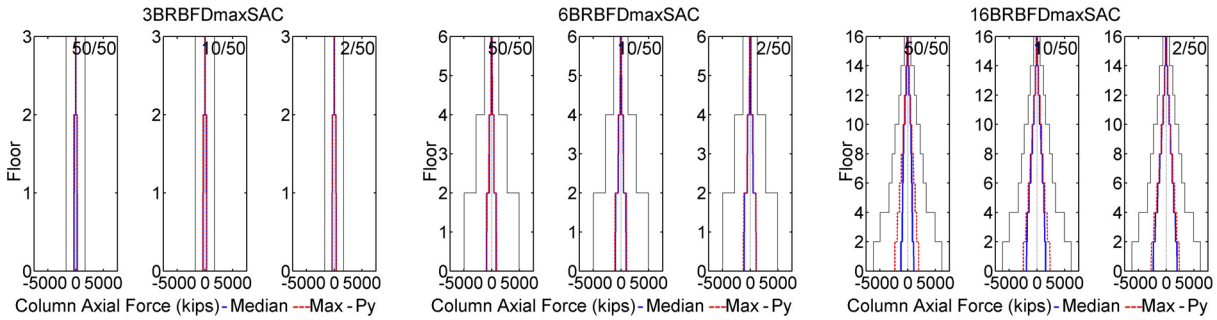

Figure 7.17 Profiles of axial forces in columns of SCBF and BRBF archetypes under SAC ground motions corresponding to three hazard levels

7.4.2 Column Flexural Moment Demand

Figure 7.18 shows the column moment demands of all archetypes at different hazard levels; only the maxima of the top and bottom ends of the column in the same story are shown. In 3SCBFDmaxSAC and 3BRBFDmaxSAC at all hazard levels, the maxima of the column moment demands reach the capacity at the first story. For 6- and 16-story archetypes, the median column moment demands increased, in general, as the hazard level change from the service-level event to the design- and MCE-level events. For 3SCBFDmaxSAC at the service-level event,

the median column moment demand in the third story was slightly greater than that measured in the second story. For 6SCBFDmaxSAC, the median and maximum column moment demands increased as the hazard levels became more severe. At the MCE-level event the maximum column moment demands reached capacity at odd stories, where the column section changed. In higher stories of 6SCBFDmaxSAC, the column moment demands were small, but approached the column moment capacity for all three hazard levels. The trend for 6BRBFDmaxSAC and 6SCBFDmaxSAC were similar. In 16SCBFDmaxSAC and 16BRBFDmaxSAC, the median column moment demands were less than 800 kips-ft, which is about 40% of the column moment capacity, on the stories higher than the 5th story at all hazard levels. In the first stories of the 16-story archetypes, the maximum column moment demands were less than 80% of column moment capacity at the design-level event. The maximum column moment demands reached the 95% and 100% of column moment capacity in the first stories of 16SCBFDmax and 16BRBFDmax, respectively, at the MCE-level event.

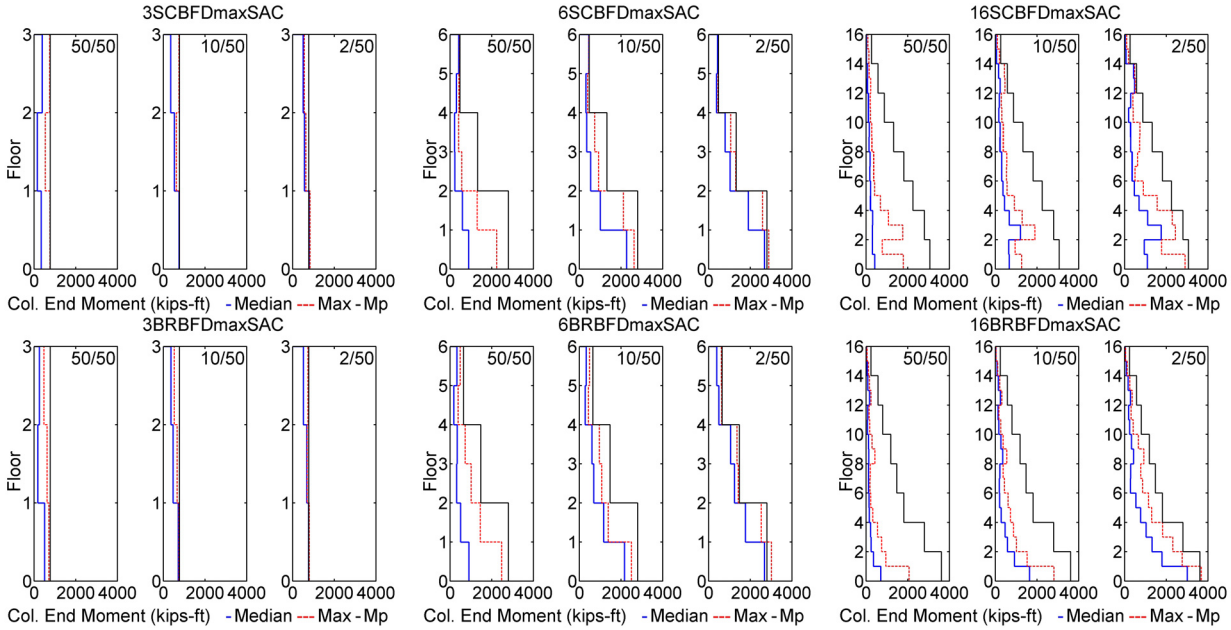

Figure 7.18 Profiles of column end moment of SCBF and BRBF archetypes under SAC ground motions corresponding to three hazard levels

7.4.3 P-M Relationship of Columns

Figure 7.19 shows the P-M relationship of the columns in the first story of all archetypes under the LA09 excitation. For the SCBF archetypes, the column axial force demand was about 600 kips in 3SCBFDmaxSAC, 2000 kips in 6SCBFDmaxSAC, and 5000 kips in 16SCBFDmaxSAC. For 3SCBFDmaxSAC, the column axial force demand was about 30% of the column axial force capacity. The column moment demands of 3SCBFDmaxSAC reached the P-M envelope in both left and right columns at both top and bottom ends. For 6SCBFDmaxSAC, the column axial force demand was about 40% of the column axial force capacity. While the column moment demands at the bottom end of the columns of 6SCBFDmaxSAC reached the column moment capacity, those at the top ends are about 30% of the column moment capacity. For 16SCBFDmaxSAC, the P-M response was obviously differ-

ent from the responses measured in 3SCBFDmaxSAC and 6SCBFDmaxSAC. The responses of 16SCBFDmaxSAC demonstrated that the columns on the first story were subjected to large axial force demands to resist lateral forces in this high-rise building. The column moment demand was about 10% of column moment capacity.

In the BRBF archetypes, the column axial force demand was about 300 kips in 3BRBFDmaxSAC, 1000 kips in 6BRBFDmaxSAC, and 2500 kips in 16BRBFDmaxSAC. For 3BRBFDmaxSAC, the column moment demands reached the P-M envelope in both left and right columns at both the top and bottom ends. For 6BRBFdmaxSAC, the column axial force demand was about 20% of the column axial force capacity, and the column moment demands were all under the P-M envelope. For 16BRBFDmaxSAC, the column axial force demands of the columns were not as high as those found in 16SCBFDmaxSAC, but the column moment demand at bottom of the column reached the P-M envelope. The 16-story BRBF archetype obviously had a greater column moment demand under the same ground motion excitation than its SCBF counterparts; the column responses of 16BRBFDmaxSAC exhibited greater flexural behavior and those of 16SCBFDmaxSAC exhibited greater tensile and compressive behavior.

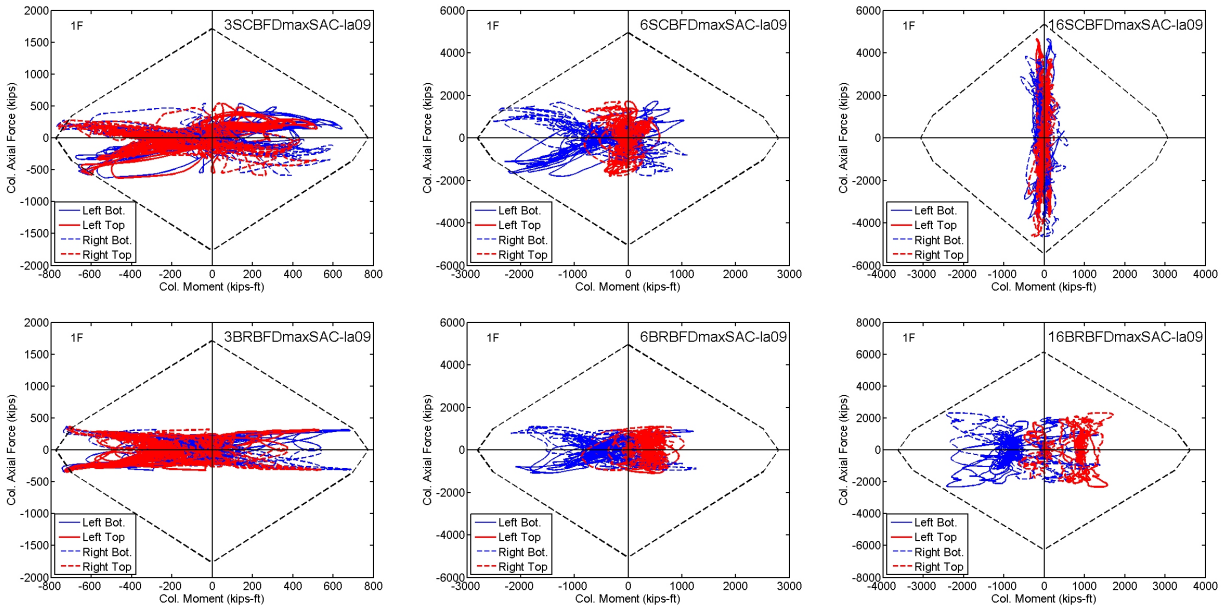

Figure 7.19 P-M interactions of the columns in the first story of SCBF and BRBF archetypes under the excitation of SAC ground motion LA09

Figure 7.20 shows the P-M relationships of the columns in the second story for all archetypes under LA09 ground motion excitation of. The axial force demands were about the same as those in the first story, as the axial force demands approximately changed every two stories. The column moment demands were reduced compared to the responses of the columns in the first story for most of the archetypes except in the case of 16SCBFDmaxSAC. The responses show that the bottom of the columns usually had slightly greater moment demands than the top of the columns in all archetypes.

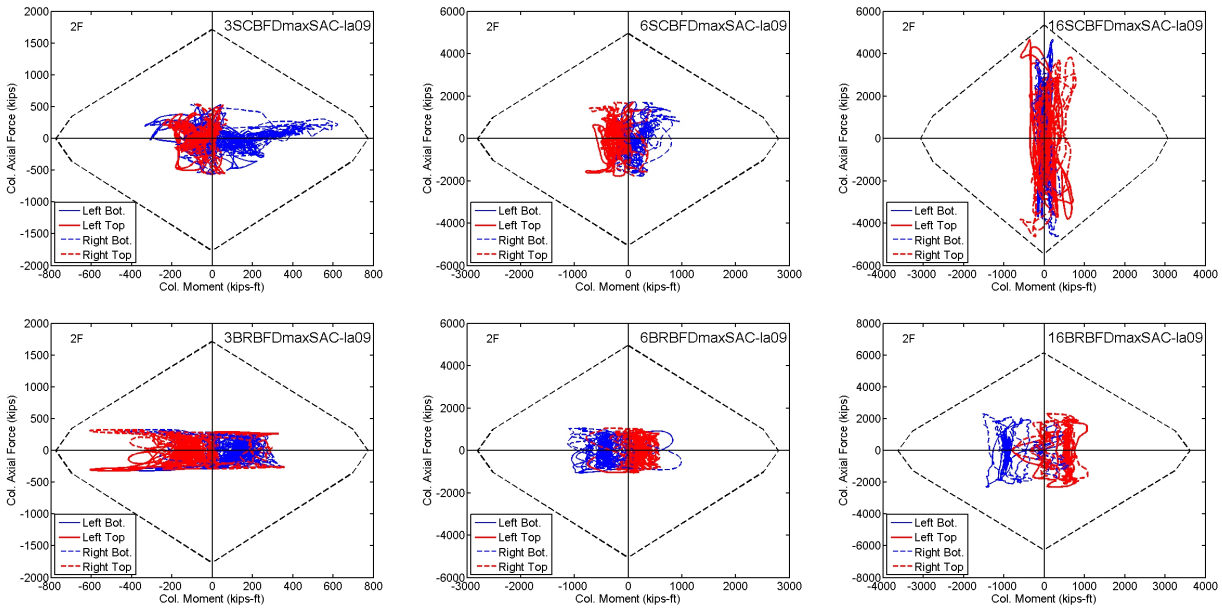

Figure 7.20 P-M interactions of the columns in the second story of SCBF and BRBF archetypes under the excitation of SAC ground motion LA09

7.4.4 Estimation of Column Compression Force Demand

The column axial force demands were bounded and change every two stories as shown in Figure 7.17. The accurate estimation of the column demands are discussed below based on the capacity and demands of the braces and beams. In the SCBF archetypes, the force demands in the braces reached the capacity in some stories and usually not in all stories. It is conservative if the column axial demands for design were estimated by considering the full capacity of braces and beams in all stories. Figure 7.21 illustrates the design estimation of the upper bound of column force demand, which is the sum of the brace and the beam capacity of the upper floors. In double-story X configuration, the estimate was calculated differently for the odd stories compared to the even stories. The vertical component of brace in story j can be expressed as:

$$V_{br,j} = P_{br,j} \cdot \sin\theta \tag{7.8}$$

where $P_{br,j} = \begin{cases} P_{cr} & j = 1,3,5,... \\ P_y & j = 2,4,6,... \end{cases}$

θ is the incline angle of the brace with respect to the horizontal.

Accordingly, the column axial force demands in story i was estimated as follows as the sum of the demands of the braces and beams in the all upper stories:

$$P_{col,i} = \begin{cases} \sum_{j=i+1}^{\#story} (V_{br,j} + V_{b,j}) + V_{b,i} & i = 1,3,5,... \\ \sum_{j=i}^{\#story} (V_{br,j} + V_{b,j}) & i = 2,4,6,... \end{cases} \tag{7.9}$$

Note that the difference between $P_{col,1}$ and $P_{col,2}$ was only $V_{b,1}$ and that between $P_{col,3}$ and $P_{col,4}$ was only $V_{b,2}$ and so forth.

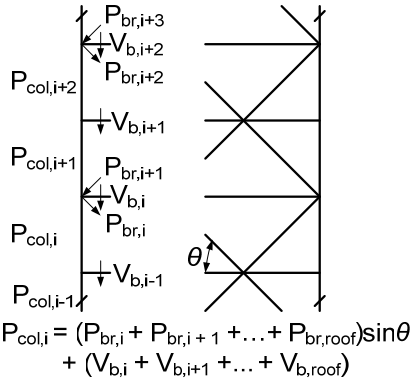

Figure 7.21 Illustration of estimation of column axial force demands

The previous analysis of the demands in beams and braces demonstrated that the demands were usually smaller than the corresponding capacity although the demands still reached the capacity in some stories under some ground motion excitations. To estimate the column axial force, the reduction factor in equation (7.10) for the brace capacity of upper stories was adopted. To estimate the axial force demand of column on floor *i*, the reduction factor was applied to each upper story (from story *i* to the roof level). The reduction factor was proposed to account for the full brace capacity on the floor in question, while reducing exponentially with the power of k for the higher floors (which varies depending on the archetypes).

For the 3- and 6-story archetypes, the k was taken as a large number such that reduction factor ϕ_{ji} was 1.0 for all the upper floors to be considered, i.e., the full brace capacity of upper floors were used to estimate column axial demands. For the 16-story archetypes, the reduction factor changed along the height; the brace capacity for estimation of column axial force demands was reduced further for the higher floors. At the instant that the maximum column axial force demands occurred in a story, the force demands in the other upper stories were usually not the maximum demands in those stories. What was more common was that the force demands in some of these upper stories reached the corresponding force capacity, but in other stories, the force demands remained small. The reduction factor was assigned to maximize the possible braces strength but reduce the braces strength on some floors as necessary for estimating column demands. In other words, the reduction factor was greater for the braces in the lower stories (with larger capacity) and less in the higher stories.

$$\phi_{ji} = 1 - \left(\frac{j-i}{\#story} \right)^k \qquad j \geq i \tag{7.10}$$

If we apply the reduction factor for the braces, the column axial force demands can be rewritten as:

$$P_{col,i} = \begin{cases} \sum_{j=i+1}^{\#story} (V_{br,j} \cdot \phi_{ji} + V_{b,j}) + V_{b,i} & i = 1,3,5,... \\ \sum_{j=i}^{\#story} (V_{br,j} \cdot \phi_{ji} + V_{b,j}) & i = 2,4,6,... \end{cases} \tag{7.11}$$

where V_b depends on the moment demands at beam ends. As demonstrated in the response of SCBF archetypes, most of the beam end moments were usually less than the beam moment capacity. The corresponding beam shear was neglected when estimating the column axial force in the SCBF archetypes. For BRBF archetypes, the beam end moment demands were closer to the corresponding capacity, and therefore the accumulative beam shear acting on columns was more significant compared to the SCBFs. As shown in Figure 7.22, by ignoring V_b in SCBF archetypes and including $V_{b,j} = 2M_{p,j} / span$ in BRBF archetypes, we obtain the estimated column axial force demands and the percent errors. Note that the percent errors in top stories were large because the calculation was normalized by the values of the column axial force demands (which were small in top stories). For the 3- and 6-story archetypes, reduction factor ϕ for all braces was taken as 1.0. This corresponded to a large number of k, and 100% of the brace capacity was considered to estimate the column axial forces.

For 16-story archetypes, the reduction factors for braces were calculated with an exponent k of 0.95. For example, when calculating the column axial force demand in the second story, 100% of the brace capacity was considered in the second story while only 12% of the brace capacity was considered for the roof. With the appropriate reduction factors, the percentage errors for all archetypes were reduced to less than 10% except for the top stories, where the absolute errors were not greater than the other stories.

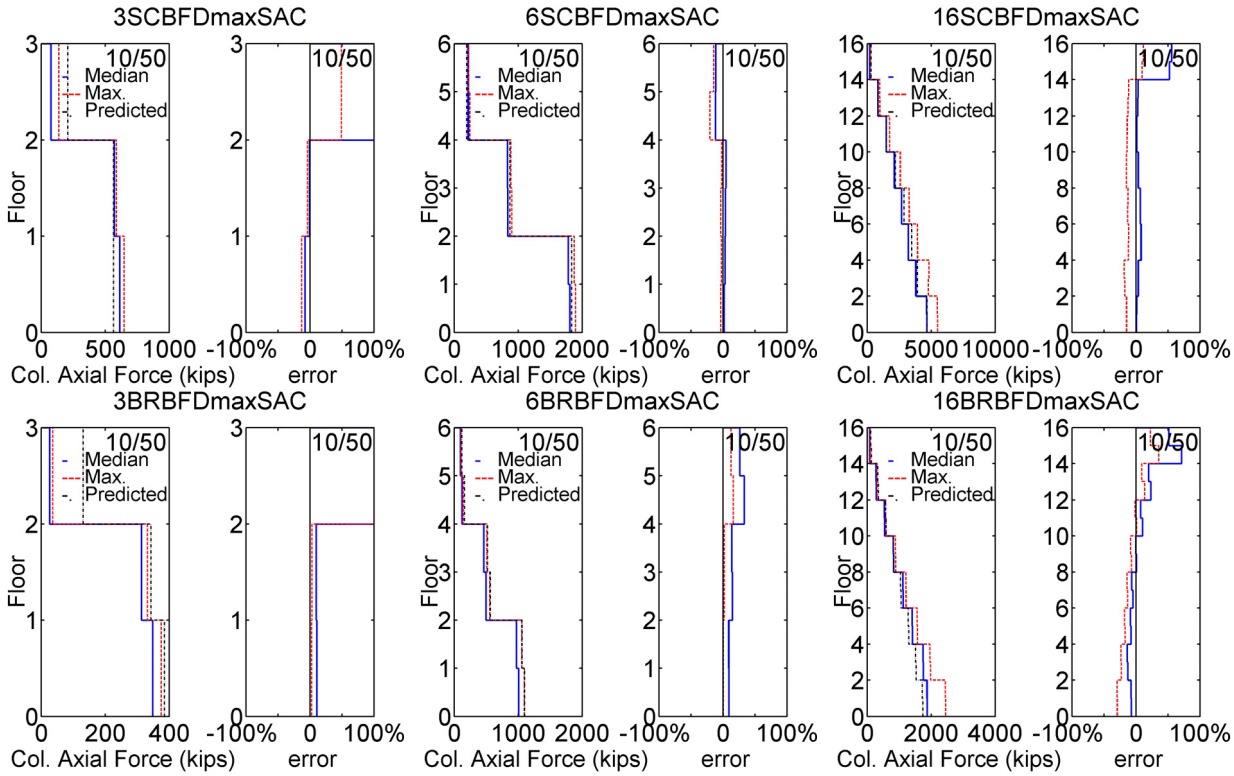

Figure 7.22 Profiles of the estimated axial compressive forces in columns and the percent errors of SCBF and BRBF archetypes under the design-level SAC ground motions

7.5 Summary

The EDPs of structural components in braced frame buildings were evaluated including the force and deformation demands in braces, beams and columns. These demands at various hazard levels are expected to provide indices to improve the design criteria of the structural components in steel braced frame buildings.

Braces:

The out-of-plane deformation is approximately proportional to square root of DR. Note that when the DR is less than the DR that initiates buckling of the brace, the out-of-plane deformation has not occurred yet. The proposed relationship between out-of-plane deformation and DR estimates the out-of-plane deformation accurately at various hazard levels.

Comparing the SCBF archetypes with their BRBF counterparts, the brace ductility demand of BRBFs is generally smaller at various hazard levels. The smaller brace ductility demand and better ductility performance of BRBF archetypes lead to a more reliable seismic resisting structural system compared to SCBFs.

The median damage indices (DI) of braces were approximately identical for two braces in the same story for most of the archetypes. While the maximum DI values of the BRBF archetypes were similar for the two braces in the same story, those of the SCBF archetypes showed different shapes of DI profile. The drift concentration of a few ground motions resulted in an asymmetric profile of the brace damage for SCBF archetypes. The brace damage profile of BRBF archetypes shows uniform and symmetric response at various hazard levels.

DI provides an index to monitor the fatigue life of braces. In most cases, braces were either 30% exhausted in terms of fatigue life or had nearly completely ruptured.

Beams:

In general, the axial force demands of SCBF archetypes were slightly greater than those of the BRBF archetypes. For designing beams for even stories, where the braces connect in beam-column connections, the estimation of beam axial force demand becomes very conservative if considering the full tensile capacity of braces and neglecting the compressive capacity of braces in adjacent stories. For designing beams for odd stories, where the braces connect in the mid-span of beams, the estimation of beam axial force demand is acceptable if considering the full capacity of braces in adjacent stories, unless severe drift concentration occurs.

For the beam moment demands, the analyses showed that most of the median beam moment demands in SCBF archetypes were less than the beam moment capacity. For BRBF archetypes, median and maximum beam moment demands reached the capacity in many stories at the design- and MCE-level events. It is then expected that the beams in the BRBF archetypes experienced more nonlinear flexural behavior and, therefore, dissipated more energy through beam plastic rotations than their SCBF counterparts.

In all BRBF archetypes, the beam axial force demands were all about 20% of the capacity and beam moment demands all reached the capacity in the three archetypes. The inelastic behavior and beam moment demands were concentrated at beam-column connections (left end of left beam and right end of right beam) rather than the middle span of the beams. In the BRBF

archetypes, the unbalanced loads had little effect on the beam moment demand in the middle span of beams. All beam moment demands in the middle span of the beams in BRBF are far less than those in the ends of the beams. In SCBF archetypes, although the unbalanced load was reduced, its effects could not be ignored. Under the unbalanced load, the moment demands in the middle span of the beams were about the same magnitude of the moment demand in the ends of the beams.

At the design-level event, the median vertical deformations in the middle span of beams were more than 1.0 inch for the first story of 3SCBFDmaxSAC and 6SCBFDmaxSAC, increasing the deformation demands of the beam-column connections by 0.5% radians. The amount of the deformation in the beam-column connections at the design-level event may not increase the structural damage to any large extent, but it may cause non-structural damage that must be addressed. At the MCE-level event for 6SCBFDmaxSAC, the vertical deformation was as high as 3.93 inches at the first story, which corresponded to about 2%-radian rotation of the beam-column connections. This greatly increased the deformation demands of the beam-column connections increasing the risk of damage to the beam-column connections.

Columns:

The profile of the column axial force demands shows the demands along the height changed every two stories, a result of the double-story X configuration. It is expected that the axial force demands of columns are related to the brace demands and capacity.

For all 3-story and 6-story archetypes, the medians and maxima of axial force demands were similar in the same story and did not change much with hazard levels. The axial force demands in 16SCBFDmaxSAC reached the capacity of the columns at the design- and MCE-level events in almost all stories. For 16BRBFDmaxSAC, the axial force demands were not as high as those in 16SCBFDmaxSAC. The 16-story BRBF archetype had higher column moment demand than their SCBF counterparts under the same ground motion excitation; the column responses of 16BRBFDmaxSAC exhibited more flexural behavior while those of 16SCBFDmaxSAC exhibited more tensile and compressive behavior. I all archetypes, the response of column moment demands also showed that the bottom of the columns usually had slightly greater moment demands than the top of the columns.

For the SCBF archetypes, the braces reached capacity in some levels but not all levels. It was conservative if the column axial demands were estimated by the full capacity of braces and beams in all upper stories. Reduction factors were used to determine the percentage of capacity of braces and beams for estimating column axial force demands. With the appropriate reduction factors, the percent errors were less than 10% except in the top stories, where the absolute errors were not greater than the other floors.

Chapter 8

Conclusions and Recommendations

To design and utilize concentrically braced frames more efficiently and with more confidence, numerical studies of several SCBF and BRBF archetypes were analyzed and interpreted on the basis of probability and statistics. Computationally efficient and accurate fiber-based models were constructed to perform an extensive set of nonlinear static and dynamic analyses. The seismic demands of conventionally braced as well as buckling restrained braced frame systems were investigated for several ground motion records corresponding to various hazard levels. The results were used to assess performance and improve the design criteria of braced frame systems. The observations reached in this study are summarized below.

8.1 Modeling

- The force-based beam-column element demonstrates an acceptable degree of accuracy and is recommended to better estimate the nonlinear responses of braced frame systems.
- An appropriate working point at the column base should be defined so that the accurate height of the first story can be included in numerical models, thus, reflecting realistic structural behavior.
- A finite element model (LS-DYNA) satisfactorily captured the local buckling behavior and changes the strength gradually before and after peak strength was reached. The fiber-based model used (OpenSees) exhibited a sudden drop in strength following buckling and when fracture criteria were met. The global buckling of braces occurred at about 0.3% radian drift ratio in the analyses.
- The OpenSees analyses suggest that statistically, the effect of low-cycle fatigue is not pronounced, but it is important to include when predicting the structural response under a single ground motion. The effect of fatigue is more important for predicting the residual displacement than the peak displacement.
- Using inelastic spectrum displacement rather than elastic spectrum displacement for the short-period SCBF systems significantly reduced the scatter in the statistical data, especially for large intensity events.

8.2 Analytical Behavior of Concentrically Braced Frames

- From the analyses, the performance of 3-story SCBF designed as per ASCE/SEI 7-05 and 1997 NEHRP are quite similar statistically. The responses of the top floor are however different due to the change in design criteria for the roof beam of chevron braced frames.
- The expected median maximum story drift ratios of SCBFs with an R of 6 at the service-level event has more than 75% probability to be greater than 0.3%, which is close to the DR that will result in buckling of the braces. Thus, following an occasional earth-

quake for which no structural damage is generally desired, it is necessary to replace one or more braces, and repair nonstructural damage to adjacent elements. The expected median maximum story drift ratios had more than 70% probability of exceeding 2.5% radian at the MCE-level event, at which point the braces fractured due to low-cycle fatigue but the integrity of the beam to column connections is likely adequate.

- The expected median maximum story drift ratios of SCBFs with an R of 3 are less than those needed to initiate buckling at the service-level event, and less than those likely to fracture the beam to column connections at the MCE-level event. Reduction of the R factor was effective in reducing the drift demand of braced frames.
- The BRBF model in Chapter 4 experienced large residual drifts at various hazard levels partly because of its relatively longer fundamental period. Because the elastic stiffness of BRBFs did not reduce dramatically after the braces yielded or were damaged, the braced frame required more force to swing back during a ground motion.
- For SCBFs, reducing the R factor reduced the tendency to form a soft story. The cost of constructing SCBFs with smaller R factors will be higher and significant elastic response can be expected, but the demands are more consistent with the ductility capacity of the connections and buckling braces considered herein.
- The analyses of the archetype buildings showed that the 3-story SCBF tended to concentrate deformation in the bottom story, the 6-story SCBF had greater story drift ratio at the roof level, and the largest drift ratio for the 16-story SCBF occurred in the middle stories. The BRBF archetypes generally had more uniform DRmax profiles than the SCBF archetypes.
- The story shears demands of all the archetypes were usually closed to the yielding capacity of each story if the archetype had experienced nonlinear behavior.
- For the 2-story SCBF archetype, R-factors of 3.3 and 3 for design were more consistent with the ductility capacity of the structural system, which also reduced the drift demand at various hazard levels and the probability of collapse at the MCE-level event.
- This research assumed that the energy dissipation profile over the height of the building during dynamic excitations was proportional to DCR distribution of the first-mode pushover analysis over the height. Under this assumption, the DR of each story was approximately proportional to D_i/C_i^2 (or $D_i \cdot V_y/C_i^2$). The analysis of the 16-story SCBF archetypes shows that, the target DR at different hazard levels can be achieved by limiting the $D_i \cdot V_y/C_i^2$ ratios. In addition, the stiffness difference at adjacent levels should also be limited to reduce damage concentration. 30% difference of $D_i \cdot V_y/C_i^2$ ratio in adjacent stories was adopted in this case study, which successfully reduced the stiffness irregularity and damage concentration of the 16-story SCBF archetype.
- In general, median PFAs at the MCE-level event were greater than those at the other hazard levels especially for the lower floor of all SCBF and BRBF archetypes. Because of the longer fundamental period and higher flexibility of BRBF archetypes, the median PFAs of SCBF archetypes were greater than those of BRBF archetypes along the height of the archetypes. As such, non-structural damage associated with floor acceleration was expected to be more severe for the SCBF archetypes compared to the BRBF archetypes.
- A relationship between out-of-plane deformation and DR is proposed. The out-of-plane deformation is approximately proportional to the square root of DR. The proposed estimate is accurate at various hazard levels.

- The low-cycle fatigue life of braces was monitored in the analyses. The analyses show that in most cases, the braces either exhausted 30% of their fatigue life or they nearly complete rupture.
- The beam moment demands of SCBF and BRBF archetypes show that the BRBF archetypes experience more nonlinear flexural behavior of beams and, therefore, are expected to dissipate more energy through beam plastic rotations than their SCBF counterparts.
- For the SCBF archetypes, although the unbalanced load had been reduced in double story configuration, its effects still cannot be ignored in beams. Under the unbalanced load, the moment demands in the middle span of the beams were similar to the moment demand in the ends of the beams.
- For double story X SCBF, the middle-span vertical deformation of beams at the design-level event may not contribute to the structural damage to any large extent, but it may cause non-structural damage which can not be ignored. At the MCE-level event for the first story of 6SCBFDmaxSAC, the vertical deformation in the middle span of beams was as high as 3.93 inches corresponding to about 2% rotation of beam-column connection. This greatly increased the deformation demands of the beam-column connections and hence increased the risk of damaging the beam-column connections.
- For double-story X configuration, the column axial force demands changed every two story. It is expected that the axial force demands of columns are related to the brace demands and capacity. The 16-story BRBF archetype had higher column moment demand than their SCBF counterparts under the same ground motion excitation; the column responses of 16BRBFDmaxSAC exhibited more flexural behavior while those of 16SCBFDmaxSAC exhibited more tensile and compressive behavior.
- To estimate the axial force demands of columns, it is conservative to consider the full capacity of braces and beams in all stories. Reduction factors were used in the capacity of braces and beams for estimating column axial force demands. With the appropriate reduction factors, the percent errors were less than 10% except for the top stories, where the absolute errors were not greater than the other stories.

8.3 Evaluation of Design Parameters Using FEMAP695 Methodology

Various archetypes of SCBF and BRBFs ranging from 2 to 16 story were evaluated. The appropriateness of seismic performance factors were investigated according to FEMA P695 (ATC-63) methodology.

- The BRBFs passed the evaluation but the 2-story SCBF designed for the upper bound of seismic design category D failed. As such, the seismic performance factors of ASCE/SEI 7-05 seem appropriate for BRBFs based on the Methodology and the archetypes, but may need adjusting for the 2-story SCBF.
- The taller archetypes were designed with the drift control criteria, and member sizes may be increased to obtain more stiffness to limit the drift. The strength is usually increased by increasing the stiffness accordingly. Low-rise archetypes typically satisfy drift requirements and member sizes need not be increased beyond those required for strength. They, thus, have less reserve capacity to resist collapse.
- The Equivalent Lateral Force Analysis (ELF) and Model Response Spectrum Analysis (RSA) resulted in more difference of member sizes for higher-rise braced frames than

lower-rise braced frames. For example, in 6-story SCBF, the difference of force demand in the members determined by ELF and RSA was within 10%. For the 16-story SCBF, the difference increased to 50%. The displacement demand under RSA was much less than that of ELF.

8.4 Recommendations for Future Work

- Full scale component and frame test data on large brace sizes will significantly improve the numerical models and increase the confidence on performance evaluation. The brace components with larger sections are usually stockier and tend to be used with smaller slenderness ratio (KL/r). Braces with smaller KL/r ratio usually have less ductility capacity although they provide higher initial compression strength. Gusset plates and brace to framing connections adjacent to the braces, based on capacity design criteria, also have higher deformation and force demand due to the larger capacity of the heavy braces. The test data should be used to improve the confidence on the quality of the parameters to design the braced frame systems in a more rational manner.
- The evaluation of braced frames should be extended to different design choices, such as different floor plans, different vertical configurations, and different numbers of braced bays. The investigation on the different brace configurations should cover a wider range of samples to improve the confidence of the evaluation.
- The torsional effect of the braced frames building is an important factor, especially when the structure is subject to near-field ground motions in two orthogonal directions, which may show obvious asymmetric excursions. Future numerical simulations should be able to model the fracture of the braces and structural behavior under multi-directional force demand.
- Complex nonlinear behavior of buckling braces and the tendency to form weak stories in SCBFs increase the difficulty of designing such a structural system using PBEE. New strategies need to be developed to reduce or redistribute the engineering demand, so that the demand can be compatible with the structural capacity by applying other engineering solutions, such as base-isolation systems, rocking mechanisms or elastic back-up frame systems.
- While the performance-based design method is a powerful tool, it requires extensive nonlinear analyses. This complex and time-consuming analysis has less appeal in practice and more efforts are required to simplify the method.

Reference

ABAQUS (2003) Version 6.4 online Documentation.

Aguero, A., Izvernari, C., and Tremblay, R. (2006), "Modelling of the Seismic Response of Concentrically Braced Steel Frames using the OpenSees Analysis Environment," *Int. J. of Advanced Steel Construction*, 2(3), 242-274.

AISC. (1997), *Seismic Provisions for Structural Steel Buildings*, American Institute of Steel Construction (AISC), Chicago, Illinois 60601.

AISC. (2002), *Seismic Provisions for Structural Steel Buildings*, American Institute of Steel Construction (AISC), Chicago, Illinois 60601.

AISC. (2005), *Seismic Provisions for Structural Steel Buildings*, American Institute of Steel Construction (AISC), Chicago, Illinois 60601.

Annan, C., Youssef, M., and El Naggar, M. (2009). "Experimental evaluation of the seismic performance of modular steel-braced frames." *Engineering Structures*, 31(7), 1435-1446.

ANSYS (2005) Theory Reference. South Pointe, 275 Technology Drive, Canonsburg (PA): ANSYS Inc.

Anthes, R. J. (1997), "Modified rainflow counting keeping the load sequence," *Internation Journal of Fatigue*, 19(7), 529-535.

Architectural Inst. of Japan, Steel Committee of Kinki Branch (1995), *Reconnaissance report on damage to steel building structures observed from the 1995 Hyogoken-Nanbu (Hanshin/Awaji) earthquake*, AIJ, Tokyo, May, p.167.

ASCE/SEI 7-05 (2005) *Minimum Design Loads for Buildings and Other Structures*, American Society of Civil Engineers, Reston, VA.

ASTM. (2003). "ASTM E 1049 - 85: Standard Practices for Cycle Counting in Fatigue Analysis." West Conshohocken, PA.

Asgarian, B. and Shojrgozar, HR.(2009), "BRBF response modification factor,".*Journal of Constructional Steel Research*, 65(2), 290-298.

Baker, J.W. (2005), *Vector-Valued Ground Motion Intensity Measures for Probabilistic Seismic Demand Analysis*, Ph.D. Dissertation, Department of Civil and Environmental Engineering, Stanford University.

Baker, J.W. and Cornell, C.A., (2006), "Spectral shape, epsilon and record selection," *Earthquake Engineering. & Structural Dynamics*, 34 (10), 1193-1217.

Balendra, T., and Huang, X. (2003), "Overstrength and Ductility Factors for Steel Frames Designed According to BS5950," *ASCE Journal of Structural Engineering*, 129(8), 1019-1035.

Basquin, O.H. (1910), "The exponential law of endurance tests," *Proceedings* of ASTM, 10:625-630, 1910.

BHRC. *Iranian code of practice for seismic resistance design of buildings: Standard no. 2800* (3rd edition) Building and Housing Research Center. 2005.

Black, C., Makris, N., and Aiken, I. D. (2004), "Component Testing, Seismic Evaluation and Characterization of Buckling-Restrained Braces," *ASCE Journal of Structural Engineering*, 130(6), pp. 880-894.

Black, G. R., Wenger, B. A., and Popov, E. P. (1980), *Inelastic Buckling of Steel Struts Under Cyclic Load Reversals*, UCB/EERC-80/40, Earthquake Engineering Research Center, Berkeley, CA.

Bonneville, D., and Bartoletti, S. (1996). "Case Study 2.3: Concentric Braced Frame, Lankershim Boulevard, North Hollywood," *1994 Northridge Earthquake; Building Case Studies Project; Proposition 122: Product 3.2, SSC 94-06*, Seismic Safety Commission State of California, pages 305-324.

British Standards Institution (BSI). (1990). "BS 5950: Structural use of steel work in building. Part1 1990." British Standards Institution, London.

Broderick, B., Elghazouli, A., and Goggins, J. (2008). "Earthquake testing and response analysis of concentrically-braced sub-frames." *Journal of Constructional Steel Research*, 64(9), 997-1007.

Chenouda, M. and Ayoub, A., (2009), "Probabilistic collapse analysis of degrading multi-degree of freedom structures under earthquake excitation," *Engineering Structures*, 31, 2909-2921.

Chopra, A. (2006), *Dynamics of Structures*, Prentice Hall, New York.

Cochran, M. and Honeck, W. (2004), *Design of Special Concentric Braced Frames*, Steel TIPS Report, Structural Steel Educational Council, Moraga, CA, May.

Coffin, L.F. Jr. (1954), "A Study of the Effects of Cyclic Thermal Stresses on a Ductile Metal," *Trans. ASME*, Vol. 76, 1954, pp. 931-950.

DASSE (2007), *Cost Advantages of Buckling Restrained Braced Frame Buildings*, DASSE Design Inc.

Downing, S. D., and Socie, D. F. (1982), "Simple Rainflow Counting Algorithms," *Int. Journal of Fatigue*, Vol. 4, pp. 31-40

Ellingwood, B., Galambos, T. V, MacGregor, J. G., and Cornell, C. A. (1980), "Development of a probability based load criteria for American National Standard Committee A58," *Special Publication No. 577*, Nat. Bureau of Standards, Washington, D.C.

Fahnestock, L.A., Ricles, J.M. and Sause, R. (2007). "Experimental evaluation of a large-scale BRBF," *Journal of Structural Engineering* **133** (9), pp. 1205–1214.

Fahnestock, L.A., Sause, R. and Ricles, J.M. (2007). "Seismic response and performance of BRBFs," *Journal of Structural Engineering* **133** (9), pp. 1195–1204.

Fajfar, P. (2000), "A nonlinear analysis method for performance-based seismic design," *Earthquake Spectra*, 16,573–591.

Fell, B.V., Kanvinde, A.M., Deierlein, G.G. and Myers, A.T. (2009). "Experimental investigation of inelastic cyclic buckling and fracture of steel braces," *Journal of Structural Engineering, American Society of Civil Engineers* **135** (1), pp. 19–32.

FEMA P695 (ATC-63) (2009), *Recommended Methodology for Quantification of Building System Performance and Response Parameters*, Applied Technology Council: Redwood City, CA.

FEMA. (1997a). *FEMA 273: NEHRP Guidelines for the Seismic Rehabilitation of Buildings*. Federal Emergency Management Agency, Washington, DC.

FEMA. (1997b). *FEMA 302: NEHRP Recommended Provisions for seismic regulations for new buildings and other structures*, Building Seismic Safety Council, Washington D.C.

FEMA. (1997c). *FEMA 303: Commentary to NEHRP Recommended Provisions for seismic regulations for new buildings and other structures*, Building Seismic Safety Council, Washington D.C.

FEMA. (2000a). *FEMA 351: Recommended Seismic Evaluation and Upgrade Criteria for Existing Welded Steel Moment Frame Buildings*. Federal Emergency Management Agency, Washington, DC.

FEMA. (2000b). *FEMA 355C: State of the Art Report on Systems Performance of Steel Moment Frames Subject to Earthquake Ground Motion Shaking*. H. Krawinkler, ed., Federal Emergency Management Agency, Washington, D.C.

FEMA. (2000c). *FEMA 355F: State of the Art Report on Performance Prediction and Evaluation of Steel Moment-Frame Buildings*. D. A. Foutch, ed., Federal Emergency Management Agency, Washington, D.C.

FEMA. (2000d). *FEMA 356: Prestandard and Commentary for the Seismic Rehabilitation of Buildings*. Federal Emergency Management Agency, Washington, D.C.

Ferch, R. (2004). Berkeley, CA, Personal Communication.

Glinka, G., and Kam, J. C. P. (1987), "Rainflow counting algorithm for very long stress histories," *International Journal of Fatigue*, 9(3), 223-228.

Gupta, A., Krawinkler, H. (1999), *Seismic Demands for Performance Evaluation of Steel Moment Resisting Frame Structures* (SAC Task 5.4.3), Report No. 132, John A. Blume Earthquake Engineering Center, Stanford University, Stanford, California.

Hachem, M. (2009). "BiSpec 1.62." Berkeley, CA, *http://www.ce.berkeley.edu/~hachem/bispec/index.html*.

Hamburger, R. O., Foutch, D. A., and Cornell, A. (2003). "Translating Research to Practice. FEMA/SAC Performance-Based Deisgn Procedures," *Earthquake Spectra*, 19(2).

Han, S. -W., Kim, W. T., and Foutch, D. A. (2007). "Seismic behavior of HSS bracing members according to width-thickness ratio under symmetric cyclic loading." *J. Struct. Eng.*, **133**(2), 264–273.

Hanson, R. D., and Martin, H. W. (1987). "Performance of Steel Structures in the September 19 and 20, 1985 Mexico Earthquakes." *Earthquake Spectra*, 3(2), 329-346.

Hines, E.M and Appel, M.E. (2007), "Behavior and Design of Low-Ductility Braced Frames," *ASCE Structures Congress*, Long Beach, California, May.

Hines, E.M and Grynuik, M.C. (2006), "Collapse Performance of Low-Ductility Chevron Braced Steel Frames in Moderate Seismic Regions," http://engineering.tufts.edu/cee/people/hines/hinesappelcheever2008finsub.pdf

Hisatoku, T. (1995), "Reanalysis and repair of a high-rise steel building damaged by the 1995 Hyogoken-Nanbu earthquake," *Proceedings*, 64th Annual Convention, Structural Engineers Association of California, Structural Engineers Assn. of California, Sacramento, CA, pages 21-40.

Hong, N., A (1991), "Modified rainflow counting method," *International Journal of Fatigue*, 1991, 13, 465-469.

Huang, Y. and Mahin, S. (2010), *Simulating the inelastic seismic behavior of steel braced frames including the effects of low cycle fatigue*, PEER-2010/104, Pacific Earthquake Engineering Research Center, University of California, Berkeley, CA.

Huang, Y., and Mahin, S. A. (2008b), "Evaluation of Steel Structure Deterioration with Cyclic Damaged Plasticity," *Proceedings*, *14th World Conference on Earthquake Engineering*, October 12-17, 2008, Beijing, China.

ICC (2000) *International Building Code*, International Code Council, Falls Church, VA
ICC (2003) *International Building Code*, International Code Council, Falls Church, VA
Jin, J., and El-Tawil, S. (2003). "Inelastic cyclic model for steel braces." *J. Eng. Mech.*, **129**(5), 548–557.
Kato, B., Tanaka, H., and Yamanouchi, H. "Field Work Investigation of Steel Building Damage due to the 1978 Miyagiken-oki Earthquake." *Proceedings of the Seventh World Conference on Earthquake Engineering*, Istanbul, Turkey, 479-486.
Kelly, D. J., Bonneville, D. R., and Bartoletti, S. J. (2000). "1994 Northridge earthquake: damage to a four-story steel braced frame building and its subsequent upgrade," *12th World Conference on Earthquake Engineering*, New Zealand Society for Earthquake Engineering, Upper Hutt, New Zealand.
Khandelwal, K., El-Tawil, S. and Sadek, F., (2009), "Progressive collapse analysis of seismically designed steel braced frames," *Journal of Constructional Steel Research*, 65(3), 699-708.
Khatib, F., Mahin, S. A., and Pister, K. S. (1988), *Seismic behavior of concentrically braced steel frames*, UCB/EERC-88/01, Earthquake Engineering Research Center, University of California, Berkeley, CA.
Kim, H and Goel, S.(1992), *Seismic evaluation and upgrading of braced frame structures for potential local failures*, UMCEE 92-24, Dept. of Civil Engineering and Environmental Engineering, Univ. of Michigan, Ann Arbor, Oct., p.290.
Kim, J. and Choi, H. (2004), "Response modification factors of chevron-braced frames," *Journal of Engineering Structure*, 27, 285-300.
Krawinkler, H, et al. (1996), "Northridge earthquake of January 17, 1994: reconnaissance report, Vol. 2—steel buildings," *Earthquake Spectra*, 11, Suppl. C, Jan., p.25-47.
Lee, K. and Foutch, D. A., (2006), "Seismic Evaluation of Steel Moment Frame Buildings Designed Using Different R-Values," *Journal of Structural Engineering*, 132(9), pp. 1461-1472.
Lee, K., and Bruneau, M. (2005), "Energy dissipation of compression members in concentrically braced frames: Review of experimental data," *J. Struct. Eng.*, 131(4), 552–559.
Lee, S., and Goel, S. C. (1987). "Seismic Behaviour of Hollow and Concrete Filled Square Tubular Bracing Members," *UMCE87-11*, University of Michigan, College of Engineering, Ann Arbor, MI 48109-2125.
Lehman, D. E., Roeder, C. W., Herman, D., Johnson, S. and Kotulka, B., (2008), "Improved seismic performance of gusset plate connections," *ASCE Journal of Structural Engineering*, , 134(6), 890-901.
Lehman, D.E., Roeder, C.W., Herman, D., Johnson, S. and Kotulka, B. (2008) "Improved seismic performance of gusset plate connections," Journal of Structural Engineering, *American Society of Civil Engineers* 134 (6), pp. 890–901.
López, W. and Sabelli R. (2004), *Seismic Design of Buckling-Restrained Braced Frames*, Steel TIPS Report, Structural Steel Educational Council, Moraga, CA, July.
LSTC (2007), *LS-DYNA Keyword User's Manual*, Livermore Software Technology Corporation, CA, US.
Mahmoudi, M. and Zaree, M. (2010), "Evaluating response modification factors of concentrically braced steel frames," *Journal of Constructional Steel Research*, 66, 1196-1204.
Manson, S. S. (1953), "Behavior of Materials under Conditions of Thermal Stress," *Heat Transfer Symposium*, University of Michigan Engineering Research Inst., pp. 9-75.

Matsuishi, M. and Endo, T. (1968), "Fatigue of metals subjected to varying stress," *Proceedings*, Kyushu Branch of Japan Society of Mechanics Engineering, Fukuoka, Japan (in Japanese), pp. 37-40.

McKenna, F. (1997), *Object Oriented Finite Element Programming: Frameworks for Analysis, Algorithms and Parallel Computing*, University of California, Berkeley, Berkeley, CA 94720.

Miner, M. A. (1945), "Cumulative Damage in Fatigue," *ASME Journal of Applied Mechanics*, Vol. 12, pp. 159-164.

Miranda, E. and H. Aslani (2003), "Building-specific loss estimation for performance-based earthquake engineering," *Working Paper*, Stanford University.

Moehle, J. P. (2003), "A Framework for Performance-Based Earthquake Engineering." *Applied Technology Council: Tenth U.S.-Japan Workshop on Improvement of Building Seismic Design and Construction Practices*; Report ATC-15-9, Redwood City, CA.

Moehle, J. P., Stojadinovic, B., Der Kiureghian, A., and Yang, T. (2005). "An Application of PEER Performance-Based Earthquake Engineering Methodology," Research Digest 2005-1, Pacific Earthquake Engineering Research Center, Berkeley, CA.

Naeim, F. (1997). *Performance of Extensively Instrumented Buildings During the January 19, 1994 Northridge Earthquake*, John A Martin And Associates, Research and Development Department, Los Angeles, CA 90015.

Naeim, F. (1998). "Performance of 20 Extensively Instrumented Buildings During the 1994 Northridge Earthquake." *The Structural Design of Tall Buildings*, 7(3), 179-215.

Neuenhofer, A., and Filippou, F. C. (1997), "Evaluation of nonlinear frame finite-element models," *J. Struct. Eng.*, 123(7), 958–966.

Newell, J. and Uang, C.M. (2006), *Cyclic Behavior of Steel Columns with Combined High Axial Load and Drift Demand*, SSRP-06/22, University of California, San Diego

Newmark, N.M. and Hall, W.J. (1982) *Earthquake Spectra and Design*, EERI Monograph, Oakland, CA

Osteraas J. and Krawinkler, H. (1989), "The Mexico earthquake of September 19, 1985—behavior of steel buildings," *Earthquake Spectra*, 5(1), pp. 51–88.

Ousterhout, J. K. (1994), *Tcl and the Tk Toolkit*, Professional Computing Series. Addison-Wesley 1994. ISBN 0-201-63337-X.

Packer, J.A. (2006) "Tubular brace member connections in braced steel frames," *Proceedings, 11th international* symposium *and IIW international conference on tubular structures*, Taylor & Francis, Québec City (Canada), pp. 3–11.

Palmgren, A. (1924), "Die Lebensdauer von Kugellagern," *Zeitschrijt des Vereines Deutscher Ingenieure* (in German), Vol. 64, pp.339-341.

Powell, J., Clark, K., Tsai, K.C., Roeder, C., and Lehman, D. (2008), "Test of a full scale concentrically braced frame with multi-story X-bracing," *ASCE 2008 Structures Congress*, Vancouver, BC, Canada.

Prakash V, Powell G, Campbell S. (1993) Drain-2DX: basic program description and user guide. Report No. UCB/SEMM/93-17. Berkeley (CA): University of California.

Rai, D., Goel, S., and Firmansjah. J. (1996), SNAP-2DX (Structural Nonlinear Analysis Program). Research Report UMCEE96-21, Dept. of Civil Engineering, Univ. of Michigan, Ann Arbor,.

Riddell, R., Hidalgo, P., and Cruz, E. (1989), "Response modification factors for earthquake resistant design of short period buildings," *Earthquake Spectra*, 5(3), 571-590.

Ruiz-Garcia, J. and Miranda, E. (2006), "Evaluation of residual drift demands in regular multi-storey frames for performance-based seismic assessment," *Earthquake Engineering & Structural Dynamics*, Vol. 35, no. 13, pp. 1609-1629. 10 Nov.

Ruiz-García, J. and Miranda, E. (2009), "Probabilistic estimation of residual drift demands for seismic assessment of multi-story framed buildings," *Engineering Structures*, 32, 11-20.

Sabelli, R. (2000), "Research on Improving the Design and Analysis of Earthquake Resistant Steel Braced Frames." FEMA / EERI.

Sabelli, R., Mahin, S. A., and Chang, C. (2003). "Seismic demands on steel braced frame buildings with buckling-restrained braces." *Engineering Structures*, 25(5), 655- 666.

Scott, Michael H., Franchin, Paolo, Gregory L. Fenves, and Filip C. Filippou (2004), "Response Sensitivity for Nonlinear Beam–Column Elements," *Journal of Structural Engineering*, 130(9), 1281–1288.

Shaw, S., Kanvinde, A., and Fell, B. (2010). "Earthquake-induced net section fracture in brace connections -- experiments and simulations." *Journal of Constructional Steel Research*, 66(12), 1492-1501.

Somerville, P. G. (1997), *Development of ground motion time histories for phase 2 of the FEMA /SAC Steel Project*, SAC BD/97-04, SAC Steel Joint Venture, Sacramento California.

Tang, X., and Goel, S. (1989), "Brace Fractures and Analysis of Phase I Structure," *ASCE Journal of Structural Engineering*, 115(8), 1960-1976.

Tremblay R. et al. (1996), "Seismic design of steel buildings: lessons from the 1995 Hyogo-ken Nanbu earthquake," *Canadian Journal of Civil Engineering*, 23(3), pp. 727–756.

Tremblay, R. (2002), "Inelastic Seismic Response of Bracing Members," *J. of Const. Steel Research*, 58, pp. 665-701.

Tremblay, R. (2008), "Influence of brace slenderness on the fracture life of rectangular tubular steel bracing members subjected to seismic inelastic loading," *ASCE 2008 Structures Congress*, Vancouver, BC, Canada.

Tremblay, R. et al. (1995), "Performance of steel structures during the 1994 Northridge earthquake," *Canadian Journal of Civil Engineering*, 22(2), pp. 338–360.

Tremblay, R., Archambault, M.-H., and Filiatrault, A (2003), "Seismic Response of Concentrically Braced Steel Frames Made with Rectangular Hollow Bracing Members," *ASCE Journal of Structural Engineering* 129(12), pp. 1626–1636.

Tremblay, R., Castonguay, P.X., Guilini-Charette, K., Koboevic, S. (2009). Seismic Performance of Conventional Construction Braced Steel Frames Designed According to Canadian Seismic Provisions. Structures Congress - Don't Mess With Structural Engineers: Expanding Our Role, p. 794-803.

Tremblay, R., Haddad, M., Martinez, G., Richard, J., Moffatt, K. (2008). "Inelastic Cyclic Testing of Large Size Steel Bracing Members," *14th World Conference on Earthquake Engineering* (WCEE), p. 05-05-0071.

Tsai, K.C., Hsiao, P.C., Wang, K.J., Weng, Y.T., Lin, M.L., Lin, K.C., **Chen, C.H.**, Lai, J.W., and Lin, S.L. (2008). "Pseudo-dynamic tests of a full-scale CFT/BRB frame-Part I: Specimen design, experiment and analysis," *Earthquake Engineering & Structural Dynamics*, Vol. 37 Issue 7, pp.1081 – 1098.

Uang, C.M. (1991), "Establishing R (or R_w) and C_d factors for building seismic provisions," *Journal of Structural Engineering*, 117(1), 19–28.

Uriz, P and Mahin, S. (2008), *Towards Earthquake Resistant Design of Concentrically Braced Steel Structures*, PEER-2008/08, Pacific Earthquake Engineering Research Center, University of California, Berkeley, CA.

Welch, Brent, Jones, Ken, and Hobbs, Jeff (2003), *Practical Programming in Tcl and Tk*, 4th Edition

Wigle, V. R., and Fahnestock, L. A. (2010). "Buckling-restrained braced frame connection performance." *Journal of Constructional Steel Research*, 66(1), 65-74.

Willibald, S., Packer, J.A. and Martinez-Saucedo, G. (2006) "Behaviour of gusset plate to round and elliptical hollow structural section end connections," *Canadian Journal of Civil Engineering* **33**, pp. 373–383.

WJE. (1998). "Oviatt Library, East and West Wings Investigation of Base Plate Damage Caused by the Northridge Earthquake," Wiss, Janey, Elstner Associates Inc., Emeryville, CA.

Yang, F., and Mahin, S.A. (2005), "Limiting Net Section Fracture in Slotted Tube Braces", *Steel Tips Series*, Structural Steel Education Council, Moraga, CA.

Yazgan, U. and Dazio, A., (2008), "Utilization of residual displacements in the post-earthquake assessment," *14th. world conference on earthquake engineering*, Paper 05-01-0445.

Yoo, J.H., Roeder, C.W., and Lehman, D.E. (2008), "FEM Simulation and Failure Analysis of Special Concentrically Braced Frame Tests," approved and awaiting publication *ASCE Journal of Structural Engineering*.

Zayas, V. A., Popov, E. P., and Mahin, S. A. (1980), *Cyclic Inelastic Buckling of Tubular Steel Braces*, UCB/EERC-80/16, University of California, Berkeley, Berkeley, California.

Appendix A:

Design of SCBF and BRBF Archetype Buildings for Evaluation of Seismic Performance Factors

Index archetypes for SCBF and BRBF are designed by adopting the design requirements of ASCE/SEI 7-05 and the referenced standards. Test data are used to support the designs as necessary. The index archetype designs of SCBF and BRBF account for the significant design features that may affect the structural collapse behavior. The structural components such as beams, columns and braces are designed to comply with the code requirement strictly.

There are a variety of archetype configurations and design choices. In the evaluation of the SCBF and BRBF, the objective is to give an overview about the performance of braced frame system. Therefore, the common options are adopted during the design. The regular structural layout and typical loading conditions are used. The archetype designs are intended to cover a reasonable range of the practical designs, but no include those designs with extreme seismic performances.

The seismic criteria, design loads, load combinations and related requirements for the SCBF and BRBF archetypes are described in the following.

A.1 ARCHETYPE DESIGN INFORMATION

All the archetypes have similar floor layout with the typical material properties and gravity loads. The material properties and gravity loads are modified from Steel TIPS [López and Sabelli, 2004; Cochran and Honeck, 2004] and SAC building designs [Gupta and Krawinkler, 1999]. The design information is summarized as following:

Structural Materials

- W sections — ASTM A992 (Fy = 50 ksi, Fu = 65 ksi)
- HSS sections — ASTM A500 Gr.B (Fy = 42 ksi for square tube sections, 46ksi for circular pipe sections, Fu = 58 ksi)
- BRB Steel Core — ASTM A36 or JIS G3136 SN 400B with supplemental yield requirements: F_{ysc} =42 ksi
- Gusset plates — ASTM A572, Grade 50 (Fyg = 50 ksi, Fu = 65 ksi)
- Weld electrodes — E70XX (notch toughness: 20 ft-lb at –20 degrees Fahrenheit)

Gravity loading

Roof Loading:

Roofing and insulation:	7.0 psf
Metal deck and concrete fill:	47.0 psf
Steel framing and fireproofing:	8.0 psf
Ceiling:	3.0 psf
Mechanical/Electrical:	2.0 psf
Total:	67.0 psf

Floor Weights:

Metal deck and concrete fill:	47.0 psf
Steel framing and fireproofing:	13.0 psf
Partition walls:	20.0 psf
Ceiling:	3.0 psf
Mechanical/Electrical:	2.0 psf
Total:	85.0 psf

Average Exterior Curtain Wall Weight including Column and Spandrel Covers: 15.0 psf
Live Loads (reducible):

Roof:	20 psf
Floor:	50 psf

Based on these loadings, the design considerations and the member sizes of all the archetypes are summarized in the following sections.

A.2 SEISMIC DESIGN LOADING CRITERIA

The seismic loads and design criteria in ASCE/SEI 7-05 are specified based on the Seismic Design Category (SDC) of the structure. SDC are determined from the ground motion intensity of the design earthquake and the Occupancy Category of the structure. FEMA P695 (ATC-63) assumes all structures to be either Occupancy Category I or II with a corresponding importance factor equal to unity. For the SCBFs and BRBFs to be evaluated, the Occupancy Category is chosen to be II. The design spectral response acceleration short periods and 1-second period are shown in Table A.1. The site coefficients (F_a and F_v) and response modification coefficient (R) are also listed in Table A.1.

Table A.1 Design parameters of SCBF and BRBF archetypes

Seismic Design Category	D_{max}	D_{min}
Occupancy Category	II (Office)	
Importance Factor	1.0	
Design Spectral Acceleration at short periods, S_{DS}	1.0g	0.5g
Design Spectral Acceleration at 1-s period, S_{D1}	0.6g	0.2g
F_a	1.0	1.36
F_v	1.5	2.27
R	6(SCBF), 8(BRBF)	

A.3 SEISMIC LOAD RESISTING SYSTEM PARAMETERS

The seismic base shear varies depending on the analysis procedure. In the design of SCBF and BRBF archetypes, the analysis procedure is determined for each archetype as per Section 12.6 in ASCE/SEI 7-05. The Equivalent Lateral Force Analysis (ELF) is used for most of the archetypes except for archetypes 16SCBFDmax, 16SCBFDmin, 12BRBFDmax, 12BRBFDmin, 16BRBFDmax and 16BRBDmin, where the Modal Response Spectrum Analysis (RSA) is used.

A.3.1 Equivalent Lateral Force Analysis (ELF)

In the ELF procedure, the seismic base shear, V, in ASCE/SEI 7-05 is defined by Equation (A.1).

$$V = C_s W \tag{A.1}$$

where

C_s: the seismic response coefficient

W: the effective seismic weight of the building

The seismic coefficient, C_s, is calculated for Short-Period and Long-Period archetypes. For short-period archetypes ($T \leq T_s$):

$$C_s = \frac{S_{DS}}{R} \tag{A.2}$$

where

S_{DS} = the design spectral response acceleration parameter in the short period range

R = the response modification factor

The occupancy importance factor, I, is unity and not shown in the equation.

For long-period archetypes *($T_s < T \leq T_L$):*

$$C_s = \frac{S_{D1}}{TR} \tag{A.3}$$

where

S_{D1} = the design spectral response acceleration parameter at a period of 1.0 s

T = the fundamental period of the structure (s)

T_L = long-period transition period (s) between the constant velocity and constant displacement response domains

Again, the occupancy importance factor is 1.0 and not shown in the equation.

In FEMA P695 (ATC-63), the calculation of seismic response coefficient from Equation A.3 is constrained by a lower bound $0.044S_{DS}$ which is used in many of the long-period archetypes, especially the higher-rise BRBFs.

In ASCE/SEI 7-05, the value of C_s is computed from another equation for very long period structures with a fundamental period, $T > T_L$. Such calculation does not apply to the evaluation here. Due to possible limitations on the low frequency content of the selected ground motion records in the Methodology, FEMA P695 (ATC-63) limits the index archetype designs to configurations with fundamental periods less than 4 seconds.

The design story drift is computed by amplifying the story drift under elastic analysis and can be expressed in Equation A.4.

$$\delta_x = C_d \delta_{xe} \tag{A.4}$$

where

C_d = the deflection amplification factor

δ_{xe} = the deflections determined by an elastic analysis

The elastic analysis is conducted by using the seismic base shear V. The elastic drifts, δ_{xe}, is determined by using seismic design forces based on the computed fundamental period of the structure without the upper limit of $(C_u)(T_a)$.

A.3.2 Modal Response Spectrum Analysis (RSA)

Some of the SCBF and BRBF archetypes are designed using the RSA procedure as per ASCE/SEI 7-05. For those archetypes, the analyses include a sufficient number of modes so the combined modal mass participation is more than 90 percent of the actual mass. The force related design parameters for each mode of response are computed from the response spectra divided by R. The value for displacement and drift quantities computed from the response spectra are multiplied by C_d, which equals R for the SCBF and BRBF archetype design. The combined responses from various modes are calculated from SRSS method.

The base shear, V, of the archetype to be evaluated is calculated using $(C_u)(T_a)$ as prescribed in ASCE/SEI 7-05, since the calculated fundamental period, T_1, of each archetype exceeds $(C_u)(T_a)$. The combined response for the modal base shear, V_t, for each archetype is less than 85 percent of the base shear, V, calculated from ELF procedure. As such, the forces in RSA procedure is multiplied by $0.85(V/V_t)$, but according to ASCE/SEI 7-05, the drifts need not to increase by the factor $0.85(V/V_t)$. The drift calculation is based on V_t, which can be much less than V, in the SCBF and BRBF archetypes. For the archetype designs which drift controls, the force demand reduces dramatically if RSA is adopted instead of ELF.

A.4 STORY DRIFT LIMIT

The design story drift determined from either ELF or RSA are limited by the allowable story drift in ASCE/SEI 7-05. For the two and three-story archetypes, the maximum story drift ratio modified by C_d factor is limited by 2.5% radians; for the six, twelve and sixteen-story archetypes, the maximum story drift ratio modified by C_d factor is limited by 2.0% radians. By changing the member sizes, the stiffness of the archetypes can be increased to satisfy the code prescript drift limits.

A.5 P-DELTA EFFECTS

The P-delta effects, which can be evaluated as per ASCE/SEI 7-05, are less likely to control the design of buildings in high seismic areas. In the SCBF and BRBF archetypes designed for SDC D_{max} and D_{min} , the P-delta effects do not dominate the design as calculated. Instead, the force controls the design of lower-rise archetypes and drift controls the design of higher-rise archetypes in general.

A.6 LOADS AND LOAD COMBINATIONS

The archetypes are designed in accordance with the seismic load effects and load combinations of Section 12.4 of ASCE/SEI 7-05 and guidance provided in FEMA P695 (ATC-63). The design ignores snow load, S, and foundation loads, H, and the basic seismic load combinations are:

$$(1.2 + 0.2S_{DS})D + Q_E + L \tag{A.5}$$

$$(0.9 - 0.2S_{DS})D + Q_E \tag{A.6}$$

where

D: Dead loads including the structural self weight and superimposed dead loads.

L: Live load including appropriate live load reduction factors.

Q_E*:* The effect of horizontal seismic forces resulting from the base shear, *V*.

The redundancy factor, ρ, is conservatively assumed to be 1.0 in all cases in FEMA P695 (ATC-63), so it is not shown in the load combination.

The overstrength is required for the seismic load effect for the design of some structural components, such as columns. Ignores snow load, S, and foundation loads, H, the load combinations for strength design of such components are:

$$(1.2 + 0.2S_{DS})D + \Omega_O Q_E + L \quad \text{(A.7)}$$

$$(0.9 - 0.2S_{DS})D + \Omega_O Q_E \quad \text{(A.8)}$$

where Ω_o is the overstrength factor.

The summary of load combinations for the design of SCBF and BRBF archetypes are shown in Table A.2.

Table A.2 Load combination of SCBF and BRBF archetypes

With or W/O Ω_o	SDC D_{max}, S_{DS}= 1.0g		SDC D_{min}, S_{DS}= 0.5g	
Where Ω_o is NOT required	SCBF and BRBF		SCBF and BRBF	
	$1.4D + Q_E + L$ $0.7D + Q_E$		$1.3D + Q_E + L$ $0.8D + Q_E$	
Where Ω_o is required	SCBF	BRBF	SCBF	BRBF
	$1.4D + 2.0Q_E + L$ $0.7D + 2.0Q_E$	$1.4D + 2.5Q_E + L$ $0.7D + 2.5Q_E$	$1.3D + 2.0Q_E + L$ $0.8D + 2.0Q_E$	$1.3D + 2.5Q_E + L$ $0.8D + 2.5Q_E$

A.7 TRIAL VALUES OF SEISMIC PERFORMANCE FACTORS

For the purpose of evaluating the appropriateness of seismic performance factors in current code, the response modification coefficient, R, and the overstrength factor, Ω_o are chosen based on ASCE/SEI 7-05. The displacement amplification coefficient, C_d, however, is equal to R for most structural systems without damping devices. Section 7.7 in FEMA P695 (ATC-63) defines the value of the deflection amplification factor, C_d, to be the same as the value of the R factor, unless the system has increased damping (i.e., greater than nominal 5% of critical).

A.8 STRUCTURAL CONFIGURATIONS AND MEMBER SIZES

The structural layouts of the archetypes are shown in Figure A.1 to Figure A.3. Regular plan view is selected to avoid excessive torsional effects. The structural layouts of 3 and 6-story archetypes are similar to the braced frames by others [DASSE, 2007]. The braced bays (for both SCBFs and BRBFs) are located at the perimeter of the structures. For 2, 3 and 6-story archetypes, one bay of braced frame is used in each side of the perimeter. For 12 and 16-story archetypes, two bays of braced frame are used in each side of the perimeter. The floor plan is 180 ft by 120 ft. Beam spans are 30 ft typically, except for the 2-story archetypes where the span is 20 ft. The configuration of double story X is adopted in the archetypes due to its benefit for design cost. The story height is 15 ft for all archetypes, except for the 2-story series which has story height of 10 ft. The archetype of the 2-story SCBF designed for SDC Dmax is designed to comply with the design of the tested specimens [Uriz and Mahin, 2008].

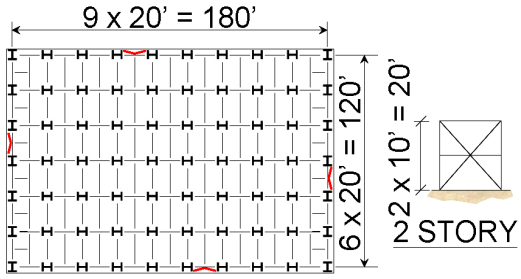

Figure A.1 Plan and elevation of 2-story braced frame archetypes

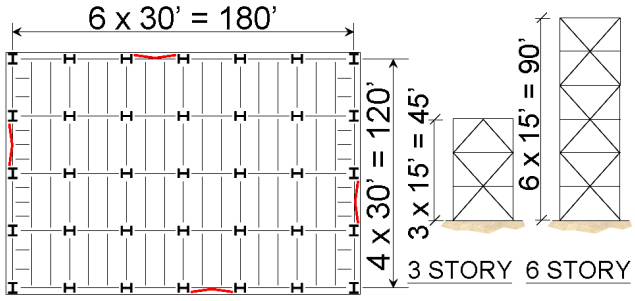

Figure A.2 Plan and elevation of 3-story and 6-story braced frame archetypes

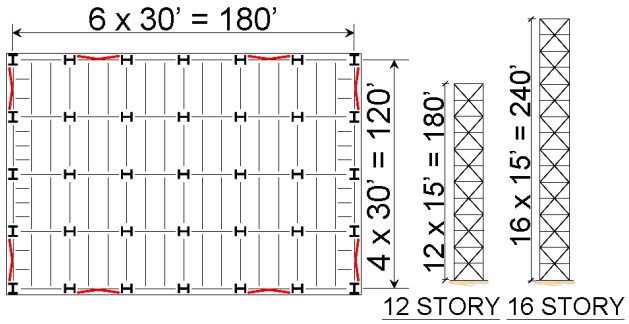

Figure A.3 Plan and elevation of 12-story and 16-story braced frame archetypes

The gravity systems are simplified as leaning columns, which is pin-connected on each floor level to account for P-Δ effects in the design. The gravity systems are assumed to have no lateral resisting capacity and their failure is not specially considered in analysis of the archetypes. Axial load on the leaning column is taken as the total dead load of the system tributary to a braced bay.

The member sizes of the archetypes shown in Table A-3 to Table A-12 are determined from the strength and drift requirements in ASCE/SEI 7-05 and the Methodology of FEMA P695 (ATC-63) which are summarized as aforementioned.

Table A.3 Member sizes of 2-story SCBF archetypes

	Floor	Columns		Braces		Beams	
		Dmax	Dmin	Dmax	Dmin	Dmax	Dmin
2 STORY SCBF	Roof	W10x45	W10x30	HSS6x6x3/8	HSS6x0.25	W24x117	W18x35
	2F	W10x45	W10x30	HSS6x6x3/8	HSS6x0.25	W24x117	w18x50

Table A.4 Member sizes of 2-story BRBF archetypes

	Floor	Columns		Braces		Beams	
		Dmax	Dmin	Dmax	Dmin	Dmax	Dmin
2 STORY BRBF	Roof	W10x39	W10x26	5 in^2	2.5 in^2	W18x35	W18x35
	2F	W10x39	W10x26	5 in^2	2.5 in^2	w18x50	W18x35

Table A.5 Member sizes of 3-story SCBF archetypes

	Floor	Columns		Braces		Beams	
		Dmax	Dmin	Dmax	Dmin	Dmax	Dmin
3 STORY SCBF	Roof	W12x120	W12x72	HSS8-3/4x0.312	HSS6-1/8x0.25	W30x173	W21x132
	3F	W12x120	W12x72	HSS8-3/4x0.5	HSS6-7/8x0.312	W21x111	W18x76
	2F	W12x120	W12x72	HSS9-5/8x0.5	HSS7-1/2x0.312	W18x65	W18x46

Table A.6 Member sizes of 3-story BRBF archetypes

	Floor	Columns		Braces		Beams	
		Dmax	Dmin	Dmax	Dmin	Dmax	Dmin
3 STORY BRBF	Roof	W12x120	W14x82	3 in^2	1 in^2	W21x62	W21x62
	3F	W12x120	W14x82	5.5 in^2	2 in^2	W18x76	W21x55
	2F	W12x120	W14x82	6 in^2	2 in^2	W21x62	W21x62

Table A.7 Member sizes of 6-story SCBF archetypes

	Floor	Columns		Braces		Beams	
		Dmax	Dmin	Dmax	Dmin	Dmax	Dmin
6 STORY SCBF	Roof	W14x68	W12x53	HSS7-1/2x0.312	HSS6x0.25	W18x97	W18x76
	6F	W14x68	W12x53	HSS9x5/8x0.375	HSS6-5/8x0.25	W24x104	W18x76
	5F	W14x176	W12x106	HSS9x5/8x0.5	HSS7x0.312	W24x131	W18x76
	4F	W14x176	W12x106	HSS11-1/4x0.5	HSS7x0.375	W18x76	W21x68
	3F	W14x342	W14x159	HSS12-1/2x0.5	HSS8-3/4x0.312	W24x146	W18x86
	2F	W14x342	W14x159	HSS12-1/2x0.5	HSS8-3/4x0.312	W21x62	W21x62

Table A.8 Member sizes of 6-story BRBF archetypes

	Floor	Columns		Braces		Beams	
		Dmax	Dmin	Dmax	Dmin	Dmax	Dmin
6 STORY BRBF	Roof	W14x90	W14x53	2.5 in^2	1 in^2	W18x76	W21x55
	6F	W14x90	W14x53	5 in^2	1.5 in^2	W21x62	W21x62
	5F	W14x193	W14x90	5.5 in^2	1.5 in^2	W18x76	W21x55
	4F	W14x193	W14x90	7 in^2	2 in^2	W21x62	W21x62
	3F	W14x342	W14x176	8 in^2	2 in^2	W18x76	W21x55
	2F	W14x342	W14x176	8 in^2	2 in^2	W21x62	W21x62

Table A.9 Member sizes of 12-story SCBF archetypes

	Floor	Columns		Braces		Beams	
		Dmax	Dmin	Dmax	Dmin	Dmax	Dmin
12 STORY SCBF (ELF)	Roof	W12x45	W12x40	HSS6-5/8x0.312	HSS5x0.25	W18x55	W18x40
	12F	W12x45	W12x40	HSS6-5/8x0.312	HSS5x0.25	W18x35	W18x35
	11F	W14x99	W14x53	HSS8-3/4x0.312	HSS6-5/8x0.25	W18x60	W18x46
	10F	W14x99	W14x53	HSS8-3/4x0.312	HSS6-5/8x0.25	W18x35	W18x35
	9F	W14x193	W14x74	HSS10x0.375	HSS6-7/8x0.312	W18x65	W18x46
	8F	W14x193	W14x74	HSS10x0.375	HSS6-7/8x0.312	W18x35	W18x35
	7F	W14x283	W14x99	HSS10x0.375	HSS7x0.312	W18x65	W18x46
	6F	W14x283	W14x99	HSS10x0.375	HSS7x0.312	W18x35	W18x35
	5F	W14x398	W14x132	HSS9-5/8x0.5	HSS7x0.312	W18x71	W18x46
	4F	W14x398	W14x132	HSS9-5/8x0.5	HSS7x0.312	W18x35	W18x35
	3F	W14x550	W14x176	HSS9-5/8x0.5	HSS7x0.312	W18x71	W18x46
	2F	W14x550	W14x176	HSS9-5/8x0.5	HSS7x0.312	W18x35	W18x35

Table A.10 Member sizes of 12-story BRBF archetypes

	Floor	Columns		Braces		Beams	
		Dmax	Dmin	Dmax	Dmin	Dmax	Dmin
12 STORY BRBF (RSA)	Roof	W12x40	W12x40	3	1.5	W18x46	W18x35
	12F	W12x40	W12x40	3	1.5	W18x35	W18x35
	11F	W14x74	W14x61	3.5	2	W18x46	W18x35
	10F	W14x74	W14x61	3.5	2	W18x35	W18x35
	9F	W14x99	W14x74	4	2.5	W18x46	W18x35
	8F	W14x99	W14x74	4	2.5	W18x35	W18x35
	7F	W14x145	W14x90	4.5	3	W18x46	W18x35
	6F	W14x145	W14x90	4.5	3	W18x35	W18x35
	5F	W14x176	W14x120	5.5	3.5	W18x50	W18x35
	4F	W14x176	W14x120	5.5	3.5	W18x35	W18x35
	3F	W14x257	W14x176	6	3.5	W18x50	W18x35
	2F	W14x257	W14x176	6	3.5	W18x35	W18x35

Table A.11 Member sizes of 16-story SCBF archetypes

	Floor	Columns		Braces		Beams	
		Dmax	Dmin	Dmax	Dmin	Dmax	Dmin
16 STORY SCBF (RSA)	Roof	W12x45	W12x40	HSS9-5/8x0.375	HSS5x0.312	W18x65	W18x50
	16F	W12x45	W12x40	HSS9-5/8x0.375	HSS5x0.312	W18x35	W18x35
	15F	W14x82	W14x53	HSS8-5/8x0.5	HSS6x0.312	W18x71	W18x50
	14F	W14x82	W14x53	HSS8-5/8x0.5	HSS6x0.312	W18x35	W18x35
	13F	W14x120	W14x68	HSS11-1/4x0.5	HSS6x0.312	W18x86	W18x50
	12F	W14x120	W14x68	HSS11-1/4x0.5	HSS6x0.312	W18x35	W18x35
	11F	W14x176	W14x90	HSS10x0.625	HSS6x0.312	W18x86	W18x50
	10F	W14x176	W14x90	HSS10x0.625	HSS6x0.312	W18x35	W18x35
	9F	W14x233	W14x109	HSS11-1/4x0.625	HSS6-5/8x0.312	W18x97	W18x50
	8F	W14x233	W14x109	HSS11-1/4x0.625	HSS6-5/8x0.312	W18x35	W18x35
	7F	W14x283	W14x132	HSS11-1/4x0.625	HSS6-5/8x0.312	W18x97	W18x50
	6F	W14x283	W14x132	HSS11-1/4x0.625	HSS6-5/8x0.312	W18x35	W18x35
	5F	W14x342	W14x159	HSS11-1/4x0.625	HSS6-5/8x0.5	W21x93	W18x60
	4F	W14x342	W14x159	HSS11-1/4x0.625	HSS6-5/8x0.5	W18x35	W18x35
	3F	W14x370	W14x193	W12x96	HSS6-5/8x0.5	W24x146	W18x60
	2F	W14x370	W14x193	W12x96	HSS6-5/8x0.5	W18x35	W18x35

Table A.12 Member sizes of 16-story BRBF archetypes

	Floor	Columns		Braces		Beams	
		Dmax	Dmin	Dmax	Dmin	Dmax	Dmin
16 STORY BRBF (RSA)	Roof	W12x40	W12x40	3	1.5	W18x46	W18x35
	16F	W12x40	W12x40	3	1.5	W18x35	W18x35
	15F	W14x82	W14x61	3.5	2.5	W18x46	W18x35
	14F	W14x82	W14x61	3.5	2.5	W18x35	W18x35
	13F	W14x109	W14x82	4.5	3	W18x46	W18x35
	12F	W14x109	W14x82	4.5	3	W18x35	W18x35
	11F	W14x159	W14x99	4.5	3	W18x46	W18x35
	10F	W14x159	W14x99	4.5	3	W18x35	W18x35
	9F	W14x193	W14x120	5.5	3.5	W18x50	W18x40
	8F	W14x193	W14x120	5.5	3.5	W18x35	W18x35
	7F	W14x233	W14x145	6	3.5	W18x50	W18x40
	6F	W14x233	W14x145	6	3.5	W18x35	W18x35
	5F	W14x342	W14x176	6.5	4	W18x50	W18x40
	4F	W14x342	W14x176	6.5	4	W18x35	W18x35
	3F	W14x426	W14x233	7	4.5	W18x55	W18x40
	2F	W14x426	W14x233	7	4.5	W18x35	W18x35

Braces in SCBF and BRBF are assumed to have pin connections to the framing. Rigid in plane offsets are assumed at the beam-column connections and brace-to-framing connections. The effective length of the braces corresponds to 70% of the work-point-to-work-point length. The braces are designed to resist more than 70% of the lateral forces. HSS round sections are used for most of the SCBF archetypes except for the locations where the demand is too large to use HSS round sections. Alternatively, the compact wide flange sections are used in those locations. For the buckling restrained braces, only the steel core areas are determined in the design of the archetypes. The effective stiffness of the BRBs are modified to 1.4 times the stiffness computed using only the steel core to account for the stiffness contribution form tapered and connection areas of BRBs.

Fully restrained connections are adopted in the design of beams. Beams are laterally supported at quarter points along the span. In SCBF and BRBF archetypes, the beams where the braces intersected at beam-column connections are also designed to carry the axial force from braces. The capacity design concept is adopted. The axial force from braces are conservatively estimated as $R_yF_yA_g$ in tension and zero in compression, where R_yF_y is the Expected Yield Strength of the braces and A_g is the brace gross area. For the beams where the braces intersected at the mid-span, the unbalanced loads due to the capacity difference of braces above and below the beams are applied. The unbalanced loads in SCBFs are estimated based on $R_yF_yA_g$

for tension braces and $0.3P_n$ for compression braces, where P_n is the nominal compression capacity of the conventional buckling braces. In BRBFs, the capacity of braces is estimated as $\omega\beta P_{ysc}$ for compression and ωP_{ysc} for tension, where ω is tension strength adjustment factor, β is compression strength adjustment factor and P_{ysc} is yield strength of steel core. ω and $\omega\beta$ are estimated as 1.15 and 1.18, respectively, which are similar to the design in Steel Tips [López and Sabelli, 2004]. Due to the configuration of double story X in elevation, the unbalanced loads of the SCBF and BRBF archetypes are cancelled out and only a small portion of the unbalanced force is applied in the beams. The beams are also designed to carry the tributary gravity load distributed along the span.

Columns of the braced frames are fixed at the base. They are orientated to resist lateral force by strong-axis bending. The columns are designed to carry the appropriate load combinations including the overstrength factor, Ω_o. W14 and W12 sections with proper axial, shear and flexural capacity are selected for the columns. Generally, the column sections are changed every two stories and the splices are assumed to be on the floor level.